POLITECNICO DI MILANO

Scuola di Ingegneria Industriale e dell'Informazione

Dipartimento di Energia

Corso di laurea magistrale in

Ingegneria Energetica

Calcium-Copper looping process for hydrogen production applied to ammonia plants

Relatore: Chiar.mo Prof. Matteo Carmelo ROMANO
Correlatore: Dott. Isabel MARTINEZ

Tesi di Laurea di:
David ARMAROLI
Matr. 820675

Anno Accademico 2015 / 2016

Index

Sommario

L'ammoniaca (NH_3) è uno dei prodotti chimici più largamente diffusi a livello mondiale. Il suo impiego nel settore dei fertilizzanti è stato decisivo per la crescita demografica della seconda metà del secolo scorso e per il nostro attuale benessere. Ciononostante, molti altri sono i suoi utilizzi: dal settore farmaceutico, a quello dei disinfettanti, a quello delle munizioni e degli esplosivi, eccetera. Attualmente il processo più efficiente e diffuso (almeno nei paesi occidentali) per la produzione della corrente gassosa di idrogeno e azoto introdotta nel reattore di sintesi dell'ammoniaca è il reforming del gas naturale.

L'obiettivo di questa tesi è proporre e analizzare un sistema completamente diverso per la produzione del gas di sintesi. Tale sistema è comunemente indicato come "calcium-copper looping process" e sfrutta il meccanismo di "sorption enhanced reforming" del gas naturale. Il processo ha luogo in tre fasi conseguenti, all'interno di letti fissi la cui alimentazione è cambiata ciclicamente. Nella prima fase ha luogo la produzione della corrente di idrogeno e la contestuale carbonatazione del sorbente: il CaO cattura la CO_2 trasformandosi in $CaCO_3$; nella seconda fase ha luogo l'ossidazione del rame presente nel letto; nella terza fase, l'ossidazione di una corrente di combustibile ad opera dell'ossigeno presente nel letto (in forma di ossido di rame) rilascia il calore necessario alla rigenerazione del sorbente.

Nella prima parte della tesi si presenta la tecnologia attuale per la produzione di ammoniaca, di cui si analizza uno schema di impianto. Nella seconda parte si passa ad analizzare il sistema oggetto di studio, prima nell'ambito della produzione di syngas grezzo, utilizzabile in centrali termoelettriche con cattura della CO_2 pre-combustione, quindi, con maggiore dettaglio, nell'ambito della produzione di idrogeno ad elevata purezza. Infine, nell'ultima parte, si confrontano le due tecnologie applicate alla produzione di ammoniaca.

Parole chiave: ammoniaca, idrogeno, steam-reforming, chemical looping, calcio-rame, sorption-enhanced reforming (SER)

Abstract

Ammonia (NH_3) is one of the most widespread chemical. Its use in fertilizer industry has been vital for the demographic growth of the twentieth century and for our present affluence. Nonetheless, ammonia has many other employments: from the pharmaceutical sector, to the disinfectants sector, to the explosive and munitions sector, and so on. Currently, the most efficient and common (at least in western countries) process to produce the hydrogen and nitrogen stream introduced into the ammonia synthesis reactor, is the natural gas reforming.

Purpose of this thesis is to analyse a completely different system to produce such hydrogen and nitrogen stream. Such system is referred to as "CaCu looping process" and exploits the "sorption enhanced reforming". The process is made of three subsequent stages, performed in fixed beds, which feed is cyclically changed. In the first stage the hydrogen production and the contextual sorbent carbonation take place: the CaO captures the CO_2 converting into $CaCO_3$. In the second stage the copper in the bed is oxidised by an air flow. In the third stage a fuel flow is oxidised by the oxygen in the bed (in the form of CuO), releasing the heat required by the sorbent regeneration.

In the first part of the thesis we present the current technology for ammonia production, of which we analyse a plant scheme. In the second part we analyse the new system, first applied to raw syngas production, as is the case of pre-combustion carbon capture power plants, then, more specifically, applied to high-purity hydrogen production. In the last part we compare the two processes, applied to ammonia production.

Keywords: ammonia, hydrogen, steam-reforming, chemical looping, calcium-copper, sorption-enhanced reforming (SER)

1) Ammonia

Ammonia (NH_3) is a compound formed by one nitrogen and three hydrogen atoms. As nitrogen has five electrons in the external shell, while hydrogen has one, three bonds are formed, with three couples of electrons involved, and the remaining two electrons of nitrogen left free. This explains the nitrogen trigonal pyramidal shape. Since the lone pair of electrons repels more than the bond pairs, the tetrahedral is not regular. This shape gives the molecule a dipole moment and so makes it polar. Besides, because of the free electrons couple, ammonia is a proton-acceptor, or, in other words, a base.

Ammonia is found, at ambient conditions, in gas phase, which can be easily liquefied thanks to the strong hydrogen bonding between molecules (at ambient pressure its boiling temperature is about -33,3 °C). The ammonia density at ambient conditions is 0,73 kg/m^3, so it is lighter than air. The presence of ammonia in environment is quite uncommon and it is due above all to the breakdown (putrefaction) of organic waste matter(1). Although it is a colourless gas, its presence can be detected for its characteristic pungent smell. Ammonia is toxic, corrosive and dangerous for the environment and so its production, transportation and uses are regulated by restrictive safety laws (see Dangerous Substances Directive 67/548/EEC). Ammonia is highly miscible with water, forming a basic solution; the most common high-concentration commercial product (“household” ammonia) is composed by up to 30% by weight of ammonia(2).

1.1) Ammonia uses

It is not an exaggeration to state that the demographic growth of the twentieth century and our present affluence could have hardly been possible without ammonia industrial-scale production. Since the 1950's, after the first and second world wars, the Haber-Bosch process to produce ammonia started to affect heavily farming. Ammonia stocks, diverted in wartime to make bombs and bullets, started being used to produce the synthetic nitrogen fertilizers, used everywhere today. Ammonia is one of the most commonly produced industrial chemicals, with about 146 500 000 tonnes produced in 2006 and 198 000 000 in 2012(2).

More than 80% of the ammonia production is destined to fertilizers production. Most of the fertilizers currently used are based on nitrogen compounds and ammonia is precursor to most of those compounds. The elements provided by fertilizers are typically nitrogen, phosphorus and potassium(7), in several forms. As shown in the graphic below nitrogen is the most used.

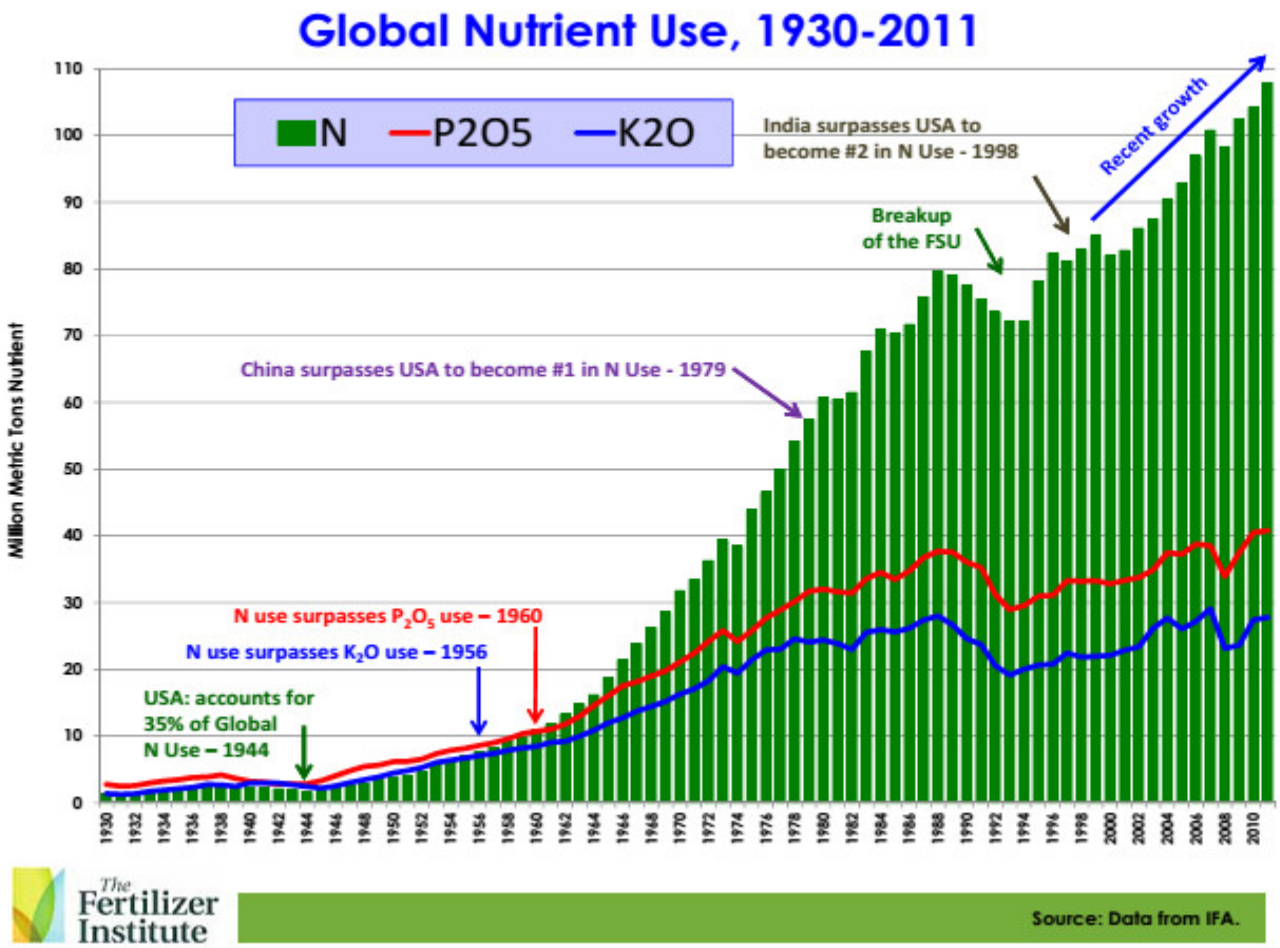

Figure 1: trend in fertilizers use: nitrogen (green line), phosphorus (red line), potassium (blue line) (4).

It can be useful to point out that plant roots need to take up nutrient from the soil usually as positive or negative ions, which therefore must be present in the soil. Nitrogen is taken up by most plants in only two forms: as nitrate ions (NO_3^-) and as ammonium ions (NH_4^+). In some dry soils, exposed to the air, ammonium ions are oxidised to nitrate ions, which are absorbed to form amino acids and hence proteins; in wet soils, as those for rice cultivation, most of the nitrogen is taken up in ammonium ions. While in western Europe the most common nitrogen-containing fertilizers are mixture of ammonium nitrate and calcium ammonium nitrate, in Asian countries, such as India and China, nitrogen is more often employed in its carbonate form, urea(6).

One of the most important ammonia derivatives is nitric acid (HNO_3), produced through the Ostwald process, in which anhydrous ammonia is oxidized to nitric oxide (NO_2), which then reacts with water to form nitric acid. Nitric acid has several uses. It is used to produce explosives (such as TNT); it is neutralized with ammonia to give ammonium nitrate (NH_4NO_3), one of the most worldwide used fertilizers; it is used to produce sodium nitrate (used in the production of fertilizers, smoke bombs, pyrotechnics, food preservatives and solid rock propellant(3)) and nitric phosphate(4). Ammonia is also precursor to ammonium sulphates and ammonium phosphate. One of the most important fertilizers derived from ammonia is urea ($CO(NH_2)_2$), with a global production in 2012 of 184 million tonnes(5). Since many soil bacteria possess the enzyme urease, which allows them to transform urea in ammonium ions and bicarbonate ions, urea is effectively absorbed by plants. Urea is produced through the Bosch-Meiser process, developed in 1922, consisting of a first exothermic reaction in which liquid ammonia reacts with gaseous carbon dioxide (CO_2) at high temperature

and pressure (around 190 °C and 140-175 bar(5)) to form ammonium carbamate (H_2N-$COONH_4$), and a second slow endothermic reaction of decomposition of ammonium carbamate in urea and water. Urea is also used to produce plastics, resins (such as urea-formaldehyde resins), adhesives and explosives (especially urea nitrate).

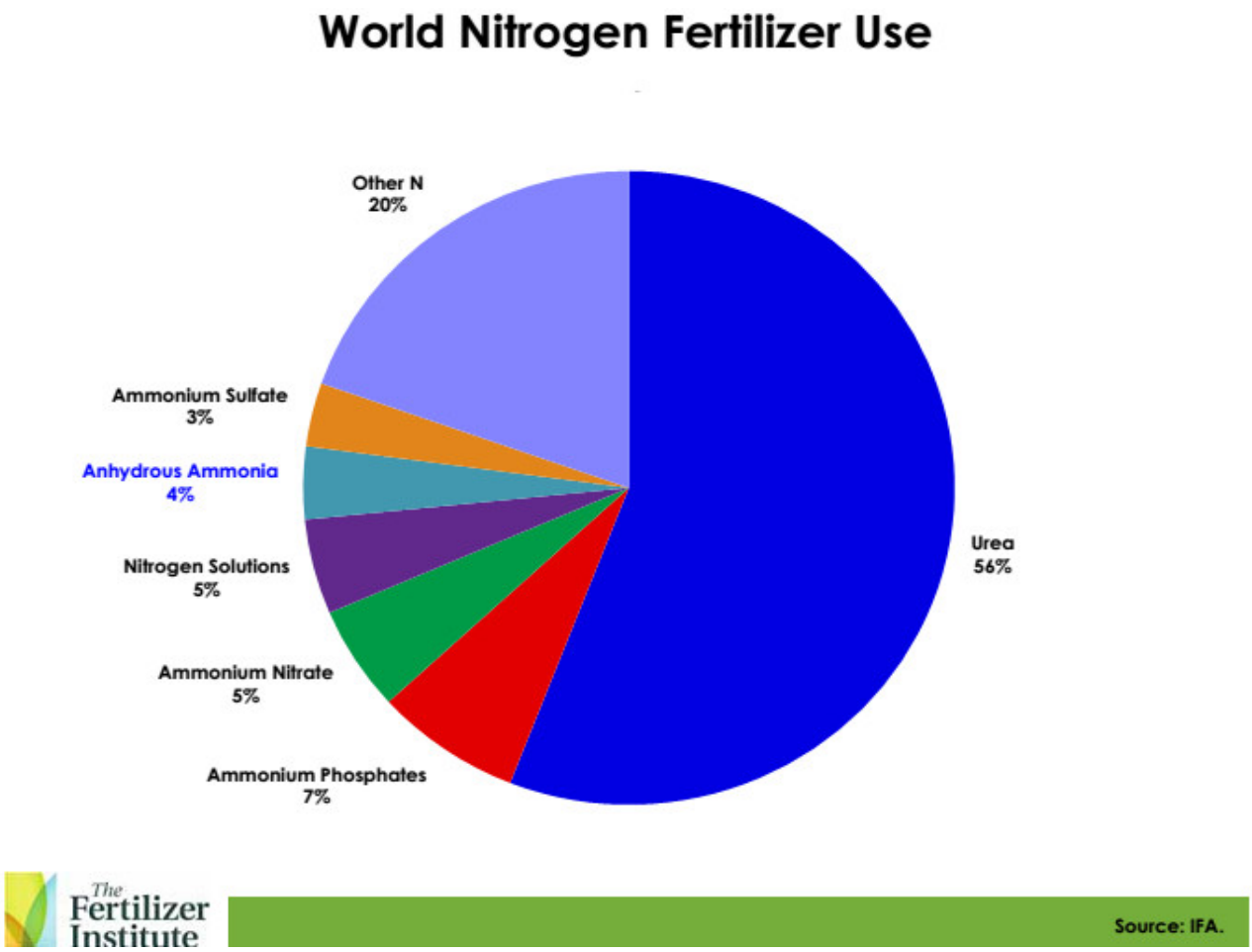

Figure 2: different kind of nitrogen fertilizers used in 2011(4)

Ammonia has also employs different from fertilizers. Ammonia is used in the synthesis of nitro-glycerine (used as vasodilator for instance), sodium hydrogen carbonate, hydrazine (used in rock propulsion systems) and many others. Ammonia is employed in production of nylon and others polyamides. Ammonia was used (and still is, in spite of its toxicity), especially before the popularization of Freons, as a very efficient refrigerant fluid (R717), either to make ice than for air- conditioning units, especially in big plants. An ammonia derivative, ammonium hydrogen sulphite, is employed in the paper industry, enabling some hardwoods to be used. Ammonia is employed in the textile industry for mercerisation treatment of cotton and to prewash wool. Although it can sound odd, ammonia is also used in food industry for its strong antiseptic properties (it has been proved that ammonia destroys 99,999% zoonotic bacteria in three types of animal feed(2)); for example ammonia is currently used to strongly reduce the microbial contamination of beef. But ammonia can also be found in our houses: solution of ammonia and water, usually with around 5-10% of ammonia by weight, are used as cleaner for glasses, porcelains and steel.

1.2) Ammonia market

Ammonia production has been constantly growing since the Haber-Bosch process (see next chapter) has been developed.

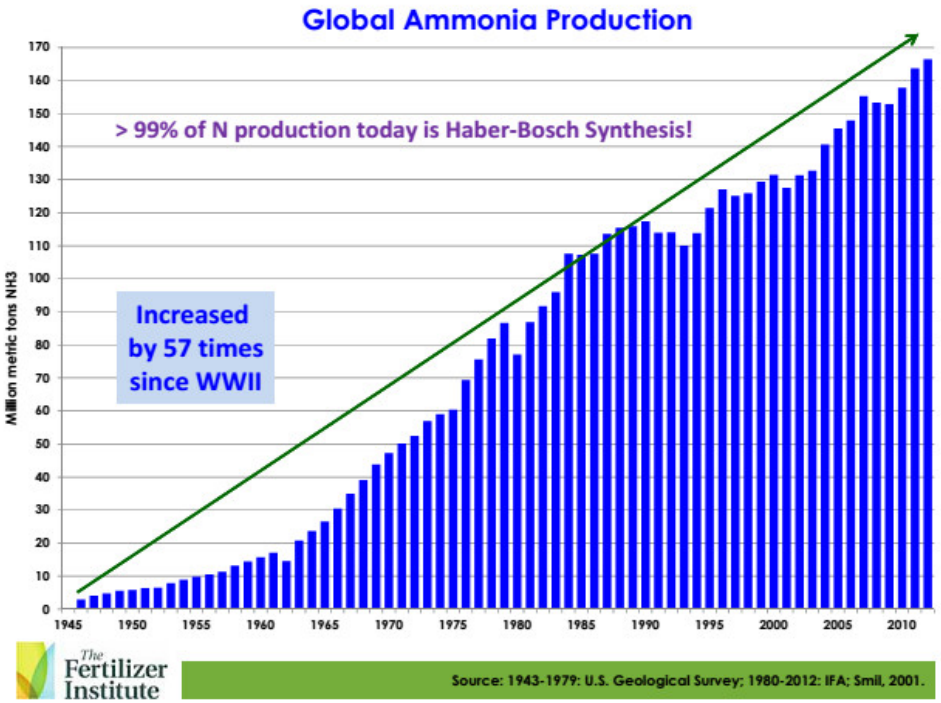

Figure 3: ammonia production trend (4)

The major ammonia producer is by far China (responsible for 32% of global production), which production is still ceaselessly growing, followed by India, US and Russia.

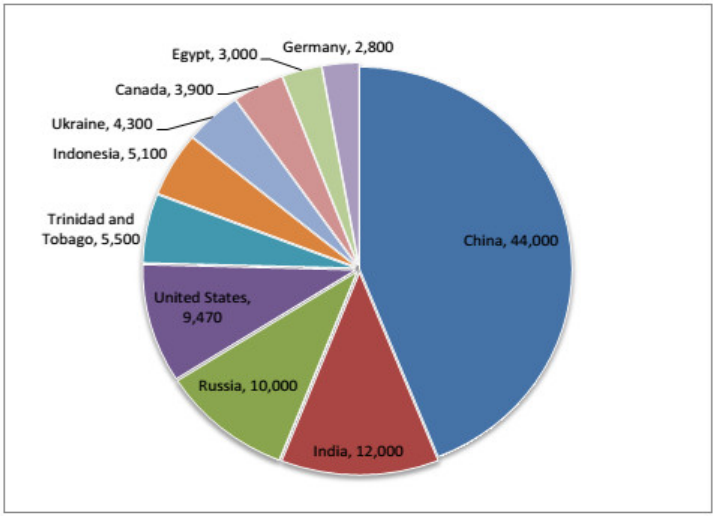

Figure 4: main ammonia producers in 2012. Data in kilotonnes (1)

The driver for ammonia consumption increase in the last decades has mainly been the demographic growth in the developing countries, accordingly with the figures above.

The EU-27 has a total capacity of around 21 million tonnes of ammonia per year, spread over just 42 plants(2). From this figure we can deduce that ammonia plants are very big, capital-intensive and prone to significant economy of scale, as will be clear when we will talk about ammonia production. The average ammonia plant in Europe produces around 1110 tonnes per day, with a trend towards the upsizing (modern plants have a capacity of around 1500 tonnes per day or even more). Nevertheless the ammonia (and so the fertilizers) production costs are mainly due to the raw material used as feedstock (primarily natural gas), as shown in the figure below.

	Share in total energy costs, %	Share in total production costs, %
Natural gas	90-94%	80-88%
Electricity	4-8%	3-6%

Figure 5: natural gas weight in ammonia production cost for European plants (1)

This has two important implications. The first is that the efficiency of the plants is decisive to reduce the production cost. The second is that the ammonia price, and subsequently that of food, is bound to that of natural gas, at least in the long run. The countries with lower natural gas price, such as Russia and US, can produce fertilizers at a lower cost, and so sell fertilizers and food in the global market at a lower price.

Table 3. EU-27 capacity and number of plants per country, 2013

COUNTRIES	CAPACITY (k tonnes)	NUMBER OF PLANTS PER COUNTRY	% EU-27
GERMANY	3,438	5	17%
POLAND	3,210	5	16%
NETHERLANDS	2,717	2	13%
ROMANIA	2,176	6	11%
FRANCE	1,495	4	7%
LITHUANIA	1,118	1	5%
BULGARIA	1,118	3	5%
UK	1,100	3	5%
BELGIUM	1,020	2	5%
SPAIN	609	3	3%
ITALY	600	1	3%
AUSTRIA	485	1	2%
SLOVAKIA	429	1	2%
HUNGARY	383	2	2%
CZECH REP.	350	1	2%
ESTONIA	200	1	1%
GREECE	165	1	1%
TOTAL EU-27	20,613	42	100.00%

Figure 6: ammonia production in Europe in 2013 (1)

The figure below, which shows ammonia and natural gas average prices in US, confirms the relation between the two. It is interesting to note that, despite the natural gas price has never recovered its pre-crisis value, the ammonia price has been keeping quite high, and it is still growing in the last years, thanks to the high demand. This means that ammonia producers, at least in US, have indeed increased their profit.

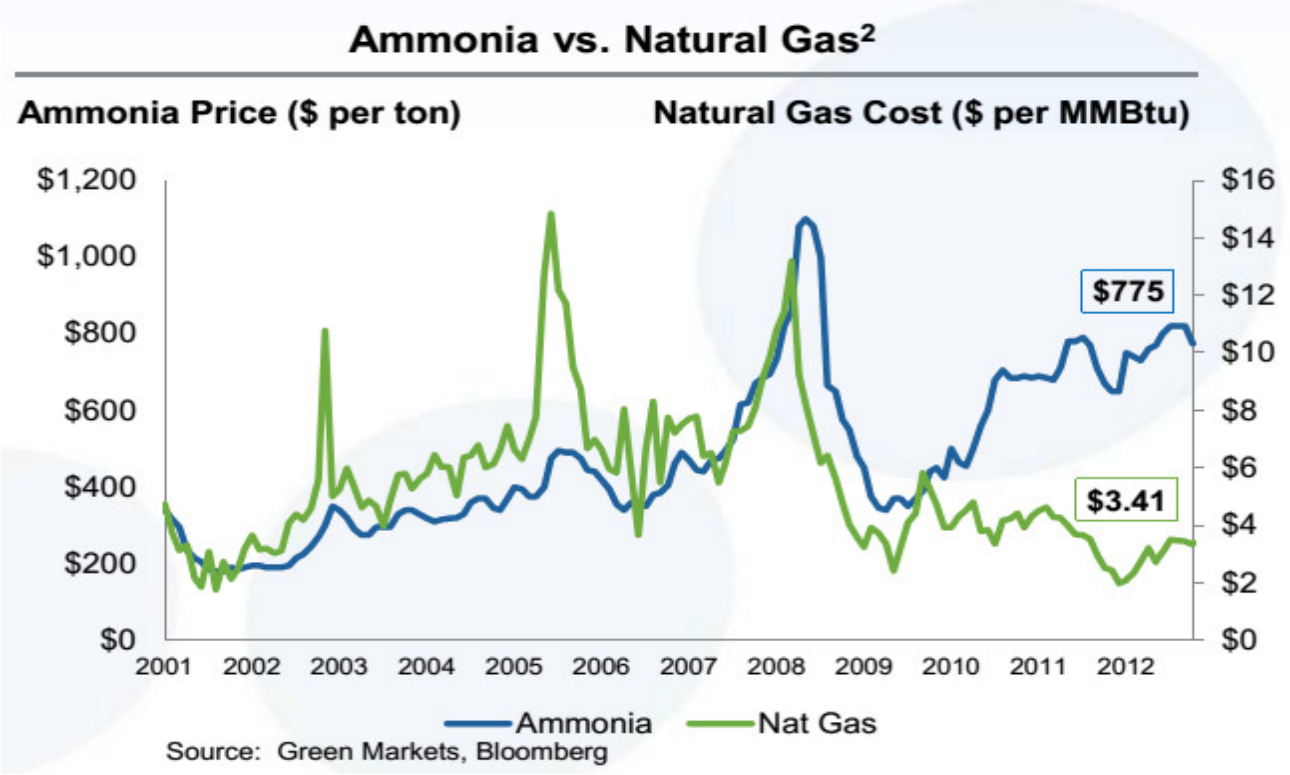

Figure 7: ammonia and natural gas prices in US (8)

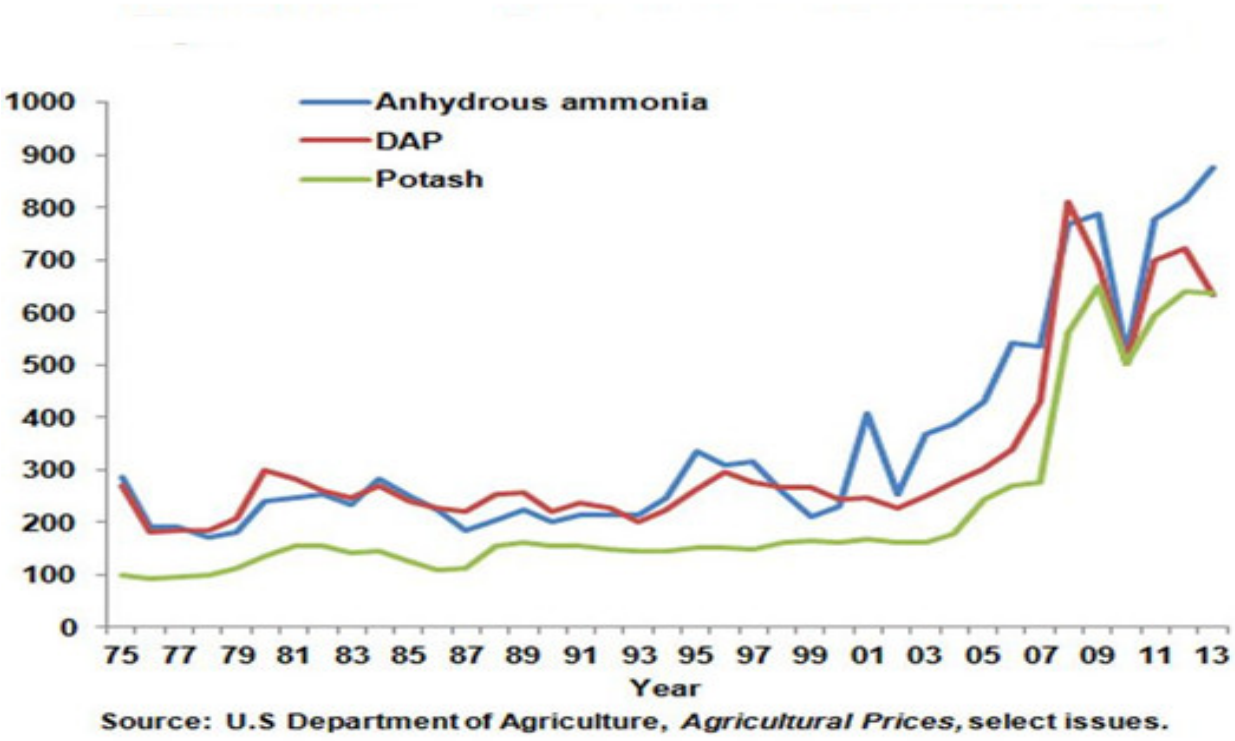

Figure 8: different fertilizers compound prices trends in US, values in $ per acre (9)

Figure 8 shows the prices trend for different fertilizers compound (ammonia, diammonium phosphate and potassium based fertilizers) in US. In the very last years the ammonia price has not gone through a decline, like other fertilizers have, because of its global demand, coming above all from developing countries. Nonetheless, the fertilizers prices, especially in the new century, are prone to a significant instability.

The ammonia plants designing, for the presence of strong economies of scale (due to the specific technological high requirements for instance), is a very “concentrated” sector. The main actors are KBR, BASF, Casale, Haldor-Topsoe, Linde AG, ThyssenKrupp(10).

2) Ammonia production

The importance of nitrogen compounds as fertilisers in agriculture is known since the 17th century (1). The first unsuccessful experiments to synthesize ammonia (NH_3) date back to the same period. In 1900, one of the most prominent chemists of the time, W. Ostwald, thought he succeeded in synthesizing ammonia, though later experiments proved he was wrong. Before 1913 the whole ammonia production process was "natural", coming from dry distillation (e.g. heating of solid material to obtain gaseous products) of animal and vegetable waste (i.e. manure and guano) and coal. At that time, the first ammonia producer was Chile, thanks to the large deposits of sodium nitrate present in the Atacama Desert (2), covering 58% of the worldwide ammonia production.

The catalytic synthesis of ammonia from nitrogen and hydrogen atoms in their molecular form (e.g. as H_2 and N_2) is one of the greatest achievements of industrial chemistry (3). This breakthrough is due to the German chemist Fritz Haber, who, together with his assistant Robert Le Rossignol, developed the process (and the instrumentation) to produce ammonia from air nitrogen. This process, patented in 1908(11), is still the foundation of modern ammonia production, with very little changes: it already comprised the main ammonia synthesis features (discussed in detail in the following sections), such as the use of an iron catalyst, high pressure and high temperature, recycle of unreacted reagents and separation of ammonia by condensation. In 1908, Haber approaches BASF (Badische Anilin & Soda Fabrik) to seek support for his work. The firm decided to supply him with the financial and technical resources required. The task to develop a reliable industrial-scale system was committed to Carl Bosch, who, together with a team of high-skilled workers, succeeded in less than five years. The first plant, in Oppau (Ludwigshafen), started the production in 1913 (3). The process is still known with the name Haber-Bosch. During the years of the World War One the production of ammonia was decisive for Germans, allowing them to produce nitric acid, a precursor to munitions (the Germans had no access to Chilean sodium nitrate, almost entirely controlled by England). After the war, the ammonia and its derivatives began to be consistently employed in farming and the global production began to increase steadily. In the years 1924-1929 the German ammonia production passed from less than 0,25 to more than 0,8 million metric tons per year (1), making Germany the first global producer in the thirties. In 1934 64% of the global production was due to the Haber-Bosch process. Haber and Bosch were both awarded with Nobel Prize in 1918 and in 1931 respectively.

Until the 50's the main source of feedstock raw gasses for ammonia production (namely high-heating value hydrogen-containing gasses) was coal gasification. The next step forward in the improvement of the technology started in USA, where the reforming of natural gas was employed to obtain synthesis gas (syngas). This process was firstly developed and commercialized, once again, by BASF, and then improved and extended to naphtha by ICI (3). With the growing availability of cheap natural gas and improved techniques for steam reforming, natural gas became the cheapest and most popular feedstock for ammonia plants (4), being the hydrocarbon with the highest hydrogen/carbon ratio. Nonetheless partial oxidation of naphtha or coal is still largely used in Asian countries like China (where 66 % of the production is based on coal (3)).

	Natural Gas	Heavy Oil	Coal
Energy Consumption	1	1.3	1.7
Investment Cost	1	1.4	2.4
Production Cost	1	1.2	1.7

Source: EFMA (2000).

Figure 1: comparison between production costs using different feedstocks, with natural gas as reference (4)

The last breakthrough in ammonia production is due to Morris W. Kellogg, who introduced the single-train steam-reforming plant concept. Such plants, still in use today, are based on the use of only one large line of production (exploiting the strong economy of scale of components) and are designed to be as much energetically integrated and self-sufficient as possible, reducing as much as possible the import of electricity (with the transformation losses related) and the import/export of low pressure steam. Modern plants are self-sufficient indeed. This new philosophy allowed to strongly increase the efficiency and to reduce the cost of plant at the same time, resulting in the quick growth of the global ammonia production capacity of the sixties (see Fig. 3, ch.1).

2.1) Inside the ammonia synthesis reactor

The reaction through which ammonia is produced is the following

$3H_2 + N_2 \leftrightarrow 2NH_3 \quad (\Delta H_r^\circ = -46{,}22\ kJ/mol, NH_3) \qquad (1)$

It is exothermic and entails a reduction in molar flow, so it is favoured at low temperature and high pressure. In the absence of a catalyst, the system does not react spontaneously at temperatures below 900 °C, at which the chemical equilibrium dictates a negligible reactants conversion. This is because a significant energy input is required for the nitrogen molecule to achieve the activated state, the nitrogen dissociation energy being 945 kJ/mol (compared to 436 kJ/mol for hydrogen). This fact explains why all the old attempts to combine molecular nitrogen (N_2) and hydrogen "thermally" failed: it is necessary either to furnish the energy in a different way or to change the path of reaction. For instance, in addition to the thermal energy, electrical energy or ionizing radiation can be exploited. The reason why these processes are economically unfeasible is that the energy supplied is used only in part for ammonia formation, whereas the greater part is dispersed. On the other hand, when a proper catalyst is employed, the molecules lose their translational degrees of freedom by fixation on the catalyst surface. As a result, the activation energy is drastically reduced (to around 103 kj/mol using an iron-based catalyst), allowing to perform the reaction at much lower temperatures.

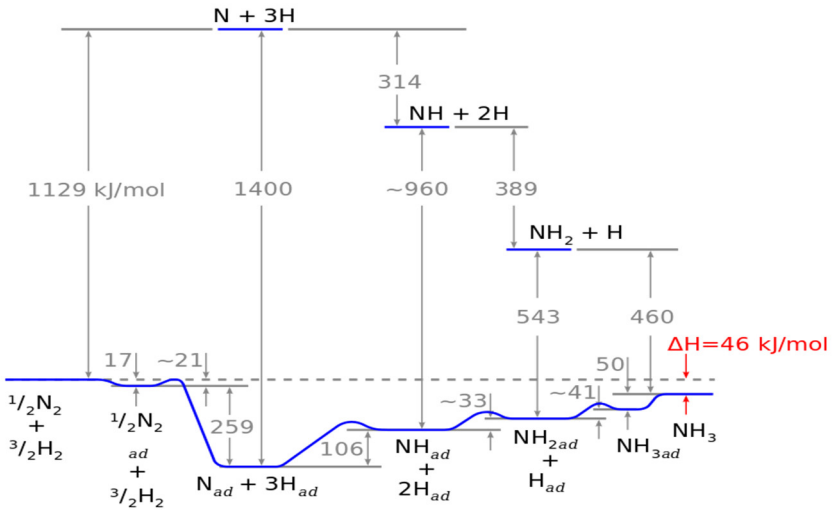

Figure 2: comparison between ammonia reaction path with and without catalyst, considering a traditional iron catalyst (3)

Generally speaking, a catalytic reaction can be divided into five main steps: (i) transport of the reactants from the gas bulk stream to the outer surface of the catalyst and then to the inner surface (pore walls) by diffusion, (ii) adsorption of the reactants on the inner surface (and in case catalyst poisoning), (iii) reaction of the adsorbed species, (iv) desorption of the products, and (v) diffusion of the reaction products towards the outer surface and from there back to the bulk phase. In the case of interest, the nitrogen adsorption and dissociation can be regarded as the rate-determining step. As can be seen from figure 2, since the adsorption is exothermic, the energy gain associated with surface atom bonds overcompensates the nitrogen dissociation energy and the first step becomes slightly exothermic.

The most widespread catalysts in ammonia reactors are iron-based and are still quite similar to those developed by Mittasch in 1950(7). They are composed of iron oxides (mainly magnetite, Fe_3O_4) and a few percent of Al, Ca and K as promoters (usually around 2,5-3,5% CaO, 2,3-5% Al_2O_3 and 0,8-1,2% K_2O(3)). Other elements, such as Mg and Si, may also be present in small amounts (3). The catalyst can be reduced in situ, with synthesis gas (magnetite reacts with hydrogen to form iron (Fe) and water), or pre-reduced by the seller. During the reduction, the oxygen present in the lattice is removed and the iron atoms themselves are redistributed. The reduction of catalyst plays an important role in its performance, since it determines its porosity. It is therefore important to keep a low reduction temperature in order to limit the reduction velocity (7). The process for catalyst production requires melting of iron minerals, to which are then added the promoters. Once the molten substance is solidified, it is shaped into grains of 1,5-3 mm, in order to maximize the surface to volume ratio. The final product obtained has a porosity around 40% and a total surface around 10-12 m^2/g(7). The activity of the catalyst can be further increased introducing Cobalt (3-6% by weight), which is built-in in crystal lattice and, during the reduction, forms an alloy with the iron.

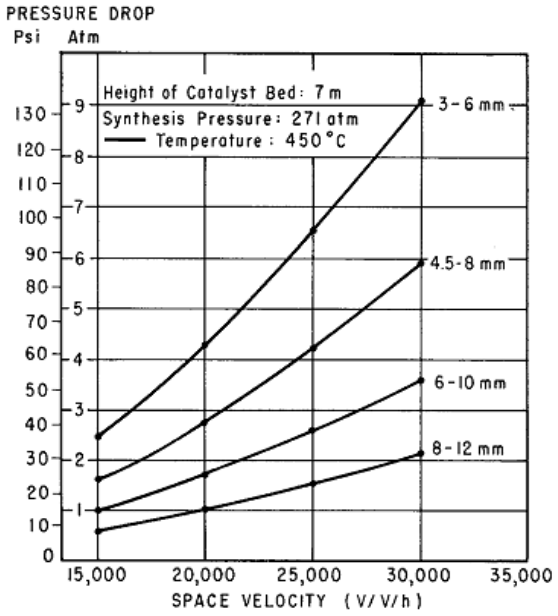

Figure 3: pressure drop in the synthesis reactor over space velocity and particles size(9)

The size and shape of catalyst is determined by two factors: catalyst performance and pressure drops. While smaller and more irregular particles allow catalyst performance to be increased, they also result into higher pressure drops. Moreover, under a certain size, there is the risk of fluidizating the catalyst. To make an idea, suffice it to say that an increase in granular size from 1,5-3 mm to 6-10 mm entails an increase in catalyst volume requirement of around 23% (3). The effect of granular size and space velocity (defined as standard cubic meters of gas processed per hour per cubic meters of catalyst) on pressure drops is shown in figure 3.

Also others catalysts are feasible, the most promising being those Ruthenium (Ru)-based. The use of Ru catalysts, with Cs or Ba as promoters, allows levels of activity one order of magnitude higher than the iron-based ones, with also a lower inhibition by ammonia(7). Despite those second-generation catalysts have already been tested in industry, their use is very limited because of their high cost.

Pure iron (Fe) cannot be used as catalyst since it deactivates very fast due to sintering. A structural promoter (such as Al_2O_3) should be therefore used as support to sustain Fe and so to promote catalyst performance, allowing an operative life of catalysts exceeding a decade (7). The Fe-based catalysts are easily poisoned by oxygen compounds, the most common being water and carbon oxides (e.g. CO and CO2). A distinction should be made between irreversible (which causes permanent damages to the catalyst) and reversible poisons. The compounds mentioned above (water and carbon oxides) can be classified as reversible, as the activity loss is gradually recovered when they are no longer present in the gas. Anyway, the continuing exposure to these

compounds (prolonged for more than 3-6 days), especially at high temperature and high concentration, can lead to an irreversible loss of activity of catalyst. This is probably the main cause of the decline of converter performance over the course of catalyst operative life. The content of those compounds at the reactor inlet should be reduced to ppm (usually no more than 5 ppm, corresponding to 12-15 ppm in the fresh synthesis gas entering the loop). On the other hand, sulphur, phosphorus, chlorine and arsenic compounds have an irreversible poisoning effect on Fe-based catalysts even at contents lower than one ppm. Fortunately, in methane-fed plants, the only poison of some relevance is sulphur, which is eliminated in a first stage, as seen later on in this chapter.

In modern plants the synthesis pressure is around 150-250 bar (7), which is more than a hundred bar lower than pressure used in old plants, thanks to the increase in catalysts performance, allowing a reduction of compression costs.

In the light of what has been said above, the reaction optimal temperature is a compromise between two opposite needs. In fact, the reaction rate for a catalytic reaction is proportional to the product of three factors: the first is the kinetic factor, which increases roughly exponentially with temperature according to the Arrhenius law; the second is the driving-force group, which indicates how far the system is from equilibrium (in our case it would require the lowest possible temperature); the third is the adsorption group, which accounts for the speed at which reactants and products are adsorbed and desorbed, respectively. The relation between the reaction rate and the thermodynamic state of the system is called rate equation and depends on the reaction path and so on the catalyst employed. The catalyst therefore dictates the minimum operative temperature of the process: under a certain temperature, the kinetic is too slow.

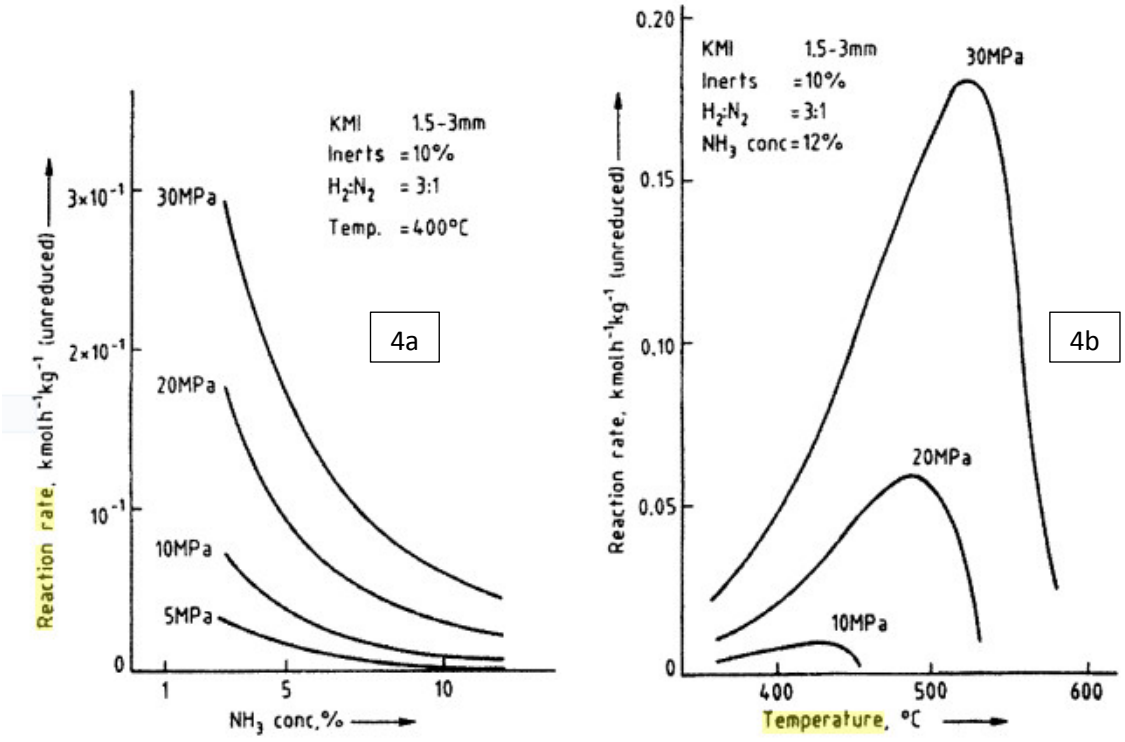

Figure 4a: reaction rate as a function of ammonia concentration for a temperature of 400°C at several pressures. Figure 4b: reaction rate as a function of temperature for several pressures for an ammonia content of 12% (8).

Figure 4a shows the reduction in reaction rate as the ammonia concentration increases. Figure 4b shows that for a pressure of 200 bar and an ammonia content of 12% the optimal temperature for maximising the reaction rate is around 490 °C. However, as appreciated, the reaction rate collapses at a slightly higher

temperature due to the decrease of the driving-force group. In modern plants the reactor outlet temperature is usually around 440-490 °C with an ammonia content of 17-21%.

The optimal temperature depends also upon the ammonia concentration. At the reactor inlet, where the ammonia concentration is low, the system is far from chemical equilibrium, and so the driving-force is high. Therefore, it is advantageous to operate at higher temperature at reactor inlet in order to increase the kinetic factor. As the gas reaches the exit of the reactor, the ammonia content increases, and the limiting factor becomes the driving-force group. Consequently, to maximize the reaction rate along the end of the reactor is therefore necessary to reduce the temperature. Since at the outlet temperatures mentioned above the kinetic is quite slow, for economic reasons, the reactors are usually not designed to reach chemical equilibrium at the exit.

The last operative parameter to be discussed is the hydrogen to nitrogen ratio in the inlet gas. As can be seen from the figure below, the NH_3 production rate shows a maximum for a certain value of this ratio. This optimal values increases when the space velocity of the gas decreases, reaching a value of three for low space velocities. The reason is that equilibrium plays a greater role at low space velocities. Usually this ratio is adjusted to three, because, in most plants, conversion near equilibrium is attained (3).

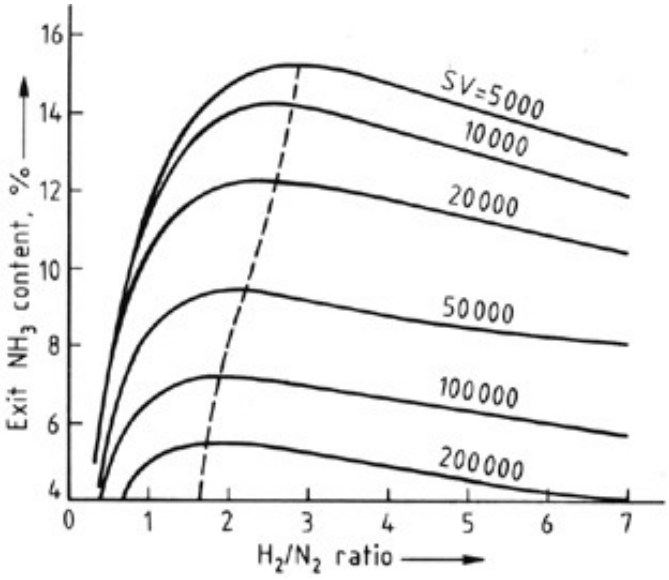

Figure 5: outlet ammonia content as a function of H_2/N_2 ratio at the inlet for several space velocities (SV) with a pressure of 97 bar(3)

The space velocity is itself an important parameter. Sure enough, its optimal value decreases when the pressure decreases. For example if the pressure raises from 150 bar to 800 bar the space velocity can be increased from 12000 h^{-1} to 35000 h^{-1}(3). Even if at higher space velocities the ammonia content in the effluent gas is lower, the increase in gas flow overcompensates it. This characteristic can be exploited to maintain a good ammonia production rate when catalyst ages, at least until the heat released by the ammonia synthesis reaction suffices to heat up the reactants to the required temperature.

The features briefly discussed above are the fundamentals to explain how the reactors are devised. As seen, to maximize the reaction rate throughout the whole reactor, and so obtain the highest reactants conversion with the smallest reactor (and catalyst) volume, the gas temperature should be very high at the inlet (the optimal value is above 600 °C) and it should be reduced gradually as the conversion proceeds, following the

optimal temperature profile. Unfortunately, the fact that the reaction is exothermic makes this temperature control very difficult to accomplish in practice.

The reactors can be classified into two main families depending on the way the gas is cooled down. In the first type of reactors the gas is "internally" cooled, with cooling tubes running throughout the catalyst bed or with catalyst inside the tubes and cooling medium on the shell side. These reactors are known as tube-cooled converters. In this case the cooling medium is usually the reactor feed gas. This class of reactors has some disadvantages related primarily to the low gas-gas heat exchange coefficient, such as an inaccurate temperature control (especially temperature peaks are very difficult to restrain) and a significant volume of the equipment. For these and other reasons this kind of converters is suited only for small production capacities and therefore of limited interest.

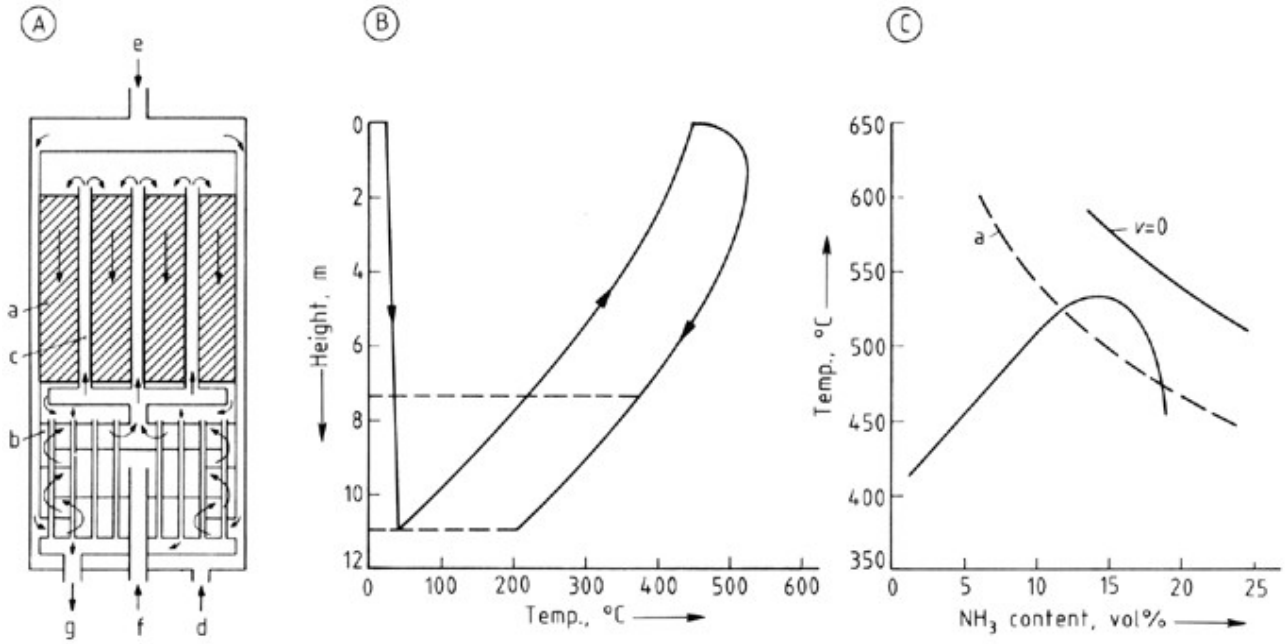

Figure 6: Counter-current tube-cooled converter (by Tennessee Valley Authority)(3)

Figure 6a shows an example of such reactor. The main flow enters in d, goes up through the heat exchanger (b) reaching around 200 °C and then is further heated inside the cooling tubes (c) to around 400 °C before being introduced into the catalytic bed (a). The flow entering in e is the vessel wall cooling gas that is mixed with the main flow in the reactor bottom. The flow entering in f is the main cooling stream. The gas temperature profile along the reactor is shown in figure 6b, while figure 6c shows the actual temperature profile against the ammonia content compared to the optimal profile (dotted line, a) and to the equilibrium temperature profile (v=0). It is a characteristic common to all the ammonia reactors that the gas enters at a temperature well below the optimal one, and then it increases due to the exothermicity of the reaction over the optimal value.

In the second and by far the most widespread type of reactors, the conversion takes place in adiabatic inter-cooled catalytic beds. In this configuration, the gas can be cooled down between two beds placed in series in two ways: either with a cold feed gas injection (named "cold shot") or with an indirect cooling, usually using boiling water. In the first cooling case, the converters are known as quench converters, whereas in the second as indirectly cooled multi-bed converters.

In quench converters only a fraction of the feed gas enters the first bed with a temperature around 400 °C. The catalyst volume is chosen so that the outlet temperature in each bed is around 500°C, which is limited

by the maximum temperature that catalyst can withstand (e.g. around 530 °C (3)). Before it enters the second stage, the gas is “quenched” by injection of cool feed gas (at 125-200°C). The same applies to subsequent beds. In this way the gas temperature follows a zig-zag path around the maximum reaction rate path, as shown in figure 7c.

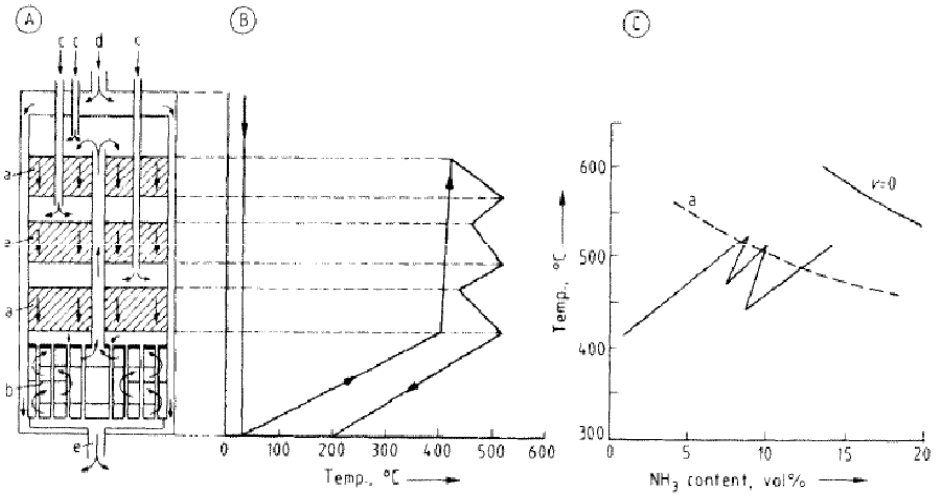

Figure 7: Multi-bed converter with quench cooling (3)

The most important disadvantage of this configuration is that not all the feed gas passes over the entire catalyst volume leading to the formation of a considerable amount of ammonia in the last beds, where the ammonia content is already high and therefore the reaction rate low. Consequently, a higher catalyst volume is required, compared to the tube-cooled converters seen above. The advantage is that no extra space is required for inter-bed heat exchangers.

Even if quench converters have seen a great success in the 60’s and 70’s for their mechanical simplicity and good temperature control, in the very last decades they are rapidly losing ground in favour of indirectly cooled converters. In these converters the heat exchanger between two consecutive beds is usually installed inside the pressure vessel (as depicted in Figure 8). However, an interesting alternative, especially for large plants, is to accommodate the beds in several vessels with an indirect cooling in between (3) (as shown in Figure 9). Note that the temperature profile shown in figure 8 is improved compared to the previous case.

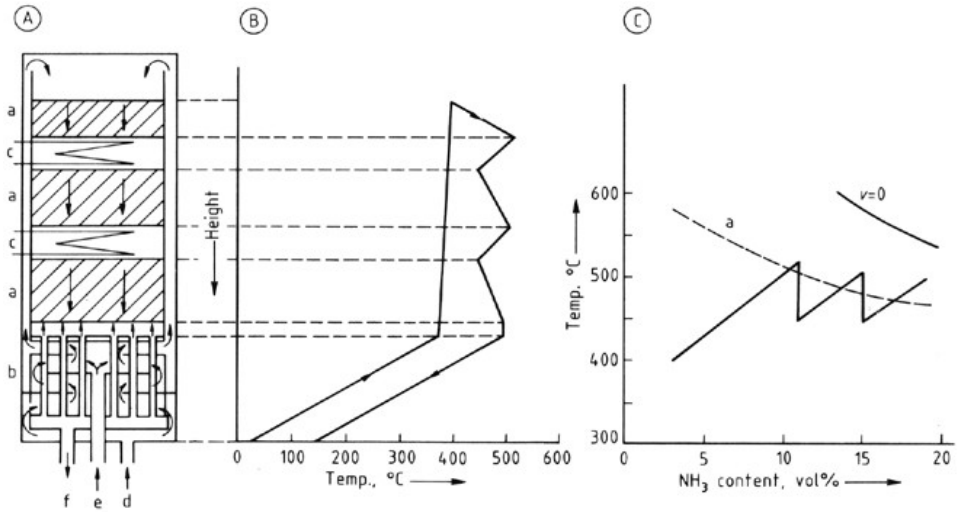

Figure 8: Multi-bed converter with indirect cooling(3)

With this concept it is possible to recover the reaction heat producing high-pressure steam (usually in the range 95-125 bar, which corresponds to temperature over 300°C, as shown in figure 9) and to reduce the equipment volume.

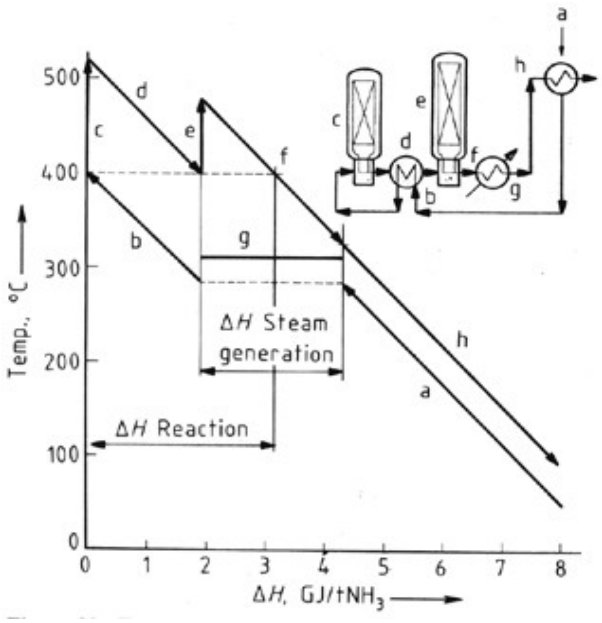

Figure 9: temperature-enthalpy diagram for a two-bed system with steam generation(3)

Another important feature to note is the direction of the reacting gas along the bed. In axial flow converters (such as those shown in figures 6-7-8), since it is not possible to increase the bed diameter above a certain limit, it is necessary to increase the bed height to rise the NH_3 production capacity. To limit the pressure drops it is hence necessary to use bigger catalyst particles, which have a lower activity. For this reason, big capacity converters nowadays are designed with radial-flow (see figure 10). In this way it is possible to design big converters with relatively small pressure drops. A successful axial-radial flow pattern has been developed and commercialized by Ammonia Casale (now Casale, see figure 11).

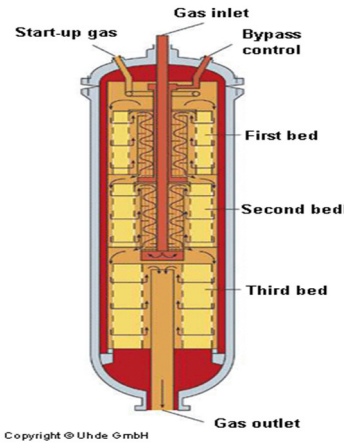

Figure 10: Radial-flow quench converter by Uhde.

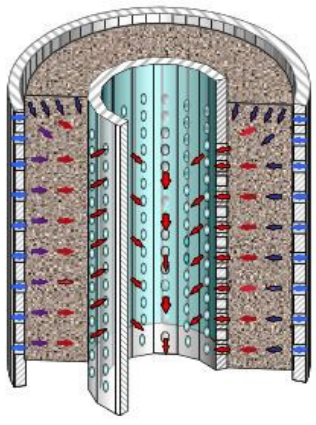

Figure 11: axial-radial flow converter by Ammonia Casale

The severe conditions of high pressure, high temperature and high hydrogen partial pressure place strict requirements on the design and construction material of converters in order to reduce the hydrogen attack (hydrogen has a very high diffusivity coefficient and tends to bond with carbon forming methane, which can then produce "pockets" in the steel), nitriding (caused by ammonia reaction with the steel surface) and stress corrosion cracking (7). Almost all converters consist of an outer pressure vessel containing a separate inner vessel, cooling synthesis feed gas flows between the two, allowing the use of cheaper materials for low-temperature external vessel (typically low-alloyed chromium-molybdenum steels). The most critical components, such as the internal "baskets", are constructed with stainless anti-corrosion steel (often Incoloy(7)).

Finally, typically operating conditions for modern synthesis loops at 220 and 140 bar are reported below (3). Consider that at 200 bar, 450 °C (which are typical outlet conditions) and 10% inerts at inlet, the ammonia content at equilibrium is around 22,2%, while the actual content doesn't exceed 20,5%. The reactants conversion per pass is in the range 25-35% (with an upward trend in most recent plants), for this reason it is mandatory, once the ammonia has been condensed and collected, to recycle such reactants. We will see the whole ammonia loop in chapter 2.1.2.

Parameters	Inlet pressure, bar	
	140	220
Inlet flow, Nm^3/h	500 000	407 000
Inlet NH_3 conc., mol %	4.1	3.8
Outlet NH_3 conc., mol %	17.1	19.9
Inlet inert conc., mol %	8.0	12.0
NH_3 separator temperature, °C	–5	–5
Relative catalyst volume	1	0.6

Figure 12: typical ammonia loop conditions

2.2) Modern ammonia production plants

The scope of this section is describing the most widespread process for producing ammonia, the steam reforming of natural gas. The process can be divided into two main sections. The aim of the first section is to obtain a syngas with the best possible composition to be introduced in the subsequent ammonia synthesis loop section. In the second phase the ammonia synthesis takes place. Although the complete process scheme of an ammonia production plant will be proposed and analysed in chapter 3, the main steps of the process are discussed in this chapter.

2.2.1) Syngas production

Based on the stoichiometry of the ammonia production reaction (1), a synthesis gas with a hydrogen/nitrogen ratio of 3 should be introduced in the synthesis reactor. It is clear from the outset that the chemical process used for producing this syngas is decisive for the efficiency and the sustainability of the whole plant. The most widespread technology for ammonia production is based on the steam reforming of natural gas according to the block diagram illustrated in the figure 13 below, which is explained in detail in the following sections.

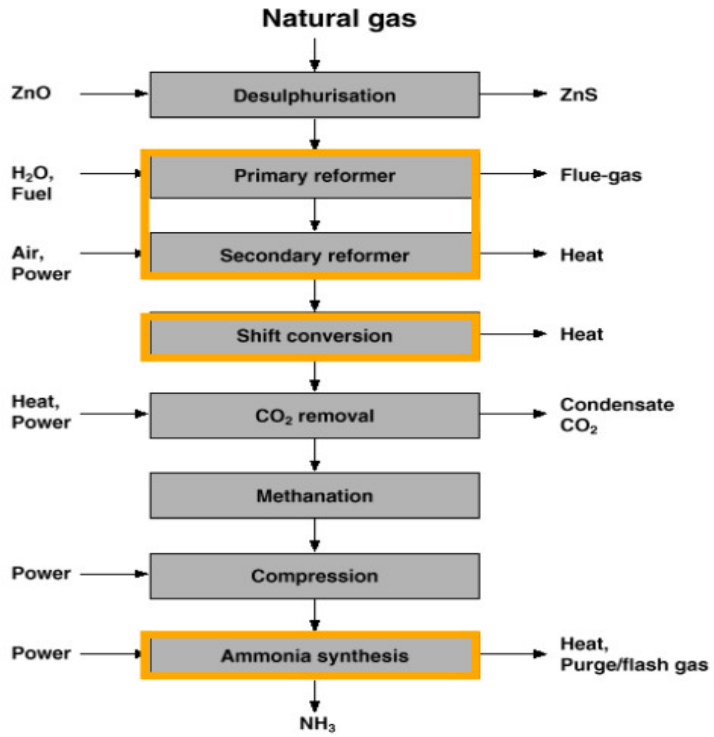

Figure 13: flow diagram of ammonia production through natural gas reforming (5)

2.2.1.1) Feedstock pre-treatment

In the first stage of the process, the desulphurization of natural gas takes place. Sulphur compounds present in the natural gas feed are poisonous for the catalysts employed in reforming, water-gas shift and ammonia synthesis reactors (see below), and should be therefore removed before entering into these reaction stages. There are several techniques for carrying out the desulphurisation of the natural gas. Adsorption on activated carbon or on molecular sieves can be employed for natural gas feedstocks with a low sulphur concentration. Nevertheless, the most common system for desulphurization consists of a non-regenerative two-stage high-temperature process. Natural gas is first mixed with hydrogen (to obtain a hydrogen concentration of around

2%) and heated to 350-400 °C to be fed to a first hydrogenation stage, where the organic sulphur compounds react with hydrogen to obtain hydrogen sulphide (H_2S) on a cobalt-molybdenum catalytic bed. Afterwards, formed H2S is irreversibly adsorbed on a second zinc oxide (ZnO) bed to form water and zinc sulphide (ZnS), which is separated in solid state. Since the amount of sulphur compounds to be removed is usually very low, this desulphurisation stage doesn't affect the energy balance of the system, and consequently the reactor outlet temperature and composition can be assumed equal to that of inlet. Using this desulphurisation process, the sulphur content in the natural gas can be reduced to less than 0.01 ppm (12).

Before being introduced in the primary reforming reactor, the feedstock, in some new plants, can undergo a pre-reforming stage. The aim of this stage is to break down the hydrocarbons heavier than methane (C_2+) present in natural gas into CO and H2, through the following steam reforming reaction:

$\mathbf{C_mH_n} + m\mathbf{H_2O} \leftrightarrow m\mathbf{CO} + (n/2+m)\mathbf{H_2}$

At the high reforming temperatures, heavy hydrocarbons are prone to decompose into solid carbon through thermal cracking. Carbon formed may deposit on the catalyst surface, leading to catalyst deactivation, and on pipes' surfaces, through a mechanism typically known as fouling. Carbon deposit on pipes' surface results in a lower convection coefficient on the inner tubes side (due to the added conduction heat resistance) that would lead to a superheating of pipes, which can be consequently damaged, and to an even faster deposition in a feedback loop. A preliminary pre-reforming stage of the natural gas would therefore avoid all these effects.

Before the pre-reforming stage, the feedstock is mixed with steam (usually drawn from the steam turbine) and heated to around 490-530 °C (3) before being sent to the pre-reformer. In the outlet stream the concentration of C_2+ hydrocarbons is usually very low (ppm). Since the reforming reaction is endothermic (the syngas exits in equilibrium with steam reforming and water-gas shift, see next chapter), the outlet temperature is lowered by 30-80 °C, depending on the concentration of heavy hydrocarbons.

The use of a pre-reforming stage allows the steam to carbon ratio to be reduced, to reduce the charge of fired tubular reformer, to extend the life of FTR catalysts and pipes and to process heavier feedstocks. Besides, through pre-reforming, some middle-temperature heat is converted into syngas chemical energy, reducing the amount of fuel to be spent.

2.2.1.2) Steam reforming

The natural gas steam reforming process is the most widespread way to produce hydrogen. Considering that methane is the main constituent of natural gas, main reactions occurring in the steam reforming process (steam reforming and water gas shift reactions) can be written as follows. :

$CH_4 + H_2O \leftrightarrow CO + 3H_2$ (ΔH_r° = 206 kj/mol,CH_4) steam reforming (SR) (2)

$CO + H_2O \leftrightarrow H_2 + CO_2$ (ΔH_r° = -41 kj/mol,CO) water-gas shift (WGS) (3)

The SR reaction is strongly endothermic, which means that a source of heat (internal or external) is necessary to sustain the reaction and that its equilibrium constant (and so the methane conversion) increases with temperature. Consequently, from a thermodynamic point of view, the SR has to be performed at the highest possible temperature for maximising methane conversion. However, maximum temperature is determined by the materials' reactor resistance as well as the catalyst performance.

The SR reaction implies doubling the molar flow, and so an increase in volumetric flow. According to Le Chatelier's principle, an increase in the operative pressure leads to a shift in the equilibrium position towards the species which occupy the smaller volume. Then, the SR reaction should be performed at a low pressure in order to maximise the methane conversion. Typical values for the pressure of the steam reformer fall down in the range of 25-40 bar. The reasons for such a high value of operating pressure are economic ones, since the plant components have to be as compact as possible to reduce their cost and the products are usually needed at a high pressure. Moreover, methane is often available at high pressure from the grid and, due to the stoichiometry of the reaction, syngas compression is more energy demanding than compressing reactants.

The ratio between carbon monoxide and dioxide in the outlet stream is itself affected by the temperature. Since the WGS reaction is exothermic the CO/CO2 ratio increases as temperature increases.

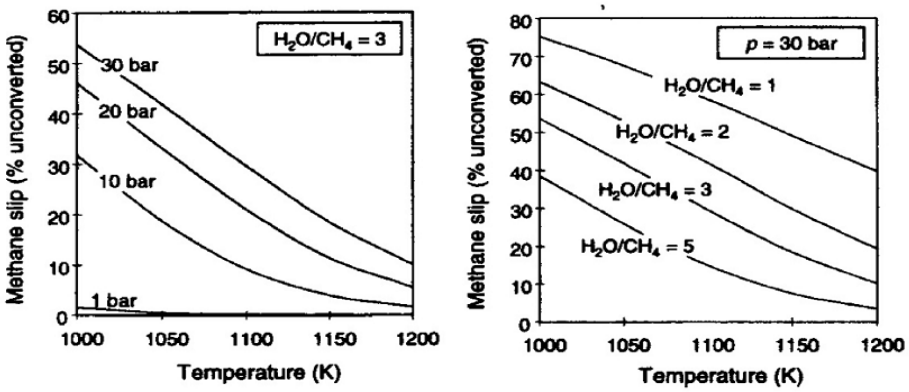

Figure 14: methane slip as a function of pressure, temperature and steam to carbon ratio(6)

The steam reforming process is globally endothermic (the heat released by the WGS is too low to balance that absorbed by the SR), and it is hence necessary to furnish the required heat somehow. This can be done in two main ways. The first way is to furnish it from outside the reforming reactor. In most of the hydrogen production plants the reforming process takes place inside of thin and long pipes (usually 7-13 cm diameter and 7-12 m length(6)), arranged inside a furnace where additional natural gas is burnt with air. The heat is therefore primarily exchanged through radiation. Those plants are known as fired tubular reformers (FTR). In this case the outlet temperature of the reformed stream is around 890-910°C which corresponds to a pipes outer wall temperature around 950 °C (6). Otherwise the heat can be supplied within the reforming reactor such as in auto-thermal reformers (ATR). In this case, air is fed to the reactor together with natural gas and vapour (usually the oxygen to methane ratio is around 0,6 (6)). Two reaction zones can be distinguished: in the first one, the combustion reactions dominate, releasing the heat necessary to sustain the reforming process, which takes place in the second catalytic zone. In this way the reactor is simpler and cheaper than in the FTR plants, and higher temperatures are permitted since there is no pipes wall temperature to be controlled, allowing a reduced methane slip to be achieved. The outlet temperature is usually in the range 950-1100 °C. As some water is produced through combustion, the steam to carbon ration can be reduced to 1-2 (where the values for FTR are in the range 2,5-4,5), with benefits for the plant energy efficiency. In both cases a Nickel-based catalyst is usually employed, made up of 15-25% of NiO on an aluminium oxide, calcium nitrate or magnesium aluminium spinel support (3). However, ATR reactors do have a disadvantage that makes them inconvenient towards FTR in conventional size hydrogen plants. If oxygen is supplied with air, nitrogen behaves like an inert, absorbing the heat of reaction and making necessary a larger amount of natural gas to be oxidised for fulfilling the energy balance. Moreover, in this case, hydrogen obtained is

diluted with nitrogen coming from air, requiring the subsequent separation of nitrogen from hydrogen when it is needed in its pure form. For these reasons in ATR plants for hydrogen production, oxygen is usually supplied almost pure (e.g. with O2 purities around 95-97%) from an air separation unit (ASU), which is itself an expensive, heavily affected by economy of scale and energy-demanding system (the primary energy required is around 0,6 kWh/Nm^3,O_2). The need of this ASU, when focused on hydrogen production, makes ATR plants more economically convenient when moving for large hydrogen production scales.

When focussing on ammonia production, an ATR-based syngas production system seems suitable since in this case the presence of nitrogen in the syngas is needed for the ammonia production process (a hydrogen/nitrogen ratio of 3 at the synthesis reactor inlet is needed). However, if the whole reforming process took place inside the ATR (supplied with air), in order to achieve the outlet temperature requested to reduce the methane slip to a reasonable level, say 1000 °C, a quantity of nitrogen far greater than the requested would be supplied, leading to the disadvantages explained above. For this reason, the reforming reaction has to be split into two sections. The first phase takes place inside a FTR reactor (primary reformer), where a partial conversion of methane is (intentionally) obtained, and afterwards the products are then sent to an ATR unit (secondary reformer). The conversion of methane in the first phase has to be determined so that the amount of nitrogen required to obtain the H_2/N_2 molar ratio at the ammonia synthesis reactor corresponds to the amount of air required to close the energy balance at ATR (that is an outlet temperature around 1000 °C which corresponds to a residual methane content lower than 0,5% on dry basis (3) and a methane slip around 1,25%). Usually the methane conversion in the first stage is in the range of 55-65 %. Since the methane conversion in FTR is limited, the outlet temperature can be itself limited (to around 780-820 °C), reducing the heating duty on FTR (which is energetically less efficient than ATR) and the piping thermal stress. For the same reason, even the FTR designing should be, at least theoretically, different from those used for the production of hydrogen. In this case, actually, it is not necessary to give the reactants the time (namely the space) to reach chemical equilibrium. The outlet temperature and the tube length (once established the superficial velocity) are both designing parameters. For a given methane conversion, decreasing the FTR outlet temperature results in a strong reduction of its heating duty and so in a strong increase of that of ATR, not only because of the reduction of the sensible heat of the reformed stream but also for the reduction of its chemical energy, due to the exothermicity of the WGS reaction. The other designing parameter is the process air temperature, which is usually varied in the range 520-610 °C to adjust the ATR outlet temperature. The steam to carbon ratio employed is in the range 2,8-3,5(3), with a trend towards the lower bound in the most modern plants. The optimum pressure value is around 30-35 bar. Once set the ammonia synthesis pressure (in the range of 150-250 bar as we will see later on), reducing the syngas production pressure results in a reduction in unconverted methane but in an increase in the compression energy costs.

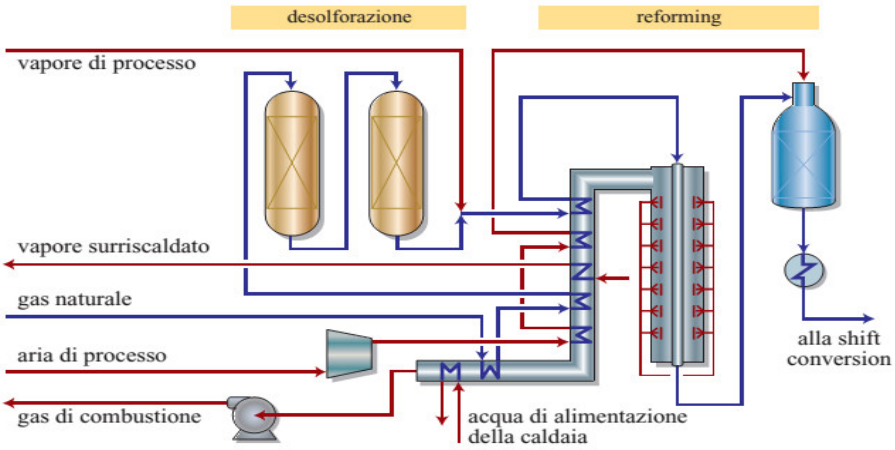

Figure 15: scheme of primary and secondary reforming sections (7)

2.2.1.3) Water-gas shift

The syngas obtained from ATR contains a substantial amount of carbon monoxide (in the range of 13-14% on a dry basis). This compound has to be converted into further H_2 and CO_2 through the WGS reaction for two reasons. On the one hand, CO has a high heating value, which can be exploited to produce further hydrogen that will be ultimately converted into ammonia. On the other hand, iron based catalyst employed in the ammonia synthesis reactor is poisoned by almost all oxygen compounds, going from CO to CO_2 or H_2O. Whereas it is quite easy to separate CO_2 from syngas, for example using a MDEA process, the same doesn't apply to CO (7).

Since the WGS is slightly exothermic the CO conversion into CO_2 and H_2 is favoured at low temperatures. When looking for high CO conversions, it is common to place two (or more) WGS adiabatic stages working at different temperatures with an intermediate cooling stage between them. High temperature heat recovered from the intermediate cooling can be exploited for producing high pressure steam, which will improve the system efficiency.

The syngas enters the first WGS stage at a temperature around 330-360 °C and exits at 410-440 °C, while the CO content slips from 12-16% to 3-3,5% (dry basis). The catalyst employed in this stage is typically iron-based, with the addition of chromium (up to 10% by weight) as a structural stabiliser, and of a little amount of copper (1-2%) as a chemical promoter (7). Such catalyst is active in the range 300-500 °C (3). Afterwards, syngas is cooled to 200-210 °C before entering in the second WGS stage. This temperature is dictated by the syngas dew-point temperature and by the catalyst activity (7). At LT-WGS reactor outlet the syngas has a temperature of 225-235 °C and a CO content of 0,1-0,3%. The catalyst employed in this stage is made up of a mixture of copper oxide (CuO) (by 40-60%) and zinc oxide (ZnO) (by 20-30%) supported over alumina (Al_2O_3) (3), which acts as a structural stabiliser.

2.2.1.4) Syngas purification

Syngas exiting the second WGS section contains around 18% of CO_2 (dry basis), a small amount of CO and a great amount of H_2O. As already mentioned, these compounds are poisonous for the ammonia synthesis catalyst and therefore their concentration must be reduced to ppm.

Water is typically removed by condensation, as shown in a next chapter.

The classical method for CO_2 removal is based on scrubbing the syngas under pressure with a solvent capable of solving carbon dioxide in a column equipped with trays or packings. Both chemical and physical solvents can be used, depending on the CO2 partial pressure in the gas phase. In the case of interest, the CO_2 pressure is in the range of 4-7 bar, which makes chemical solvents (e.g. alkanolamines) usually the preferred option. Primary and secondary amines, such as MEA or DEA, exhibit a high mass-transfer rate but have an high energy consumptions during regeneration (3). For this reason, tertiary amines (e.g. MDEA) are commonly used today. In this case, the CO_2-laden solvent is flashed, usually in steps, to around atmospheric pressure, and the spent scrubbing liquid is heated and regenerated in a stripping column, before being recycled in the scrubbing column The heat requirement for amine regeneration in this case is strongly dependent on the process employed. For example the one-stage MDEA process developed by BASF requires 73kj per mole of CO_2 captured, while the up-to-date two-stage MDEA process (again by BASF) requires just 28-30kj (3).

Alternatively to absorption with amines, physical solvents represent also a feasible option for CO2 removal (e.g. Selexol process). However, they have the disadvantage of a high capacity for adsorbing water, making necessary the previous cooling of gas to around 5 °C to separate the water. Besides, adsorption is favoured at cryogenic temperatures, leading to a high cooling cost.

Concerning the MDEA process, the heat needed in the reboiler of the stripping column is supplied by low-temperature (125-130 °C) vapour condensation, in order to reduce the volume of the equipment. The CO_2 removal efficiency reached in ammonia plants is in the range 98-99,9% (3,7). Usually the low-pressure steam is generated downstream the LT-WGS reactor, cooling the syngas to around 140-150°C. The syngas is then further cooled to around 35 °C in order to condensate the water (which is collected before the MDEA process) and to reach the optimal conditions for the absorption column. The syngas exiting the MDEA process has a CO_2 and CO contents of 0,01-0,3% and 0,2-0,5% (dry basis) respectively, which are still too high for the tolerance of the catalyst used in the synthesis reactor.

The most common and cheap way to remove the remaining carbon compounds is through “methanation”. The gas exiting the CO_2 removal stage is heated up to 260-290 °C (usually using the gas exiting the methanator itself) to be sent to the adiabatic methanation reactor in the presence of a Nickel-based catalyst. At these low temperatures the equilibrium constant of the SR reaction is quite low, so that the reaction proceeds backward, producing CH4 and consuming CO. The consumption of CO through the methanation reaction pushes the reverse WGS reaction (e.g. CO_2 conversion into CO). Despite some hydrogen is reconverted into water and some more inerts (CH_4) are produced, the low outlet carbon oxides concentration (below 10 ppm) makes this stage advantageous. The higher is the CO_2 removal section efficiency, the lower is the hydrogen loss and the methane production. Since the process is globally exothermic, some attention has to be paid to the outlet temperature. Usually the temperature rise is around 50-70 °C, but if a CO_2 slip from the CO_2 removal system occurs, the outlet temperature can quickly exceed 500 °C.

Both the removal of CO_2 and the methanation process entail the increase of water partial pressure in the hydrogen rich gas. Consequently, the gas is cooled again to 30-35°C, depending on the temperature of cooling water available, to condensate the H_2O present and separate it before entering into the ammonia synthesis reactor. The water content is reduced in this way to around 0,16-0,14%. The gas is now sent to the compression train of the synthesis loop.

2.2.2) Ammonia synthesis loop

In the compression train, the syngas is compressed from a pressure of around 25-30 bar up to 150-250 bar (over 300 bar in old plants; note that at these pressures the ideal gas hypothesis no longer stands). One of the most important features of the single-train plant pioneered by M. W. Kellogg in 1963 was the use of centrifugal compressors to compress the synthesis gas (and recycle) in the ammonia loop, as well as process air and refrigerant (in the refrigeration cycle). Since then, application of centrifugal compressors has become standard practice in almost all ammonia plants. In spite of the lower efficiency compared to reciprocating or axial compressors, these machines have also important advantages: a low investment cost (because of the higher compression ratio per stage compared to axial compressors and because single machines have been developed even for large capacities), low maintenance costs, less frequent shutdowns for preventive maintenance, high reliability and small space requirement (3). As mentioned above, in most cases they are

directly driven by the steam turbine (fed with heat recovery system steam), avoiding the losses associated with conversion and transmission of electrical power. The maximum wheel tip speed is limited to around 330 m/s by the tensile strength of the steels used. This means that a pressure increase from 25 to 200 bar would require 18-20 impellers. However, a compressor shaft can accommodate no more than 8-9 impellers, in order to avoid excessive vibrations. It is therefore necessary to accommodate several compressor casings in series (usually 3, or 2 in low-pressure ammonia loop plants), with a compression ratio of 1,8-3,2 each (3). Since it is necessary to recompress the recycle gas before sending it into the converter, because of the pressure drops, the shaft of the final casing also bears the impeller for the compression of the recycle gas (3). The feedstock is cooled down to 40-50 °C, depending on the temperature of the cooling water available, before the second and, if present, the third compressor, reducing the compression power consumption. In this way is also possible to condense and collect some of the residual water, which can then be almost totally removed by an adsorption system.

The ammonia loop can be performed in three main ways, sketched in figure 16.

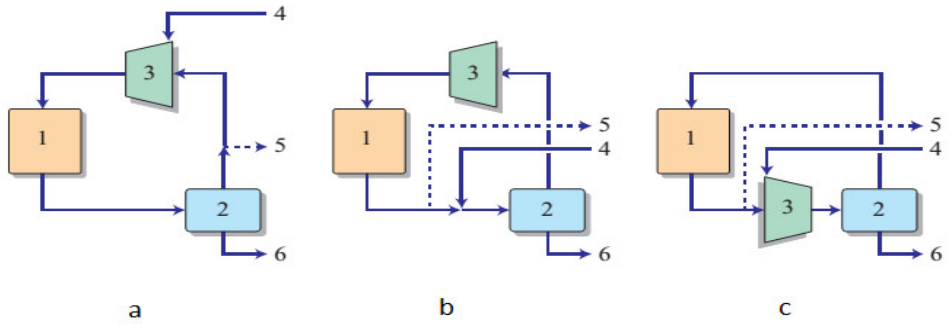

Figures 16a-b-c: three main ammonia loop concepts. Where 1 is the ammonia converter, 2 is the ammonia separator, 3 is the recycle compressor, 4 is the fresh feed, 5 is the purge, 6 is the liquid ammonia(7)

In any case, it can be noted that a purge stream is necessary, in order to keep a constant inert content (CH_4 and Ar) at the converter inlet (usually around 7-12%). The purge ratio (defined as the ratio between the purge flow and the purge split inlet flow) is an important parameter, which has to be optimized. On the one hand, increasing the purge ratio leads to a reduction both in the flow entering the reactor and in its inerts content, allowing a reduction of the equipment (and catalyst) volume and an increase in ammonia content at the converter outlet. On the other hand, more reactants are thrown out, leading to a loss of ammonia production efficiency. Anyway, the purge ratio is very small (1-1,6% as order of magnitude), which means that the great majority of the flow entering the converter comes from the recycle (the recycle mass flow is usually three-fold or more the fresh gas mass flow).

In the scheme in figure 16a both the purge split and the fresh syngas inlet are placed downstream the ammonia separator. This is the most efficient scheme because the ammonia is collected before being diluted with the fresh gas, and so at its highest partial pressure, whereas the purge is pulled out at the lowest ammonia content. In this way the ammonia content at the synthesis reactor inlet is the lowest possible. Moreover, the gas flow to be compressed is the lowest, since the ammonia has already been removed. However, the main disadvantage of this scheme is that all the impurities present in the fresh gas are directly introduced in the synthesis reactor. Therefore, in case this ammonia loop scheme is used, it is necessary removing efficiently any impurity present in the syngas before the ammonia synthesis process as well as using lubricant-less compressors (such as centrifugal ones (7)), in order to avoid the presence of lubricant on the catalyst. Otherwise, if the impurities content in the feed gas could be harmful for the catalyst, the feed can be introduced upstream the ammonia separator (figures 16b-16c), so that the impurities can be absorbed

and removed by condensing ammonia. Scheme in figure 16b has the advantage of a lower mass flow to be compressed compared to that in figure 16c, since the ammonia has already been drained at the compressor inlet. On the other hand, the compressor in scheme 16b has to be designed so to avoid the mixing between the fresh gas and the recycle (in fact, scheme in figure 16b is referred to as “4 nozzles scheme” while that in figure 16c as “3 nozzles scheme”).

The ammonia is removed by condensation, which is favoured by the high pressure of the loop. It is hence necessary to cool the ammonia-rich gas as much as possible, in order to reduce to a minimum the ammonia content in the recycle. The cooling is performed in a series of heat exchangers, in order to exploit the temperature levels available in the most efficient way. Usually, in modern plants, after the ammonia-laden gas has been cooled down with recycle gas and, then, with cold water, to around 30-45 °C (depending on the temperature of the water available), it is further cooled down with a refrigeration cycle to around -25°C (3,7). Compression cycle with ammonia as refrigerant fluid is usually employed, with one or more temperature levels. The refrigeration energy cost is significant because of the high compression ratio (usually the ammonia in the cycle evaporates at around -30 °C or less, and condenses at 35 °C at least, corresponding respectively to a pressure of 1,1 and 17 bar) and the relatively high mass flow to be cooled (since the ammonia content in this stream is relatively low, as a consequence of the low conversion per pass). It is therefore very important to design the synthesis loop and the refrigeration cycle with the aim to reduce such cost. The liquid ammonia obtained is flashed to around 20 bar in a let-down vessel to release the dissolved gases. Such gases are usually scrubbed to remove evaporated ammonia and then used as fuel in the primary reformer.

The low-temperature purge (stream 5 of fig. 16) is scrubbed with water to remove the ammonia (which is highly miscible in water) at around 135-145 bar (3), reducing the ammonia content to less than 200 ppm. This step is necessary in order to limit the NO_x formation, since the purge is used as fuel in the fired tubular reformer combustion chamber. Usually the scrub system is composed of two scrubbers, one at low pressure in which the low-pressure desorbed gases are washed, and one at high pressure for washing the purge. The laden water is regenerated in a stripper, from which the gaseous ammonia is separated from water (10). Since the purge flow is very low and its ammonia content is relatively low as well, the energy regeneration cost is negligible.

Since the purge gas contains mostly hydrogen, it can be advantageous to recover and recycle it. There are three main ways to do it. When cryogenic units are employed, after the scrub, ammonia is completely removed by molecular sieve adsorbers, the dry ammonia-free gas is sent into the cold box, where it is cooled down to around -188 °C(3), partially liquefying methane and argon (and some nitrogen). The liquid inert-rich phase is flashed and the resulting gas is used to cool the inlet gas and then sent into the combustion chamber. The gas phase contains mainly hydrogen. The hydrogen recovery efficiency for cryogenic units is around 90-95% (25% for nitrogen, 25% for argon and 4% for methane(7)). An interesting alternative is the membrane separation (for instance Monsanto’s Prism), exploiting selective gas permeation through membranes to separate them. In this case there is no necessity for an advanced dryer and ammonia-removal system. Since the rate of permeation decreases along the separation bank, due to the decrease in hydrogen partial pressure, usually two separators operate in series, the second one with a lower pressure on the sweep side. In this way two streams of permeated hydrogen are obtain, the first up to 70 bar, the second around 25-28 bar (3). The overall hydrogen recovery is around 90-95% with a high purity. The third and probably the most widespread way to recover the hydrogen is the “pressure swing adsorption” (PSA). The process was initially developed by Union Carbide, under the name HYSIV, and then marketed by Honeywell UOP, under the name Polybed PSA (3). Currently it is commercialized by several companies. This process exploits the different adsorption capability of solid beds (usually zeolites) for different gases: the hydrogen crosses the bed uncaptured while other gases remains trapped in the solid pores. The bed is then regenerated reducing the

pressure. In this way a high-pressure (up to 60 bar) hydrogen stream and a low-pressure purge gas stream are obtained. The hydrogen recovery efficiency can reach 90%, with final H_2 purities higher than 99.999% (7).

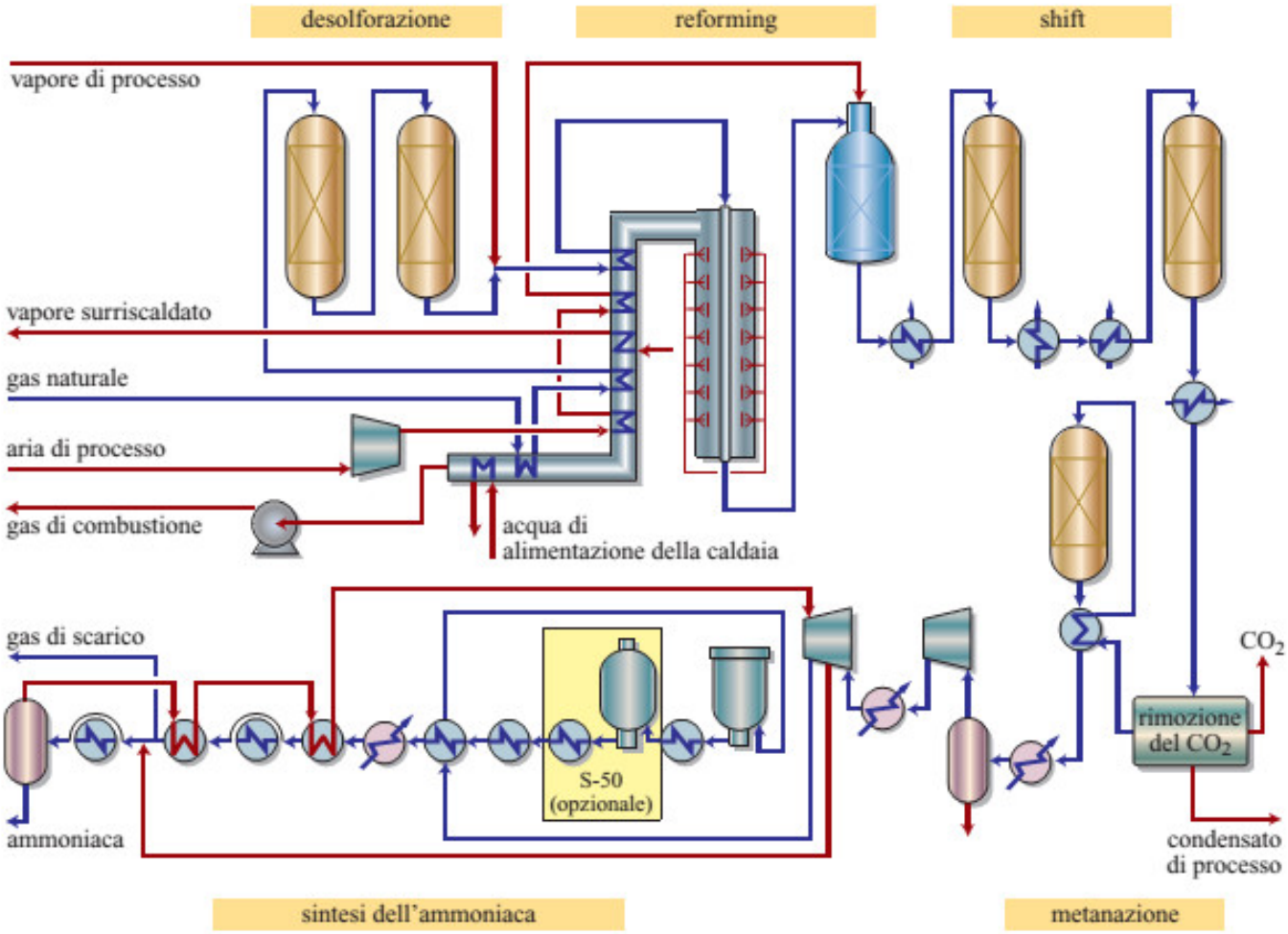

Figure 17: process scheme of an ammonia production plant by Haldor Topsoe(7)

2.2.3) Performances and improvements

Typically, for evaluating the performance of an ammonia production plant, the key parameter is the primary energy consumption (in GJ) required to produce one ton of ammonia. If there is an electric energy or vapour export/import into the ammonia production plant, it can be taken into account in this energy consumption by adding or subtracting the primary energy related to their production. It has to be noted that the parameter itself is prone to a certain ambiguity, since it is affected, for example, by the ammonia phase (the delivery of 3 bar ammonia vapour allows a reduction of 0,6 GJ/t compared to liquid ammonia at ambient temperature, while delivery as liquid at -33 °C would need an extra 0,3 GJ/t(3)). Anyway, ammonia is usually delivered liquid at ambient temperature at 17-20 bar, so this is probably the most logical reference conditions to be used for performance comparison. There are also external factors affecting the performance, the most

important one is probably the temperature of the available cooling water: an increase from 20 to 30 °C entails an increase of around 0,7 GJ/t in energy consumption(3). Also the natural gas composition plays a role.

It is possible to evaluate the theoretical minimum energy consumption referring to the ammonia synthesis reaction from methane, air and vapour:

$CH_4 + 0{,}3035\ O_2 + 1{,}131\ N_2 + 1{,}393\ H_2O \leftrightarrow CO_2 + 2{,}262\ NH_3$ ($\Delta H_r° = -86$ kJ/mol)

As can be seen, from 1 kilomole of methane (corresponding to 0,8 Gj of primary energy), 2,262 kilomoles (or 38,454 kg) of ammonia are obtained, which means that the theoretical consumption is 20,9 GJ/t. In the figure below the performance of actual ammonia production plants are shown. The current reference value is around 28 GJ/t (but technology would be available to reach 27 GJ/t (3)). As can be noted, great improvements have been achieved from the dawn of the technology to the present day.

	GJ/t NH_3 (LHV)	% theory
Classical Haber – Bosch (coke)	80 – 90	(338 – 431)
Reforming, 0.5 – 10 bar (1953 – 55)	47 – 53	225 – 254
Reforming, 30 – 35 bar (1965 – 75)	33 – 45	139 – 215
Low energy concepts (1975 – 84)	29 – 33	139 – 158
Modern concepts (since 1991)	< 28	134
Stoichiometric CH_4 demand	20.9	= 100

Figure 18: ammonia plants primary energy consumption throughout the years compared to the theoretical value(3)

Almost 70% of the exergy losses of the process occur in the reforming section (primary reforming particularly) and in the steam generation (3). From a first-law analysis it can be seen that almost all the losses are transferred to the cooling water, meaning that a great deal of low-temperature heat is produced. Therefore, the water heat integration system plays a remarkable role in the overall efficiency.

Finally, the carbon dioxide emissions minimum value, if the carbon dioxide captured by MDEA is stored, is around 0,35-0,38 t_{CO2}/t_{NH3} for the best available technology, corresponding to 76-78% of carbon capture ratio.

The main steps that have allowed the improvement of the ammonia production technology mentioned above are briefly listed below.

- The desulphurization of natural gas, initially performed through adsorption on active carbons, has been replaced by catalytic hydrogenation followed by absorption on ZnO pellets (see chapter 2.1.1.1).
- Reforming section: reduction of the flue gas temperature, combustion air and fuel preheating, increased operative pressure, lowering of the steam to carbon ratio, installing a pre-reformer unit, and, above all, shifting some reformer duty from primary to secondary reformer(3).

- Shift conversion: improved LT-WGS catalysts allow a lower operative temperature and so a lower CO content, while a new generation of HT-WGS catalysts, less prone to low-steam to carbon deactivation and hydrocarbon formation, allow lower S/C ratio to be used.
- Carbon dioxide removal: modern processes, as BASF aMDEA or Benfield LoHeat, allow a reduction in the regeneration energy duty.
- Ammonia synthesis section: improved converter design (with indirect cooling), larger catalyst volume, refrigeration cycle to condense the ammonia and hydrogen recovery systems.
- Turbomachinery: developments in compressors and turbines manufacturing.
- Heat recovery system: increase of pressure and superheating temperature of steam; inclusion of steam superheater downstream of the secondary reformer(3), despite the metal dusting issue, thanks to new and more expensive material.

3) Reference ammonia plant

In this chapter it is analysed in detail a modern natural gas-reforming ammonia plant, with the aim to evaluate its performance. Whereas several elements are typical of modern plants as pointed out in the previous chapter, many others are free design choices. Therefore, logically enough, the designers still play an important role in the plant efficiency. The main goal of this section is to design a plant representative of the best available technology. The production capacity of the plant considered is 1500 tons of ammonia per day.

3.1) Reference ammonia plant scheme

Before to give the complete plant scheme, which is quite complex due to the heat integration system, the process illustrated in detail in chapter 2 is summarized in the simplified figure below (fig. 1). After desulphurization, the charge is mixed with steam (drawn from the turbine) to achieve a steam to carbon ratio of 3 and fed into an adiabatic pre-reformer. After being heated to 620 °C (with the FTR flue-gas), the charge is sent into the fired tubular reformer (FTR). Its exit temperature is set to 820 °C (corresponding to a methane conversion of 57,9%. The next step is the auto-thermal reformer (ATR), in which an air flow is fed so to reach a H_2/N_2 ratio of three at the ammonia reactor inlet. The ATR air inlet temperature is chosen so to reach the target outlet temperature (in this case the former is 538 °C and the latter is 1000 °C). Then, the syngas is purified. After being cooled down, it undergoes two water-gas shift stages, reducing its CO content to 0,26% (dry basis). After cooling down to 35°C and removing the condensed water, the CO_2 is removed with a MDEA process, obtaining a CO_2 content of 0,3% (dry basis). Since the oxygen compounds content is still too high for the ammonia reactor catalyst, a methanation is introduced as last purification step. The syngas produced is sent to the ammonia loop compression train, in which it reaches 200 bar. After mixed with recycle flow and heating up to 320 °C, it is introduced into the ammonia reactor, from which it exits at 450°C with an ammonia content of 20%. After several cooling stages, the high-pressure liquid ammonia is collected and flashed to 20 bar to set free the dissolved gasses. The purge stream is scrubbed with water to remove the remaining ammonia then fed into a PSA to recover the hydrogen. The PSA flue-gas are used as fuel in the FTR.

The water/steam heat recovery system allows to produce 55,9 kg/s of steam at 510°C and 110 bar to feed the steam turbine. Of them, 26,7 kg/s are drawn from the steam turbine as process steam at 33 bar.

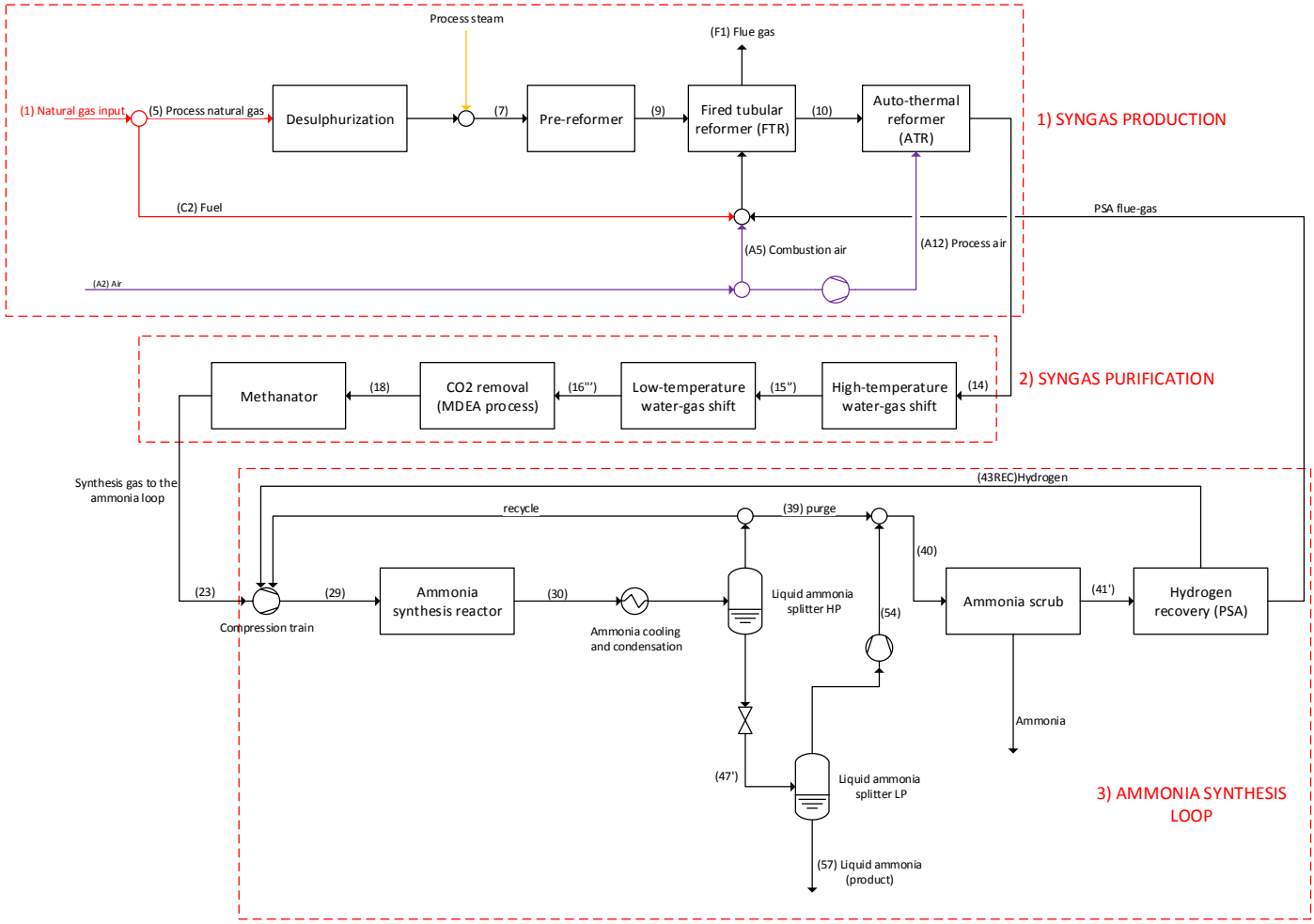

Figure 1: simplified scheme of the ammonia plant

Figure 2 shows the complete scheme. In this figure it possible to note the heat recovery section of the FTR flue-gas, the details of the ammonia loop (particularly the way the ammonia-rich flow is cooled down), the refrigeration cycle scheme (a two-pressure stage cycle has been chosen to improve its performance; see green lines) and the water/steam heat integration system. To make it as clear as possible, different colours are used depending on the flows (see colours legend). It is recommended to focus on “process” streams before, ignoring the water/steam streams (blue and orange lines), in this way the scheme should be easier to understand.

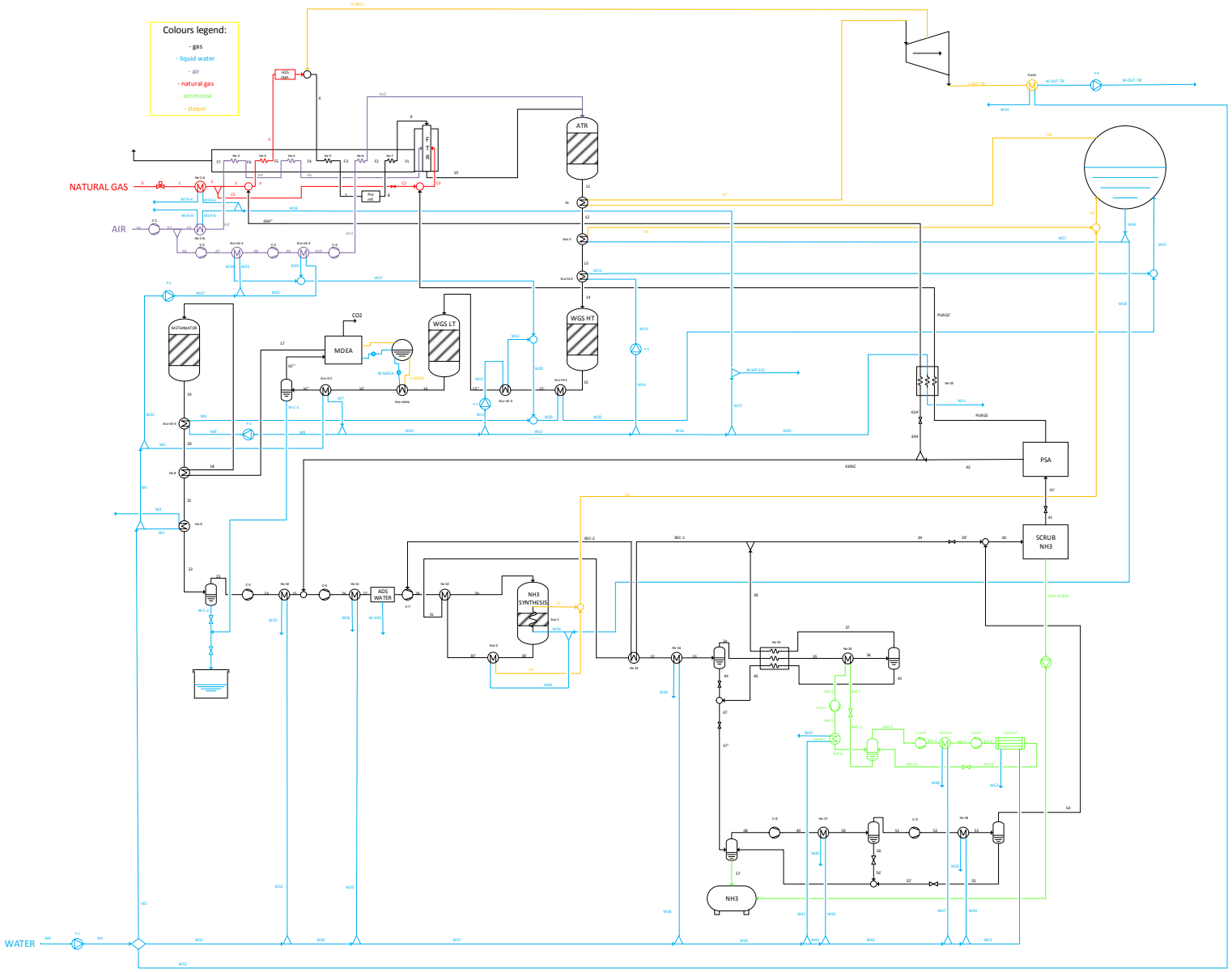

Figure 2: complete ammonia plant scheme

For the sake of clarity, Figures 3, 4 and 5 represent zoomed pictures of the complete process plant scheme depicted in Figure 2.

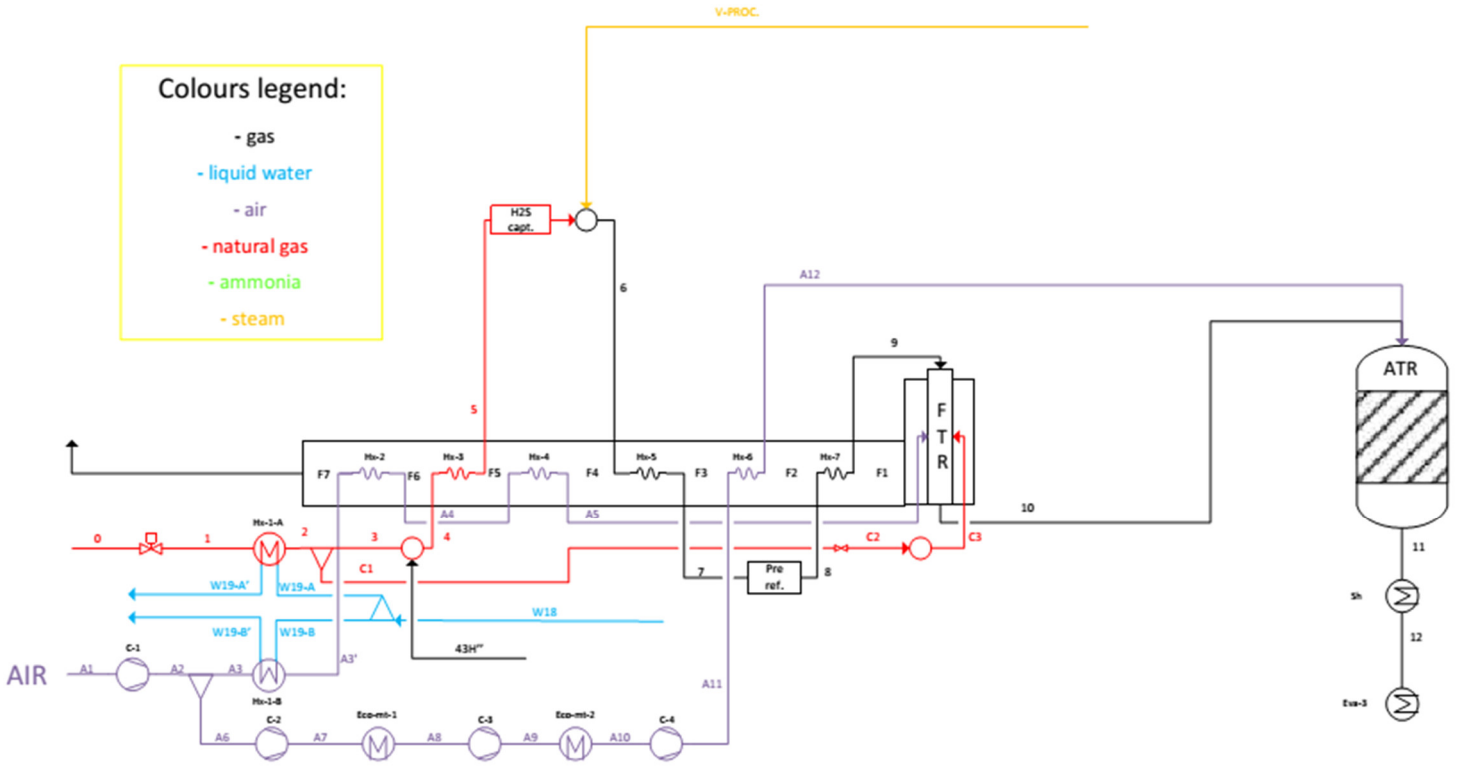

Figure 3: syngas production section

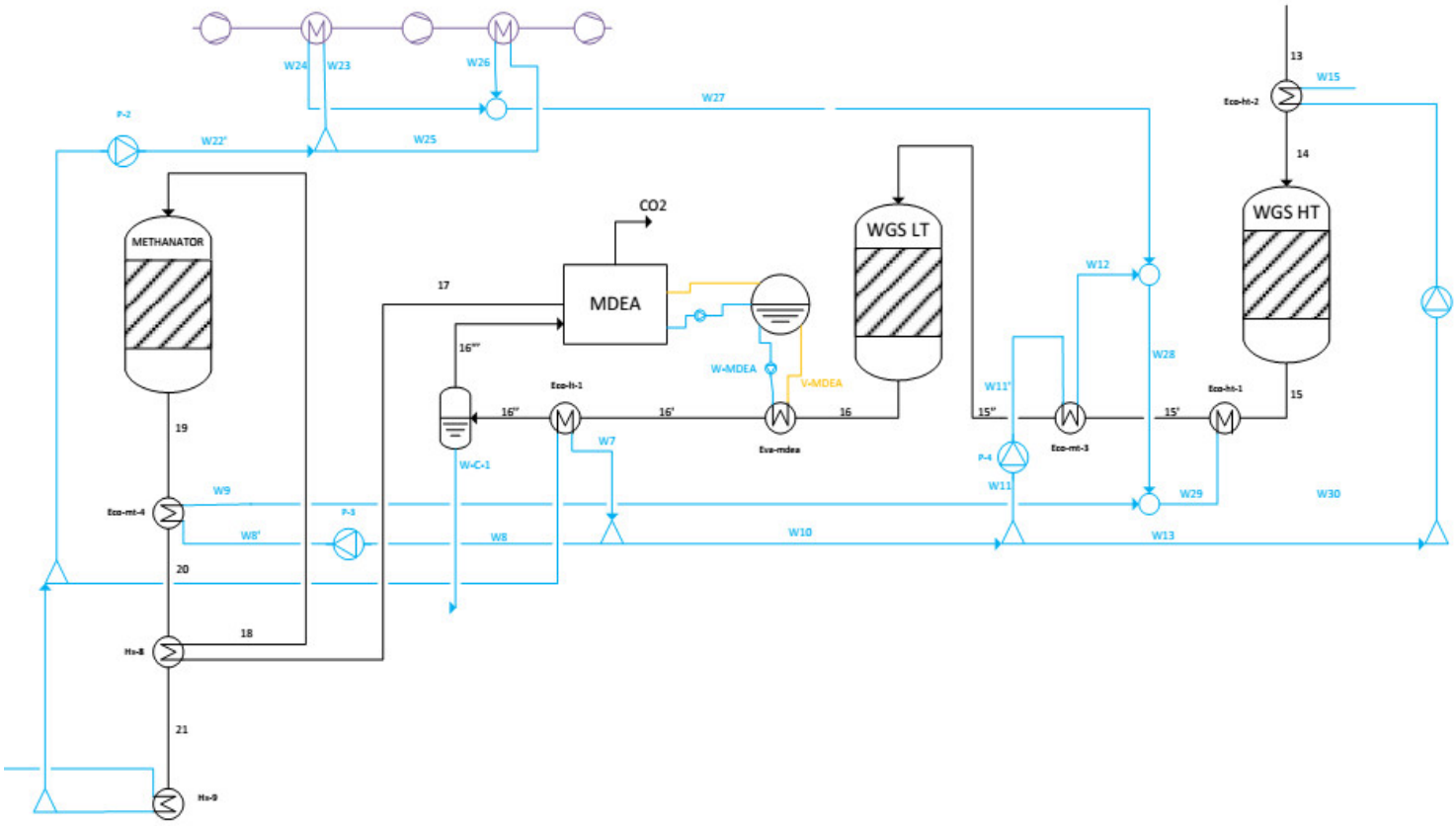

Figure 4: syngas purification section

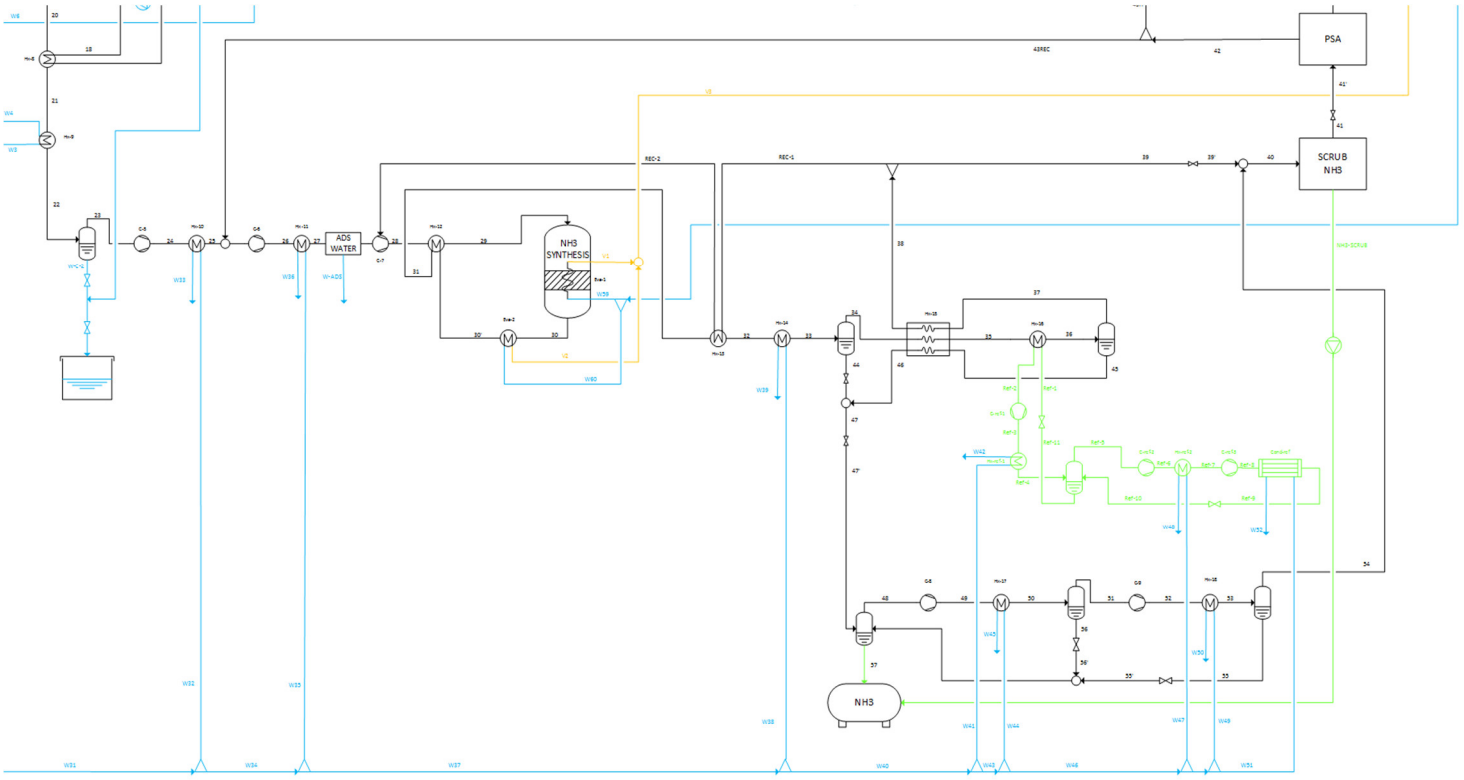

Figure 5: ammonia synthesis loop section

Note that stream 35 is cooled down to -20°C in the heat exchanger hx-16, in order to reduce to a minimum the ammonia content in the recycle and purge streams. To do so, a two-stage refrigeration cycle is employed (green lines in Figures 2 and 5). Since the ammonia-rich liquid collected by the high-pressure liquid-splitters (after streams 33 and 36) contains a significant amount of incondensable gasses, it has to be flashed to around 20 bar (stream 47). In this way some liquid ammonia evaporates (stream 48), therefore, after re-liquefying (streams 56 and 55), it has to be sent back to the ammonia tank. The ammonia liquid output stream (57) has a purity higher than 99%. Since a little amount of ammonia remains in the PSA off-gas (around 0,2%), there must be some tools to control and limit the NO_x emissions (such as SCR or SNCR, using the available ammonia).

3.2) Stream tables

SYNGAS PRODUCTION															
					MOLAR COMPOSITION										
stream	T [°C]	P [bar]	m [kg/s]	n [kmol/s]	Ar	CH4	H2O	CO	CO2	H2	C2H6	N2	O2	C3H8	C4H10
1	16,0	33,1	10,48	0,58	0,0%	89,0%	0,0%	0,0%	2,0%	0,0%	7,0%	0,9%	0,0%	1,0%	0,1%
2	115,0	33,0	10,48	0,58	0,0%	89,0%	0,0%	0,0%	2,0%	0,0%	7,0%	0,9%	0,0%	1,0%	0,1%
3	115,0	33,0	8,20	0,46	0,0%	89,0%	0,0%	0,0%	2,0%	0,0%	7,0%	0,9%	0,0%	1,0%	0,1%
4	114,6	33,0	8,22	0,46	0,0%	87,2%	0,0%	0,0%	2,0%	2,0%	6,9%	0,9%	0,0%	1,0%	0,1%
5	365,0	32,7	8,22	0,46	0,0%	87,2%	0,0%	0,0%	2,0%	2,0%	6,9%	0,9%	0,0%	1,0%	0,1%
6	350,4	32,7	34,90	1,95	0,0%	20,8%	76,1%	0,0%	0,5%	0,5%	1,6%	0,2%	0,0%	0,2%	0,0%
7	490,0	32,4	34,90	1,95	0,0%	20,8%	76,1%	0,0%	0,5%	0,5%	1,6%	0,2%	0,0%	0,2%	0,0%
8	438,5	32,3	34,90	2,03	0,0%	21,9%	69,2%	0,0%	2,4%	6,2%	0,0%	0,2%	0,0%	0,0%	0,0%
9	620,0	32,1	34,90	2,03	0,0%	21,9%	69,2%	0,0%	2,4%	6,2%	0,0%	0,2%	0,0%	0,0%	0,0%
10	820,0	31,8	34,90	2,54	0,0%	7,4%	40,7%	5,8%	6,2%	39,7%	0,0%	0,2%	0,0%	0,0%	0,0%
11	1000,1	31,7	54,28	3,43	0,2%	0,2%	32,7%	9,3%	4,9%	37,4%	0,0%	15,3%	0,0%	0,0%	0,0%
12	703,6	31,5	54,28	3,43	0,2%	0,2%	32,7%	9,3%	4,9%	37,4%	0,0%	15,3%	0,0%	0,0%	0,0%
13	514,7	31,4	54,28	3,43	0,2%	0,2%	32,7%	9,3%	4,9%	37,4%	0,0%	15,3%	0,0%	0,0%	0,0%
14	350,0	31,3	54,28	3,43	0,2%	0,2%	32,7%	9,3%	4,9%	37,4%	0,0%	15,3%	0,0%	0,0%	0,0%
15	428,1	31,1	54,28	3,43	0,2%	0,2%	25,7%	2,2%	12,0%	44,4%	0,0%	15,3%	0,0%	0,0%	0,0%
15'	219,6	30,9	54,28	3,43	0,2%	0,2%	25,7%	2,2%	12,0%	44,4%	0,0%	15,3%	0,0%	0,0%	0,0%
15''	200,0	30,7	54,28	3,43	0,2%	0,2%	25,7%	2,2%	12,0%	44,4%	0,0%	15,3%	0,0%	0,0%	0,0%
16	223,8	30,5	54,28	3,43	0,2%	0,2%	23,6%	0,2%	14,0%	46,5%	0,0%	15,3%	0,0%	0,0%	0,0%
16'	150,1	30,3	54,28	3,43	0,2%	0,2%	23,6%	0,2%	14,0%	46,5%	0,0%	15,3%	0,0%	0,0%	0,0%
16''	35,0	30,1	54,28	3,43	0,2%	0,2%	23,6%	0,2%	14,0%	46,5%	0,0%	15,3%	0,0%	0,0%	0,0%
16'''	35,0	30,1	39,74	2,62	0,3%	0,2%	0,2%	0,3%	18,3%	60,7%	0,0%	20,0%	0,0%	0,0%	0,0%
17	35,0	30,0	18,88	2,15	0,3%	0,3%	0,2%	0,3%	0,3%	74,1%	0,0%	24,4%	0,0%	0,0%	0,0%
18	280,0	29,9	18,88	2,15	0,3%	0,3%	0,2%	0,3%	0,3%	74,1%	0,0%	24,4%	0,0%	0,0%	0,0%
19	322,8	29,7	18,88	2,12	0,3%	0,9%	1,2%	0,0%	0,0%	72,8%	0,0%	24,8%	0,0%	0,0%	0,0%
20	300,0	29,6	18,88	2,12	0,3%	0,9%	1,2%	0,0%	0,0%	72,8%	0,0%	24,8%	0,0%	0,0%	0,0%
21	61,4	29,5	18,88	2,12	0,3%	0,9%	1,2%	0,0%	0,0%	72,8%	0,0%	24,8%	0,0%	0,0%	0,0%
22	35,0	29,4	18,88	2,12	0,3%	0,9%	1,2%	0,0%	0,0%	72,8%	0,0%	24,8%	0,0%	0,0%	0,0%
23	35,0	29,4	18,49	2,10	0,3%	0,9%	0,2%	0,0%	0,0%	73,6%	0,0%	25,0%	0,0%	0,0%	0,0%

(the table continues in the next page)

					MOLAR COMPOSITION										
stream	T [°C]	P [bar]	m [kg/s]	n [kmol/s]	Ar	CH4	H2O	CO	CO2	H2	C2H6	N2	O2	C3H8	C4H10
43H''	100,0	33,0	0,02	0,01	0,0%	0,0%	0,0%	0,0%	0,0%	100,0%	0,0%	0,0%	0,0%	0,0%	0,0%
A1	16,0	1,0	67,83	2,34	1,0%	0,0%	0,0%	0,0%	0,0%	0,0%	0,0%	78,0%	21,0%	0,0%	0,0%
A2	38,0	1,2	67,83	2,34	1,0%	0,0%	0,0%	0,0%	0,0%	0,0%	0,0%	78,0%	21,0%	0,0%	0,0%
A3	38,0	1,2	48,45	1,67	1,0%	0,0%	0,0%	0,0%	0,0%	0,0%	0,0%	78,0%	21,0%	0,0%	0,0%
A3'	90,0	1,2	48,45	1,67	1,0%	0,0%	0,0%	0,0%	0,0%	0,0%	0,0%	78,0%	21,0%	0,0%	0,0%
A4	271,8	1,2	48,45	1,67	1,0%	0,0%	0,0%	0,0%	0,0%	0,0%	0,0%	78,0%	21,0%	0,0%	0,0%
A5	352,0	1,2	48,45	1,67	1,0%	0,0%	0,0%	0,0%	0,0%	0,0%	0,0%	78,0%	21,0%	0,0%	0,0%
A6	38,0	1,2	19,38	0,67	1,0%	0,0%	0,0%	0,0%	0,0%	0,0%	0,0%	78,0%	21,0%	0,0%	0,0%
A7	195,0	3,8	19,38	0,67	1,0%	0,0%	0,0%	0,0%	0,0%	0,0%	0,0%	78,0%	21,0%	0,0%	0,0%
A8	40,0	3,6	19,38	0,67	1,0%	0,0%	0,0%	0,0%	0,0%	0,0%	0,0%	78,0%	21,0%	0,0%	0,0%
A9	198,0	11,2	19,38	0,67	1,0%	0,0%	0,0%	0,0%	0,0%	0,0%	0,0%	78,0%	21,0%	0,0%	0,0%
A10	40,0	10,8	19,38	0,67	1,0%	0,0%	0,0%	0,0%	0,0%	0,0%	0,0%	78,0%	21,0%	0,0%	0,0%
A11	194,8	32,8	19,38	0,67	1,0%	0,0%	0,0%	0,0%	0,0%	0,0%	0,0%	78,0%	21,0%	0,0%	0,0%
A12	538,0	32,7	19,38	0,67	1,0%	0,0%	0,0%	0,0%	0,0%	0,0%	0,0%	78,0%	21,0%	0,0%	0,0%
C1	115,0	32,8	2,28	0,13	0,0%	89,0%	0,0%	0,0%	2,0%	0,0%	7,0%	0,9%	0,0%	1,0%	0,1%
C2	107,0	1,3	2,28	0,13	0,0%	89,0%	0,0%	0,0%	2,0%	0,0%	7,0%	0,9%	0,0%	1,0%	0,1%
C3	105,6	1,2	3,14	0,17	2,9%	77,0%	0,0%	0,0%	1,5%	2,7%	5,3%	9,7%	0,0%	0,8%	0,1%
CO2			20,85	0,47	0,0%	0,0%	0,0%	0,0%	100,0%	0,0%	0,0%	0,0%	0,0%	0,0%	0,0%
F1	1010,0	1,2	51,59	1,84	1,2%	0,0%	15,9%	0,0%	8,3%	0,0%	0,0%	71,7%	3,0%	0,0%	0,0%
F2	766,4	1,2	51,59	1,84	1,2%	0,0%	15,9%	0,0%	8,3%	0,0%	0,0%	71,7%	3,0%	0,0%	0,0%
F3	658,0	1,2	51,59	1,84	1,2%	0,0%	15,9%	0,0%	8,3%	0,0%	0,0%	71,7%	3,0%	0,0%	0,0%
F4	466,2	1,2	51,59	1,84	1,2%	0,0%	15,9%	0,0%	8,3%	0,0%	0,0%	71,7%	3,0%	0,0%	0,0%
F5	400,0	1,2	51,59	1,84	1,2%	0,0%	15,9%	0,0%	8,3%	0,0%	0,0%	71,7%	3,0%	0,0%	0,0%
F6	301,8	1,1	51,59	1,84	1,2%	0,0%	15,9%	0,0%	8,3%	0,0%	0,0%	71,7%	3,0%	0,0%	0,0%
F7	147,6	1,1	51,59	1,84	1,2%	0,0%	15,9%	0,0%	8,3%	0,0%	0,0%	71,7%	3,0%	0,0%	0,0%
PURGE'	100,0	1,2	0,86	0,04	12,0%	38,6%	0,0%	0,0%	0,0%	11,4%	0,0%	38,0%	0,0%	0,0%	0,0%
VAP	346,8	33,0	26,68	1,48	0,0%	0,0%	100,0%	0,0%	0,0%	0,0%	0,0%	0,0%	0,0%	0,0%	0,0%
W-C-1	35,0	30,1	14,54	0,81	0,0%	0,0%	100,0%	0,0%	0,0%	0,0%	0,0%	0,0%	0,0%	0,0%	0,0%
W-C-2	35,0	29,4	0,40	0,02	0,0%	0,0%	100,0%	0,0%	0,0%	0,0%	0,0%	0,0%	0,0%	0,0%	0,0%

Table 1: syngas production stream table

AMMONIA SYNTHESIS LOOP

					MOLAR COMPOSITION					
stream	T [°C]	P [bar]	m [kg/s]	n [kmol/s]	H2	N2	Ar	NH3	CH4	H20
23	35,0	29,4	18,49	2,10	73,6%	25,0%	0,3%	0,0%	0,9%	0,2%
24	123,2	58,0	18,49	2,10	73,6%	25,0%	0,3%	0,0%	0,9%	0,2%
25	40,0	57,5	18,49	2,10	73,6%	25,0%	0,3%	0,0%	0,9%	0,2%
26	123,4	109,3	18,55	2,13	74,0%	24,7%	0,3%	0,0%	0,9%	0,2%
27	40,0	108,3	18,55	2,13	74,0%	24,7%	0,3%	0,0%	0,9%	0,2%
28	144,7	200,0	65,00	6,66	67,0%	22,4%	1,8%	1,6%	7,2%	0,0%
29	320,0	199,0	65,00	6,66	67,0%	22,4%	1,8%	1,6%	7,2%	0,0%
30	450,0	196,0	65,00	5,64	52,0%	17,4%	2,1%	20,0%	8,6%	0,0%
30'	348,3	195,0	65,00	5,64	52,0%	17,4%	2,1%	20,0%	8,6%	0,0%
31	164,7	194,0	65,00	5,64	52,0%	17,4%	2,1%	20,0%	8,6%	0,0%
32	76,8	193,0	65,00	5,64	52,0%	17,4%	2,1%	20,0%	8,6%	0,0%
33	30,0	192,0	65,00	5,64	52,0%	17,4%	2,1%	20,0%	8,6%	0,0%
34	30,0	192,0	55,35	5,08	57,7%	19,3%	2,3%	11,4%	9,3%	0,0%
35	8,9	191,0	55,35	5,08	57,7%	19,3%	2,3%	11,4%	9,3%	0,0%
36	-20,0	190,0	55,35	5,08	57,7%	19,3%	2,3%	11,4%	9,3%	0,0%
37	-20,0	190,0	47,11	4,59	63,7%	21,3%	2,5%	2,3%	10,2%	0,0%
38	25,0	189,0	47,11	4,59	63,7%	21,3%	2,5%	2,3%	10,2%	0,0%
39	25,0	189,0	0,60	0,06	63,7%	21,3%	2,5%	2,3%	10,2%	0,0%
39'	25,0	189,0	0,60	0,06	63,7%	21,3%	2,5%	2,3%	10,2%	0,0%
40	25,4	189,0	1,07	0,09	51,7%	17,2%	5,4%	8,2%	17,5%	0,0%
41	25,4	189,0	0,95	0,08	56,3%	18,7%	5,9%	0,1%	19,0%	0,0%
41'	20,7	60,0	0,95	0,08	56,3%	18,7%	5,9%	0,1%	19,0%	0,0%
42	20,7	58,0	0,08	0,04	100,0%	0,0%	0,0%	0,0%	0,0%	0,0%

(the table continues in the next page)

					MOLAR COMPOSITION					
stream	T [°C]	P [bar]	m [kg/s]	n [kmol/s]	H2	N2	Ar	NH3	CH4	H20
43H	20,7	58,0	0,02	0,01	100,0%	0,0%	0,0%	0,0%	0,0%	0,0%
43H'	21,2	33,0	0,02	0,01	100,0%	0,0%	0,0%	0,0%	0,0%	0,0%
43H''	100,0	33,0	0,02	0,01	100,0%	0,0%	0,0%	0,0%	0,0%	0,0%
43REC	20,7	58,0	0,06	0,03	100,0%	0,0%	0,0%	0,0%	0,0%	0,0%
44	30,0	192,0	9,65	0,57	1,1%	0,4%	0,5%	96,6%	1,4%	0,0%
45	-20,0	190,0	8,24	0,48	0,4%	0,1%	0,5%	97,8%	1,1%	0,0%
46	25,0	189,0	8,24	0,48	0,4%	0,1%	0,5%	97,8%	1,1%	0,0%
47	27,7	189,0	17,89	1,05	0,8%	0,3%	0,5%	97,2%	1,3%	0,0%
47'	25,1	20,0	17,89	1,05	0,8%	0,3%	0,5%	97,2%	1,3%	0,0%
48	25,3	20,0	0,90	0,05	15,0%	5,0%	6,8%	54,5%	18,7%	0,0%
49	148,7	61,0	0,90	0,05	15,0%	5,0%	6,8%	54,5%	18,7%	0,0%
50	40,0	60,7	0,90	0,05	15,0%	5,0%	6,8%	54,5%	18,7%	0,0%
51	40,0	60,7	0,59	0,04	22,3%	7,4%	9,7%	33,6%	27,0%	0,0%
52	175,2	191,0	0,59	0,04	22,3%	7,4%	9,7%	33,6%	27,0%	0,0%
53	40,0	190,4	0,59	0,04	22,3%	7,4%	9,7%	33,6%	27,0%	0,0%
54	40,0	190,4	0,47	0,03	27,5%	9,1%	11,4%	19,9%	32,1%	0,0%
55	40,0	190,4	0,12	0,01	1,1%	0,4%	2,8%	89,4%	6,3%	0,0%
55'	22,3	20,0	0,12	0,01	1,1%	0,4%	2,8%	89,4%	6,3%	0,0%
56	40,0	60,7	0,30	0,02	0,2%	0,1%	0,8%	97,0%	1,9%	0,0%
56'	31,9	20,0	0,30	0,02	0,2%	0,1%	0,8%	97,0%	1,9%	0,0%
57	25,3	20,0	17,42	1,02	0,0%	0,0%	0,2%	99,4%	0,4%	0,0%
NH3SCRUB	25,4	189,0	0,12	0,01	0,0%	0,0%	0,0%	100,0%	0,0%	0,0%
PURGE	20,7	58,0	0,87	0,04	11,4%	38,0%	11,9%	0,2%	38,5%	0,0%
PURGE'	100,0	58,0	0,87	0,04	11,4%	38,0%	11,9%	0,2%	38,5%	0,0%
REC-1	25,0	189,0	46,51	4,53	63,7%	21,3%	2,5%	2,3%	10,2%	0,0%
REC-2	146,7	189,0	46,51	4,53	63,7%	21,3%	2,5%	2,3%	10,2%	0,0%
W-ADS	40,0	108,3	0,061	0,003	0,0%	0,0%	0,0%	0,0%	0,0%	100,0%

Table 2: ammonia synthesis loop stream table

In the following page is reported the stream table for the heat integration system. We have assumed that water is available at 20 °C. Note that the water consumption is remarkable, making necessary a big natural source (such as rivers or lakes) or, in the worst case, a big cooling tower. We have used a steam cycle with one only pressure level, which is the most common choice for ammonia plants (bear in mind that the steam turbine power output is below 40 MW, as we will see later on). The steam enters the turbine with a pressure of 110 bar (corresponding to a boiling temperature of 318 °C) and a temperature of 510 °C. A significant amount of low-temperature (up to 135 °C) heat is also produced: of 488,3 MW entering with the fuel heating value, a total of 114,9 MW are lost in hot water at different temperatures, of which 19,4 MW in water between 100 and 135 °C. Such energy output represents the main efficiency loss, also because ammonia plants, logically, are built far away from residential areas and so there is no chance to exploit it with a district heating system.

HEAT INTEGRATION SYSTEM (WATER)							
stream	T [°C]	P [bar]	m [kg/s]		stream	T [°C]	P [bar]	m [kg/s]
W0	20	1	931,1		W33	100	6	15,6
W1	20	6	931,1		W34	20	6	284,8
W2	20	6	109,0		W35	20	6	16,2
W3	20	6	20,4		W36	100	6	16,2
W4	45	6	20,4		W37	20	6	268,6
W5	20	6	88,6		W38	20	6	132,2
W6	20	6	78,8		W39	53	6	132,2
W7	135	6	78,8		W40	20	6	136,4
W8	135	6	9,6		W41	20	6	4,6
W8'	135	110	9,6		W42	61	6	4,6
W9	170	110	9,6		W43	20	6	131,8
W10	135	6	69,2		W44	20	6	3,0
W11	135	6	15,0		W45	64	6	3,0
W11'	135	110	15,0		W46	20	6	128,8
W12	170	110	15,0		W47	20	6	5,6
W13	135	6	54,2		W48	47	6	5,6
W14	135	6	21,5		W49	20	6	0,9
W14'	135	110	21,5		W50	97	6	0,9
W15	315	110	21,5		W51	20	6	122,3
W16	135	6	32,7		W52	42	6	122,3
W-MT-ECC.	135	6	18,1		W53	20	6	521,6
W17	135	6	32,3		W54	48	6	521,6
W18	135	6	14,2		W55	315	110	55,9
W19-A	135	6	6,1		W56	315	110	55,9
W19-A'	40	6	6,1		W57	315	110	18,1
W19-B	135	6	8,0		W58	315	110	37,8
W19-B'	60	6	8,0		W59	315	110	21,8
W20	135	6	0,4		W60	315	110	16,0
W21	55	6	0,4		W-OUT-TB	53	0,16	29,2
W22	20	6	9,8		W-OUT-TB'	53	1,50	29,2
W22'	20	110	9,8		W-MDEA	127	2,70	9,1
W23	20	110	4,8					
W24	170	110	4,8		V1	319	110	21,8
W25	20	110	5,0		V2	319	110	16,0
W26	170	110	5,0		V3	319	110	37,8
W27	170	110	9,8		V4	319	110	18,1
W28	170	110	24,8		V5	319	110	55,9
W29	170	110	34,4		V6	319	110	55,9
W30	315	110	34,4		V7	510	110	55,9
W31	20	6	300,4		V-PROC.	347	33	26,7
W32	20	6	15,6		V-OUT-TB	55	0,16	29,2
					V-MDEA	132	2,70	9,1

Table 3: heat integration system stream table

The two-stage refrigeration cycle proposed has an evaporation and condensation temperature of -25 °C and 45 °C respectively and an energy efficiency ratio (EER) of 2,37.

REFRIGERATION CYCLE (ammonia)				
stream	T [°C]	P [bar]	VAPOUR FRACT.	m [kg/s]
Ref-1	-25,2	1,50	0,094	7,17
Ref-2	-23,4	1,49	1	7,17
Ref-3	76,3	4,77	1	7,17
Ref-4	30,0	4,72	1	7,17
Ref-5	2,5	4,72	1	8,75
Ref-6	61,8	9,44	1	8,75
Ref-7	35,0	9,44	1	8,75
Ref-8	95,1	18,00	1	8,75
Ref-9	38,2	17,90	0	8,75
Ref-10	2,5	4,72	0,136	8,75
Ref-11	2,5	4,72	0	7,17

Table 4: refrigeration cycle stream table

3.3) Calculation method and main assumptions

We have used Aspen Plus V8.8 to perform the calculations. Note that, due to the high ammonia synthesis pressure, the ideal gas hypothesis no longer stands for that section, so, according to the Aspen database recommendations, we have used the Redlich-Kwong-Soave equation of state with Boston-Mathias modifications.

THERMODYNAMIC MODEL (from Aspen database)	
syngas production section	RKS
ammonia synthesis section	RKS-BM
heat integration system (water-steam)	IAPWS
refrigeration cycle (ammonia)	REFPROP

Table 5: thermodynamic model

REACTORS						
REACTOR	**CALCULATION METHOD**	**m [kg/s]**	**T,in [°C]**	**T,out [°C]**	**P,in [bar]**	**ΔP [bar]**
PRE-REF.	equilibrium	34,9	490,0	**438,5**	32,4	0,2
FTR	methane conversion=57,9%; CO/CO2 ratio=1,0145	34,9	620,0	820,0	32,1	0,3
ATR	equilibrium	54,3	761,0	1000,1	31,8	0,1
WGS HT	equilibrium for wgs (restricted eq.)	54,3	350,0	**428,1**	31,3	0,2
WGS LT	equilibrium for wgs (restricted eq.)	54,3	200,0	**223,8**	30,7	0,2
METHANATOR	equilibrium	18,9	280,0	**322,8**	29,9	0,2
NH3 synthesis	equilibrium at Teq = Tout + 15 °C	65,0	320,0	450,0	199	3,0

Table 6: reactors calculation method. The resulting outlet temperatures for adiabatic reactors are in bold type.

As pointed out in chapter 2.2.1.2, the methane conversion in the FTR is a design choice. After setting such conversion and the outlet temperature, the carbon monoxide to carbon dioxide ratio depends on the tubes length and the gas superficial velocity (anyway, its value is around 0,75-1,1). The topic of the conversion in the ammonia synthesis reactor has already been discussed in chapter 2.1 and 15 °C is a reasonable chemical equilibrium temperature approach (although lower values are achievable with higher investment cost).

COMPONENTS PERFORMANCES	
COMPONENT	EFFICIENCY
MDEA PROCESS (CO_2 removal)	ε,co2 = 98,5 %, ε,co = 2,9 %, Q,duty = 42 kj/mol,CO2
ADS WATER (H_2O removal)	ε,H2O = 100%
SCRUB NH_3 (NH_3 removal from purge stream)	ε,NH3 = 99 % (selectivity 100%)
PSA (H_2 recovery from purge stream)	ε,H2 = 90 % (selectivity 100%)

Table 7: components performances

3.4) Heat exchange diagrams (T-Q)

In the following we report the T-Q diagram both for the FTR flue-gas cooling section and for the syngas cooling section. Moreover, we have shown the heat exchange diagrams for the exchangers hx-15 and hx-16 of the ammonia loop, since those are the ones with the lowest temperature approach.

For high-pressure steam, the subcooling and superheating temperature differences are 3 and 1 °C respectively, so that the high-temperature economizers produce liquid water at 315 °C and the evaporators produce steam at 319 °C. Although the evaporator “eva-1” is inside the synthesis reactor, and so we cannot draw a precise heat exchange diagram, the gas temperature is sufficiently high to perform the water

evaporation (as shown in chapter 2.1). Generally speaking, the approach temperature differences are chosen considering the fluids phase (and so their heat exchange coefficient and density) and the effect of the exchangers efficiency on the overall plant efficiency.

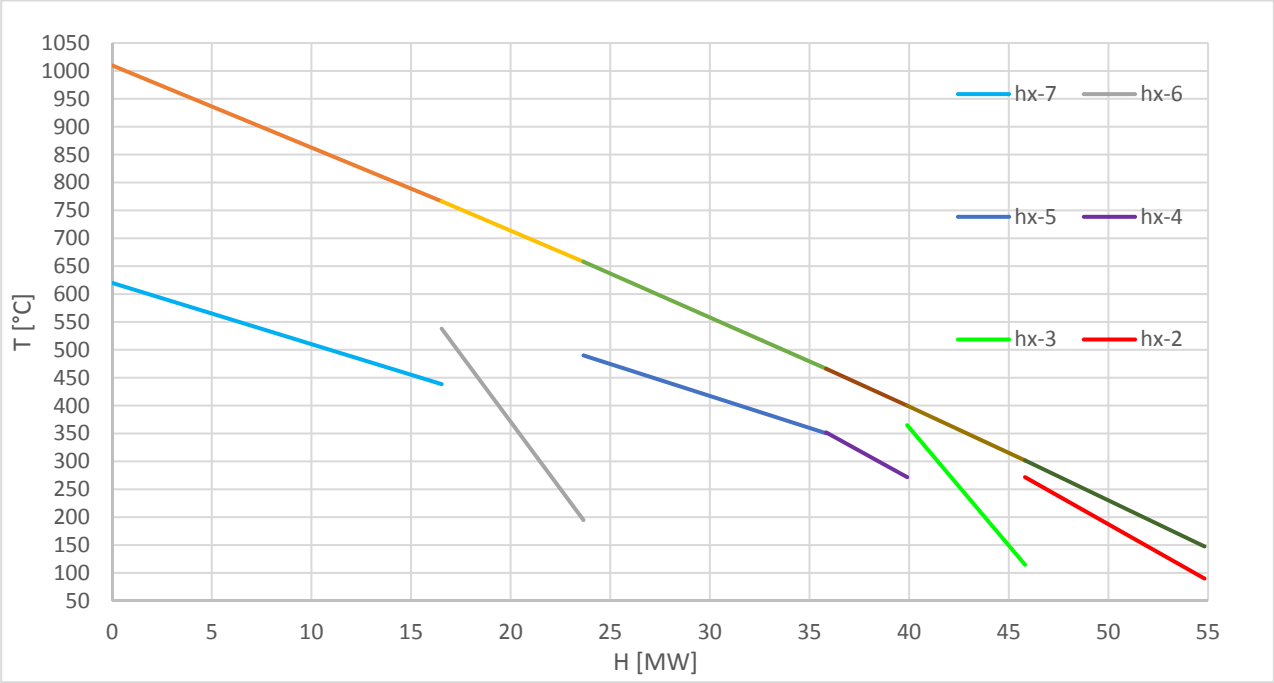

Figure 6: T-Q diagram for the FTR flue-gas cooling section

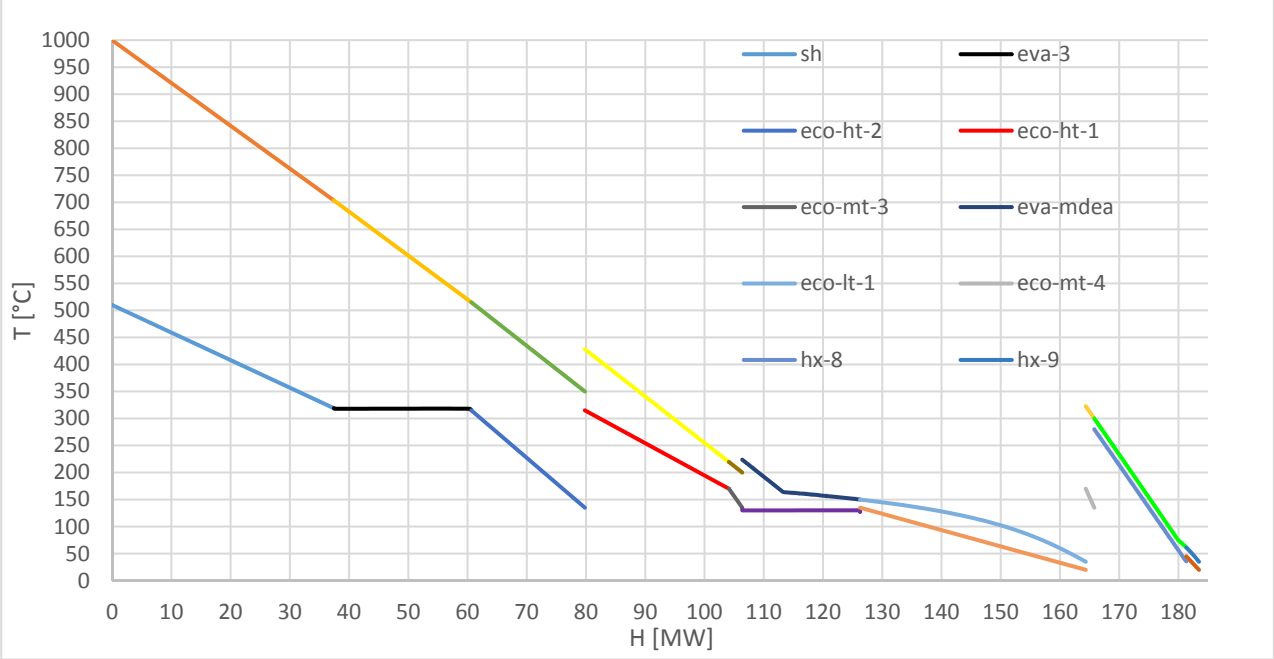

Figure 7: T-Q diagram for the syngas cooling

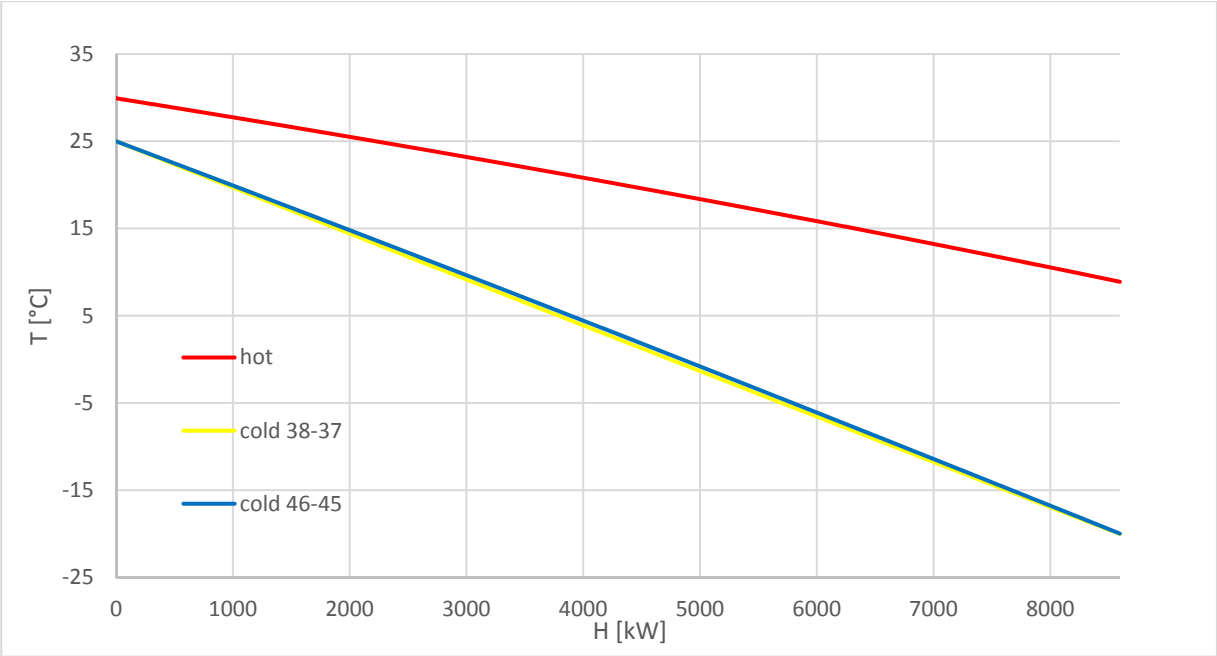

Figure 8: T-Q diagram for the exchanger hx-15

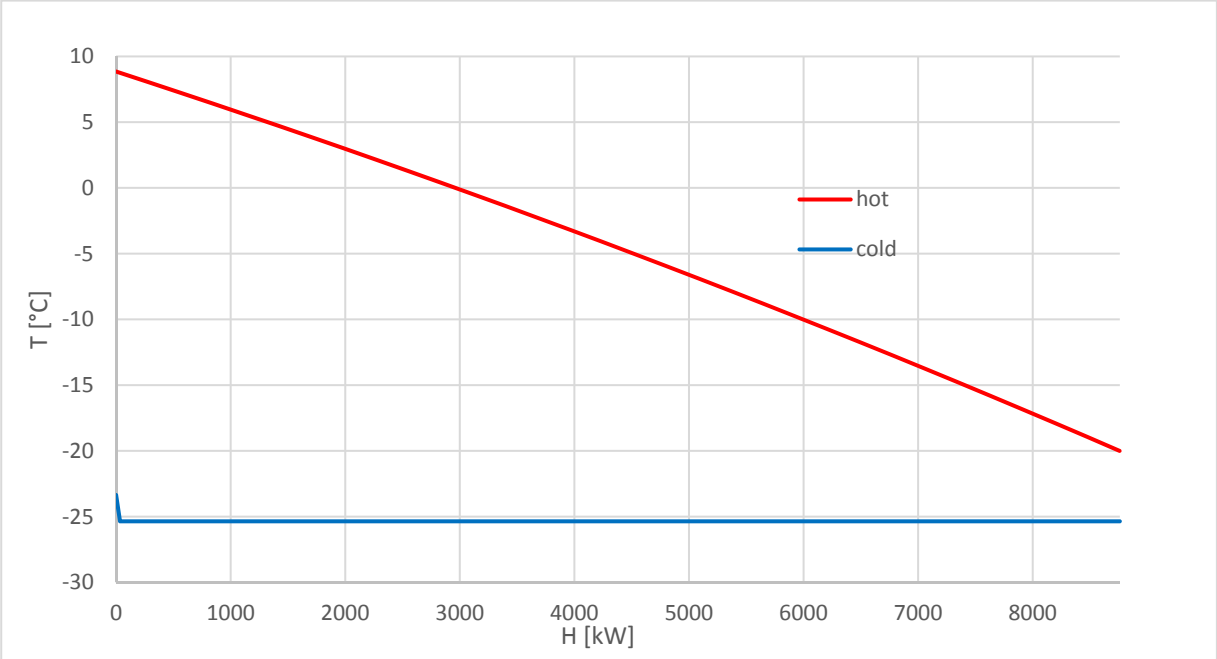

Figure 9: T-Q diagram for the exchanger hx-16

3.5) Turbomachinery mechanical power output and consumption

COMPRESSORS AND PUMPS					
COMPRESSORS			PUMPS		
η,is=	0,75				
η,mech.=	0,98				
RESULTS: POWER CONSUMPTION (shaft)					
C-1 (air)	1526	kW	P-1	475	kW
C-2 (process air)	3145	kW	P-2	104	kW
C-3 (process air)	3170	kW	P-3	110	kW
C-4 (process air)	3117	kW	P-4	171	kW
C-5 (syngas)	5629	kW	P-5	245	kW
C-6 (syngas)	5561	kW	P-6	4	kW
C-7 (syngas)	6840	kW			
C-8 (incondensables)	218	kW			
C-9 (incondensables)	161	kW			
C-ref-1	1533	kW			
C-ref-2	1115	kW			
C-ref-3	1126	kW			
total	33138	kW		1109	kW
net mechanical energy consumption			34247		kW

Table 8: compressors and pumps power consumption

STEAM TURBINE		
η,is=	0,82	
η,mech.=	0,98	
T,in=	510	°C
P,in=	110	bar
T,out=	55	°C
P,out=	0,158	bar
RESULTS		
x,out=	0,878	
P,mech.=	38403	kW

Table 9: steam turbine

Remind that almost half the high-pressure steam entering the turbine is drawn as process steam at 33 bar (see tab. 3).

We have assumed a constant isentropic efficiency of 75% for every compressor. To be precise, we should make a distinction between centrifugal compressors, for which 75% is a good value, and fans. Anyway, the power consumption of fans is very low and so the approximation is reasonable. The plant has an electric power output of 3948 kW (considering a generator efficiency of 95%).

3.6) General results

Since there is an electric power output, it makes sense to introduce a new performance index (in addition to those discussed in chapter 2.2.3), which is the primary energy corrected consumption per ton of ammonia produced:

$$PRIMARY\ ENERGY\ CORRECTED\ CONSUMPTION\ \left[\frac{Gj}{t_{NH3}}\right] = \frac{\dot{m}_{NG} * LHV_{NG}}{\dot{m}_{NH3}} - \frac{P_{el,out}}{\eta_{el,ref} * \dot{m}_{NH3}}$$

Where $\eta_{el,ref}$ is the electric power production reference efficiency (here equal to 55%. Bear in mind that, while the reference efficiency for combined cycles reaches 60%, their average efficiency, nowadays, does not exceed 50%; besides, the renewables share has to be accounted).

Similarly, the carbon dioxide corrected emission is:

$$CARBON\ DIOXIDE\ CORRECTED\ EMISSION\ \left[\frac{t_{CO2}}{t_{NH3}}\right] = \frac{\dot{m}_{CO2,out}}{\dot{m}_{NH3}} - \frac{P_{el,out} * E_{CO2}}{\dot{m}_{NH3}}$$

Where E_{CO2} is the specific emission of the reference power plant (here equal to 0,103 kg_{CO2}/MJ_E).

The results are shown in tab. 10 and they are in agreement with those mentioned in ch. 2. The CO_2 captured by the MDEA process is considered compressed and stored, so, the only carbon emission is due to the FTR flue-gas (and to the negligible amount of carbon compounds in the liquid ammonia produced). The CO_2 compression cost is shown at the end of chapter 5, in the comparison between the traditional and the proposed new technology.

GENERAL RESULTS		
steam to carbon ratio (S/C)=	3	
total natural gas consumption=	10,48	kg/s
of which for energy purposes=	2,28	kg/s
ammonia production=	17,36	kg/s
	1500	t/d
PCI,ng=	46,59	MJ/kg
P,el,output=	3948	kW
primary energy net consumption*=	28,13	Gj/t,NH3
primary energy corrected consumption=	27,72	Gj/t,NH3
carbon capture ratio=	77,3%	
carbon dioxide net emission**=	0,363	t,CO2/t,NH3
carbon dioxide corrected emission=	0,339	t,CO2/t,NH3

Table 10: general results

* it doesn't take into account electrical power output/input.

** due to the FTR flue-gas, since the carbon dioxide captured by the MDEA process is considered stored.

4) Calcium-Copper looping process for hydrogen production

Consider the hydrogen production process described in chapter 2. One of the most important issue is to maximize the methane conversion (and so the hydrogen yield). There are several ways to increase the methane conversion through the steam-reforming process, all of them seem to have also disadvantages. Looking to the thermodynamics of reforming reaction of CH_4 (R1), it can be noticed that CH_4 conversion may be favoured by increasing the reforming temperature, reducing the operating pressure or increasing the amount of steam (e.g. the steam to carbon ratio) introduced in the reformer. However, some disadvantages appear from any of these options. Increasing the equilibrium temperature entails an increase in the amount of natural gas burnt in the FTR furnace for supplying energy needed for reforming; besides there are constraints due to the materials employed. Reducing the pressure entails an increase both in compression costs and in equipment volume. Increasing the steam to carbon ratio entails a reduction in the power produced by the steam turbine, besides it increases the amount of high-temperature heat to supply and so, generally, the fuel consumption.

The system proposed here exploits an alternative way for improving CH_4 conversion within a reforming process, which is called "sorption enhanced reforming" (SER). In the proposed process, the reforming reaction is carried out in the presence of a solid sorbent that reacts with the carbon dioxide (CO_2) generated from the water gas shift reaction (R2), removing it from the gas phase. The removal of CO_2 pushes the WGS to consume CO, which, in turn, pushes the SR to consume CH_4. Consequently, set pressure and temperature, the hydrogen yield is higher than that of a traditional reforming process.

$CH_4 + H_2O \leftrightarrow CO + 3H_2$ (steam-reforming, $\Delta H_r^\circ = 206$ kj/mol) (R1)

$CO + H_2O \leftrightarrow H_2 + CO_2$ (water-gas shift, $\Delta H_r^\circ = -41$ kj/mol) (R2)

In this case, it is proposed the calcium oxide (CaO) as CO_2 sorbent, which reacts with the CO_2 following exothermic reaction given in (R3). CaO is an inexpensive solid, mostly produced through calcination of calcium carbonate ($CaCO_3$), which is typically contained in limestones (according to reaction (R4)). CaO is used above all in building industry to produce cement, but it finds also minor applications in other sectors, such as petroleum and paper industry (1). It is also used for flue-gas desulphurization in power production plants.

$CaO^{(s)} + CO_2 \rightarrow CaCO_3^{(s)}$ (CaO carbonation, $\Delta H_r^\circ = -178{,}8$ kj/mol) (R3)

$CaCO_3^{(s)} \rightarrow CaO^{(s)} + CO_2$ ($CaCO_3$ calcination, $\Delta H_r^\circ = 178{,}8$ kj/mol) (R4)

Since both CaO and $CaCO_3$ are solids, under suitable conditions, the CO_2 capture reaction can proceed until all the CaO is converted. The other advantage of this system is that, thanks to the capture of carbon dioxide in solid phase, from which can then be easily set free and stored, it performs an intrinsic carbon capture (allowing to avoid the CO_2 removal section).

The carbonation reaction is exothermic and entails a reduction in the number of moles in the gas phase, which means that it is thermodynamically favoured at low temperature and high pressure. As an explanation of the last sentence, consider the chemical equilibrium constant for the carbonation reaction, which under the hypothesis of ideal gas can be written as:

$$K_{carb}(T) = \frac{1}{p} * \frac{1}{x_{CO_2}} \rightarrow x_{CO_2} = \frac{1}{p} * \frac{1}{K_{carb}(T)}$$

This equation states that, once pressure and temperature are set, the CO_2 concentration is also fixed, and it increases as pressure decreases and temperature increases. Anyway, it is worth to make clear that carbonation can take place only if CaO is available: when it has been fully converted, the CO_2 can no longer be captured, even if equilibrium condition would dictate so.

Besides, it has been experimentally proved that, at a pressure of 30 bar, at temperatures above 860-870 °C the carbonation reaction is negligible, and therefore gas composition is dictated by SR and WGS alone (see fig. 1). The figure below shows a comparison between methane conversion in traditional steam-reforming (SR) process (continuous lines) (e.g. in the absence of a CO2 sorbent), and in a sorption enhanced reforming (SER) process (dotted lines).

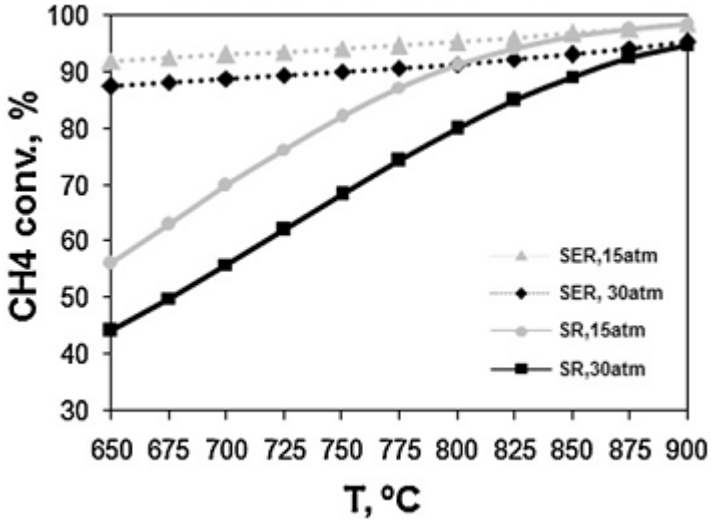

Figure 1: comparison between methane conversion for SR and for SER systems, under the hypothesis of ideal gas and chemical equilibrium, with S/C=5(2).

It can be also noted in Figure 1 that for the SER, the effect of temperature on methane conversion is quite soft. This fact can be demonstrated looking to the overall reaction in the SER process (e.g. calculated as the sum of reactions of SR (1), WGS (2) and carbonation reactions (3)), which is almost thermally neutral:.

$CH_4 + CaO^{(s)} + 2H_2O \leftrightarrow CaCO_3^{(s)} + 4H_2 \quad \Delta H_r^\circ = -13{,}7$ kj/mol (*)

The slight increase in methane conversion with temperature shown in the graph, is due to the fact that however low is the CO and CO_2 content in the outlet syngas, it cannot be zero; besides the feed is usually pre-reformed, so that not only CH_4 and H_2O are present. Therefore all the three reactions mentioned above have to be taken into account. Note that reaction (*) entails an increase in gas moles number and so the SER process is favoured at low pressures.

Another interesting feature of the process is that the heat released by carbonation, and to a lesser extent by water-gas shift, is sufficient to compensate that absorbed by steam-reforming, which makes unnecessary burning additional natural gas as in the conventional SR process.

Finally, in SER systems there is no need for WGS reactors, since the presence of the carbonation reaction allows CO content in the syngas produced to be very low. This entails not only an economic investment

saving, but also an energetic advantage, since the heat released by WGS is partially recovered by SR inside the reaction front (on the contrary, the heat released downstream of the WGS reactors is recovered by liquid or boiling water).

Once the CaO bed has been fully converted to CaCO3, it is necessary to regenerate it through calcination (R4), releasing the CO2 that has been separated during the SER process. The calcination reaction is strongly endothermic and it is favoured at high temperatures and low pressures. Different process schemes can be found in the literature on how to supply the required heat in the calcination process. In calcium-copper looping systems, originally proposed by J.C. Abanades and R. Murillo(10), a second copper looping is employed for supplying the energy needed for calcination. As shown in the figure below (Fig. 2), the Ca-Cu chemical looping process can be divided into three main stages, taking place in packed beds. In stage A hydrogen production takes place through the SER reactions. At the beginning of stage A, the bed is made up of three solids:

- CO2 sorbent that consists of CaO, typically supported over an inert material for improving its chemical stability along cycles
- Oxygen carrier, in this case Cu supported over an inert material (typically Al2O3 or MgAl2O4)
- Reforming catalyst, typically Ni-based with Al2O3 or MgAl2O4 working as support

At the end of this stage all the (active) CaO in the bed is converted into $CaCO_3$. During the subsequent stage B, a stream of air is fed into the bed to oxidise the Cu (and secondarily the Ni) to CuO (and NiO), resulting in an outlet gas stream made up mainly of nitrogen. In stage C the regeneration of the CO2 sorbent takes place thanks to the energy provided by CuO reduction with the fuel introduced into this stage (e.g. CH4, CO or H2 are typically proposed). In fact, a stream of pre-reformed natural gas and steam is fed, which reduces the copper and nickel oxides in the bed to Cu and Ni. Since the reactions of bed reduction and feed oxidation are overall exothermic, the heat they release allows the $CaCO_3$ calcination to occur. The CuO to $CaCO_3$ molar ratio is dictated by the energy balance in this stage C: the heat released by the bed reduction has to balance the heat absorbed by $CaCO_3$ calcination. The exiting gas stream is composed only of steam and carbon dioxide, which can then be easily separated. As a result at the end of stage C the bed composition is that of the beginning of stage A, and the system can start again, working in a continuous manner (namely in a loop).

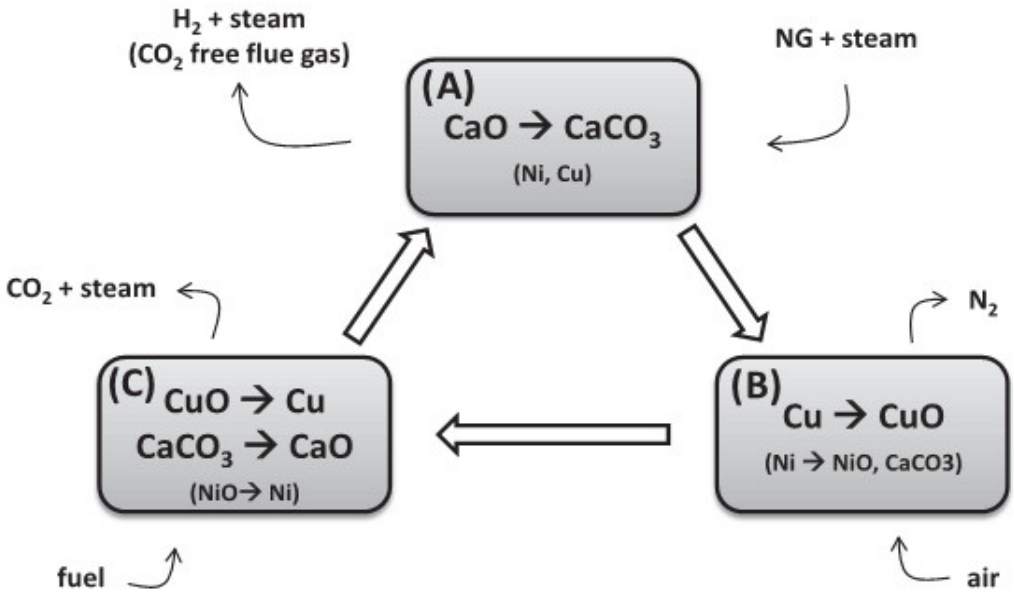

Figure 2: Conceptual scheme of a Ca-Cu looping process (6).

4.1) General assumptions

Before describing in detail the mode of operation of the stages and the calculation procedure followed, it is briefly discuss here the main assumptions and simplifying hypothesis adopted.

The gas mixtures are considered as ideal gases. Once set the reduced temperature ($T_r = T/T_c$), the ideal gas hypothesis stands under a certain reduced pressure ($p_r = p/p_c$). Of course, the lower is the reduced pressure, the better the ideal gas model fits the real gas behaviour; the opposite occurs, to a certain extent, with temperature. Since the operating pressure does not exceed 44 bar in any case, we can assume this (very convenient) hypothesis not too far from reality.

The reactors are adiabatic, or, to be precise, the thermal power dispersed to the environment through the reactor walls is negligible in comparison to the energy flow crossing the bed. Even though there are studies assessing the potentiality of fixed bed reactors working close to isothermal conditions (with a cooling medium flowing on the outer walls), it has been widely demonstrated that the highest performances are reached with adiabatic reactors (3).

A plug flow pattern for the gases in the reactor axial direction has been assumed (3), meaning that the gradient modulus of every property (in particular velocity, temperature, gas and solid composition) in radial direction is null. This allows to use one only spatial coordinate (z).

The bed void fraction, which affects the gas superficial velocity and the pressure drops, is kept constant (ε = 0,5; consider that the void fraction of a mono-sized spherical particles bed after a prolonged shaking is about 0,395(4)). The particles are considered as spheres of constant diameter (3) (d = 2,2 cm). The particle size is a trade-off between two opposite necessities: on one hand, reducing the particles size leads to an increase in the solid activity and so a reduction of solid volume; on the other hand both the pressure drops and the risk of solid losses (elutriation) increase.

The solid composition is considered homogeneous throughout the bed and no catalyst deactivation is taken into account. The catalyst employed is alumina supported nickel (with 18% nickel by mass). The amount of catalyst has to be enough for reforming reaction to occur at a sufficient reaction rate during stage A as to reach methane conversion close to equilibrium. It has been shown that a catalyst (supported) to sorbent mass ratio of 0,3 is sufficient to reach this condition (7) (given as mass of active catalyst including the support per mass of CaO in the sorbent), so we have used this value. Alumina is also used as support material for CaO (15% alumina by mass) and Cu (35% alumina by mass).

Whereas the copper oxidation (stage B) and reduction (stage C) reactions have been proved to be very fast (5), the chemical activity of CaO along carbonation-calcination cycles is a thorny matter. It is acknowledged that the CaO conversion to $CaCO_3$ is usually not complete, since once the outer particle shell has been converted to carbonate, the CO_2 diffusion inward is very slow. Moreover, in case of hybrid particles, made of CaO, Cu and a support material, it has been found that the copper is responsible for a significant reduction in calcium oxide activity. In fact, as CuO becomes unstable and starts to decompose at around 870 °C, even if its melting point is higher, it tends to wrap the solid particles(5). In that case, experiments have shown that Cu/CuO reduces the carbonation rate, but does not affect significantly the CaO conversion: the carbonation requires more time because of the presence of Cu/CuO. To avoid this phenomenon, we have considered three kinds of “simple” particles: CaO, Cu and Ni, all of them supported by Al_2O_3. It has been demonstrated that the use of an inert material, such as MgO, as support for the CaO, can enhance the performance of the CO_2 sorbent along cycles (5). The CaO activity is significantly affected by the operating temperature, and by its preparation and origin (5). In any case, an important reduction of CaO activity has been observed as it

undergoes an increasing number of calcination-carbonation cycles. As an example, it has been found that for a CaO composite synthesized by mechanical mixing, a carbonation conversion of 83,7% is reached in the first cycle, while the figure drops to 18,7% after 68 cycles (with different preparations the figure after 68 cycles is around 27%) (5). This is one of the main technical problem of Ca-Cu looping processes. Three main consequences are due to this problem. First, it is necessary to replace periodically the solid. Though natural calcium oxide is quite inexpensive and could be used as raw material in cement production (if pure), the one we are considering here is synthetic and much more expensive. The copper and nickel cost is even greater. Second, the gas superficial velocity has to be limited (to around 0,5 m/s for stage A(3)(7)), in order to give the carbonation the time to proceed. In this regard, we had better make clear that the carbonation is the "slow" reaction, which dictates, even at the beginning of the solid service life, the maximum superficial velocity in stage A (as shown in the following). As the solid ages, the kinetics slows down and the time required by carbonation rises. This entails an increase in the equipment volume and cost. Third, an important quota of CaO behaves like inert, absorbing heat during stage C and so affecting the process performances. This phenomenon also precludes the use of cheap CaO from natural origin (mainly limestone), since it undergoes a rapid loss of reactivity, and imposes the use of CaO-based synthetic materials, for which a reactivity over 30% has been observed even after a lot of cycles(3). We have assumed that 30% of CaO is "active", while the remaining 70% behaves like inert. The activity of the copper is instead assumed to be 100%, as several studies reported it to be close to this value(3)(5).

The natural gas composition is the following: 89% CH_4, 2% CO_2, 7% C_2H_6, 1% C_3H_8, 0,11% C_4H_{10}, 0,89% N_2.

The use of packed beds, instead of fluidized beds, not only simplifies the plant and its management (since there is no need for solids transport and solid-gas separation systems), but it has also a positive effect on the solid duration. Attrition between the particles seems not to be a problem and no significant mass loss has been observed (5). Obviously, in order to have a continuous production several beds working in parallel are required.

The gas chemical equilibrium has been calculated at the stages inlet pressure, regardless of the pressure drops. This assumption is justified by the fact that for stage A, in which the conversion is limited by equilibrium, the pressure drop is quite low, whereas for stages B and C the conversion can be considered complete. Anyway, the pressure drops will be evaluated using the Ergun's law.

The solid and gas temperatures are assumed to be equal at any point ($T=T_g=T_s$ is a function of the axial coordinate (z) and time). This assumption is justified by the high gas-solid heat transfer coefficient (reported to be around 0,13 kW/m^2K for stage A(3); the figure is expected to be higher for stages B and C since the gas velocity is higher). The gas-solid mass transfer coefficient can be evaluated using an analogy starting from the heat transfer coefficient (a value around 0,17 m/s is reported for stage A(3)). Therefore, a fast gas-solid mass transfer can be assumed for all the stages.

The last matter to discuss here concerns once again the CaO reactivity. Consider a fixed bed reactor. When the gas going up through the reactor meets the unconverted solid (in this case CaO) a reaction front forms in which the reaction (in this case carbonation) takes place.

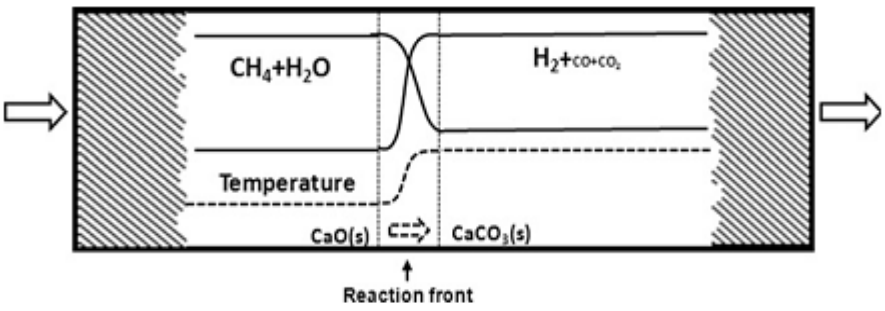

Figure 3: general scheme of the composition and temperature profiles in the reaction front during the SER in a fixed-bed reactor(3).

In the reaction front is concentrated the composition gradient (for the reaction front definition itself) and the temperature gradient (since the heat transfer coefficient is high, as said above). If the reaction rate is high enough (compared to the reactants flow entering the reaction front) there will be a very thin reaction front. The reaction rate depends on the gas diffusion velocity on the solid particles surface and on the reaction kinetic. It has been proved that with a low gas superficial velocity (around 0,5 m/s) and with a properly prepared (synthetic) CaO the SER reactions take place inside a narrow reaction front so that the outlet composition and temperature profile over time follow a step function (see figure 4 case k=3,5 s^{-1}, which corresponds to a carbonation rate around $1{,}11 \cdot 10^{-4}$ kmol/kg·s)(3). The same hypothesis applies also to stages B and C(2)(8)(9).

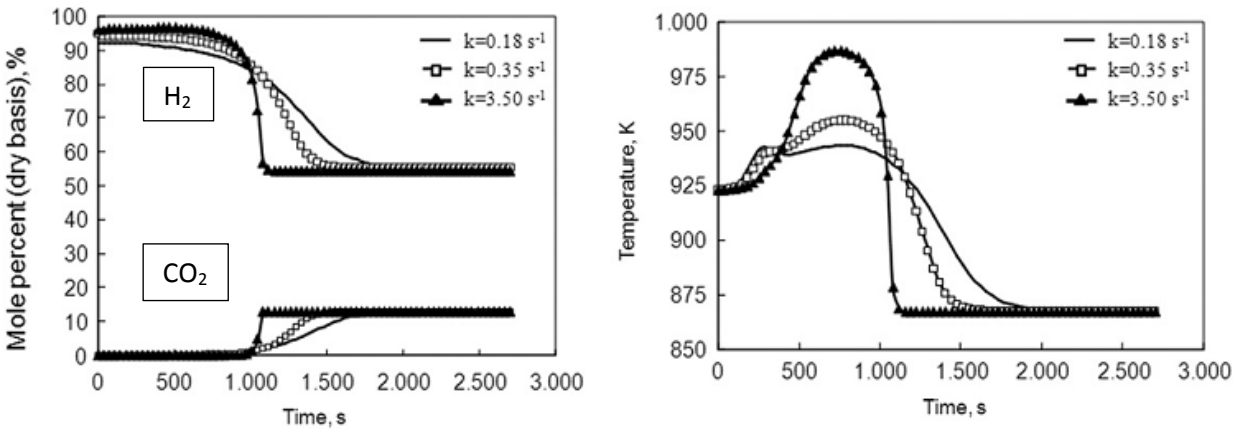

Figure 4: stage A: effect of carbonation kinetics on the product gas composition on a dry basis and on the temperature profile with the reaction time on stream (P=3.5 MPa, S/C=5)(3).

As a consequence, we have assumed that the axial composition and temperature profile inside the bed follow exactly a step function.

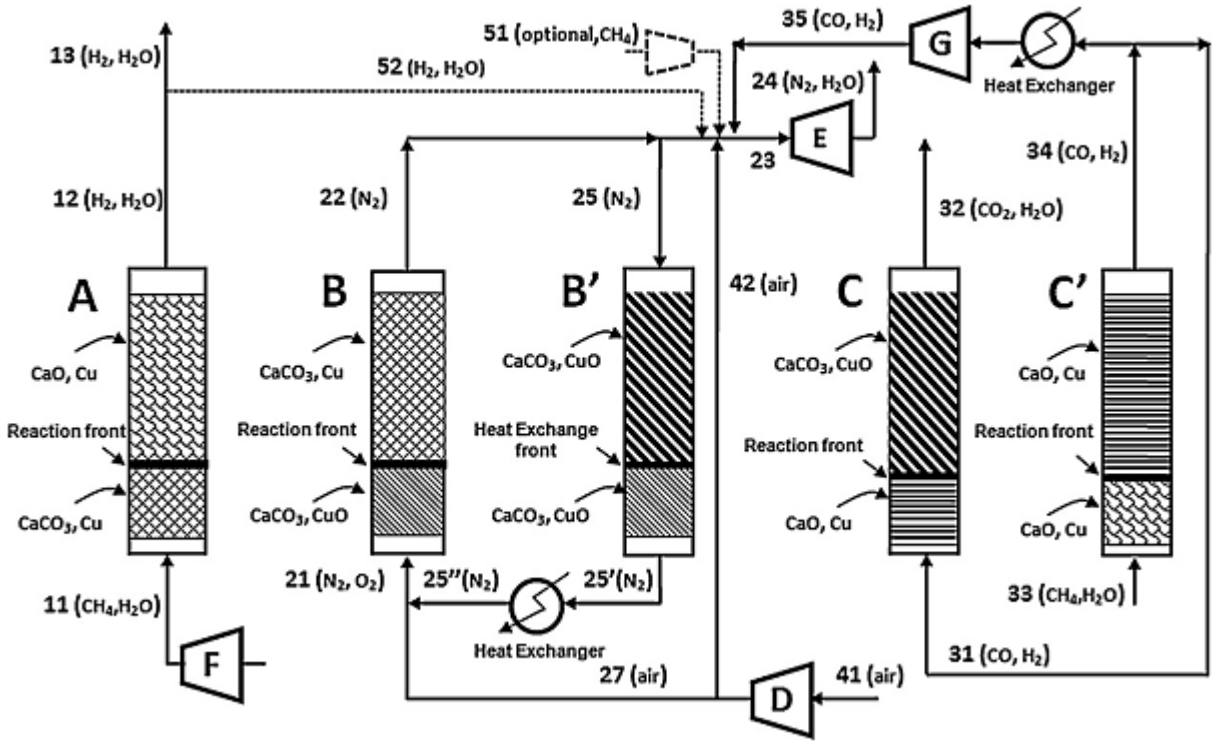

Figure 5: illustration of the Ca-Cu chemical loop(2)

Undoubtedly the assumptions made need to be validated using further experimental data, although there is some experimental evidence of some of them in published works in the literature(11)(12) . Nevertheless, they allow to use a relatively simple model, which is necessary if we aim to assess the performance of the system under different conditions. In particular, no transport partial differential equation has to be solved and the chemistry kinetic is neglected (the reactants are considered to be instantaneously converted into products as they meet).

4.2) Stage A: enhanced steam reforming

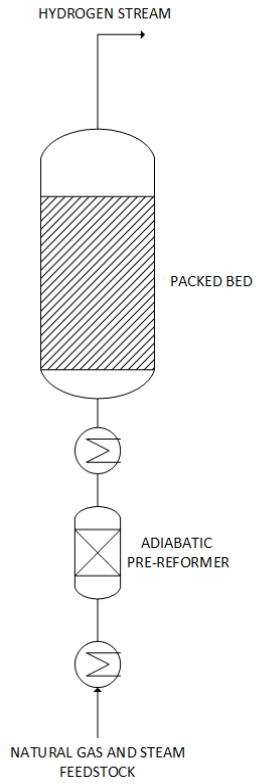

Figure 6: reactor operating in stage A

The natural gas and steam feed is firstly pre-reformed before being sent to stage A. The objective of this pre-reforming is to break down the hydrocarbons heavier than methane, which would lead to solid carbon deposition inside the solid bed; moreover some middle-temperature heat is requalified and converted into syngas chemical energy. An adiabatic pre-reformer stage is considered, working with an inlet temperature around 490 °C (due to the endothermicity of the reforming reactions of hydrocarbons, the outlet temperature is around 420-460 °C for a standard natural gas). The syngas produced is heated to around 700 °C ($T_{gas,in,A}$) to be introduced into the bed. The effect of the gas inlet temperature, as well as of the other operating parameters such as pressure or steam-to-carbon ratio, on the system performance will be evaluated in the sensitivity analysis chapter. The initial composition and temperature of the bed is that of the end of stage C. In figure 6 it is shown the initial temperature of stage A. It is possible to see that the bed is split into two parts: the initial part of the bed is at $T_{gas,in,C}$ (around 700 °C) and the second part of the bed at $T_{max,C}$ (around 860-870 °C). The reason for this temperature profile will be discussed when explaining stage C in the following sections. The initial solid composition of stage A is that of figure 9, zone "c". Figures 7, 8, 9 represent respectively temperature, gas and solid composition profiles over the axial coordinate for stage A at an intermediate time. The plots have been obtained with a steam-to-carbon ratio for stage A of 4 and with a pressure for stages A and B of 25 bar. As already mentioned, the real profiles will not have an exactly step shape, nonetheless this is a convenient and realistic enough assumption.

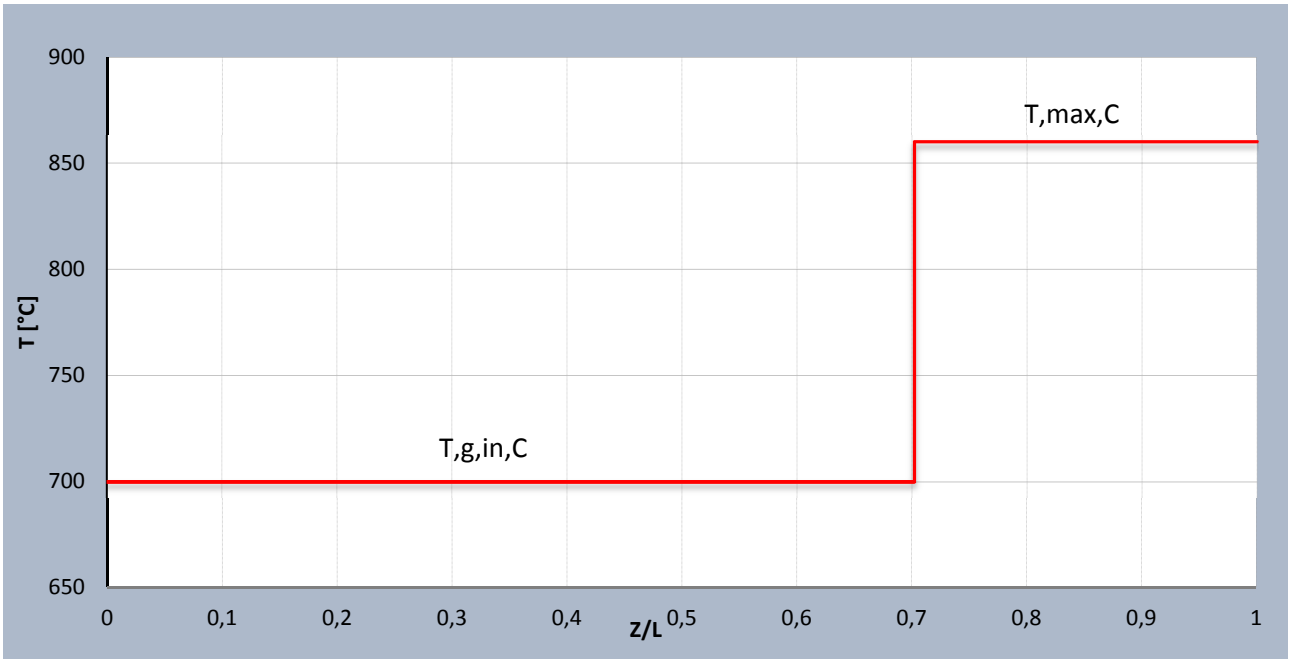

Figure 7: Axial temperature profile at the beginning of stage A (S/C=4; P,A=P,B=25 bar)

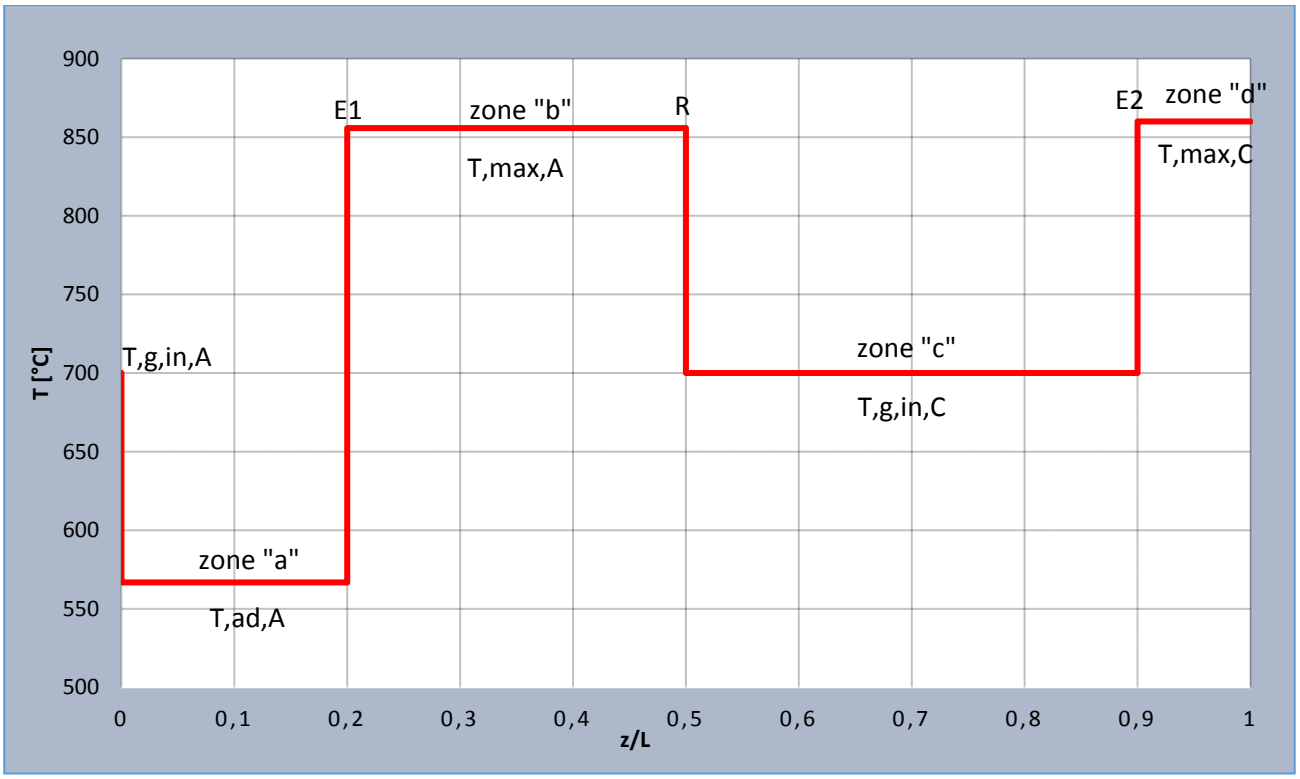

Figure 8: Axial temperature profile at an intermediate time for stage A (S/C=4; P,A=P,B=25 bar). R= reaction front. E1=heat exchange front. E2=second heat exchange front.

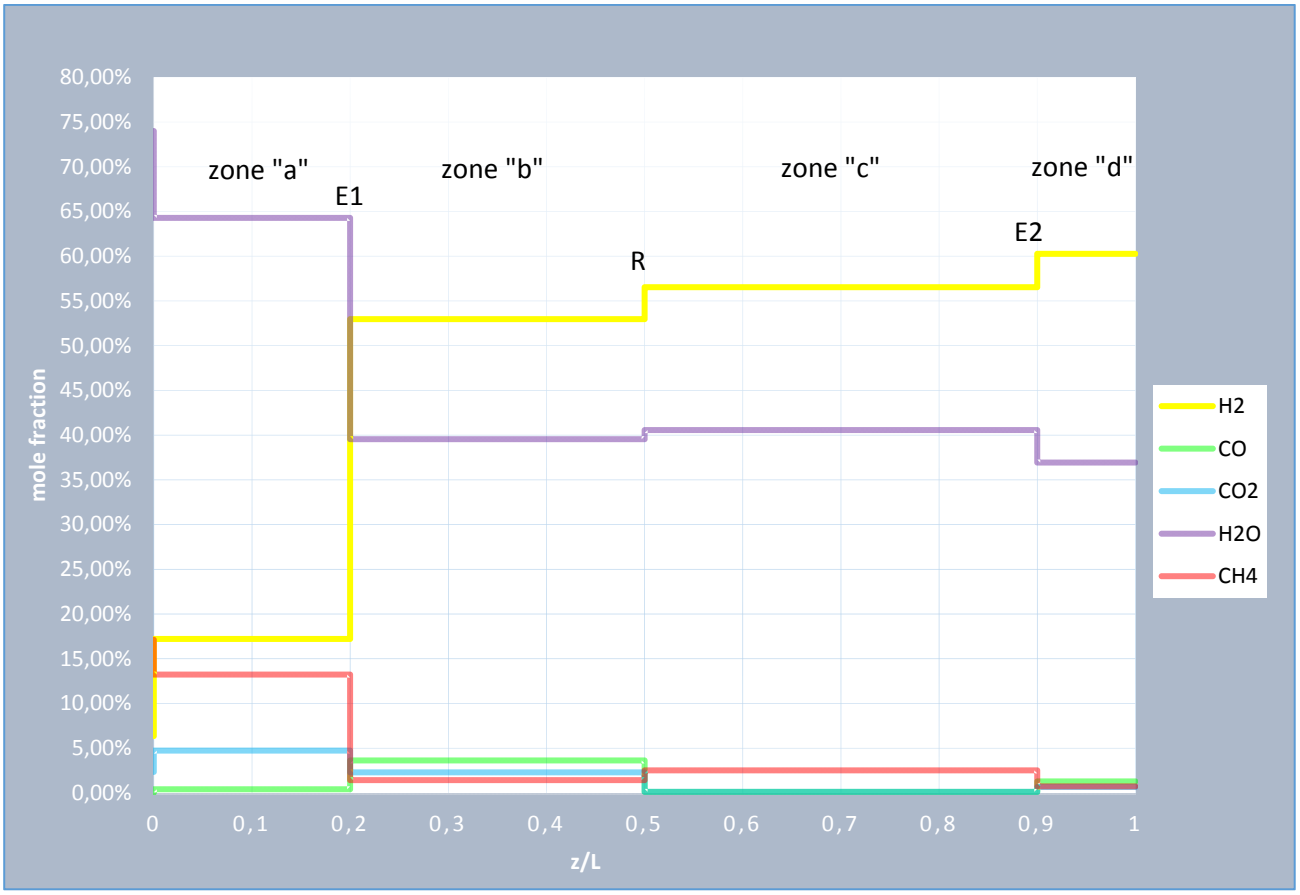

Figure 9: Axial profile of the gas molar composition for stage A at an intermediate time (S/C=4; P,A=P,B=25 bar).

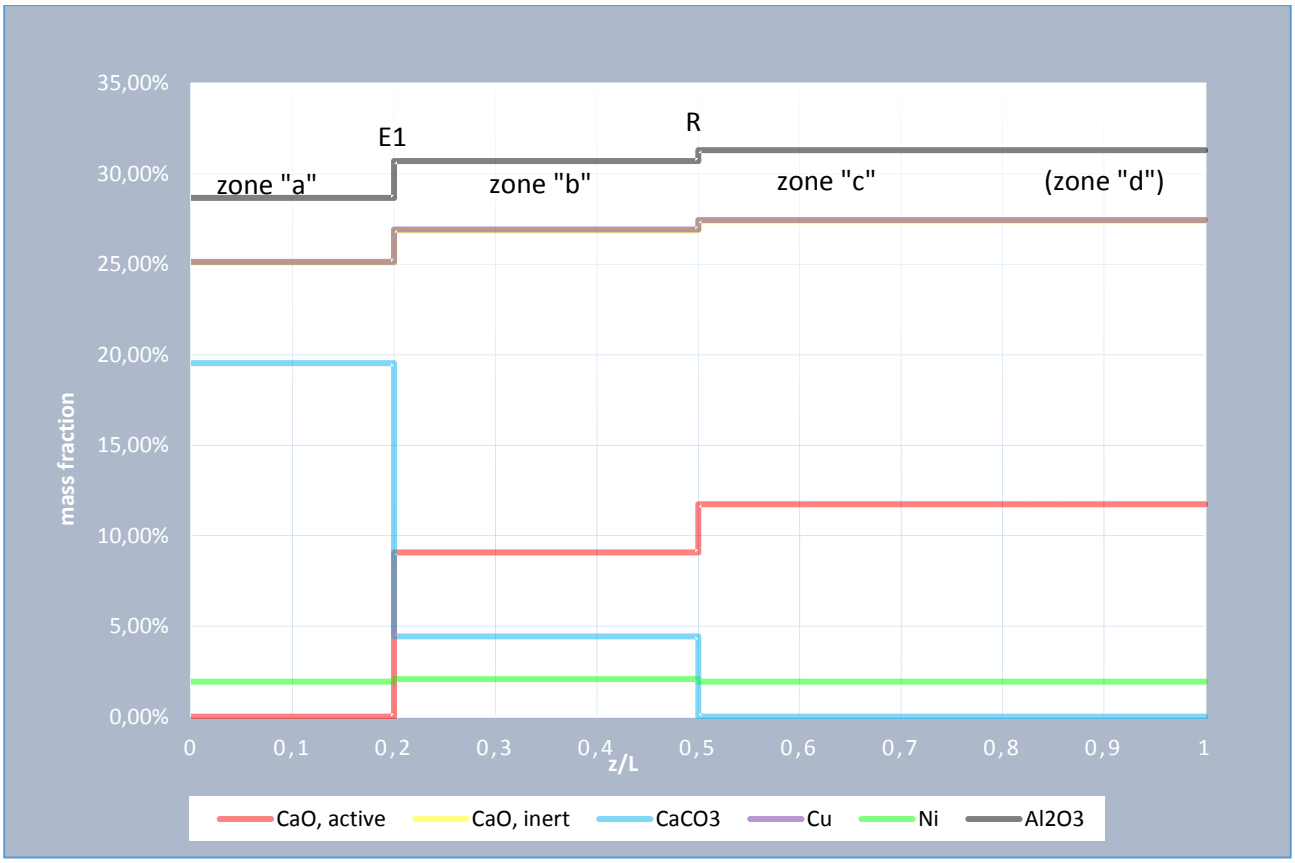

Figure 10: Axial mass composition of the solid for stage A at an intermediate time (S/C=4; P,A=P,B=25 bar). The solid composition in zones "c" and "d" is the same, so the front E2 is not visible. The inert CaO and Cu profiles are almost completely overlapped.

Consider the pre-reformed natural gas entering to the solid bed at the beginning of stage A. In the very first part of the bed the feed gas finds the unconverted solid at $T_{g,in,C}$ (around 700 °C), and it reacts reaching the equilibrium through the SR, WGS and carbonation reactions at $T_{g,in,C}$ (as the reaction front outlet gas temperature has to be equal to that of the solid inlet). After a certain period, the reaction front has covered a certain distance, leaving behind the CaO (partially) converted. Since the SER reactions are overall exothermic, some heat is released into the bed, resulting in an increase of the temperature up to a value of $T_{,max,A}$, and so into the formation of the correspondent heat exchange front (E1) . As a function of the relation between the velocities of the reaction and heat exchange fronts, there may be two options: the heat exchange front lags behind the reaction front, or the opposite. Calculations of these velocities in this stage have shown that the former case is true, so that the heat released in the reaction front is "stored" in the zone behind it. Therefore the gas is firstly heated up to $T_{,max,A}$ by the solid in the heat exchange front and then cooled down to $T_{,g,in,C}$ exiting the reaction front. Looking to figures 7 and 8, it can be appreciated that the gas enters at $T_{,g,in,A}$, and it finds the first fraction of the solid already converted (so that there is no active CaO for reacting with the CO2), and therefore reactions of SR and WGS occur, resulting in a temperature decrease. The temperature reached at this first part of the reactor ($T_{ad,A}$) corresponds to that from equilibrium through the SR and WGS reactions. After crossing zone "a", the gas meets the hot, partially converted solid left behind by the reaction front. The gas exits the heat exchange front (E1) at the solid inlet temperature ($T_{,max,A}$), in equilibrium with SR, WGS and carbonation. In fact, at such a high temperature as $T_{,max,A,}$ the carbonation of CaO in the reaction front is not complete and some active CaO is left behind. On the contrary, at $T_{,ad,A}$ it is possible to assume that all the active CaO has been converted to $CaCO_3$, so that no active CaO is left behind by the heat exchange front. After crossing zone "b", the gas reaches the reaction front, from which it exits at $T_{,g,in,C}$ in equilibrium with SR, WGS and carbonation. Therefore, some carbon is captured inside the heat

exchange front (where the gas meets for the first time the hot, unconverted, CaO) and some in the reaction front (where the gas is cooled down and the carbonation can proceed). Before to get out, the gas exiting the reaction front (in which carbon is mainly present in the form of methane) crosses zone "c" and reaches the last part of the bed, at $T_{,max,C}$, in the second heat exchange front (E2). Here the gas is heated up to $T_{,max,C}$ so that most of the residual methane is converted. In spite of the high temperature, there is no risk of calcination in zone "d", since there is no carbonate.

Stage A ends when the heat exchange front (E1) reaches the top of the bed, which is left at $T_{,ad,A}$. As a result, the syngas outlet temperature and composition changes with time. In the first period the syngas exits at $T_{,max,C}$ with the composition of zone "d". This is the best possible composition, since the carbon content is the same as for zone "c" but the residual methane is much lower and therefore the hydrogen content is higher. In the second period it exits at $T_{,g,in,C}$ with the composition of zone "c". In the third (and last) period it exits at $T_{,max,A}$ with the composition of zone "b". The last one is the worst composition, as it contains a significant amount of carbon compounds, since at $T_{,max,A}$ the carbonation is negligible. The higher is $T_{,max,A}$, the higher is the carbon content of the gas exiting with composition "b" as a consequence of the exothermicity of carbonation.

Finally, it has been considered the possibility of having CaO hydration during the process. If the steam partial pressure exceeds a limit value, the following reaction may occur:

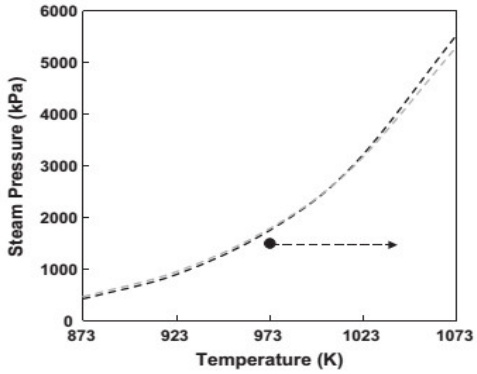

Figure 11: CaO hydration equilibrium(6)

$$CaO + H_2O \rightarrow Ca(OH)_2$$

The formation of $Ca(OH)_2$ is competitive with carbonation, reducing the amount of available CaO for reacting with the CO_2. If $Ca(OH)_2$ is formed in the outer part of the particles, an inner core of unreacted CaO inside a $Ca(OH)_2$ shell will result, preventing the CO_2 diffusion towards the inner core and so leaving some CaO unconverted. Moreover, the higher volume of the $Ca(OH)_2$ with respect to that of CaO may result in the breakdown of the CaO particles. For these reasons, the operating conditions of stage A, which is the one working under conditions closest to hydration ones, have to be chosen so to maintain the steam partial pressure under the equilibrium value that is indicated in figure 10. As appreciated from this figure, hydration is favoured at low temperatures and high steam partial pressures. Therefore, it is important to check for this problem is zone "c", where the temperature decreases, and in zone "a" where the steam partial pressure is maximum. In zone 'c', the temperature is around 700°C, corresponding to a limit steam partial pressure around 17,6 bar, while the real steam partial pressure (in the case above, with S/C=4 and p=25 bar) is 10,1 bar, so that there should be no hydration. On the contrary, in zone "a", the temperature is lower and the steam concentration is higher, but since there is no active CaO in this zone, theoretically, there should be no problem. Actually, the hydration issue under the operating conditions in stage A is being studied in detail through experimental tests by different research groups worldwide, which will provide future guidelines for the development of SER processes using CaO-sorbents.

4.2.1) Stage A: calculation method

In this section it is briefly explained the procedure followed to evaluate the performance of stage A. Despite the complexity of the process to be studied, it is possible to evaluate its performance considering mass and energy balances, regardless of the time variable and of the size of the bed. Once the operating conditions have been set and the beds number and size determined, it will be possible to account for the gas flow over time.

For making a first calculation of stage A, it is considered a solid bed containing 1 kmol of active CaO as a reference value. The amount of Cu needed will be determined with the energy balance to stage C of the process. For making a first calculation of stage A, an initial amount of Cu can be assumed (i.e. 2 kmol Cu), which will be updated when solving the corresponding energy balance. The corresponding amount of Ni and Al_2O can be determined with the assumptions about the solid composition made in chapter 4.1. Making a guess about the solid fraction left hot at the end of stage C, the solid composition and temperature at the beginning of stage A is determined.

The calculation can be split into seven main steps ("nothing is particularly hard if you divide it into small jobs"). The operating conditions for stage A to which the following results refer to are those given in table 1. No pressure drop is taken into account so far.

stage A		
T,gas,in,pre-ref=	490	°C
P,in,pre-ref=	25	bar
p,in,A=	25	bar
S/C=	4	
T,gas,in,A=	700	°C

Table 1: operating conditions for stage A, in the case considered here.

Step 1:

The amount of natural gas required to convert the whole bed is not known. It is considered a natural gas molar flow of 1 kmol/s fed into the pre-reformer, together with the corresponding steam flow. This assumption on the mass flow rate does not affect the results, it just allow to compute the gas molar flow crossing the several bed sections. With a higher natural gas molar flow higher fronts velocities would result, but the compositions and temperatures would remain the same. Therefore, in the first step of the calculation process, the composition of the gas exiting the adiabatic pre-reformer (that is the composition of the gas entering stage A) is calculated imposing the chemical equilibrium and the energy balance into this adiabatic process. Table 2 shows the composition of the gas at pre-reformer inlet and outlet (the natural gas composition has been specified in ch. 4.1).

	n, in, pre-ref [kmol/s]	n, out, pre-ref [kmol/s]
H2	0,00	0,35
N2	0,01	0,01
CO	0,00	0,00
CO2	0,02	0,13
AR	0,00	0,00
CH4	0,89	0,95
H20	4,34	4,11
C2H6	0,07	0,00
C3H8	0,01	0,00
C4H10	0,00	0,00
T [°C]	490	428,45

Table 2: Adiabatic pre-reformer inlet and outlet streams.

Step 2:

The composition and temperature in zone "a" during stage A of the Ca-Cu process is calculated, imposing the chemical equilibrium of SR and WGS and the energy balance. Table 3 shows the results of this calculation.

	n, in, A [kmol/s]	n, zone "a" [kmol/s]
H2	0,35	1,02
N2	0,01	0,01
CO	0,00	0,02
CO2	0,13	0,28
AR	0,00	0,00
CH4	0,95	0,78
H20	4,11	3,80
T [°C]	700,00	566,81

Table 3: streams entering stage A and crossing zone "a" of stage A

Step 3:

Since the reaction front gas outlet temperature is already known ($T_{,g,in,C}$), it is possible to determine the gas composition in zone "c", imposing the equilibrium of SR, WGS and carbonation, starting from the composition in zone "a" (the values are reported in the next step). Note that the solid composition in zones "a" and "c" is known: in the first zone all the active CaO has been converted to $CaCO_3$, in the second there is no $CaCO_3$ (since the reaction front is yet to come).

Step 4:

In this step the gas and solid compositions in zone "b" as well as $T_{,max,A}$ are computed simultaneously, imposing one energy balance and one carbon balance for both the reaction front and the heat exchange front (E1).

Considering that v_{gas} is the superficial velocity of the gas inside the bed and v_{front} is the velocity at which the heat exchange front E1 moves along the bed, the gas molar flow entering this heat exchange front E1 can be calculated as:

$$n_{gas,in,E1} = (v_{gas} - v_{front}) \cdot A \cdot (1 - \varepsilon_s) \cdot \rho_{gas,in,E1} \cdot \frac{1}{M_{gas,in,E1}} \quad \text{[kmol/s]} \quad (1)$$

In this fixed bed operation, the solid is still while the fronts cross it. Therefore, the solid molar flow entering the heat exchange front could be written as:

$$n_{solid,in,E1} = v_{front} \cdot A \cdot \varepsilon_s \cdot \rho_{solid,in,E1} \cdot \frac{1}{M_{solid,in,E1}} \quad \text{[kmol/s]} \quad (2)$$

Where ε_s is the bed package density.

Consider now an ideal case in which the front is not moving and the solid is entering the front with a velocity so that the mass and energy balances at the front are fulfilled. The gas molar flow entering the front, if it is not moving, is:

$$n_{gas,in,E1,fake} = v_{gas} \cdot A \cdot (1 - \varepsilon_s) \cdot \rho_{gas,in,E1} \cdot \frac{1}{M_{gas,in,E1}} \quad \text{[kmol/s]} \quad (1a)$$

To fulfil the balances, the ratio between gas and solid molar flows has to be the same as in the real case, hence the solid molar flow entering the front is:

$$n_{solid,in,E1,fake} = v_{front} \cdot \frac{v_{gas}}{v_{gas} - v_{front}} \cdot A \cdot \varepsilon_s \cdot \rho_{solid,in,E1} \cdot \frac{1}{M_{solid,in,E1}} \quad \text{[kmol/s]} \quad (2a)$$

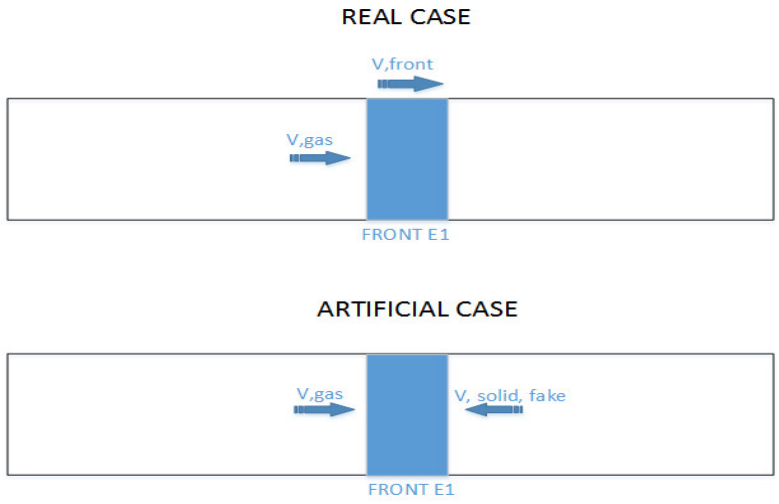

Figure 12: heat exchange front in the real and in the artificial case

The advantage of such abstraction is that the gas flow entering the front is the real gas flow, which is known once the natural gas feed flow has been set. For example, the gas fake molar flow entering the front E1 is equal to the gas molar flow computed in step 2 (zone "a").

Once made these considerations, the whole problem can be reduced, formally, in a two equations in two unknowns system. The two unknowns, for which we have to guess a first attempt value, are the temperature in zone "b" ($T_{,max,A}$) and the $CaCO_3$ molar concentration in the solid in zone "b" (x_{CaCO3}^{b}). The gas fake molar flow entering the front E1 is known (it is equal to the gas molar flow in zone "a"). Then we can compute the gas molar flow in zone "b", imposing the equilibrium of SR, WGS and carbonation at $T_{,max,A}$, which corresponds to the gas molar flow exiting the front E1. The carbon flow captured in the front E1 is now known. It is possible to determine the solid fake molar flow entering the front E1 using a carbon balance:

$$n_{C,captured,E1,fake} = n_{C,gas,in,E1,fake} - n_{C,gas,out,E1,fake} = n_{solid,E1,fake} \cdot (x^{a}_{CaCO3} - x^{b}_{CaCO3}) \quad \text{[kmol/s]}$$

Remind that the total solid molar flow entering and exiting the front are equal, since carbonation does not entail a change in the mole number. The molar concentration of $CaCO_3$ in the solid in zone "a" is equal to the molar concentration of active CaO in the solid in zone "c" (which is known).

Similarly we can compute the solid fake molar flow entering the reaction front (remind that there is no $CaCO_3$ in zone "c"):

$$n_{C,captured,R} = n_{C,gas,in,R} - n_{C,gas,out,R} = n_{solid,R} \cdot x^{b}_{CaCO3} \quad \text{[kmol/s]}$$

Now that the solid fake molar flows crossing the fronts are known, we can write two energy balances, one at the heat exchange front and one at the reaction front, to determine $T_{,max,A}$ and $x_{CaCO3}{}^{b}$.

	n, zone "b" [kmol/s]	n, zone "c" [kmol/s]
H2	3,54	3,53
N2	0,01	0,01
CO	0,24	0,01
CO2	0,15	0,01
AR	0,00	0,00
CH4	0,10	0,16
H20	2,64	2,53
T [°C]	855,78	700,00

Table 4: streams in zones "b" and "c" of stage A

solid molar composition			
	a	b	c
CaO,active	0,00%	11,20%	14,21%
CaO,inert	33,16%	33,16%	33,16%
Cu	29,33%	29,33%	29,33%
Al2O3	20,85%	20,85%	20,85%
Ni	2,44%	2,44%	2,44%
CaCO3	14,21%	3,01%	0,00%

Table 5: solid molar composition in zones "a", "b" and "c" of stage A

Step 5:

The gas molar flow crossing zone "d" is calculated imposing the equilibrium condition of SR and WGS at $T_{,max,C}$. Due to the high temperature in this zone, carbonation reaction is no longer favoured. In fact, the gas entering E2 has a carbon content dictated by equilibrium at $T_{,g,in,C}$, which is lower than $T_{,max,C}$. Therefore, considering carbonation equilibrium at $T_{,max,C}$, a carbon content in zone "d" higher than that in zone "c" would result, meaning that some carbon dioxide has been set free by the solid in E2. However, since there is no $CaCO_3$ to calcine in zone "d", CO_2 concentration in the gas phase cannot increase in this region. However, due to the increase in the temperature, H2 content in the gas phase raises as a result of the SR and WGS equilibrium.

	n, zone "d" [kmol/s]
H2	3,89
N2	0,01
CO	0,08
CO2	0,04
AR	0,00
CH4	0,05
H20	2,39
T [°C]	860

Table 6: stream crossing zone "d" of stage A

Step 6:

Finally it is calculated the amount of natural gas to be fed to stage A of the process to convert the whole bed (in terms of kmol) and, at the same time, the amount and composition of the gas produced.

First, we can calculate the amount of natural gas required to convert the hot bed fraction (at $T_{,max,C}$) in zone "d" and so the amount of syngas exiting with composition "d". We have used a simple energy balance to do so: the heat released by cooling the hot bed fraction from $T_{,max,C}$ to T,g,in,C has to be equal to the energy absorbed by the gas to pass from composition "c" (at $T_{,g,in,C}$) to composition "d" (at $T_{,max,C}$).

The amount of gas exiting with composition "c" and "b" can then be calculated imposing an overall energy balance and an overall carbon balance, as follows. Bear in mind that all the temperature and compositions are known by now.

$$H_{solid}^{initial} - H_{gas}^{initial} = H_{solid}^{final} - H_{gas}^{final} \qquad \text{[kj]}$$

$$n_{carbon}^{gas,initial} = n_{carbon}^{gas,final} + n_{CaCO3,solid}^{final} \qquad \text{[kmol]}$$

	n,in,A [kmol]	n,out,b [kmol]	n,out,c [kmol]	n,out,d [kmol]	n,out,A [kmol]	x,out	x,out,dry
H2	0,47	2,36	1,04	1,44	4,84	55,72%	91,41%
N2	0,01	0,01	0,00	0,00	0,01	0,14%	0,22%
CO	0,00	0,16	0,00	0,03	0,19	2,24%	3,68%
CO2	0,17	0,10	0,00	0,02	0,12	1,39%	2,28%
AR	0,00	0,00	0,00	0,00	0,00	0,00%	0,00%
CH4	1,27	0,06	0,05	0,02	0,13	1,47%	2,41%
H20	5,47	1,76	0,74	0,88	3,39	39,04%	

Table 7: total number of moles exiting stage A, corresponding to a sorbent (active CaO) amount of 1 kmol.

Step 7:

In the last step velocities of the reaction and heat exchange fronts are calculated, which allows determining position of each front at any time during stage A. This is important not only to verify the initial hypothesis that E1 lags behind R, but it can also be used to validate the results of step 6. Besides, it is useful to check that the front R does not reach the end of the reactor before the front E2, as supposed for the calculations.

The velocity of the fronts can be evaluated by equation 2a of step 4, once the solid fake molar flows entering the fronts have been evaluated using the mass/energy balances. In step 4 we found $n_{solid,fake,E1}$ = 5,29 kmol/s and $n_{solid,fake,R}$ = 10,62 kmol/s. It is possible to determine the solid fake flow entering E2 using an energy balance at such front, which gives $n_{solid,fake,E2}$ = 5,62 kmol/s.

Considering a cross-section of 1 m^2, the following heat exchange and reaction fronts velocities result: V_{E1} = 0,17 m/s, V_R = 0,33 m/s and V_{E2} = 0,17 m/s. As mentioned above, these values refer to a natural gas inlet flow of 1 kmol/s and a section area of 1 m^2, which are just reference values (in fact, the corresponding gas superficial velocity in zone "b" is around 50 m/s, which is not acceptable). In chapter 4.7.1 we address the issue of the beds size and number and the stages duration, now we are just interested in the system performance.

To validate the results obtained with our simplified method, in table 8, we have compared them with those obtained with a "complete" method, originally developed by V. Spallina et al. (13).

RESULTS VALIDATION						
operating conditions						
P [bar]=	20					
T,gas,in,pre-ref. [°C]=	490					
T,gas,in,A [°C]=	700					
S/C=	4					
results comparison: complete (reference) vs simplified method						
	zone "a"		zone "b"		zone "c"	
gas composition (%mol)	ref.	simpl.	ref.	simpl.	ref.	simpl.
H2	18,5%	18,0%	54,0%	53,4%	56,9%	57,5%
N2	0,2%	0,2%	0,1%	0,1%	0,1%	0,1%
CO	0,7%	0,4%	3,0%	3,7%	0,1%	0,1%
CO2	4,8%	4,9%	2,0%	2,4%	0,0%	0,2%
AR	0,0%	0,0%	0,0%	0,0%	0,0%	0,0%
CH4	12,8%	13,0%	1,5%	1,2%	2,4%	2,2%
H20	63,0%	63,6%	39,4%	39,1%	40,6%	39,9%
solid composition (%mass)						
CaO,active	0,0%	0,0%	8,5%	9,0%	10,5%	11,5%
CaO,inert	26,5%	24,7%	28,0%	26,4%	28,7%	26,9%
Cu	25,0%	25,7%	26,5%	27,5%	27,2%	28,1%
Al2O3	29,0%	28,8%	31,0%	30,8%	31,6%	31,4%
Ni	2,0%	1,9%	2,0%	2,0%	2,0%	2,1%
CaCO3	17,0%	19,3%	3,0%	4,3%	0,0%	0,0%
T [°C]=	561	564	847	844	700	700

Table 8: results validation, stage A

4.3) Stage B: bed oxidation

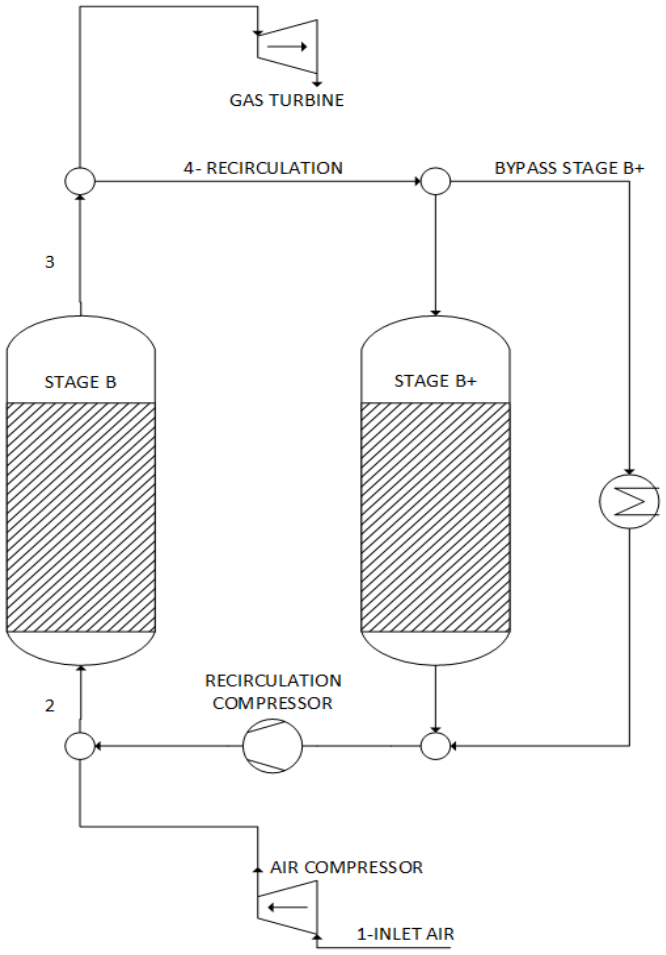

Figure 13: reactors operating in stages B and B+

During stage B the copper (and nickel) oxidation takes place, so that, in the subsequent stage C the oxygen is available for the fuel oxidation, which supplies the required energy for the $CaCO_3$ calcination. Since the Cu oxidation is strongly exothermic, there is a sharp temperature rise inside the reaction front.

$Cu^{(s)} + \frac{1}{2}O_2 \rightarrow CuO^{(s)}$ ΔH^0_r = -156,1 kj/mol

$Ni^{(s)} + \frac{1}{2}O_2 \rightarrow NiO^{(s)}$ ΔH^0_r = - 240 kj/mol

In order to increase the overall energy efficiency, the stage B outlet gas temperature should be as high as possible. Unfortunately, there are some limitations. Firstly, it has been proved that CuO tends to decompose and agglomerate at temperatures above 950 °C (8) (other studies report an even lower temperature (5)). Secondly, and more importantly, there is the issue of $CaCO_3$ calcination, that must be avoided. In fact, when the $CaCO_3$ is heated up to a high temperature in a CO_2-poor atmosphere (as that of stage B), it tends to release the CO_2 captured (according to the equilibrium condition mentioned at the beginning of chapter 4). The calcination in stage B has to be kept to a minimum since it affects the carbon capture ratio (defined as

the ratio between the carbon dioxide molar flow exiting stage C and the carbon molar flow entering the plant with natural gas).

Calcination can be effectively limited in two ways: increasing the pressure (calcination entails an increase in moles number) and reducing the oxidation temperature. The oxidation temperature depends on the oxygen concentration in the gas entering the reaction front (and the Cu concentration in the solid) and on its temperature. It has been demonstrated in literature (2)(8) that to limit the oxidation temperature during stage B operation to reasonable values (around 830-850°C), it is necessary to recirculate a fraction of the O2-depleted gas stream exiting stage B to maintain O2 contents at stage B inlet below 6% (usually around 2,8-4%). Thus, the non-recycled gas from stage B is sent to a gas turbine, while the recycled fraction is cooled down before being mixed with the inlet air to stage B. The oxygen content in the inlet stream of stage B is regulated by the recirculation ratio, which is defined as the ratio between the recirculation flow and the flow exiting stage B. For achieving O2 contents of around 1.5-3% at stage B inlet, such recirculation ratio results to values around 85-89%. In addition, the other parameter to control is the gas inlet temperature (point 2 in figure 11). Such temperature is usually in the range 150-340 °C. Considering the possibility of acting on both operating variables, for a given objective value of $T_{,max,B}$, the higher is $T_{,gas,in,B}$, the higher must be the recirculation ratio.

As will be seen later on, the electric consumption associated to the fan needed for recirculating this O2-depleted gas into stage B represents an important operating cost to be considered when deciding about these operating variables.

The plots below represent temperature, gas and solid composition profiles at an intermediate time for stage B. The operating conditions chosen for these figures are $p_{,B}$ = 25 bar, $T_{,gas,in,B}$ = 300 °C and $T_{,max,B}$ = 830 °C.

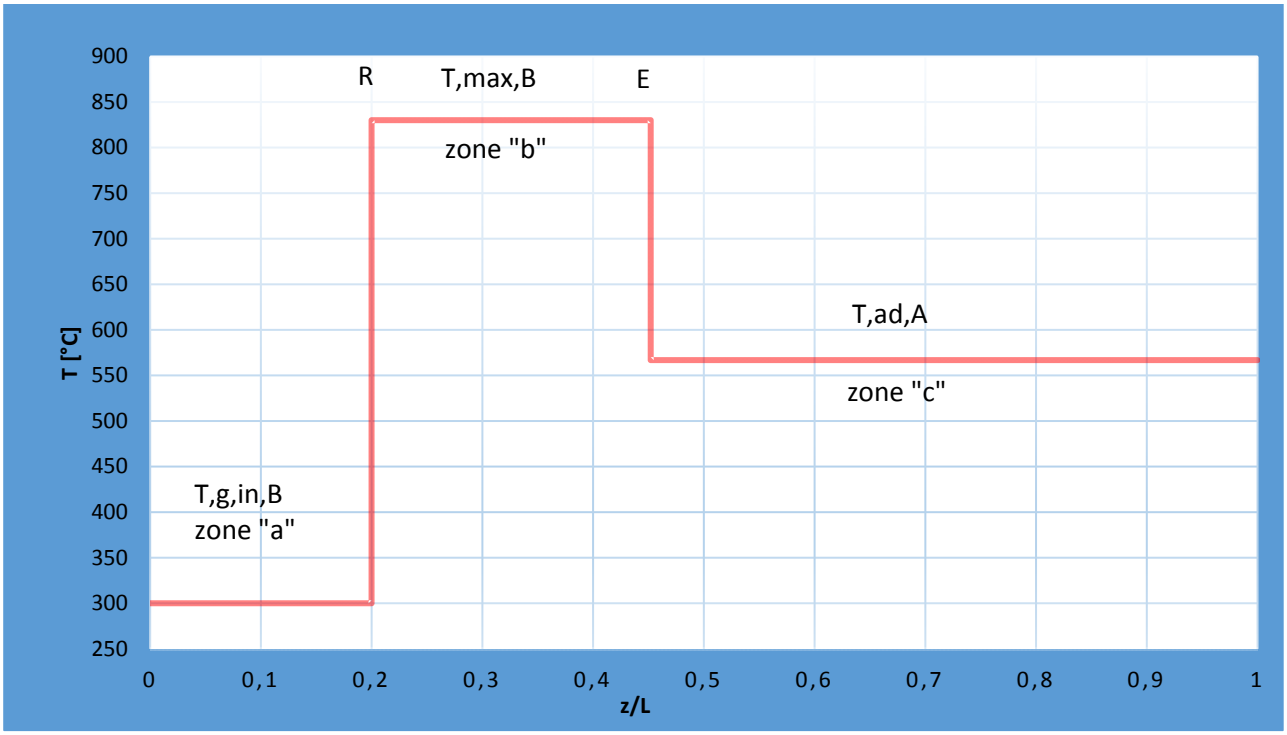

Figure 14: stage B: axial temperature profile at an intermediate time

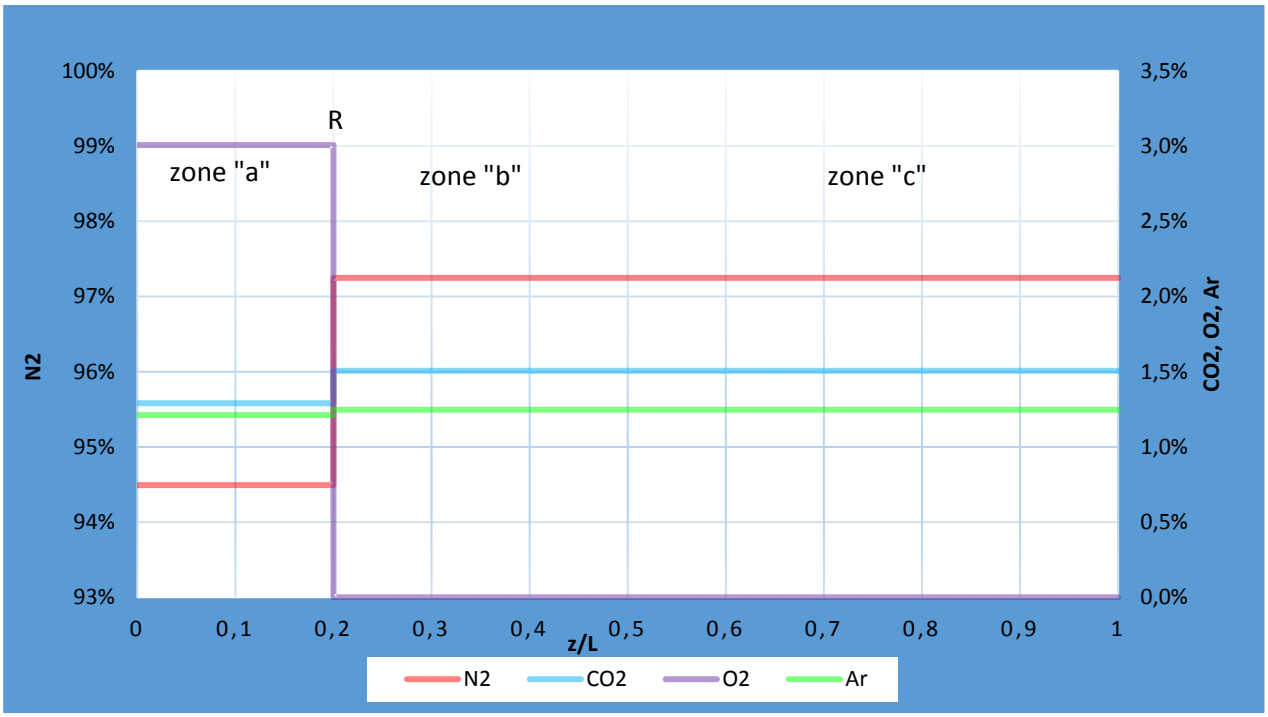

Figure 15: stage B: axial gas molar composition profiles at an intermediate time. N2 content on the left axis. CO2, O2, Ar contents on the right axis.

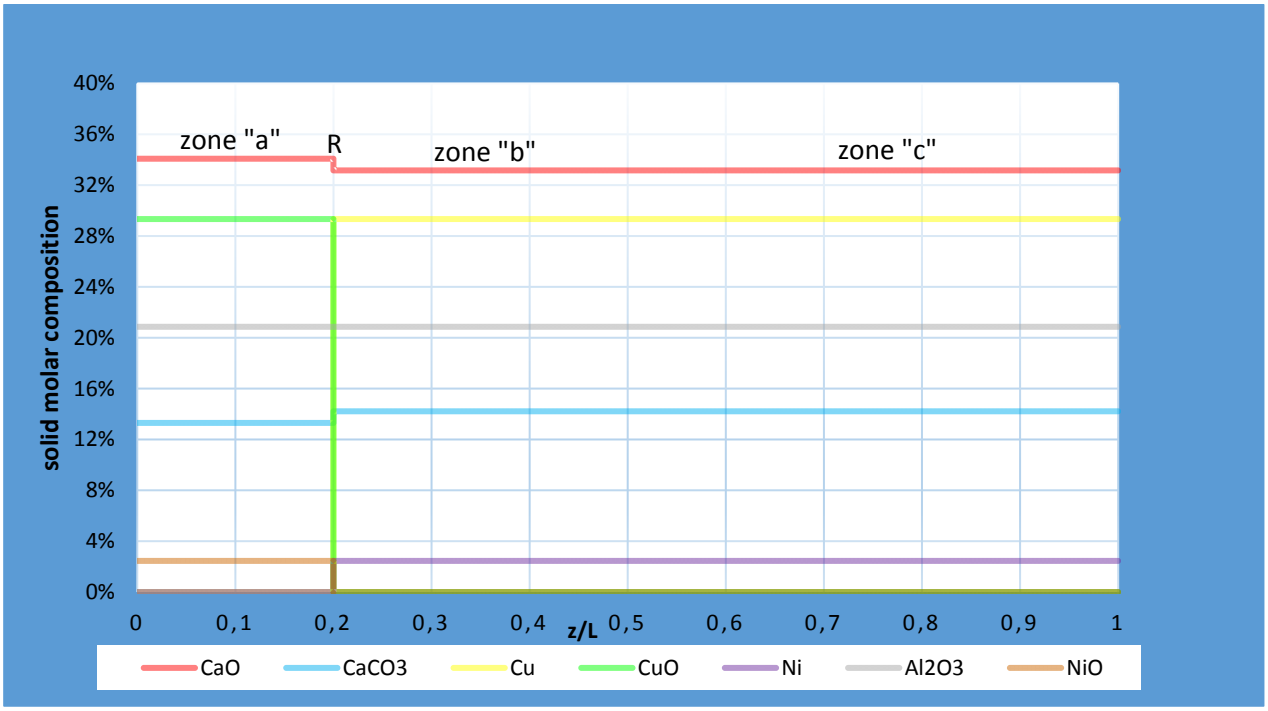

Figure 16: stage B: axial solid molar composition at an intermediate time.

The high oxygen dilution required for limiting temperature during stage B leads to a low reaction front velocity inside the reactor, which results into a heat exchange front going faster (see fig. 13). For this reason, the maximum oxidation temperature achieved during this stage is not affected by the initial solid temperature ($T_{,ad,A}$).

Inside the reaction front takes place not only the solid oxidation, but also the partial calcination of the $CaCO_3$ present in the bed. Therefore, the CO_2 partial pressure in the gas exiting such reaction front is that corresponding to equilibrium at T,max,B. In the conditions mentioned above, the CO2 content in the outlet gas is around 1,5%, which corresponds to a calcination of 6,4% of the $CaCO_3$ present in the bed at the beginning of stage B.

Stage B ends when the reaction front reaches the end of the bed. As figure 12 reveals, the gas outlet temperature changes with time. In a first period the nitrogen-rich stream exits at $T_{,ad,A}$ (the solid initial temperature for stage B), then it exits at T,max,B. In order to maximise the overall efficiency it would be reasonable to recirculate the gas exiting at $T_{,ad,A}$ and the required fraction of that exiting at $T_{,max,B}$ and so send to the gas turbine the remaining gas at $T_{,max,B}$. However, from an operational point of view, it is much simpler to mix the gas exiting from the several stages B working in parallel in a vessel, obtaining a gas at an adiabatic mixing temperature ($T_{,rec}$). Therefore, the temperature of the gas recirculated is $T_{,rec}$.

At the end of stage B the bed is fully oxidized and its temperature is $T_{,g,in,B}$. Such temperature is too low for the subsequent stage C to initiate since reduction reactions are not favoured at such a low temperature. Moreover, considering the energy balance into stage C, the higher is the bed temperature at the beginning of stage C, the lower is the amount of Cu needed in the process and so the amount of fuel required to reach the $T_{,max,C}$ target. Based on these facts, a heat exchange stage is introduced into the Ca-Cu process between stages B and C (called stage B+), for heating up the solid bed. During stage B+ the recirculation flow from stage B (flow 4 in fig. 11) is sent into a reactor which has completed stage B. In this way, its temperature can be raised to the recirculation temperature ($T_{,rec}$). Actually, since the recirculation ratio needed for achieving a reduced O2 content at stage B inlet is very high, only a fraction of the recirculated flow is required to perform stage B+. Consequently, the recirculated flow at $T_{,rec}$ is split into two flows: one is sent to stage B+, whereas the other is cooled in a heat exchanger. It is important to note that, if all the recirculated flow at $T_{,rec}$ is sent to stage B+, the heat exchange front in such stage would reach the end of the reactor before the end of stage B and so some gas would exit stage B+ at $T_{,rec}$, being then necessary to cool it down in a heat exchanger.

4.3.1) Stage B: calculation method.

The calculation procedure of this stage is explained in this section for the operating conditions given in table 8.

stage B		
T,g,in,B =	300	°C
p,B =	25	bar
T,max,B =	830	°C

Table 9: operating conditions for stage B, in the case analysed here

Step 1

The amount of Cu and Ni present in the solid bed is known (in this case respectively 2,06 and 0,17 kmoles), and therefore the total amount of oxygen (and so of air) to be fed (5,32 kmoles air) is also known assuming that the O_2 conversion is complete and that the stoichiometric amount of O_2 is fed into this reactor. To make it as simple as possible, an air inlet flow of 5,32 kmol/s is assumed. The air (molar) composition is 78% N_2, 21% O_2 and 1% Ar.

The stream entering stage B (flow 2 in fig. 22) depends on the recirculation ratio (named R in the following), which is chosen so to reach the $T_{,max,B}$ target. For a given value of R, the inlet gas flow is known (the numbers in superscript refer to the flows of fig. 12):

$$n_{N2}^2 = n_{N2}^3 = \frac{n_{N2}^1}{1-R}$$

$$n_{Ar}^2 = n_{Ar}^3 = \frac{n_{Ar}^1}{1-R}$$

$$n_{O2}^2 = n_{O2}^1, \quad n_{O2}^4 = n_{O2}^3 = 0$$

$$n_{CO2}^2 = n_{CO2}^4 = R \cdot n_{CO2}^3, \quad n_{CO2}^4 = (n_{N2}^4 + n_{Ar}^4) \cdot \frac{x_{CO2}^4}{1 - x_{CO2}^4}$$

Where x_{CO2}^4 is the carbon dioxide content in the gas exiting the reaction front (and so in the outlet gas):

$$x_{CO2}^4 = \frac{1}{p \cdot K_{carbonation(T,max,B)}}$$

The gas fake molar flow entering and exiting the reaction front are respectively equal to the gas flow entering and exiting stage B. We can determine the solid fake molar flow crossing the reaction front imposing the oxygen balance. Since we have considered 1 second as reference time for stage B, we find that the solid fake flow entering the reaction front is numerically equal to the amount of solid in the bed at the beginning of stage B (7,04 kmol/s).

Finally we can find R with an energy balance at the reaction front, imposing the $T_{,max,B}$ target (R = 88,2%). Since the reaction front outlet and inlet gas composition is known, the amount of $CaCO_3$ calcined is also known.

gas molar flow			
	n, air [kmol/s]	n, in, B [kmol/s]	n, out, B [kmol/s]
N2	4,15	35,14	35,14
CO2	0,00	0,48	0,54
Ar	0,05	0,45	0,45
O2	1,12	1,12	0,00

solid composition		
	n, B, initial [kmol]	n, B, final [kmol]
CaO	2,33	2,40
CaCO3	1,00	0,94
Cu	2,06	0,00
CuO	0,00	2,06
Ni	0,17	0,00
NiO	0,00	0,17
Al2O3	1,47	1,47

Table 10: molar flow entering and exiting stage B and solid composition at the beginning and at the end of stage B

Step 2

At this point it is known the solid initial and final temperature and composition of stage B. Since we also know the composition and inlet temperature of the gas it is possible to use an overall energy balance (between the gas and solid at the beginning and at the end of stage B) to determine the fraction of gas exiting cold (at $T_{,ad,A}$), and the remaining fraction exiting at $T_{,max,B}$. In this case 55,8% of the gas exits at $T_{,max,B}$. This data allows us to determine the recirculated flow average temperature (T_{rec} = 715,1 °C).

Step 3

We can calculate the velocity of the two fronts. We have already computed the fake solid molar flow entering the reaction front in step 1. Now we can determine the fake solid flow entering the heat exchange front with an energy balance to such front, finding $n_{solid,\ fake,\ E}$ = 15,92 kmol/s. The fronts velocities are calculated with the expression given in the previous section (expression 2a, step 4, section 4.2.1), considering an air inlet flow of 5,32 kmol/s and a bed section area of 1 m^2. We find V_E = 0,57 m/s and V_R = 0,25 m/s.

Step 4

In this last step it is verified that the amount of gas recirculated at stage B suffices to heat up the bed of stage B+ to T_{rec}. To do so, we first calculate the energy released by the cooling of the recirculated gas from T_{rec} to $T_{,g,in,B}$, which is the initial temperature of stage B+ and so the temperature at which the gas is expelled from that stage. Then it is calculated the energy required to heat up the solid of stage B+ to T_{rec}. Since the first is bigger than the latter, the bed can be fully heated up to T_{rec} and a fraction of the recirculated flow can bypass stage B+ (the bypass fraction is 45,5%).

4.4) Stage C: sorbent regeneration.

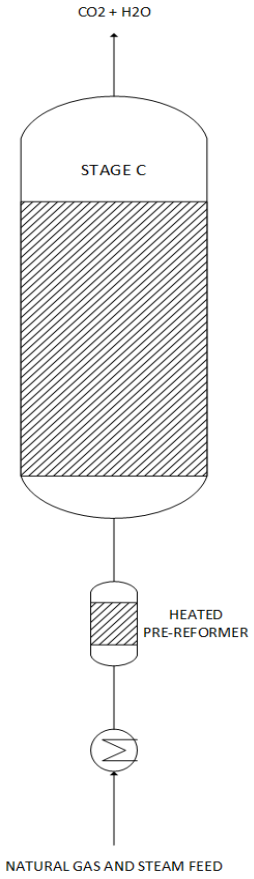

Figure 17: reactor operating in stage C

In this stage the $CaCO_3$ calcination takes place thanks to the energy released by reduction of CuO using fuel gas. The calcination reaction is strongly endothermic and entails an increase in gas moles number. Thus, to shift the equilibrium towards the desired products, it is necessary to perform it at high temperature and low pressure. For avoiding high calcination temperatures, which would both compromise the stability of the Cu material (as seen before) and increase the fuel consumption, stage C is performed at atmospheric (or slightly upper-atmospheric) pressure. At this pressure the calcination proceeds rapidly to a complete $CaCO_3$ conversion at temperatures above 850 °C (2). The calcination is usually performed at temperatures around 860-870 °C. In fact, a higher calcination temperature leads to a higher reaction rate, but the price is an increase in fuel consumption and in the amount of Cu needed (2).

The heat required by the calcination is supplied by the CuO (and NiO) reduction with CH_4, CO or H_2 (produced through previous methane reforming):

$4CuO^{(s)} + CH_4 \rightarrow 4Cu^{(s)} + CO_2 + 2H_2O$ $\quad \Delta H^0_R = -195{,}3$ kj/mol (1)

$CuO^{(s)} + CO \rightarrow Cu^{(s)} + CO_2$ $\quad \Delta H^0_R = -131{,}9$ kJ/mol (2)

$CuO^{(s)} + H2 \rightarrow Cu^{(s)} + H2O$ $\quad \Delta H^0_R = -89{,}6$ kJ/mol (3)

Note that CuO reduction with CO is more advantageous than that with CH_4, since the former releases 131,9 kj for every CuO converted, whereas the latter only 48,8 kj. Consequently, a lower copper to calcium ratio is required when the regeneration is performed with pre-reformed methane, which in turn entails a lower amount of fuel consumption. To make an idea, if the calcination is performed at atmospheric pressure at 850 °C with pure methane, the Cu to active Ca molar ratio required is 3,1; such ratio drops to 1,3 with pure carbon monoxide and to 1,9 with hydrogen (2). Therefore, the advantages of pre-reforming mentioned in previous chapters (2.2.1.1 and 4.2) intensify for stage C. The steam to carbon ratio used is very low (around 1) for several reasons: the pressure is very low and so the methane conversion is favoured; the steam has to be heated in the reaction front by CuO reduction, dictating an higher Cu to Ca ratio and so an higher fuel consumption; even low-pressure steam comes at a price (reduction in steam turbine power output); the CO_2 production through WGS has to be avoided since it could carbonate the regenerated CaO. As shown in literature (2), no carbon deposition has been observed is stage C even with a low steam to carbon ratio.

The gas exiting stage C is composed only of water and carbon dioxide (partly captured in stage A and released by $CaCO_3$ calcination). The two can be easily separated cooling the gas, then, if required, the carbon dioxide can be compressed and stored.

The system originally proposed by Abanades and Murillo(10) consisted of a stage C and a subsequent stage C+. In stage C a pre-reformed natural gas stream is fed for carrying out bed reduction. During the subsequent stage C+, the heat stored in the high temperature solid is exploited for the pre-reforming of stage C feed gas. In this way, the pre-reformed feed from stage C+ enters stage C and the solid at the end of stage C+ is left at a suitable temperature (650 °C) for starting stage A.

In the system proposed here, the stages C and C+ are performed in one only reactor, with no performance reduction. The advantage is a reduction in the number of beds required and so in the investment cost; besides the process management becomes easier. Finally, using an external heated pre-reformer allows to recover high-temperature heat, to the benefit of the overall performance. The feed exits such pre-reformer in chemical equilibrium (with SR and WGS) at $T_{,gas,in,C}$, hence, as we are going to see, the solid bed remains at $T_{,gas,in,C}$ at the end of stage C. The value of $T_{,gas,in,C}$ can be set appropriately for stage A to operate efficiently (around 700 °C).

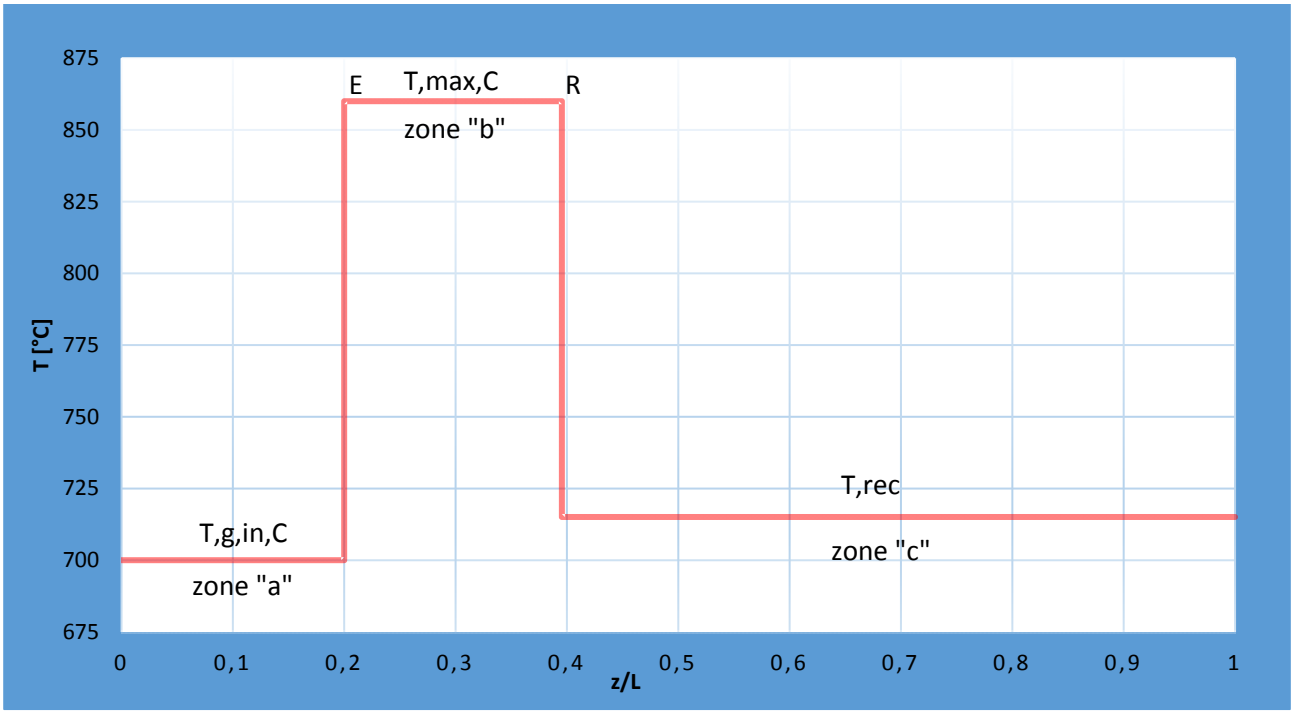

Figure 18: stage C: axial temperature profile at an intermediate time

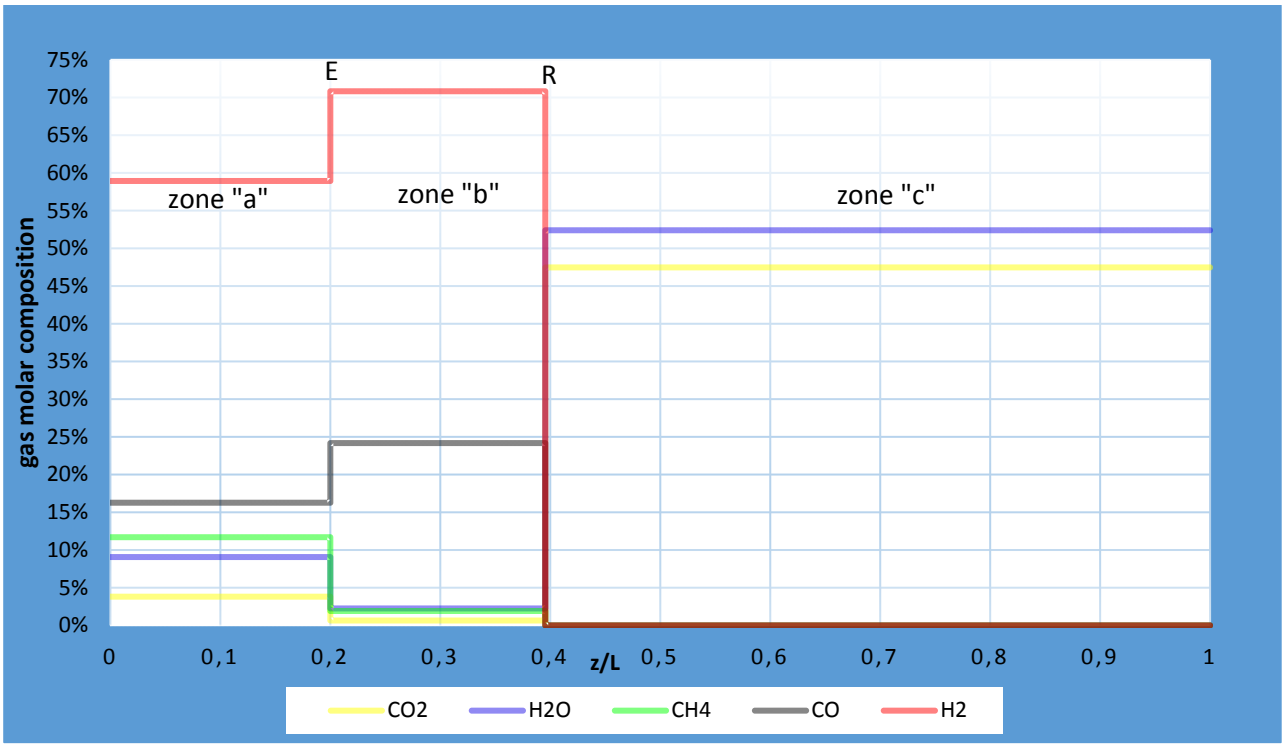

Figure 19: stage C: axial gas molar composition profile at an intermediate time

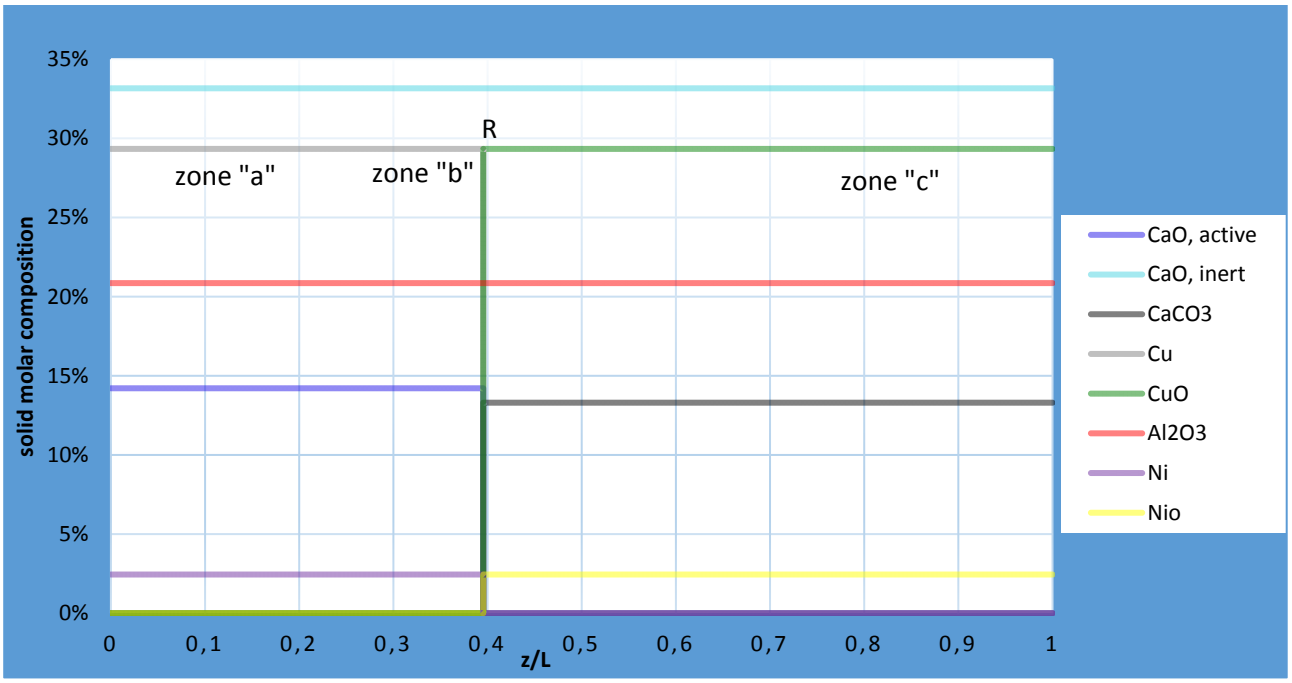

Figure 20: stage C: axial solid molar composition profile at an intermediate time

The Cu to active Ca ratio is chosen so that the calcination temperature ($T_{,max,C}$) achieved during stage C operation is that required. As in stages A and B, when the inlet gas meets the unconverted solid a reaction front forms. In this case, as in case A, the reaction front is faster than the heat exchange front. Thus, the gas first meets the hot converted solid in the heat exchange front, from which it exits in equilibrium with SR and WGS at $T_{,max,C}$. Then it meets the unconverted solid in the reaction front, where the bed reduction and calcination take place.

Stage C ends when the reaction front reaches the top of the bed. At this point the heat exchange front is still behind. As a consequence, at the end of stage C the solid bed is partly at $T_{,g,in,C}$ and partly at $T_{,max,C}$ (see figure 5). The outlet gas temperature is constant and equal to T_{rec} (calculated in the previous chapter and equal to 715 °C) during the whole duration of stage C.

4.4.1) Stage C: calculation method.

The results below refer to these operating conditions:

stage C		
T,g,in,c=	700	°C
T,max,c=	860	°C
p,in,C=	1,8	bar
P,in,pre-ref=	2	bar
S/C=	1	

Table 11: operating conditions for stage C, in the case analysed here

Step 1

Consider a natural gas molar flow of 1 kmol/s (with the corresponding steam). We can calculate the flow exiting the heated pre-reformer (equal to that entering stage C) imposing the equilibrium (of SR and WGS) at $T_{,g,in,C}$.

	n,in,P.R. [kmol/s]	n,out,P.R. [kmol/s]
H2	0,00	2,01
N2	0,01	0,01
CO	0,00	0,56
CO2	0,02	0,13
AR	0,00	0,00
CH4	0,89	0,40
H20	1,08	0,31
C2H6	0,07	0,00
C3H8	0,01	0,00
C4H10	0,00	0,00

Table 12: heated pre-reformer entering and exiting streams, corresponding to a natural gas molar flow of 1 kmol/s

Step 2

We can compute the molar flow in zone "b", imposing the equilibrium of the gas flow in zone "a" at $T_{,max,C}$.

	n, zone "a" [kmol/s]	n, zone "b" [kmol/s]
H2	2,01	2,87
N2	0,01	0,01
CO	0,56	0,98
CO2	0,13	0,03
AR	0,00	0,00
CH4	0,40	0,08
H20	0,31	0,09

Table 13: streams in zones "a" and "b" of stage C

Step 3

The gas flow in zone "b" corresponds to the gas fake flow entering the reaction front. Assuming a complete oxidation of the gas, it is possible to calculate the required fake flow of CuO and NiO entering the reaction front (using an oxygen balance), and so the solid fake flow entering the reaction front. Hence, the carbon dioxide released by the solid in the reaction front is known (considering a complete carbonate calcination), and so the gas flow exiting such front is also known (using a carbon and hydrogen balance). Finally, it is possible to use an energy balance at the reaction front to find the Cu to active Ca ratio required to obtain the $T_{,max,C}$ target.

	n, zone "b" [kmol/s]	n, zone "c" [kmol/s]
H2	2,87	0,00
N2	0,01	0,01
CO	0,98	0,00
CO2	0,03	2,83
AR	0,00	0,00
CH4	0,08	0,00
H20	0,09	3,12

	n,initial [kmol]	n,final [kmol]
CaO activo	0,06	1,00
CaO inerte	2,33	2,33
CaCO3	0,94	0,00
Cu	0,00	2,06
CuO	2,06	0,00
Al2O3	1,47	1,47
Ni	0,00	0,17
NiO	0,17	0,00

Table 14: streams in zones "b" and "c" and solid composition at the beginning and at the end of stage C

Step 4

With an overall energy balance we can determine the fraction of bed left at $T_{,max,C}$ (hot) and that at $T_{,g,in,C}$ (cold). In this case the cold fraction is 70,2%.

Step 5

We can calculate the front velocities as for the previous stages. With a bed section area of 1 m^2 and a natural gas molar flow of 1 kmol/s we find V_R = 0,51 m/s and V_E = 0,29 m/s.

4.5) Performances and sensitivity analysis

In this chapter it is evaluated the performance of the system proposed above, with different operating conditions. It is possible to use several performance indexes; anyway, three are the aspects to evaluate: the energy efficiency, the carbon capture efficiency and the quality of the syngas produced (namely its composition).

To evaluate the energy efficiency, the most widespread index for hydrogen plants is the "cold gas efficiency" (CGE). It is defined as the ratio between the chemical energy (low heating value, LHV) of the hydrogen produced and the chemical energy (LHV) of the fuel (in this case natural gas) consumed.

$$CGE = \frac{\dot{m}_{H2} \cdot LHV_{H2}}{\dot{m}_{NG} \cdot LHV_{NG}}$$

In our case $\dot{m}_{H2}$ is the hydrogen flow produced by stage A (or better, by the stages A working concurrently) and $\dot{m}_{NG}$ is the natural gas flow entering stage A and stage C pre-reformers. This index represents the fraction of the natural gas energy effectively converted into hydrogen energy: the remaining fraction is mainly due to

the thermal energy of the syngas produced and, if present, to that of the flue-gas (and, to a lesser extent for traditional plants, to the syngas carbon monoxide and unconverted methane chemical energy). Therefore, if we fix the syngas composition, the lower is its temperature, the higher is the CGE. Note that this index does not take into account possible heat or electricity input/output, which, however, are unknown at this stage.

To evaluate the carbon capture efficiency we have used the carbon capture ratio, defined as the carbon flow captured divided by the carbon flow entering the plant with the fuel.

$$CCR = \frac{\dot{m}_{C,captured}}{\dot{m}_{C,in}}$$

In our case $\dot{m}_{C,captured}$ is the carbon flow exiting stage C and $\dot{m}_{C,in}$ is the carbon flow entering stage A and C pre-reformers with the fuel. For a modern fired-tubular reforming plant with a CCR around 74-75%, the CGE does not exceed 77-78%.

Finally, the syngas composition quality means basically its hydrogen content (on a dry basis).

Note that these indexes refer to a plant without any hydrogen purification system, so that the methane and carbon monoxide in the syngas are considered lost (their energy is not accounted in the CGE). In this case, a very important parameter is therefore the methane slip (defined as the ratio between the methane flow exiting and entering stage A).

If not otherwise specified the operative conditions are the following:

stage A			stage B			stage C		
T,gas,in,pre-ref=	490	°C	T,g,in,B=	300	°C	T,g,in,C=	700	°C
P,in,pre-ref=	20	bar	P,in,B=	20	bar	T,max,C=	860	°C
p,in,A=	20	bar	T,max,B=	830	°C	P,in,C=	1,8	bar
S/C=	4					P,in,pre-ref=	2	bar
T,g,in,A=	700	°C				S/C=	1	

Table 15: reference operating conditions for the sensitivity analysis

4.5.1) Effect of the steam to carbon ratio at stage A.

The graphs below report the effect of the steam to carbon at stage A with different pressures (we have used the same pressure for stage A and B in any case). It is possible to see that the S/C affects heavily the methane slip and so the other parameters. The high methane slip proved the main obstacle to high performance. For example, at 20 bar, to reduce the methane slip under 5% a S/C of 4,8 is required (the situation get still worse at higher pressures). As already pointed out, the use of such a high S/C entails several disadvantages.

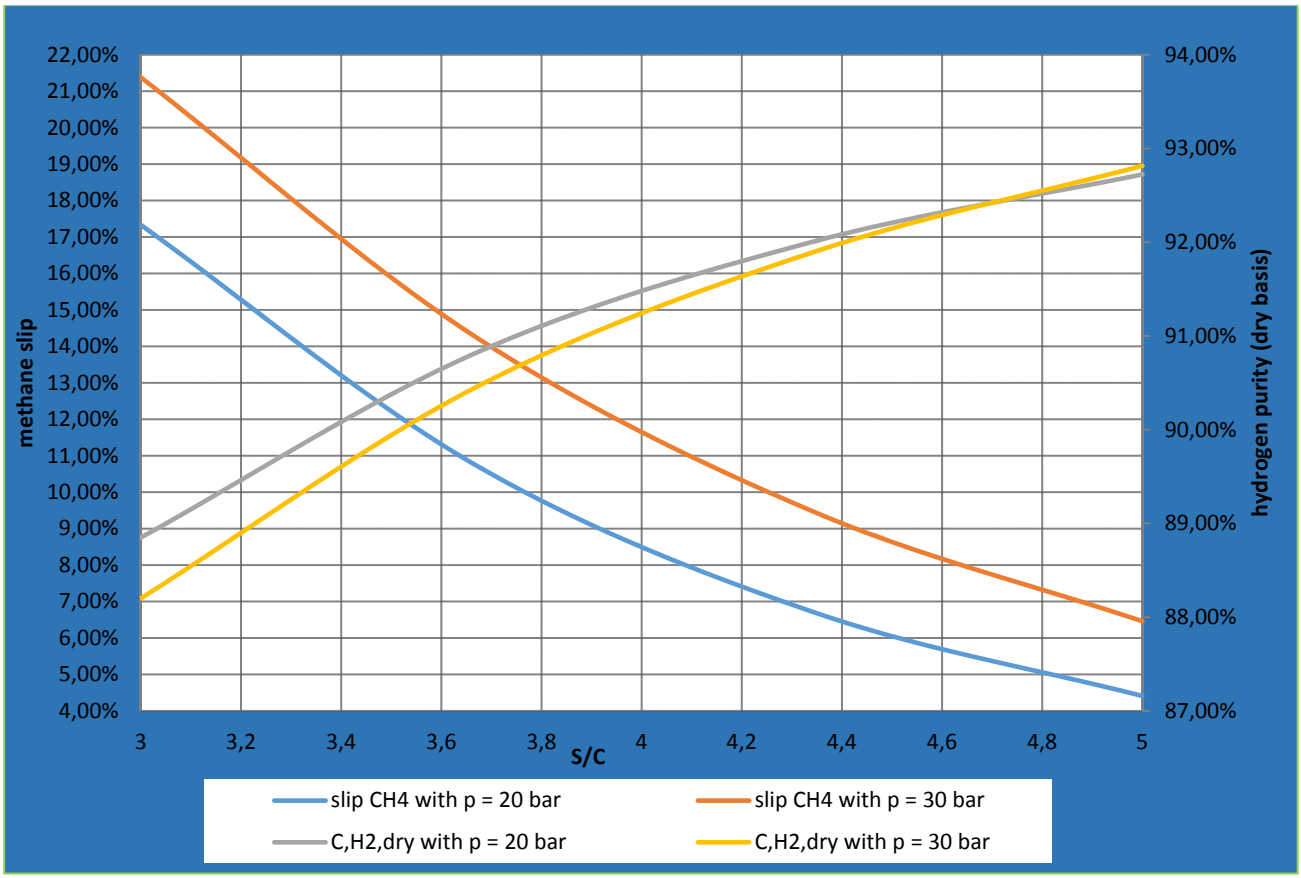

Figure 21: effect of the S/C at stage A on methane slip (left axis) and on hydrogen purity (right axis), with a pressure of 20 and 30 bar at stage A (equal to that of stage B).

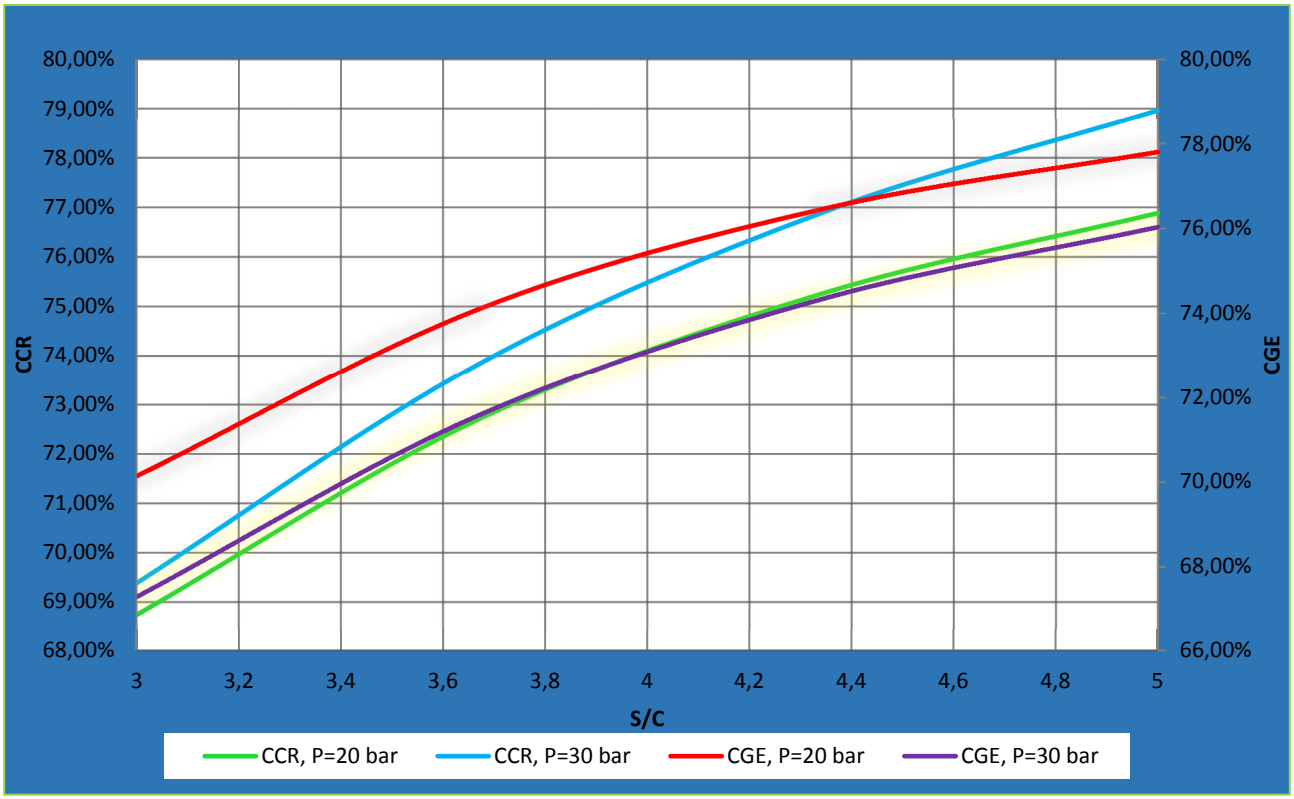

Figure 22: effect of the S/C at stage A on the cold gas efficiency (right axis) and carbon capture ratio (left axis), with a pressure for stage A (equal to that of stage B) of 20 and 30 bar.

4.5.2) Effect of pressure of stage A (equal to that of stage B).

As the graphs below reveal, the effect of pressure of stage A is quite marked on the methane slip, especially at low S/C. Anyway, they also reveal that it is possible to operate at reasonably high pressures. On the other hand, a higher pressure fosters carbonation in stage A and reduces calcination in stage B, to the benefit of the CCR.

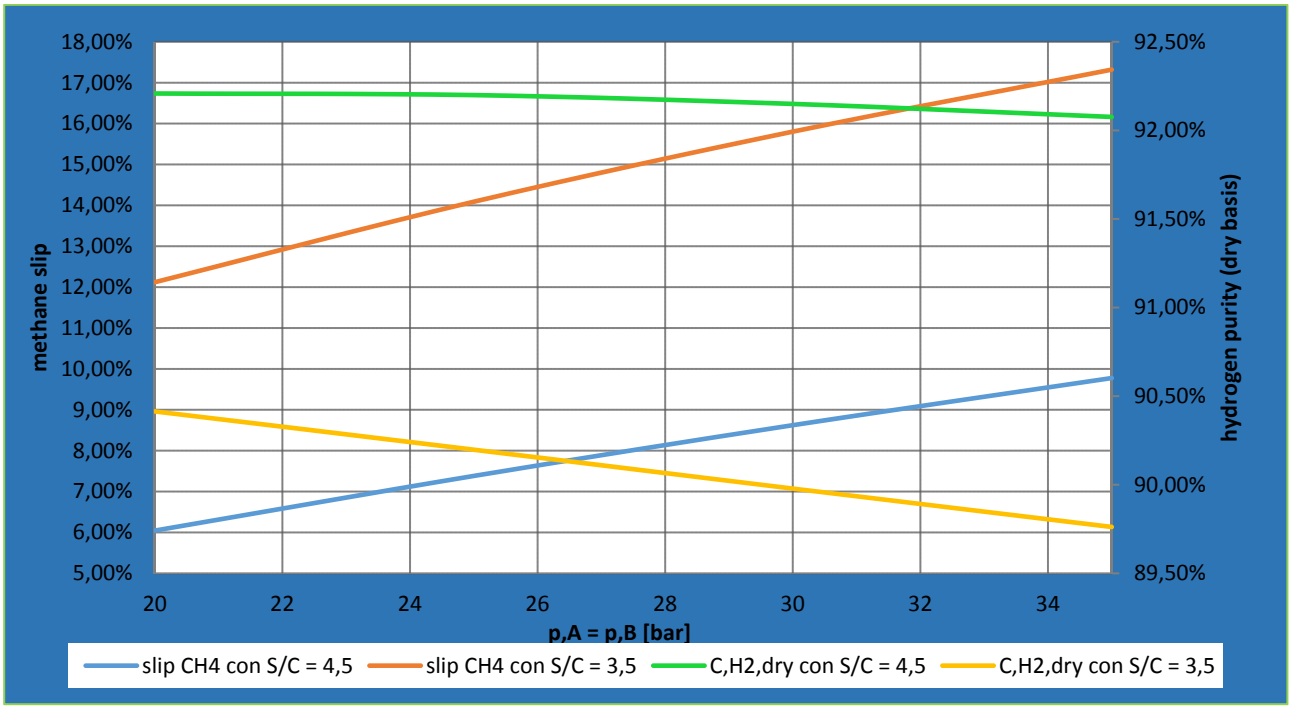

Figure 23: effect of pressure of stage A (equal to that of stage B) on methane slip (left axis) and on hydrogen purity (right axis), with a S/C of 3,5 and 4,5.

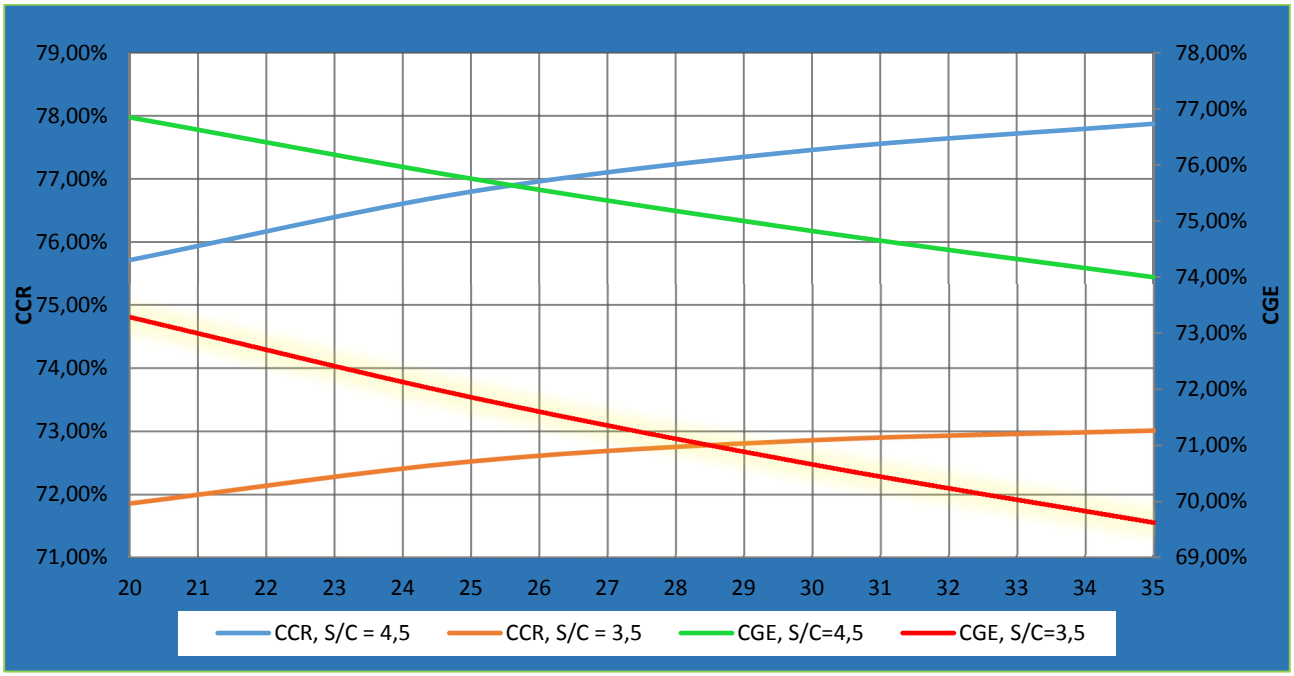

Figure 24: effect of pressure of stage A on cold gas efficiency (right axis) and carbon capture ratio (left axis).

4.5.3) Effect of stage A gas inlet temperature.

An increase in stage A inlet gas thermal energy translates partly into an increase in chemical energy of the gas produced, and so an increase in CGE. The limit, of course, is the availability of high-temperature heat to perform the inlet gas heating. On the other hand, an increase in $T_{,g,in,A}$ entails an increase in $T_{,max,A}$ and in the fraction of gas exiting at $T_{,max,A}$ and so a decrease in the CCR.

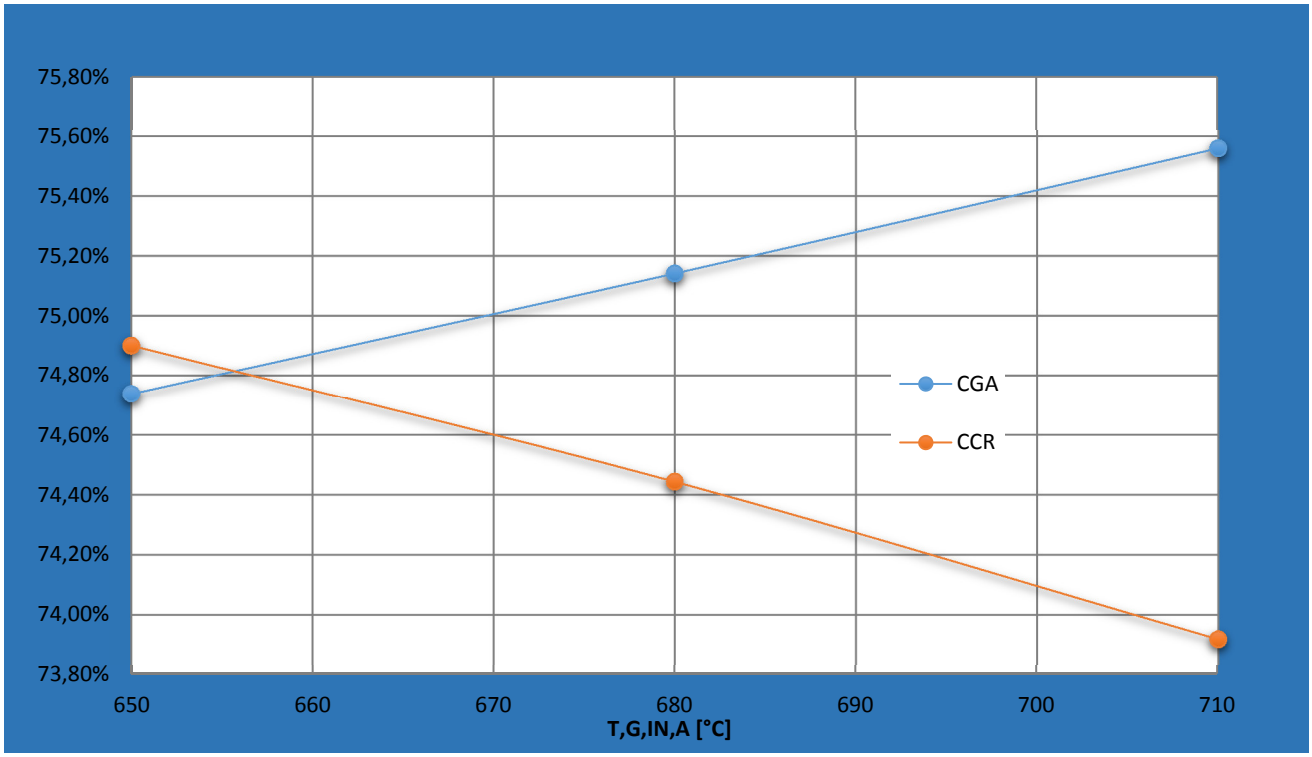

Figure 25: effect of stage A gas inlet temperature on cold gas efficiency and carbon capture ratio

4.5.4) Effect of stage B gas inlet temperature.

As figure 27 reveals, stage B gas inlet temperature doesn't affect appreciably the CCR (since $T_{,max,B}$ and $p_{,B}$ are fixed), while it has an influence on the CGE. Once $T_{,max,B}$ has been fixed, an increase in $T_{,g,in,B}$ involves an increase in the recirculation ratio and so a reduction of the oxygen content in the inlet gas, which in turn entails a reduction of the velocity of the reaction front. As a result, the fraction of gas expelled at $T_{,ad,A}$ decreases to the benefit of that at $T_{,max,B}$; thus the recycle average temperature (T_{rec}) increases as $T_{,g,in,B}$ increases. Since the solid bed temperature at the beginning of stage C is T_{rec}, increasing $T_{,g,in,B}$ involves, to a certain extent, decreasing the amount of fuel required at stage C. This justifies the trend of the CGE in the graph below.

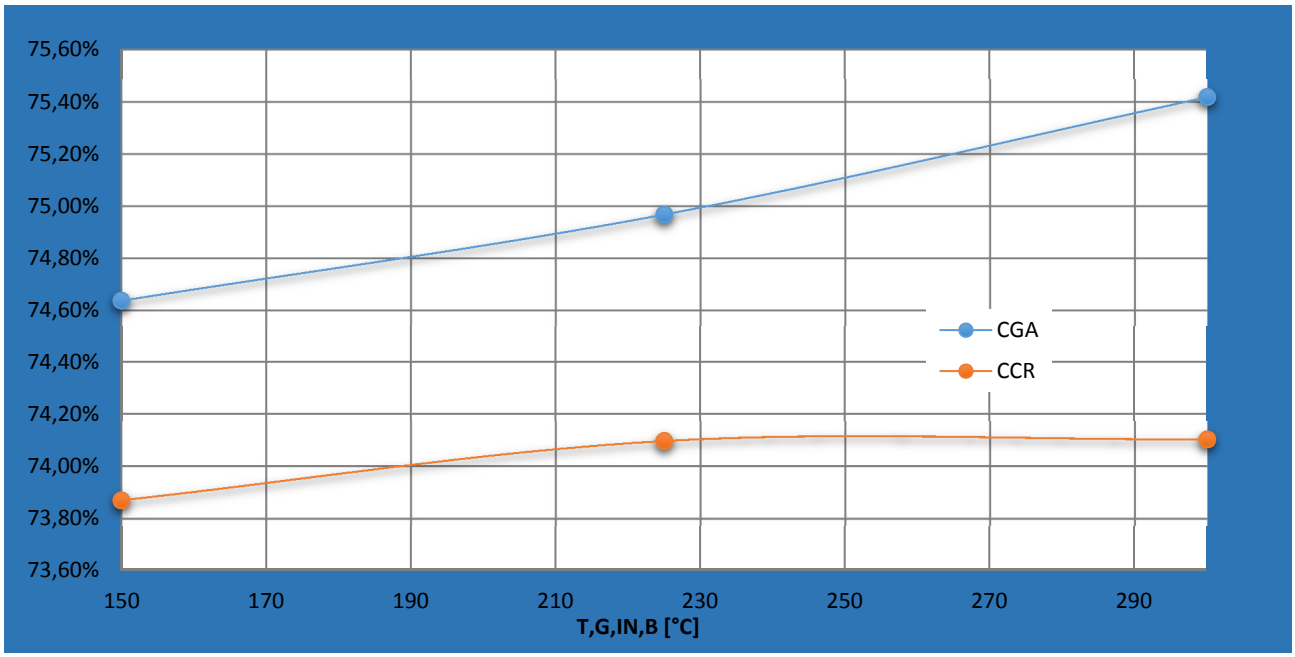

Figure 26: effect of stage B inlet temperature on cold gas efficiency and carbon capture ratio

4.5.5) Effect of stage B maximum temperature.

An increase in maximum temperature of stage B results in a higher T_{rec} and so in a higher solid initial temperature at stage C, to the benefit of the cold gas efficiency. On the other hand, it entails an increase in calcination at stage B and so a drop of carbon capture ratio. A temperature of 830 °C is chosen as a good trade-off between the two opposite effects.

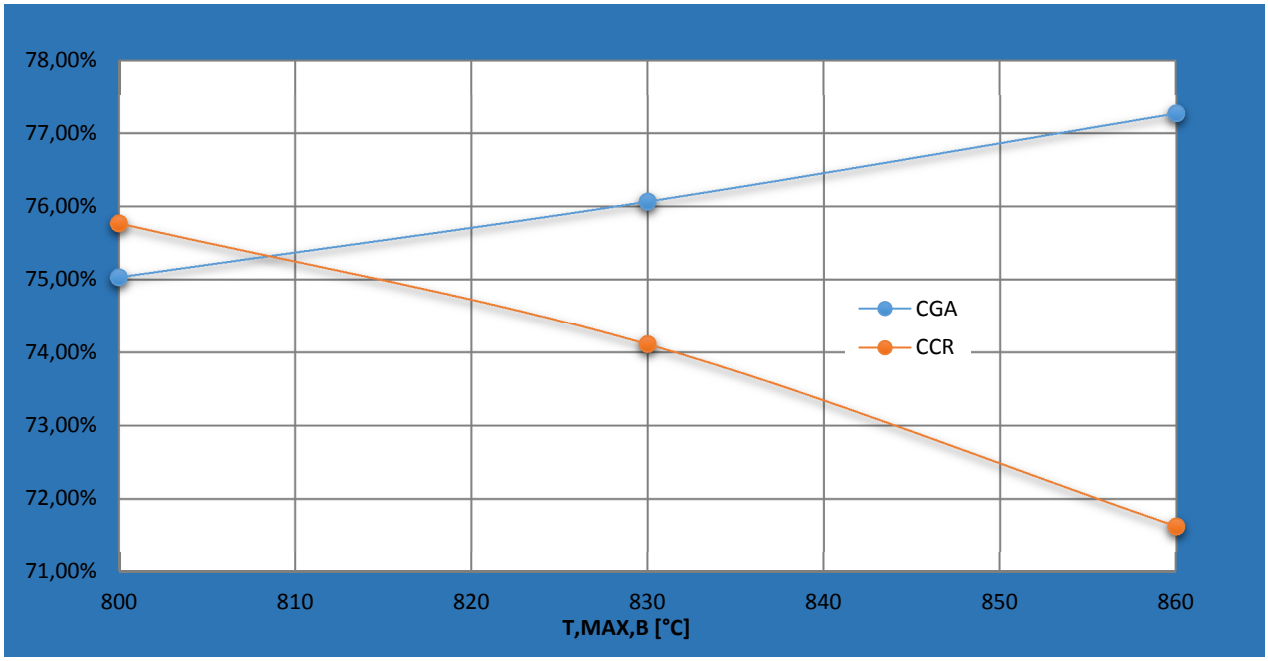

Figure 27: effect of stage B maximum temperature on cold gas efficiency and carbon capture ratio.

4.5.6) Effect of the steam to carbon ratio at stage C.

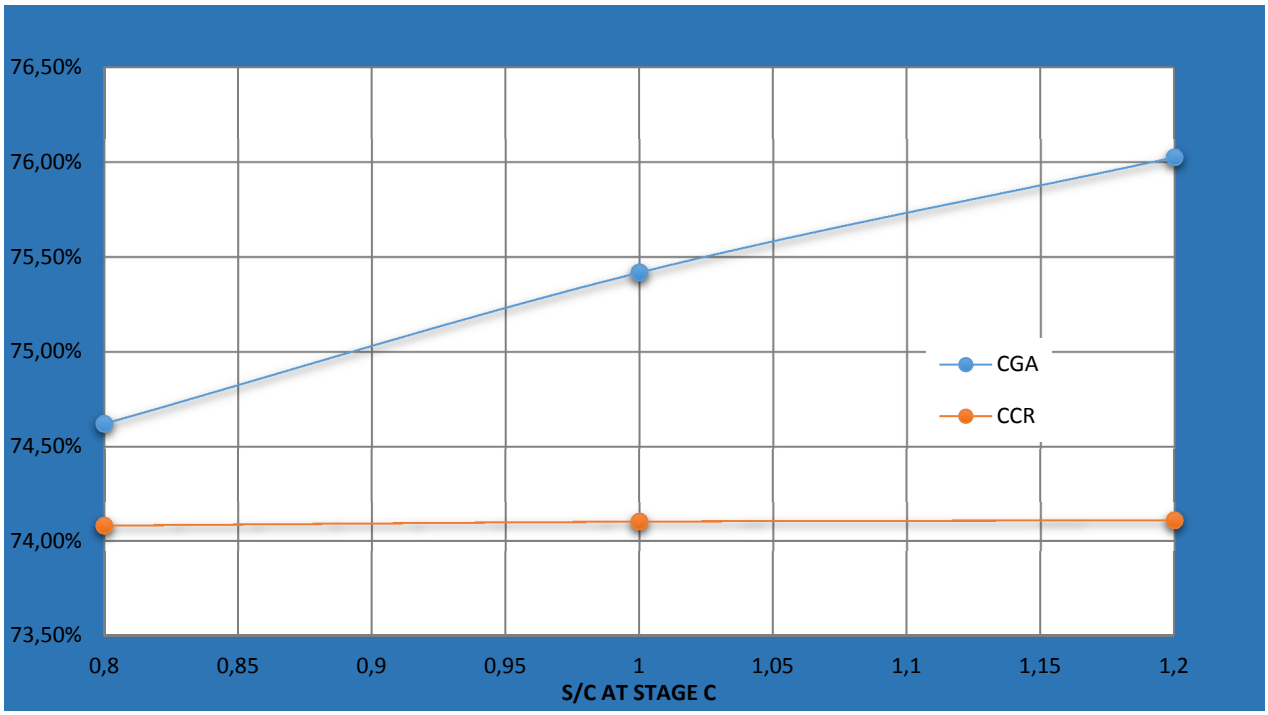

Figure 28: effect of the steam to carbon ratio at stage C on cold gas efficiency and carbon capture ratio.

The steam to carbon ratio at stage C seems to have no effect on CCR, whereas it has an effect on CGE. The reason of that lies in the influence of the S/C on the composition of the gas exiting the pre-reformer of stage C: the higher is the steam content at the inlet, the higher is the methane conversion and the heat required at the pre-reformer, and so the higher is the chemical energy of the fuel stream entering stage C. However, for the reasons cited in chapter 4.3.1, a value of 1 may be a good choice: it should not be forgotten that the high-temperature heat required by the heated pre-reformer has to come from the hot streams of the plant, without any combustion.

4.5.7) Effect of stage C gas inlet temperature.

An increase in the heated pre-reformer outlet gas temperature leads to an increase in chemical and thermal energy of the gas entering stage C, to the benefit of CGE. Conversely, it has a negative effect on CCR, both because the gas fraction exiting with composition “c” from stage A has a higher carbon content (as a consequence of its higher temperature) and because the fraction with composition “b” increases.

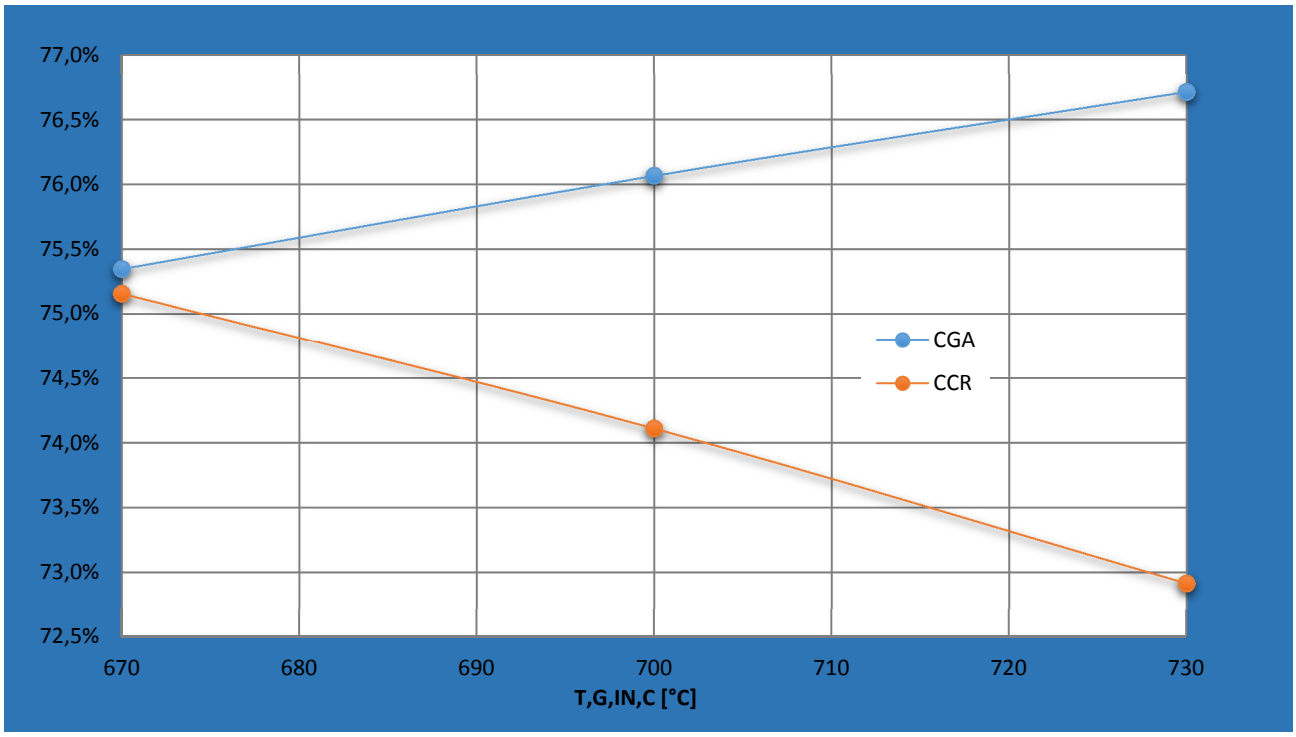

Figure 29: effect of stage C gas inlet temperature on cold gas efficiency and carbon capture ratio.

In conclusion, the main drawback of the system proposed seems to be the methane slip. For instance, with the usual steam-reforming operative conditions of S/C = 3,5 and p = 30 bar, it is around 15,8%. Here we had better make a distinction between hydrogen production for pre-combustion carbon capture power plants, in which the syngas produced (with a hydrogen content usually around 90% on a dry basis) is wholly sent into the combustion chamber, and high-purity hydrogen production plants. In the first case, although the unconverted methane and carbon monoxide heating value is fully recovered in the combustion chamber (and so the cold gas efficiency as defined above is not a very representative parameter), the presence of carbon compounds in the syngas affects the carbon capture ratio. Thus, for such plants, if we aim to limit the emissions, the most important index is probably the carbon capture ratio. On the contrary, in high-purity hydrogen plants, there is a syngas purification system (usually PSA, but also membrane systems are available) that separates hydrogen from other compounds, which can be recycled as fuel at stage C. In this way, not only the unconverted carbon compounds heating value is recovered, but the carbon itself is captured, leading to a very high carbon capture ratio. In this case, the cold gas efficiency is probably the most important index. It is clear from the outset that the two systems are indeed different.

4.6) Possible improvements for pre-combustion carbon capture power plants.

Whereas in this work we are concerned in high-purity hydrogen production, which will be discussed in the next chapter (4.7), here we briefly address the problem of increasing the carbon capture ratio in plants without syngas purification systems.

The main carbon loss is due to stage A, so we had better focus on this stage. As for the carbon loss due to calcination in stage B, we have seen that there are basically two ways to hinder such phenomenon: increasing the pressure or reducing the maximum temperature, the effects of both have already been investigated.

If we look at stage A we can note that the main carbon loss is due to the syngas exiting at $T_{,max,A}$ (zone "b" with reference to figures 7 and 8), because of the strong exothermicity of carbonation. The key to reduce the carbon loss, therefore, lies in a reduction of the gas fraction exiting at $T_{,max,A}$ or in a reduction of $T_{,max,A}$ itself. It can be done in several ways, for example reducing $T_{,g,in,C}$ or $T_{,g,in,A}$. The drawback is the reduction in methane conversion (and so in cold gas efficiency).

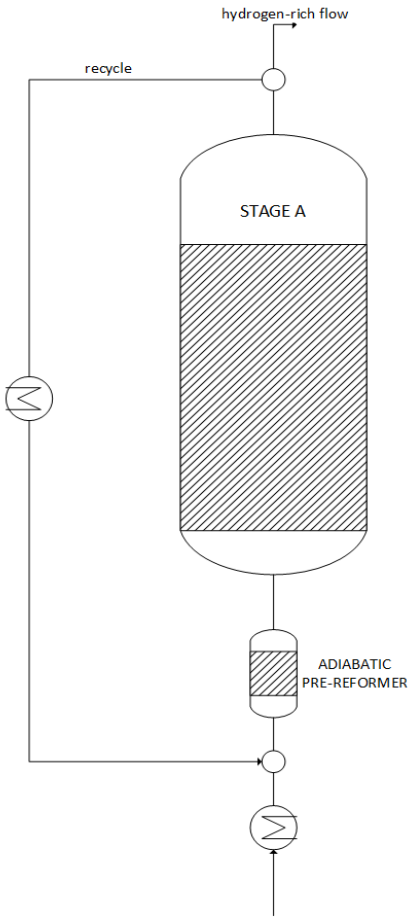

Figure 30: stage A with recycle.

We propose here two possible process changes to achieve an increase in carbon capture ratio. The first, and also the most straightforward, is recycling some of the syngas exiting stage A as shown in figure 29. This leads to a significant reduction of $T_{,max,A}$, thanks to the strong dilution of the reactants (mainly with steam), so that the heat released by SER reactions in the reaction front is spread on a greater gas flow. To give an idea, with S/C = 4 and p = 20 bar, in the base case we have found $T_{,max,A}$ = 843,5 °C, whereas with a recirculation ratio of 50% it slips to 744,3 °C. Besides, the velocity of the reaction front, set all the other operating conditions, slightly decreases (because of the reactants dilution), so that also the fraction of gas exiting at $T_{,max,A}$ slightly decreases. Another advantage is the increase in the steam to carbon ratio at the pre-reformer inlet, since the recycled gas is rich in steam. The result is a relevant increase in carbon capture ratio (see the end of the chapter, fig. 33). The main drawback is that the methane entering stage A is strongly diluted with hydrogen (since the recirculated flow is rich in hydrogen) thus its conversion drops, and so does the cold gas efficiency. Moreover, if we fix the gas maximum superficial velocity in stage A and the inlet natural gas molar flow, the use of a recirculation involves a significant increase in the flow entering stage A and so an increase in beds size. Undoubtedly, the system becomes more expensive and more difficult to manage.

The second path to a carbon capture ratio gain deals with both a reduction of $T_{,max,A}$ and (especially) a reduction of the gas fraction at $T_{,max,A}$. The core idea is to subtract energy from the gas, in a way less harmful for methane conversion as possible. In fact, fixed the bed composition and temperature at the beginning and

at the end of stage A and the gas inlet temperature, the energy balance dictates that if we remove energy from the gas its outlet energy lowers. To do that, we have split stage A into two stages, say A1 and A2, that operate in series. In this way, the whole gas flow exiting stage A2 is cooled down and sent into stage A1 ($T_{,gas,in,A1}$ = 700 °C), where the carbon capture can complete (see figure 30). Since the gas exiting stage A2 is not in chemical equilibrium at $T_{,g,in,A1}$, when it meets the catalyst, at the bottom of the bed of stage A1, it reacts, reaching the equilibrium with SR and WGS at $T_{,ad,A1}$ (higher than $T_{,g,in,A1}$). Stage A1 can be solved similarly to stage A of the base case, except for the fact that its input is stage A2 output, so that an iterative procedure is required. For this same reason, stage A1 and A2 start and finish at the same time. In particular, they finish when the bed of stage A2 has been fully carbonated and left at $T_{,ad,A2}$. At this time, a fraction of the bed of stage A1 is left fully carbonated at $T_{,ad,A1}$ and the other part is left partially carbonated at $T_{,max,A}$. With a S/C = 4 and p = 35 bar, for the base case we have found $T_{,max,A}$ = 874 °C with 55% of the total moles number exiting stage A at such temperature; for the modified process $T_{,max,A}$ is 846 °C and only 24% of the gas exits at such temperature. Unfortunately, also in this process the increase in carbon capture ratio comes at the price of a reduction in methane conversion, and so cold gas efficiency. Besides, as there is one more stage, the total number of beds required for a continuous operation increases, leading to an increase in investment cost and management complexity.

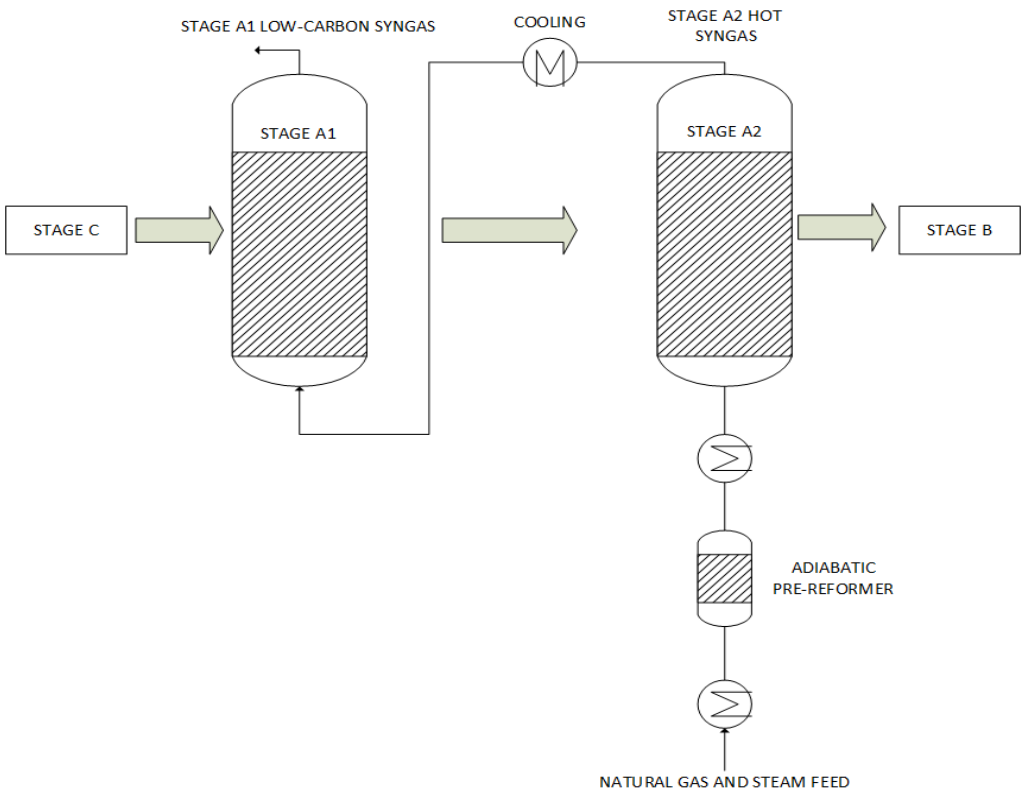

Figure 31: stage A split into A1 and A2.

The graphs below report a comparison between the base case, the case with a 50% recycle ratio at stage A and the case with stage A split into A1 and A2. The reference conditions are those listed in chapter 4.5. The changes proposed above leads to a carbon capture ratio increase up to 10 percentage points (in the case with 50% recirculation ratio at stage A) over the base case, with figures over 84%. Also the hydrogen purity increases appreciably. On the other hand, the plant cost and complexity rise significantly.

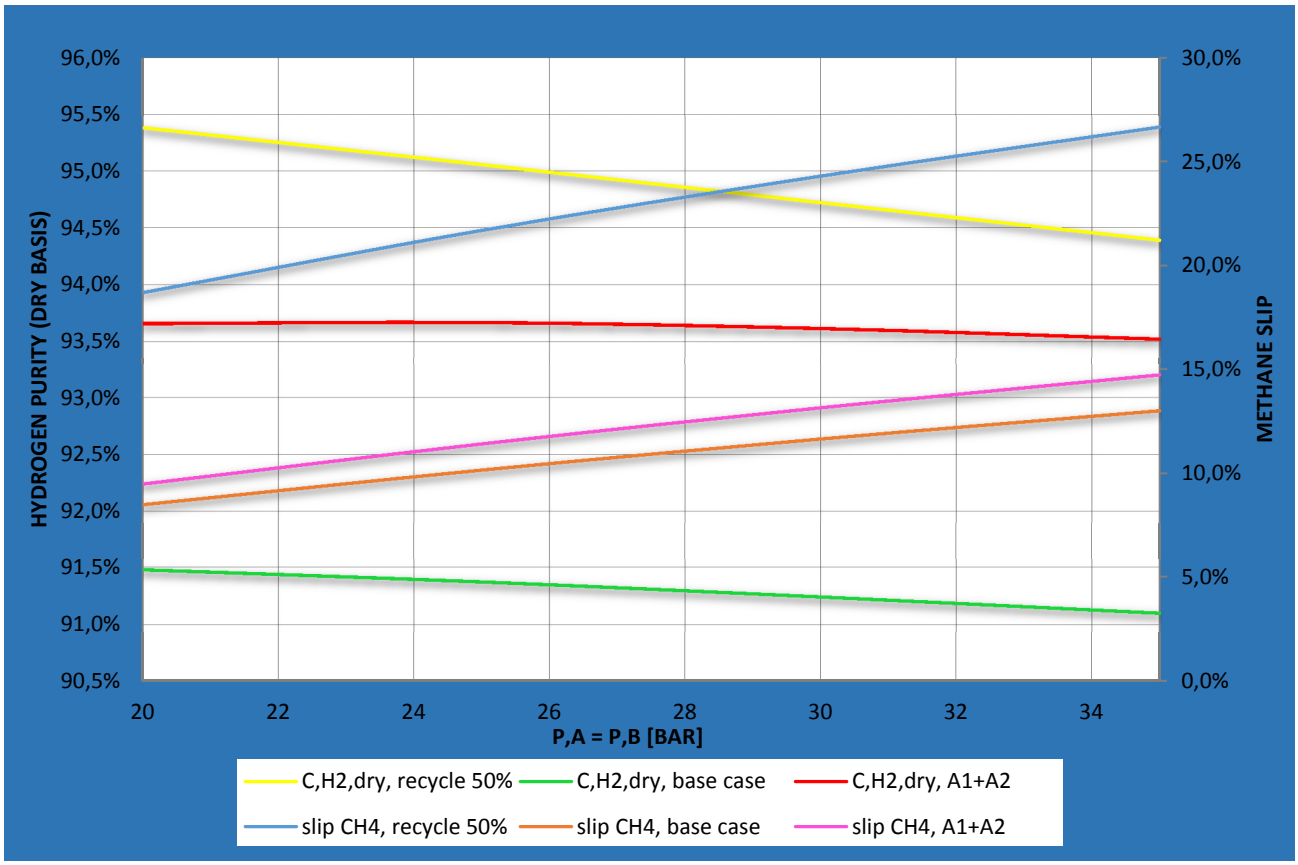

Figure 32: comparison between the hydrogen purity (left axis) and the methane slip (right axis) for the three systems analysed.

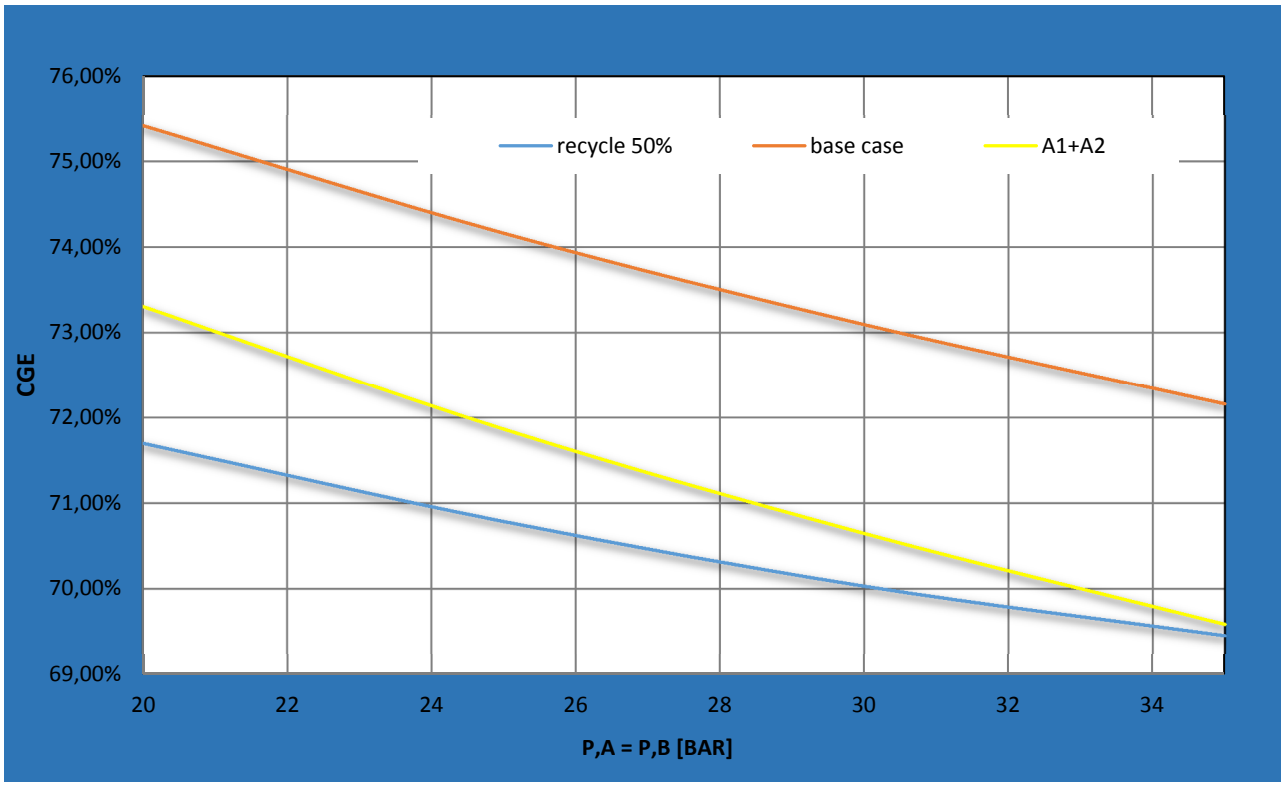

Figure 33: comparison between the cold gas efficiency of the three systems analysed.

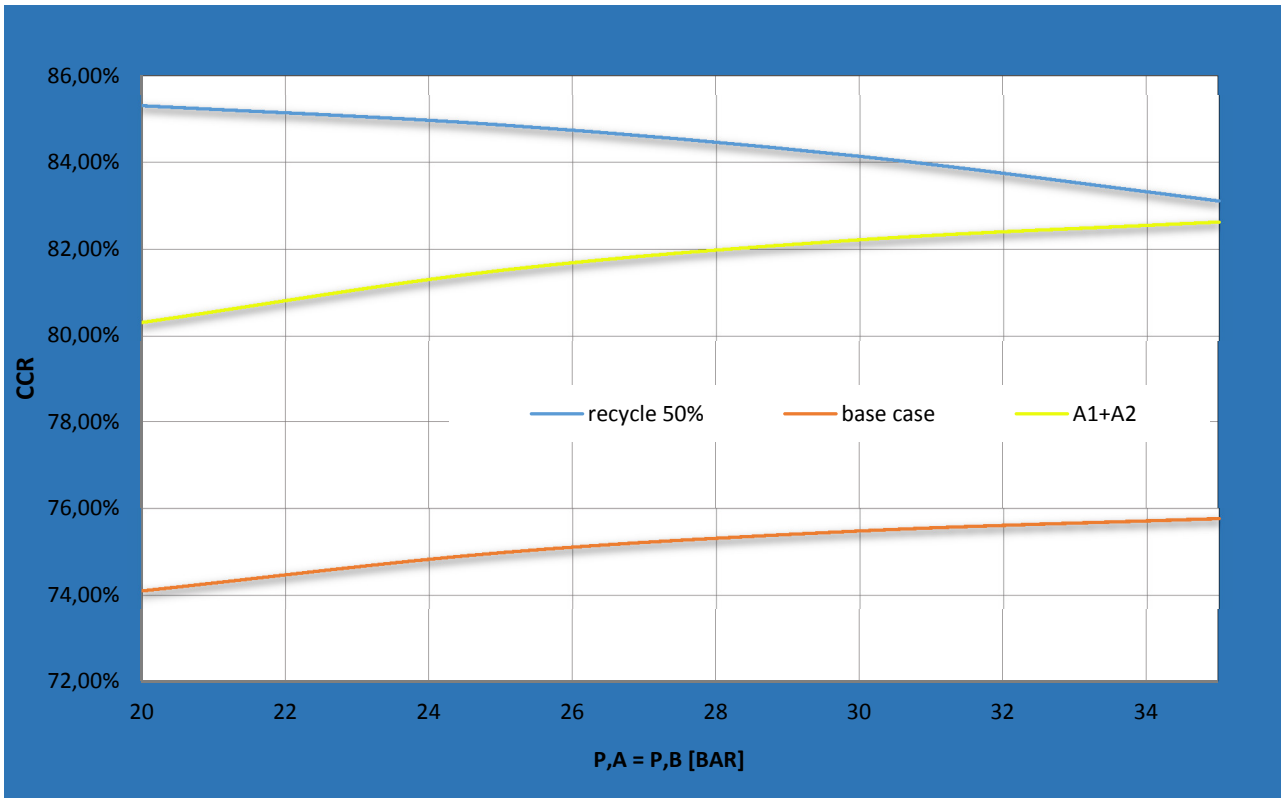

Figure 34: comparison between the carbon capture ratio of the three systems analysed.

4.7) Ca-Cu looping process for high-purity hydrogen plants.

In this chapter we focus on high-purity hydrogen production, which is important when integrating this process into an ammonia production plant. Looking back on the previous chapter, we can see that the raw syngas hydrogen purity does not exceed 92% in the base case (and 95% with a recirculation ratio of 50% at stage A), the remaining being methane, carbon monoxide and dioxide. Such carbon compounds concentration is too high not only for the ammonia synthesis reactor, but also for the methanator: if we sent this syngas into the methanator, there would be an unacceptable hydrogen consumption and a relevant methane content in the outlet stream. Hence it is required a purification system, the most promising seems to be a PSA. From this moment on we analyse the system made of a Ca-Cu looping process (in the base configuration) and a PSA, the off-gas of which are used as fuel in stage C.

Analysing such system, we have found out a very interesting feature. After setting all the operating conditions to reasonable values (see previous chapters), there is always a certain (reasonable) value of steam to carbon ratio (at stage A) that allows stage C to operate only with PSA off-gas, without any additional fuel (see figure 34). Since this seems to be the most efficient way of performing the process, we have focus on this condition.

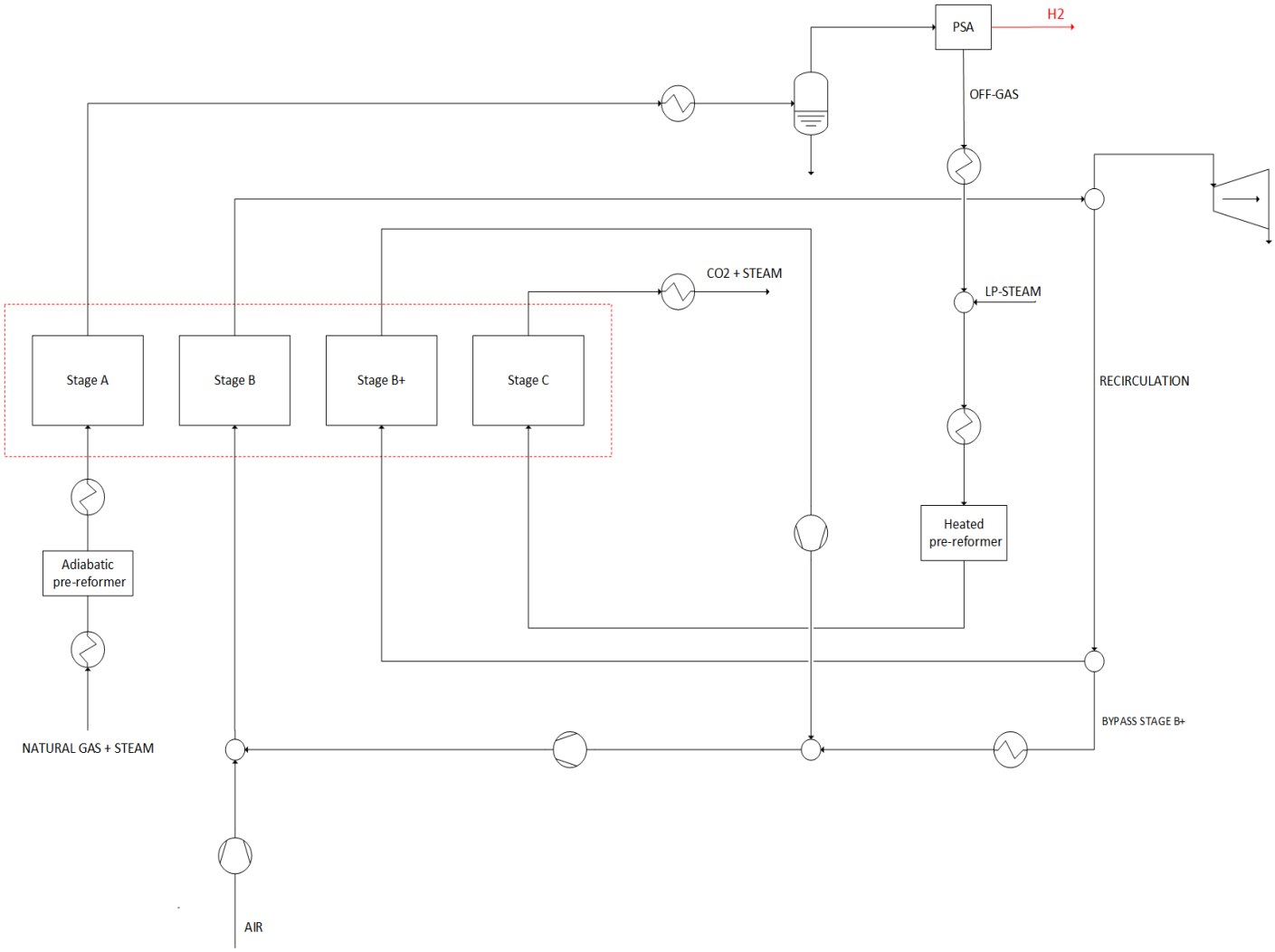

Figure 35: conceptual design of a Ca-Cu process for high hydrogen purity. Note that stage C is fed only with PSA off-gas, without any additional fuel. The contents of the red dotted rectangle, representing the CaCu process, will be shown later on.

Since our main goal here is to maximise the cold gas efficiency, we can set several operating conditions from the outset, in the light of the analysis of chapter 4.5. The inlet temperature of stages A and C should be as high as possible, the main limit being the availability of high-temperature heat to perform the heating. The other conditions are chosen as good compromise values. The following table reports a summary. We have assumed a constant PSA efficiency of 90% with 100% purity.

stage A			stage B			stage C		
T,in,pre-ref=	490	°C	T,g,in,B=	300	°C	T,g,in,C=	700	°C
T,g,in,A=	700	°C	T,max,B=	830	°C	T,max,C=	860	°C
						P,in,C=	1,8	bar
						P,in,pre-ref=	2	bar
						S/C=	1	

Table 16: operating conditions considered for the high-purity hydrogen production. These are the conditions considered during chapters 4.7 and 5.

Neither the pressure of stage A (assumed equal of that of stage B) nor its steam to carbon ratio have been chosen. In fact, the former has important and opposed effects on performances and investment cost, which we will try to evaluate in more detail in the following. The latter is chosen so to feed stage C only with PSA off-gas and so it is determined after fixing all the other conditions. Generally speaking, the higher is stage A pressure, the higher will be the methane slip and so the off-gas enthalpy flow. To balance this effect, the higher is the pressure, the higher is the S/C required. The graph below reports the S/C required as a function of pressure at stage A and B. Such ratio is comprised between 2,7 and 2,95 for a wide range of pressures, which is a reassuring result.

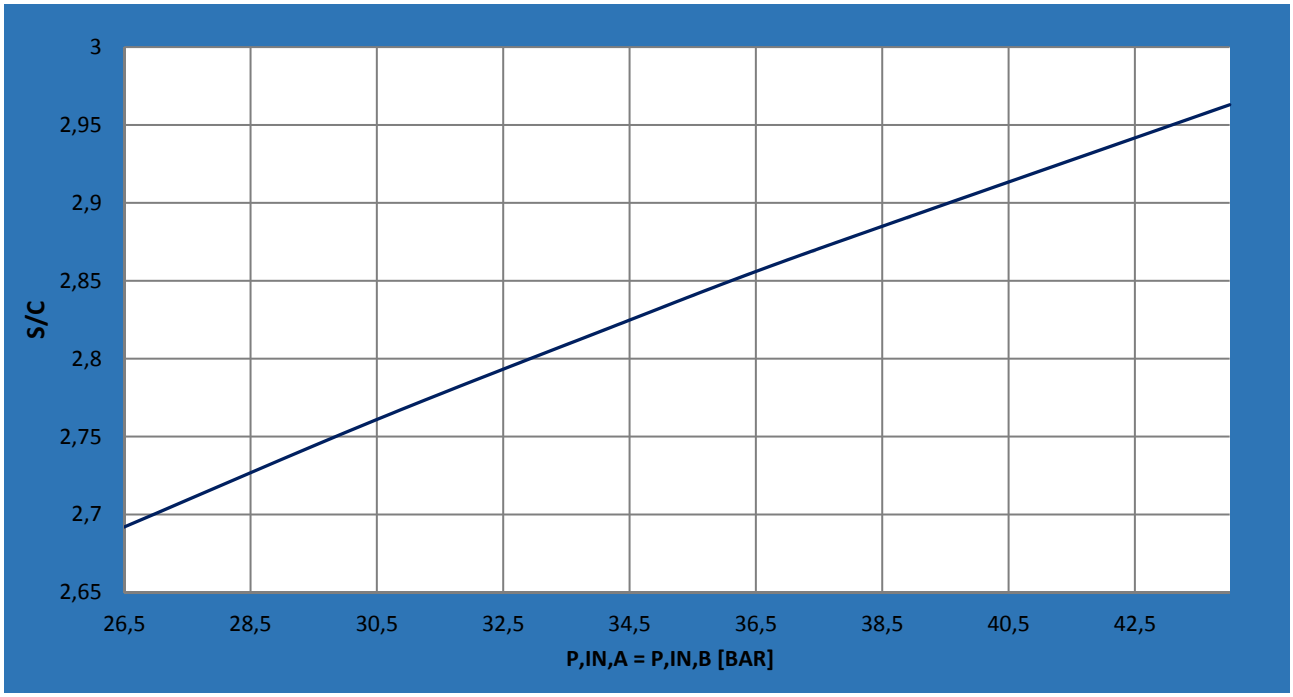

Figure 36: S/C required at stage A to feed stage C only with PSA off-gas as a function of stage A and B pressure.

The following graph (fig. 36) reports the CGE and the CCR as function of stage A and B pressure, with the corresponding S/C (see figure 35). Although the former decreases and the latter increases as the pressure increases (for the reasons mentioned in chapter 4.5), the change is very small. Increasing the pressure from 26,5 to 44 bar, the cold gas efficiency passes from 81,1% to 79,7%, while the carbon capture ratio passes from 96,6% to 97,9%. This very important feature paves the way to high-pressure processes, with significant advantages in terms of equipment volume and cost, PSA performance and compression costs.

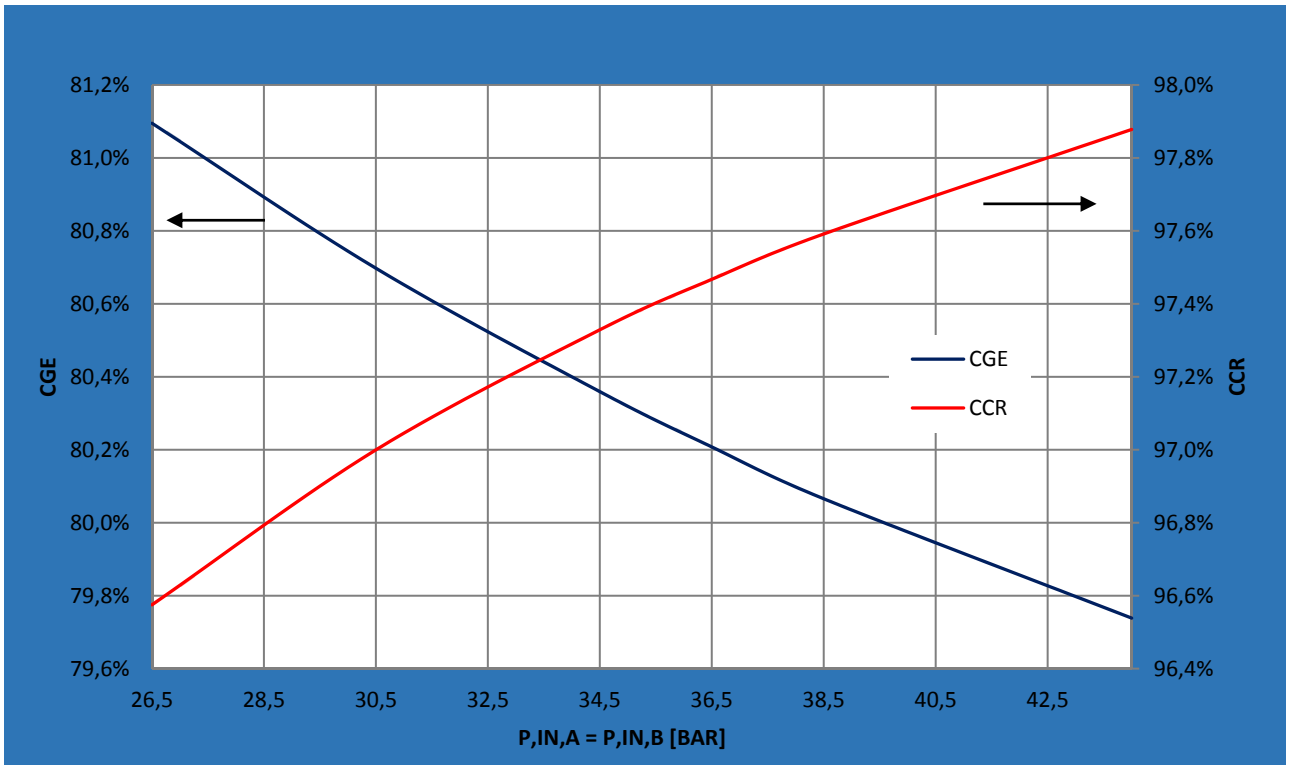

Figure 37: effect of stage A and B pressure on cold gas efficiency (left axis) and carbon capture ratio (right axis) for the system CaCu looping process + PSA

4.7.1) Beds number and size, pressure drops and thermal dissipations: economic considerations.

4.7.1.1) Beds number and size

After setting all the process thermodynamic and chemical parameters, it is possible to determine the optimal beds number and size. Such choice depends on economic considerations: on one hand there is the investment cost, on the other there are the operating costs. The former will be spread on the single years using a carrying charge factor. A full economic analysis would be not only a demanding task, but above all it would be full of uncertainties. Fortunately, in this section, we have to consider only the costs related, directly or indirectly, to the beds number and size. To this group belong the solid cost, the reactors cost, the valves cost and so on (basically everything inside the red dotted rectangle of figure 34). The operating costs related to the beds number and size are only those due to the pressure drops, which will be accounted for as a reduction of the electrical power output. Since we have to compare different Ca-Cu looping plant

configurations, and not the Ca-Cu looping plant with a traditional FTR plant, the burden of these uncertainties is lighter.

The first step requires to decide, arbitrarily, the number of reactors (beds) operating in every stage. In order to avoid significant variations of the hydrogen flow we can set to three the minimum number of stages A in parallel. The same applies to stage B, to limit the flow and temperature variations of the stream entering the gas turbine (and also the nitrogen stream entering the ammonia loop). Moreover, for every stage B there must be a stage B+. As a result, the minimum number of reactors required is 10: 3 for stages A, 3 for stages B, 3 for stages B+ and 1 for stage C. In the following we consider this configuration with a pressure of stage A and B of 34,5 bar, as an example of the procedure followed. Bear in mind that the Ca-Cu process has already been "solved" at this point, hence the streams entering and exiting the stages are all known. We have decided to set the beds size imposing a gas superficial velocity of 0,5 m/s for stage A, because of the CaO activity issue (see chapter 4.1). Eventually we will check that the gas superficial velocity for every stage is reasonable. For every stage we consider the section in which the superficial velocity is maximum (the worst section).

1) Consider stage A. After setting the plant capacity, the natural gas inlet flow is known. For a hydrogen molar flow of 1,53 kmol/s, a natural gas inlet flow of 0,55 kmol/s is required, that is 0,18 kmol/s for every stage A (remember that we are considering three stages A in parallel). The corresponding molar flow for the worst section (in this case zone "d" of figure 7) is known (0,93 kmol/s). We can now determine the cross section (A) required imposing the gas superficial velocity:

   $\dot{n}_{gas\ zone\ "d"} = v_g \cdot A \cdot (1 - \varepsilon_s) \cdot \rho_g \cdot \frac{1}{M_g} \quad \left[\frac{kmol}{s}\right] \quad \rightarrow$ A = 10,19 m^2 (r = 1,80 m)

   We can fix the length to radius ratio (l/r) to a reasonable value, in this case 6, therefore l = 10,81 m. The lower limit of such ratio is mainly due to two reasons: the radial dispersion and the stages duration inferior limits (due mainly to the valves operation but also to the process dynamic performances). The upper limit is due to the need to limit the pressure drops and the plant cost.
   The solid volume can be computed as $V_{sol} = A \cdot l \cdot \varepsilon_s = 55{,}09\ m^3$ (this is the solid volume of one bed at the beginning of stage A).

2) It is possible to calculate the amount of syngas produced by the complete conversion of such bed, as well as the syngas molar flow. In particular, the syngas composition and temperature changes with time (as seen in chapter 4.2), therefore we have to calculate the duration of every phase of stage A:

   $\Delta t, d = \frac{n_{tot,out,d}}{\dot{n}_{out,d}} = 26{,}05\ min$

   $\Delta t, c = \frac{n_{tot,out,c}}{\dot{n}_{out,c}} = 11{,}75\ min$

   $\Delta t, b = \frac{n_{tot,out,b}}{\dot{n}_{out,b}} = 33{,}70\ min$

   $\rightarrow \Delta t, tot, A = 71{,}50\ \text{min} \quad (= 71m\ 30s)$

3) Consider stage B. To have the same number of stages B and A working in parallel at any time, they must have the same duration ($\Delta t, tot, B = 71{,}50\ m$). Generally speaking, if N_a and N_b represent respectively the number of stages A and B working in parallel, we can say that $\Delta t, tot, B = \Delta t, tot, A \cdot \frac{N_b}{N_a}$.
The duration of stage B can be calculated as $t, tot, B = \frac{1}{2} \cdot \frac{n_{Cu}+n_{Ni}}{\dot{n}_{air,in} \cdot x_{O2,air}}$, assuming a complete oxidation of the bed. Therefore the air molar flow required is 0,61 kmol/s (for every stage B), which corresponds to a gas molar flow of 4,20 kmol/s in the worst section. The gas velocity in such section is 2,19 m/s. The figure is higher than that of stage A because of the high recirculation ratio (which implies a high molar flow).

4) The duration of stage B+ is equal to that of stage B and the gas molar flow in the worst section is known (2,04 kmol/s), considering that the recirculation ratio at stage B is 88,5% and that 45,2% of such recirculation flow bypasses stage B+. The corresponding gas superficial velocity is 0,95 m/s.

5) The duration of stage C must be $\Delta t, tot, C = \Delta t, tot, A \cdot \frac{N_c}{N_a}$, where N_c and N_a are respectively the number of stages C and A working concurrently. In this case $\Delta t, tot, C = 23{,}82\ min$. The feed flow entering the heated pre-reformer is known (from stage A) as well as the molar flow in the worst section (in this case zone "b" of figure 17), equal to 0,91 kmol/s. The corresponding gas velocity is 8,43 m/s. Such velocity is the highest one, not only because there is one only stage C, but above all because its pressure is very low (and so its volumetric flow is high).

From this brief considerations we can draw the conclusion that the number of stages A, B and C in parallel (referred to as N_a, N_b, N_c) has an important effect both on the solid amount, and so on the plant cost, and on the gas velocity, and so on the pressure drops.

4.7.1.2) Pressure drops

After setting the beds size and number, we can evaluate the pressure drops for every stage. Firstly it has to be pointed out that the gas composition and temperature changes not only along the axial direction, but also with time, as the fronts move forward. Consequently the pressure drops change with time. A detailed calculation of such pressure drops would be time-demanding, inaccurate and useless. Hence we evaluate the maximal pressure drop for every stage, based on the worst section. To do so, we use the most widespread empirical correlation for fixed beds, the Ergun's law, applied to spherical monosized particles:

$$\frac{\Delta p}{l} = \frac{150 \cdot (1-\varepsilon)^2 \cdot v \cdot \mu}{\varepsilon^3 \cdot d^2} + \frac{1{,}75 \cdot (1-\varepsilon) \cdot \rho \cdot v^2}{\varepsilon^3 \cdot d} \quad \left[\frac{Pa}{m}\right]$$

Where ε is the bed void fraction (0,5), v is the gas superficial velocity, μ is the gas dynamic viscosity, d is the particles diameter, ρ is the gas density. The first term on the right hand side represents the pressure loss through viscous effects and is the dominant in the laminar flow region; the second term is the loss due to

inertial forces and will be dominant at high Reynolds numbers (4). In our case the second term dominates. The results are shown in the following table. It should be noticed that the pressure drop in stage C is remarkable, because of its high gas velocity.

pressure drops				
	stage A	stage B	stage B+	stage C
ε =	0,5	0,5	0,5	0,5
d,p [m] =	0,022	0,022	0,022	0,022
M [kg/kmol] =	7,87	28,33	28,33	11,60
T [K] =	1133,0	1103,0	990,1	1133,0
P [bar] =	34,16	34,16	34,16	1,78
ρ [kg/m^3] =	2,85	10,55	11,75	0,22
v [m/s] =	0,50	2,19	0,95	8,43
μ [Pa*s] =	3,26E-05	4,23E-05	3,94E-05	3,62E-05
Δp/l,A [Pa/m] =	10,12	57,44	23,32	189,48
Δp/l,B [Pa/m] =	227,08	16126,88	3408,38	4964,45
Δp/l,tot [Pa/m] =	237,20	16184,32	3431,70	5153,93
ΔP,tot [bar] =	0,026	1,749	0,371	0,557
ΔP/P,in =	0,07%	5,07%	1,09%	30,95%

Table 17: pressure drops calculation for the case with N_a=N_b=3 and P_a=P_b=34,5 bar

Such pressure drops entail an increase in compression costs and so a reduction in the electrical power output, if there is one, otherwise there will be an increase in the electrical power input. Although there is a difference between the energy purchase and sale price and there should be turbomachinery efficiencies to account, we can consider the cost of the pressure drops as a reduction in the power sold, even if it will come out that there is a net power input (even more so for the reasons we will see later on). Such costs are due to the recompression of the pure hydrogen flow, of the pure nitrogen flow required by the ammonia plant (in our case), of the recirculation flow at stage B, of the carbon dioxide flow from stage C and to the reduction in the gas turbine power output. We have assumed an electricity price of 55 €/MWh. The following table reports the cost due to the pressure drops in the case analysed. The main costs are due to the recompression of the recirculation flow at stage B (for its high mass flow) and to the recompression of the CO2 flow (for the high pressure drop of stage C). Together the two account for roughly 90% of the pressure drops cost, which, in this case, is estimated at 5160 €/d.

pressure drops cost						
η,is=	0,75					
η,mech=	0,98					
η,el=	0,96					
hydrogen flow				recirculation flow at stage B			
m,H2=	3,07	kg/s		m,N2,rec=	171,31	kg/s	
T,in=	323,00	K		p,in=	32,38	bar	
p,in=	2,77	bar		p,out=	34,50	bar	
p,out=	2,79	bar		cp=	1,07	kj/kg*K	
cp=	14,46	kj/kg*K		(γ-1)/γ=	0,28		
(γ-1)/γ=	0,29			P,pale=	2511,12	kW	
P,shaft=	51,18	kW		P,el=	2669,13	kW	68,3%*
P,el=	54,40	kW	1,4%*				

Continues

nitrogen flow			
m,N2 for ammonia=	14,31	kg/s	
m,N2,in,psa=	17,89	kg/s	
m,N2,in,tot=	39,68	kg/s	
m,N2,gt=	21,79	kg/s	
T,in=	323,00	K	
p,in=	32,42	bar	
p,out=	34,17	bar	
cp=	1,04	kj/kg*K	
(γ-1)/γ=	0,29		
P,shaft=	97,85	kW	
P,el=	104,01	kW	2,7%*

carbon dioxide flow			
m,CO2=	25,82	kg/s	
p,in=	1,24	bar	
p,out=	1,80	bar	
cp=	0,88	kj/kg*K	
(γ-1)/γ=	0,22		
P,pale=	792,81	kW	
P,el=	842,69	kW	21,6%*

gas turbine			
p,in,gt=	34,50	bar	
p,in,tg'=	32,75	bar	
cp=	1,17	kj/kg*K	
(γ-1)/γ=	0,26		
P,gas turbine, shaft=	254,15	kW	
P,el,gas turbine=	239,10	kW	6,1%*

P,tot,el=	3,91	MW
electricity cost =	55	€/MWh
total cost =	215,01	€/h
	5160,32	€/d
	1883517,46	€/y

Table 18: pressure drops cost evaluation

* Fraction of the total recompression cost.

4.7.1.3) Thermal dissipations

Since we have assumed the adiabaticity of every stage for our calculations, we have to evaluate in this section the amount (thickness) of insulating required to fulfil this hypothesis. Similarly to the pressure drops, the thermal dissipations change with time, as the gas temperature inside the reactors change with time. Once again we have considered the worst case, that is the one in which the gas temperature is at its maximum value (in this case 860 °C, which is roughly the maximum temperature for stages A and C). The convective thermal resistance on the inner side (hot gas side) has been neglected as a further safety margin (anyway, it is far lower than the conductive resistance or the external convective resistance). Therefore we have assumed an inner wall temperature of 860 °C.

The internal refractory thickness is chosen to limit the maximal steel temperature, which, of course, depends on the steel employed. Even though on the market there are high-temperature applications steels, with very good tensile performances, particularly those Chromium-Molybdenum, we have chosen a cheaper "standard" steel, the SA 516 grade 70. The maximal steel temperature is fixed to 300 °C, at which the design steel stress is 136 MPa. The advantage of fixing a low steel temperature lies not only in a lower steel stress but also, if we set the external wall temperature, in an increase of the refractory thickness to the advantage

of the more expensive external insulating thickness. In this case, considering a gas pressure of 35 bar, the steel thickness required is 11,1 cm.

To determine the refractory and the external insulating thickness we have to impose an external wall temperature, in this case 70 °C could be a good value. The external convective heat transfer coefficient can be evaluated with the correlations available for natural convection on vertical plates, after assessing the Rayleigh number. Since the Rayleigh number based on the reactor height (L = 12,4 m) is $Ra_L = 7{,}22*10^{12} > 10^9$, the flow regime is turbulent and the Nusselt number can be evaluated with the following correlation:

$$Nu_L = 0{,}15 \cdot (Ra_L * Pr)^{\frac{1}{3}} \quad \rightarrow \quad h_{ext} = 5{,}73 \ \frac{W}{m^2 \cdot K}, \ \text{where } Ra_L = Gr_L \cdot \mathrm{Pr} = \frac{g\beta(T_{wall,ext} - T_\infty)L^3}{\nu^2} \cdot \frac{\nu}{\alpha}$$

The (maximal) heat flux through the vertical walls of the cylindrical reactors is

$$\Phi = h_{ext} \cdot \left(T_{wall,out} - T_\infty\right) = 286{,}4 \ \frac{W}{m^2}$$

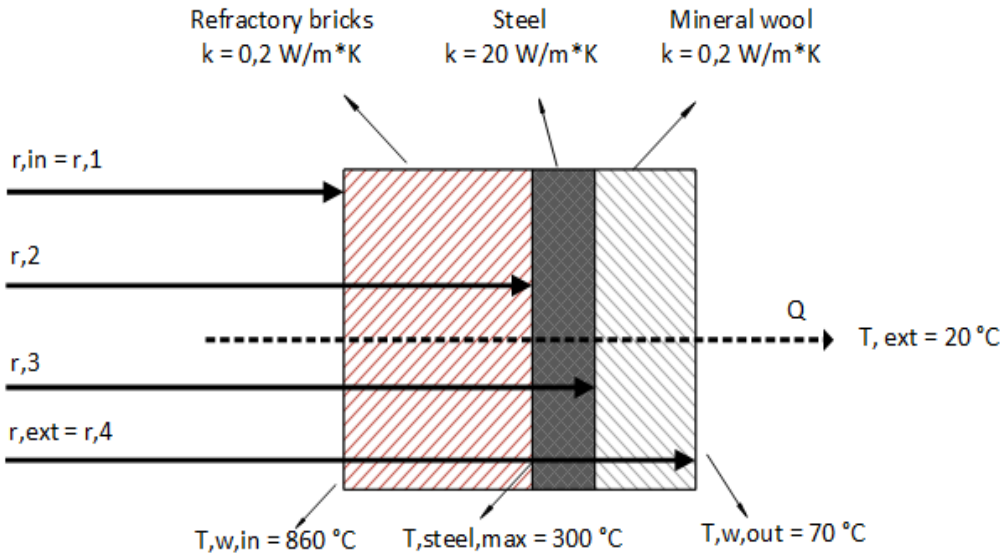

Figure 38: reactor thermal scheme

The insulating (mineral wool) thickness can be determined with the following relation:

$$Q_{lat} = \Phi \cdot 2\pi r_{ext} \cdot L = \frac{(T_{steel,max} - T_{wall,out})}{R_{steel} + R_{insulating}}, \ \text{where the conductive resistances in cylindrical geometry are}$$

$$R_{steel} = \frac{\ln\frac{r3}{r2}}{2\pi L k_{steel}}, \quad R_{ins.} = \frac{\ln\frac{r4}{r3}}{2\pi L k_{ins.}} \left[\frac{K}{W}\right] \quad \rightarrow \quad t_{ins.} = 15{,}4 \text{ cm.}$$

Similarly the refractory thickness:

$$Q_{lat} = \frac{(T_{wall,in} - T_{steel,max})}{R_{refractory}}, \ \text{with } R_{ref.} = \frac{\ln\frac{r2}{r2}}{2\pi L k_{ref}} \left[\frac{K}{W}\right] \quad \rightarrow \quad t_{ref.} = 32 \text{ cm.}$$

Finally, the thermal dispersions are accounted for as temperature drops (ΔT) of the gas streams exiting the reactors. The following table sums up the results.

T,wall,in=	860	°C					external convective coefficient		
T,max,steel=	300	°C							
T,wall,ext=	70	°C					L,bed=	10,81	m
T∞=	20	°C					L,reactor=	12,43	m
k, ref.=	0,2	W/m*K					T,f=	45	°C
k, steel	20	W/m*K					β=	0,0031	1/K
k, ins. =	0,2	W/m*K		r,1=	1,801	m	Pr=	0,72	
t, ref.=	0,321	m	→	r,2=	2,122	m	ρ=	1,11	kg/m^3
t, steel=	0,111	m	→	r,3=	2,233	m	ν=	1,72E-05	m^2/s
t, ins.=	0,154	m	→	r,4=	2,387	m	Gr=	1,00E+13	
							Ra=	7,22E+12	
							Nu=	2598,98	
Q,lat=	53,40	kW	(maximal dissipation per reactor on lateral walls)				k=	0,027	W/m*K
Q,tot=	63,65	kW	(maximal dissipation per reactor)				h,ext=	5,73	W/m^2*K
Q,tot=	636,50	kW	(maximal overall thermal dissipation)						

maximal temperature drops

ΔT,stage A=	1,85	°C
ΔT,stage B=	0,46	°C
ΔT,stage B+=	0,95	°C
ΔT,stage C=	1,08	°C

Table 19: calculation of the refractory and external insulating thickness required and of the temperature drops.

The maximal temperature drop is below 2 °C for every stage: the adiabaticity is a good hypothesis.

4.7.1.4) Economic considerations

To evaluate the investment cost mentioned at the beginning of chapter 4.7.1 we have to assume a cost for the solid in the beds. Since this is the most important investment cost (among those directly related to the Ca-Cu looping system), this is a very influential hypothesis (and probably the heaviest uncertainty). After calculating the material cost, we add the labour and installation costs (assumed to be equal to those of material), the indirect costs, the owner's costs and the contingencies costs. The result is the total plant cost. Such cost is spread over the years using a carrying charge factor of 13%. The minimum number of valves per reactor required to perform the cyclical operation is 8. The ensuing table sums up the results for the case considered above (N_a = 3, N_b = 3, N_c = 1, P_a = P_b = 34,5 bar).

R, bed=	1,80	m
L, bed=	10,81	m
L, reactor=	12,43	m
T,max,in=	863,4	°C
P,max,in=	34,5	bar
T, external wall=	70	°C
T,steel, max =	300	°C
Steel design stress (@ 300 °C) =	136	MPa

valves per reactor=	8	cost per valve=	€ 50.000
N, valves, total=	80	total valves cost=	€ 4.000.000

reactor material	thickness [cm]	amount per reactor [m^3]	total amount [m^3]	cost [€/m^3]	total cost
fire bricks (internal refractory)	32,06	53,65	536,51	216,0	€ 115.886
steel (SA 516 grade 70)	11,11	20,63	206,32	5581,4	€ 1.151.548
mineral wool (external insulating)	15,42	30,58	305,77	750,0	€ 229.326

solid bed material (supported by allumina)	amount per reactor [t]	total amount [t]	support (Al2O3) massic fraction	cost [€/t]	total cost
CaO	112,19	1121,91	15%	10000,00	€ 11.219.148
Cu	98,11	981,08	35%	15000,00	€ 14.716.267
Ni	28,61	286,09	82%	50000,00	€ 14.304.414

total material cost=	€ 45.736.589

labour and installation factor=	1	
total direct plant cost=	€ 91.473.178,07	
indirect costs factor=	0,14	
indirect costs=	€ 12.806.244,93	
owner's costs & contingencies factor=	0,15	
owner's & contingencies costs=	€ 15.641.913,45	
total plant cost=	€ 119.921.336	
carrying charge factor (CCF)=	0,13	
plant cost per year=	15.589.774	€/y
cost due to the pressure drops=	1.883.517	€/y
total cost per year=	17.473.291	€/y

Table 20: evaluation of the material cost for CaCu process alone

The total plant cost found here, by no means representative of the real plant cost, is useful to compare several configurations and choose the optimal number of beds operating in parallel for every stage (N_a, N_b, N_c). The results above show that the investment is the dominant cost (compared with the pressure drops

cost), therefore the goal will be to minimise such cost. In other words, it is generally worthwhile to accept higher pressure drops if it involves a reduction of the total volume of solid.

In the following we show the results of a sensitivity analysis aimed to evaluate the investment cost (per year) and the pressure drops cost for several number of stages. In figure 38 the number of stages A in parallel is set to 3 and the number of stages B (equal to that of B+) is varied from 3 to 6. On the x-axis, in brackets, there is the total number of beds (reactors) required. In figure 39 the number of stages A is set to 4. In any case the number of stages C is set to one, because the pressure drops play a minor role in the total cost and so it advantageous to reduce the solid volume. In any case, the main recompression cost is due the recirculation flow at stage B, hence increasing the number of stages B in parallel entails a reduction in the pressure drops cost.

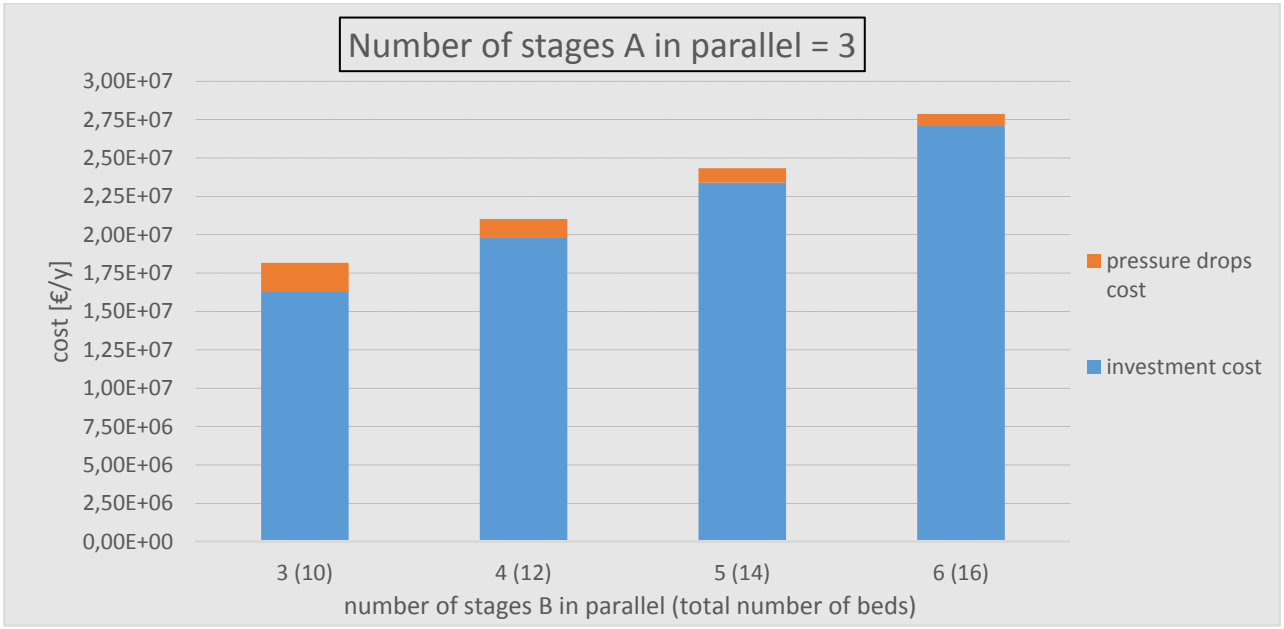

Figure 39: investment cost and pressure drops cost on varying number of stages B in parallel, with 3 stages A in parallel.

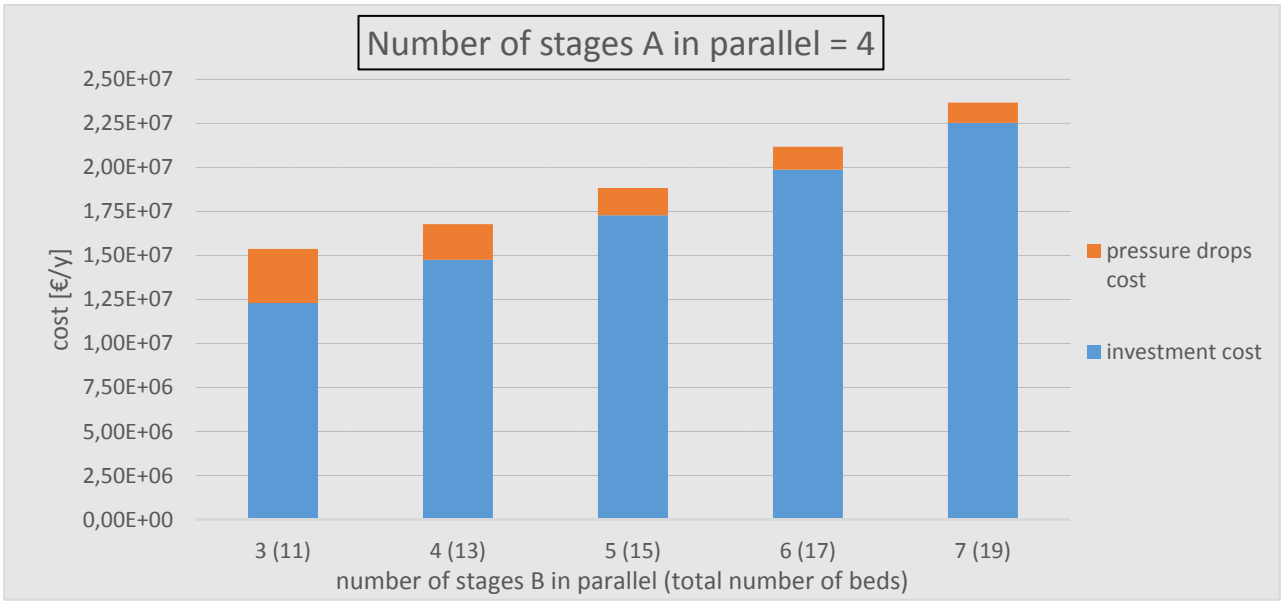

Figure 40: investment cost and pressure drops cost on varying number of stages B in parallel, with 4 stages A in parallel.

We have decided to limit the maximal number of stages A in parallel to four to contain the plant complexity and give a lower limit to the stages duration. From the graphs above we can conclude that the optimal configuration is those with 4 stages A and 3 stages B, despite the high pressure drops. In fact, since we have determined the beds size imposing the gas maximal velocity in stage A, increasing the number of stages A leads to a lower molar flow per stage A and so to a reduction of the beds size. Consequently, increasing the number of stages A leads to a reduction in the total solid volume. Of course there are some by-products: an increase in plant size (more reactors), an increase in pressure drops, a stages duration reduction, an increase in pipes and instrumentation amount, an increase in the gas velocity in stages different than A, which can cause a widening of the reaction fronts and a faster solid wear. Since the solid represents the main cost, and so the main uncertainty, we have performed another sensitivity analysis, similar to the previous one, with a solid cost reduced to 40% (that is, reduced by 60%).

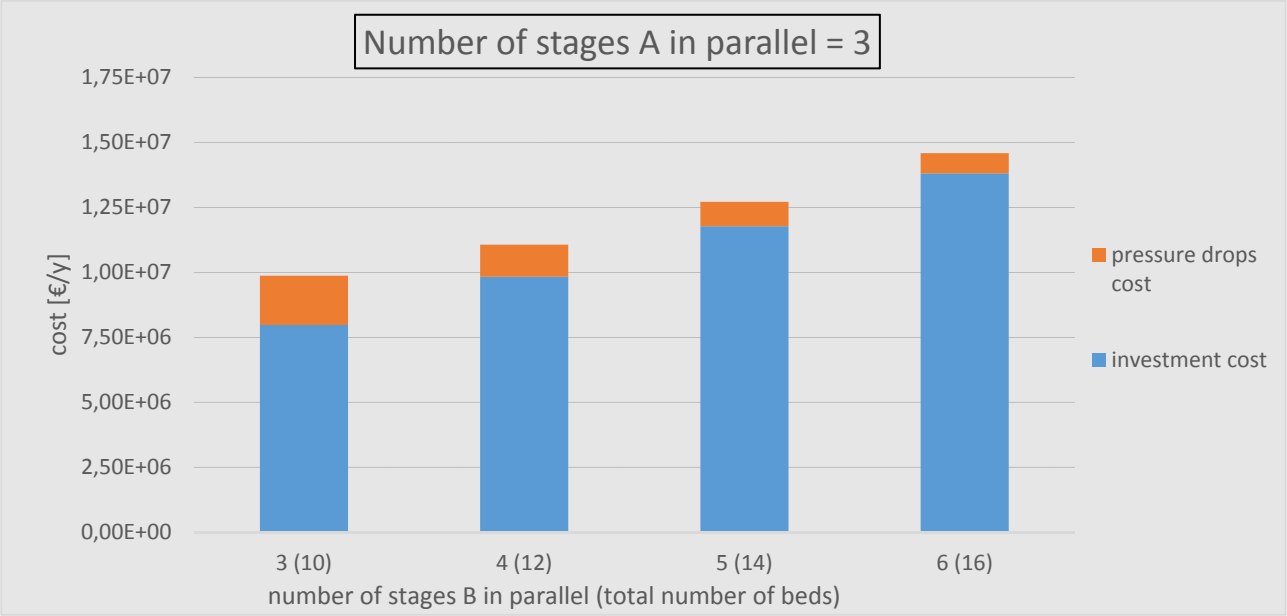

Figure 41: investment cost and pressure drops cost on varying number of stages B in parallel, with 3 stages A in parallel. Solid cost reduced to 40% of the original value.

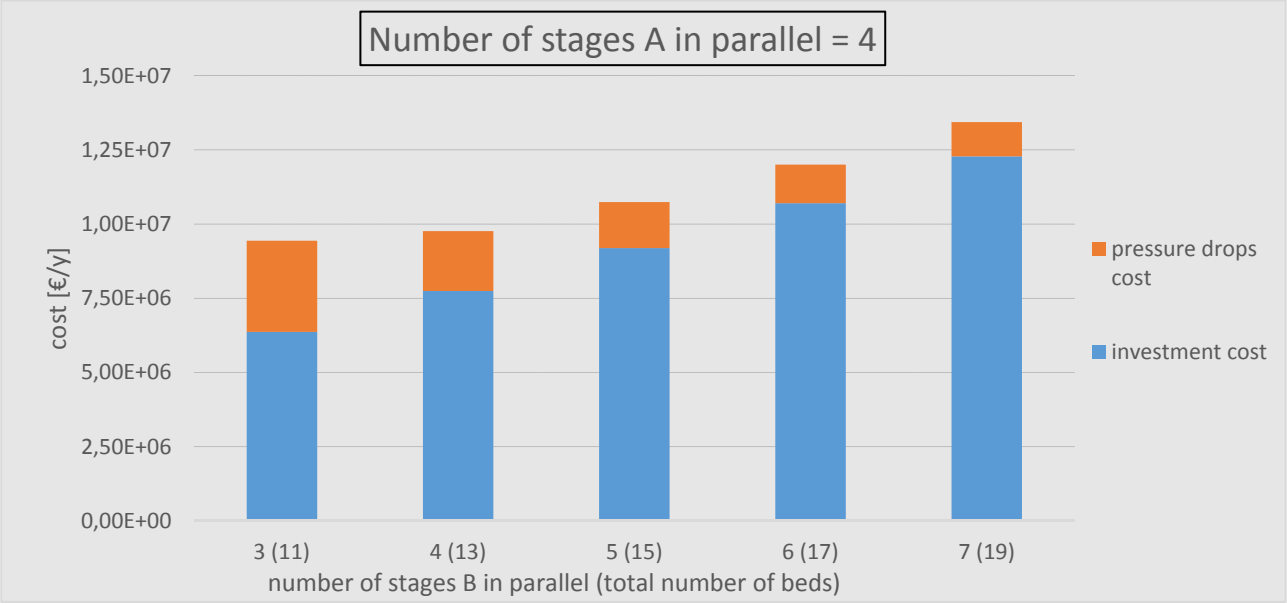

Figure 42: investment cost and pressure drops cost on varying number of stages B in parallel, with 4 stages A in parallel. Solid cost reduced to 40% of the original value.

This new analysis confirms that the optimal configuration is that with $N_a = 4$ and $N_b = 3$, therefore, from this moment on we will consider this configuration. Once again, we want to make clear that the costs above are not representative of the real plant cost, they just allow to choose the best plant configuration. The table below sums up the results for the case with $P_A = P_B = 34{,}5$ bar, while figure 42 represents the dynamic operation of the process.

R, bed=	1,56	m	P,max,in=	34,5	bar
L, bed=	9,36	m	T, external wall=	70	°C
L, reactor=	10,8	m	T,steel, max =	300	°C
T,max,in=	863,4	°C			
	stage A	stage B	stage B+	stage C	
Number	4	3	3	1	
Δt [min] =	61,9	46,44	46,44	15,48	
V, max [m/s] =	0,5	2,92	1,27	11,24	
ΔP [bar] =	0,022	2,69	0,57	0,85	
valves per reactor=	8			cost per valve=	€ 50.000
N, valves, total=	88			total valves cost=	€ 4.400.000
reactor material	thickness [cm]	amount per reactor [m^3]	total amount [m^3]	cost [€/m^3]	total cost
fire bricks (internal refractory)	31,52	40,09	441,02	216	€ 95.260
steel (SA 516 grade 70)	9,62	13,69	150,58	5581,4	€ 840.451
mineral wool (external insulating)	15,37	23,47	258,20	750	€ 193.647
solid bed material (supported by allumina)	amount per reactor [t]	total amount [t]	support (Al2O3) massic fraction	cost [€/t]	total cost
CaO	72,87	801,58	15%	10000,00	€ 8.015.756
Cu	63,72	700,96	35%	15000,00	€ 10.514.345
Ni	18,58	204,40	82%	50000,00	€ 10.220.089

Table 21: summary of the results for the case with N_a=4, N_b=3 and P_a=P_b=34,5 bar.

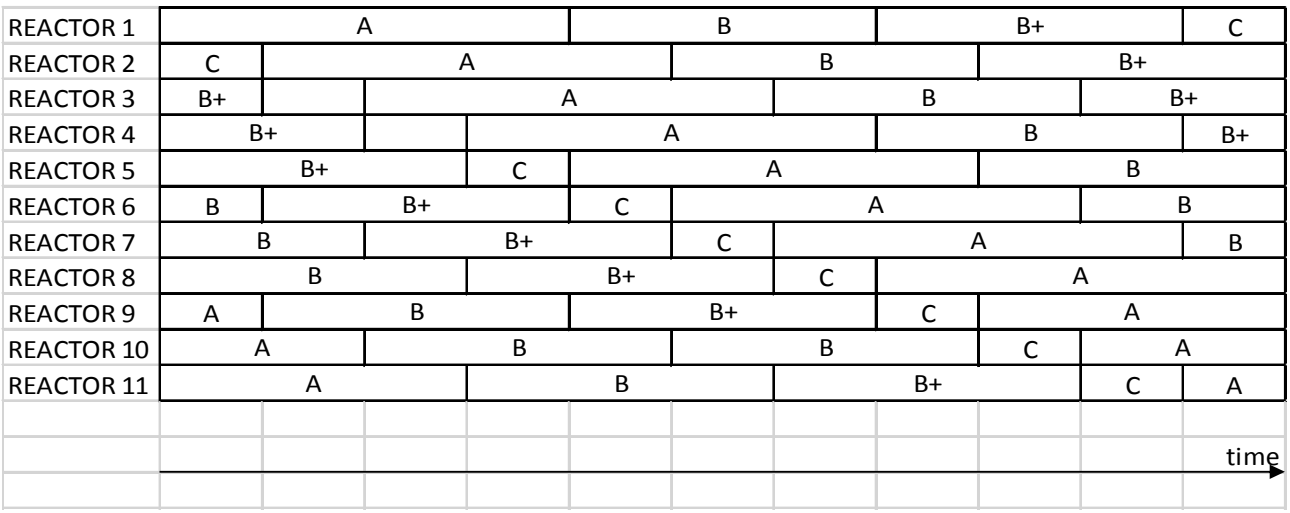

Figure 43: dynamic operation of the process.

We have left in suspense the issue of the optimal pressure for stages A and B. Even if the aspects to account are many, we can make here some useful considerations. Firstly, as we have seen that the investment cost is the most important entry in the overall management cost (which, in this case, does not include the fuel cost, since the effect of the pressure drops is accounted for as a reduction of power output), it is vital to evaluate the effect of pressure on such cost. The graph below, which shows the investment costs (those listed above) and the pressure drops cost on varying the pressure of stage A and B, testifies evidently the important benefit of operating at high pressure. Even if such effect was easily predictable (since an increase in pressure entails an increase in density and so, set the molar flow and the gas velocity, a reduction in the cross area), its extent, as well as the effect on the pressure drops, were not. The pressure drops cost slightly increases as the pressure of stages A and B increases, as a consequence of the rise in pressure drop in stage C.

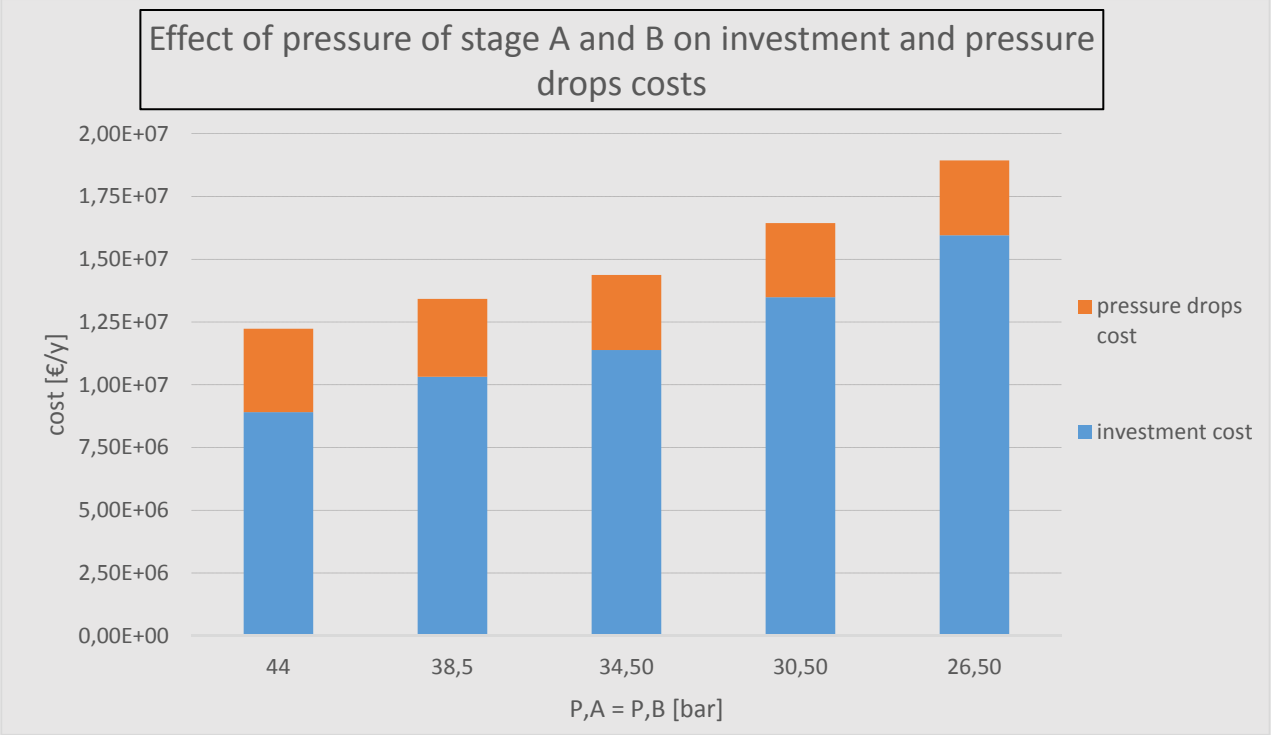

Figure 44: effect of pressure of stages A and B on investment and pressure drops costs.

Everything seems to come out in favour of high pressures. Actually, high pressures entail by-products too, the main probably being the pressure drop in stage C. As we have seen, increasing the pressure of stage A allows to reduce the beds cross area, but, in this way, the gas velocity in stage C increases, since the gas density and molar flow in stage C is not affected by stage A pressure. When $P_A = P_B$ exceeds 33 bar, the outlet pressure of stage C (if we set the inlet value to 1,8 bar) becomes subatmospheric (in this configuration). On the other hand, increasing the pressure of stage A and B seems to have a (small) positive effect on the relative pressure drops of stages A, B and B+ (see figure 44). Besides, however small, the pressure has an effect on cold gas efficiency, meaning that increasing the pressure entails a little increase in fuel consumption (see figure 36). Then, we have to remark that the calculations have been performed under the ideal gas hypothesis, which loses accuracy at high pressures. Lastly, there is an effect that requires solving in detail the plant to be correctly assessed. In fact, whereas in traditional reforming plants an increase in operating pressure entails a significant reduction in compression costs, here we have to consider that the oxygen compressed by the air compressors is trapped in stage B and released at low pressure in stage C, therefore it is not expanded in the gas turbine. Note that decreasing the pressure of stage B is not a solution: it would

lead to a sharp increase in pressure drops. To evaluate effectively the influence of pressure on compression costs we have to analyse at least two plants operating at two different pressures. This is what we will do in chapter 5, in the case of an ammonia plant.

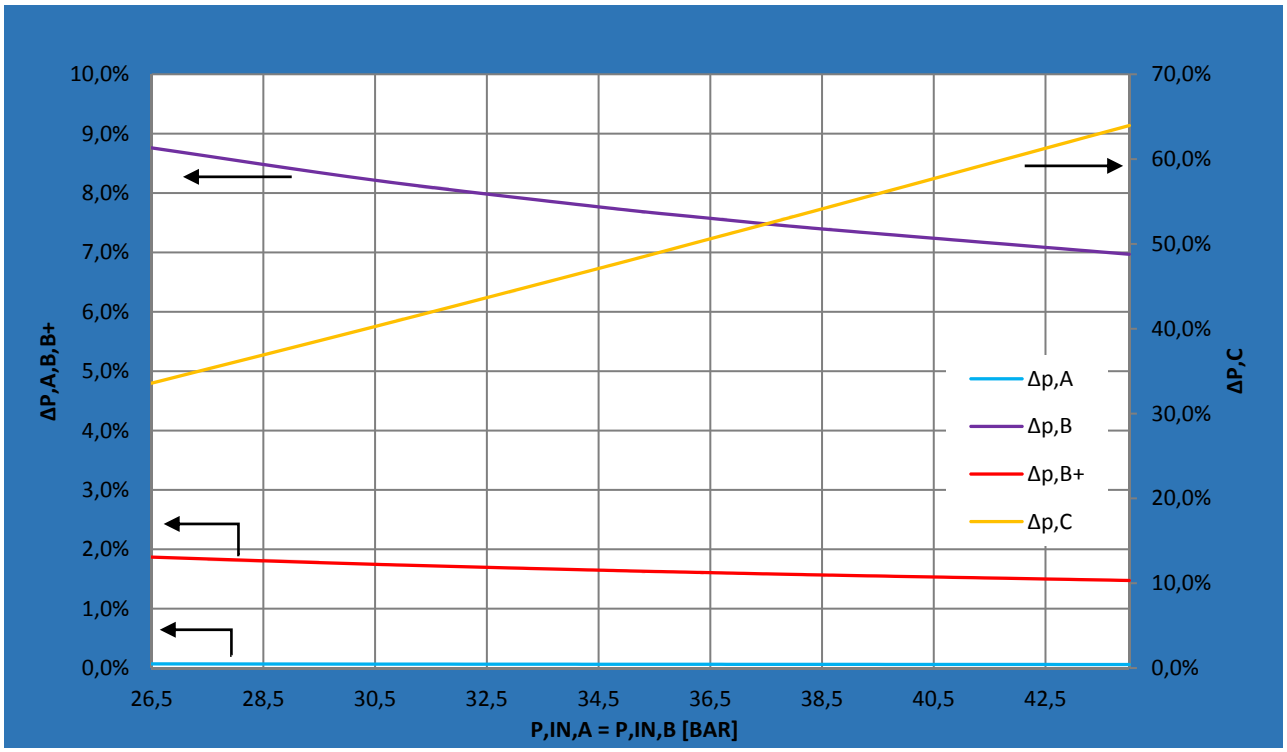

Figure 45: effect of pressure of stages A and B on relative pressure drops. The curve of the pressure drops of stage A is close to zero

Finally, in the following page there is an example of a complete Ca-Cu looping process scheme for high-purity hydrogen production (fig. 45). The heat integration system has been omitted: a complete scheme for ammonia production will be proposed and analysed in the next chapter. The aim of the figure is to explain how the reactors can be connected to work cyclically. Note that 8 valves per reactor are required at least, since there are four feeding lines (one for stage) and four drain lines (one for stage). The operating mode of the valves (close/open) determines the stage in which every reactor is working.

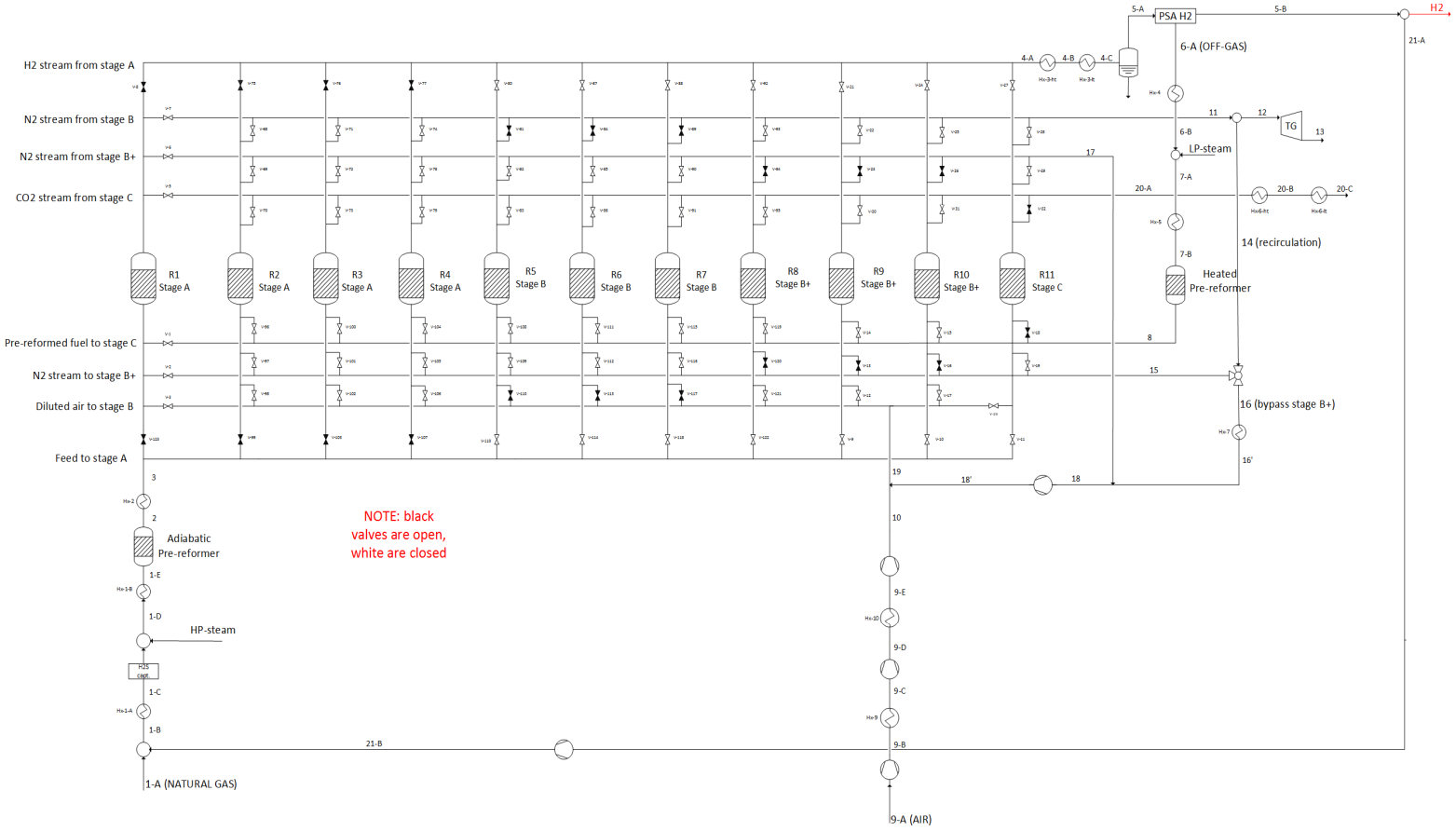

Figure 46: example of a complete CaCu looping process scheme for high-purity hydrogen production

5) CaCu looping process in ammonia production plants

In this chapter, the CaCu looping process for hydrogen production proposed in chapter 4.7 is applied to ammonia plants. In this case, such a process has the intrinsic advantage of producing two hydrogen and nitrogen separate flows, which can then be mixed in a proper proportion. Besides, since the process produces a third flow, made only of carbon dioxide and steam, it can be employed in urea plants as well, requalifying part of the carbon dioxide produced.

As pointed out above, neither the hydrogen nor the nitrogen flow has a high enough purity to be directly introduced in the ammonia loop. It is proposed in this work using a PSA system also for the nitrogen flow, for which an 80% efficiency has been assumed (while that of hydrogen has an efficiency of 90%). We have assumed 100% purity for both N2 and H2 products coming out from the two different PSA units. Note that the chance to use two PSA units is related to the availability of two separate flows: if we had hydrogen and nitrogen mixed in one only flow, together with others (unwanted) compounds, we wouldn't be able to obtain the hydrogen to nitrogen ratio required with a PSA (we cannot set both the hydrogen and nitrogen capture efficiency). Finally, the convenience of using two PSA is due to high purity of the two streams (the hydrogen stream entering the PSA has a purity of 85-86%, while the nitrogen one exceeds 97%). The same does not apply to traditional plants, in which the high concentration of carbon compounds in raw syngas dictates the necessity for a water-gas shift and a carbon dioxide removal section.

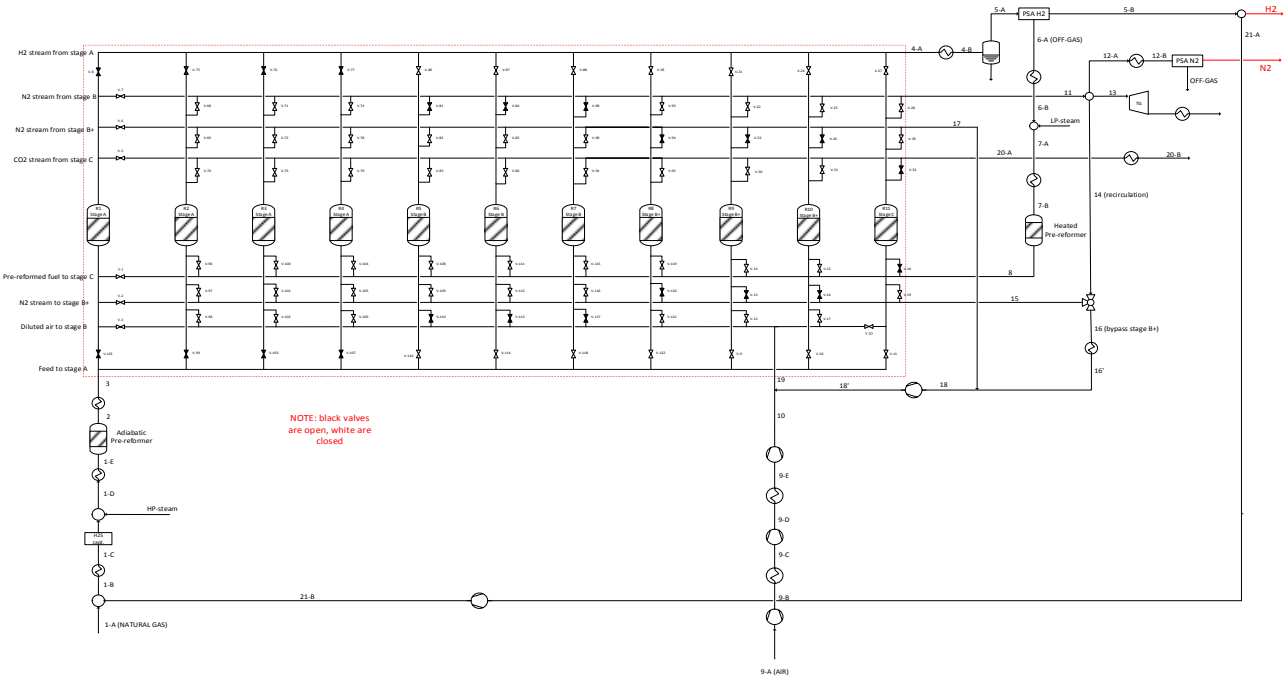

Figure 1: Ca-Cu looping process scheme in ammonia production plants (without heat integration system)

In the following we will analyse three different plants, for all of them the scheme shown in Fig.1 can be applied. The hydrogen-rich stream from stages A is cooled to 40 °C and, after the condensed water removal, it is sent into the PSA. The stream exiting the PSA is mixed with the nitrogen stream and fed to the ammonia synthesis loop. The PSA flue-gas are properly mixed with low-pressure steam (to reach a S/C of 1), heated up and fed to the heated pre-reformer. As already said, the gas exiting such reformer is the only feed of stage

C. The nitrogen-rich stream from stages B, taken out the recycled fraction, is partly cooled to 40 °C and sent to the nitrogen PSA and partly sent to the gas turbine. In particular, after setting the amount of ammonia to be produced, the amount of nitrogen and hydrogen required is known ($n_{NH3}^{tot} \cong \frac{1}{2} n_{N2}^{in,loop} \cong \frac{3}{2} n_{H2}^{in,loop}$ where the approximately is due to the negligible N_2 and H_2 slip as gas dissolved in the liquid ammonia). Therefore, the nitrogen flow to be fed to PSA is $n_{N2}^{in,PSA} = \frac{1}{0,8} n_{N2}^{in,loop}$ (since the efficiency of the nitrogen PSA is 80%). The remaining part is fed to the gas turbine (stream 13 in fig. 1). Looking to figure 1, it is possible to note that there is a stream of pure hydrogen mixed with the fresh natural gas (stream 23B). As seen in chapter 2, this very little hydrogen flow is required for the natural gas desulphurization.

The availability of a pure hydrogen-nitrogen flow downline of the PSAs has momentous consequences for the ammonia loop section, of which is given a simplified scheme in figure 2. Firstly, it means that no inert is introduced into the synthesis reactor, leading both to a conversion increase and to a reduction in the volumetric flow rate crossing the reactor (and so to a reduction in the equipment cost). Secondly, no purge stream is required. In fact, even if small amounts of inert compounds escape the PSAs, they can be removed from the loop dissolved in the liquid ammonia. Consequently, there are no hydrogen (and nitrogen) losses due to the purge stream: all the reactants are converted into ammonia (except for the negligible losses due to the dissolution in liquid ammonia). Moreover, both the scrub and the PSA for the purge stream treatment are spared. Finally, there is no NO_x formation due to the combustion of the residual ammonia in the purge stream.

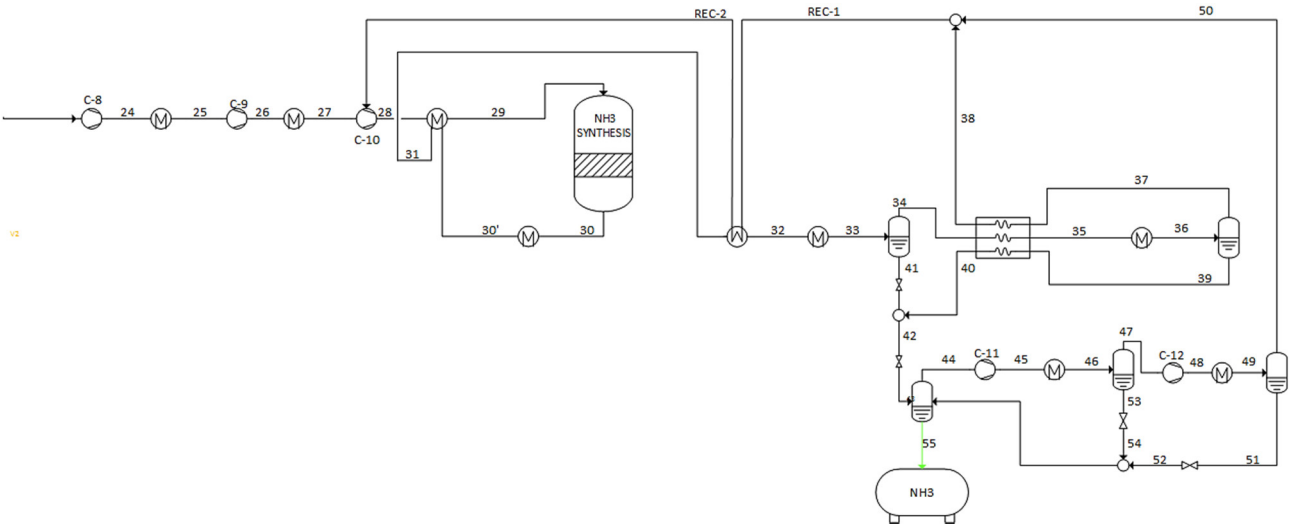

Figure 2: ammonia synthesis loop for the CaCu looping process, without heat integration system

In the first and second case we consider the same scheme with two different pressures, in order to assess the effect of pressure on performance and solid cost. In the third case we use a heated pre-reformer also for stage A. Two reasons lie behind this modification. The first is the will to avoid any chance of CaO hydration. In fact, in chapter 4.2 it is said that there should be no hydration in zone "a" of stage A because there is no active CaO in that zone. Actually, the matter has still to be studied in detail. The issue can be completely overcome if the gas entering stage A is in chemical equilibrium at a temperature $T_{,g,in,A}$ so that $P_{,water,in} < P_{,water,limit(T,g,in,A)}$. In fact, in this way the gas temperature does not drop to $T_{,adiabatic}$ in the first zone of the bed, and CaO hydration is no longer favoured. The second reason is simply a cold gas efficiency gain, since this allows to turn some thermal energy into chemical energy. Anyway, the availability of the high-temperature heat required to make such a pre-reforming should not be taken for granted.

5.1) Case 1: Base case with P,A = P,B = 34,5 bar.

Figure 3 shows the simplified scheme of the syngas production section. In this scheme, the details of the fixed bed reactors connections are omitted, as well as the water/steam heat recovery system, it is displayed instead the heat integration system between the process gas streams. In particular, the gas from stages A (stream 4A of fig. 3), which is the hottest available, its temperature being 835 °C in this case, supplies the heat required to perform the pre-reforming of the feed of stage C. The heat required by the feed of stage A is supplied by the recycle stream of stage B that bypasses stage B+ (stream 16A), which is the greatest hot flow available. Finally, the little nitrogen flow to be sent to the PSA (stream 12A), heats up the feed of stage C (to 566 °C in this case) before it enters the pre-reformer. The flow obtained by mixing the H_2 and N_2 pure flows (stream 23) is sent to the ammonia loop compression train.

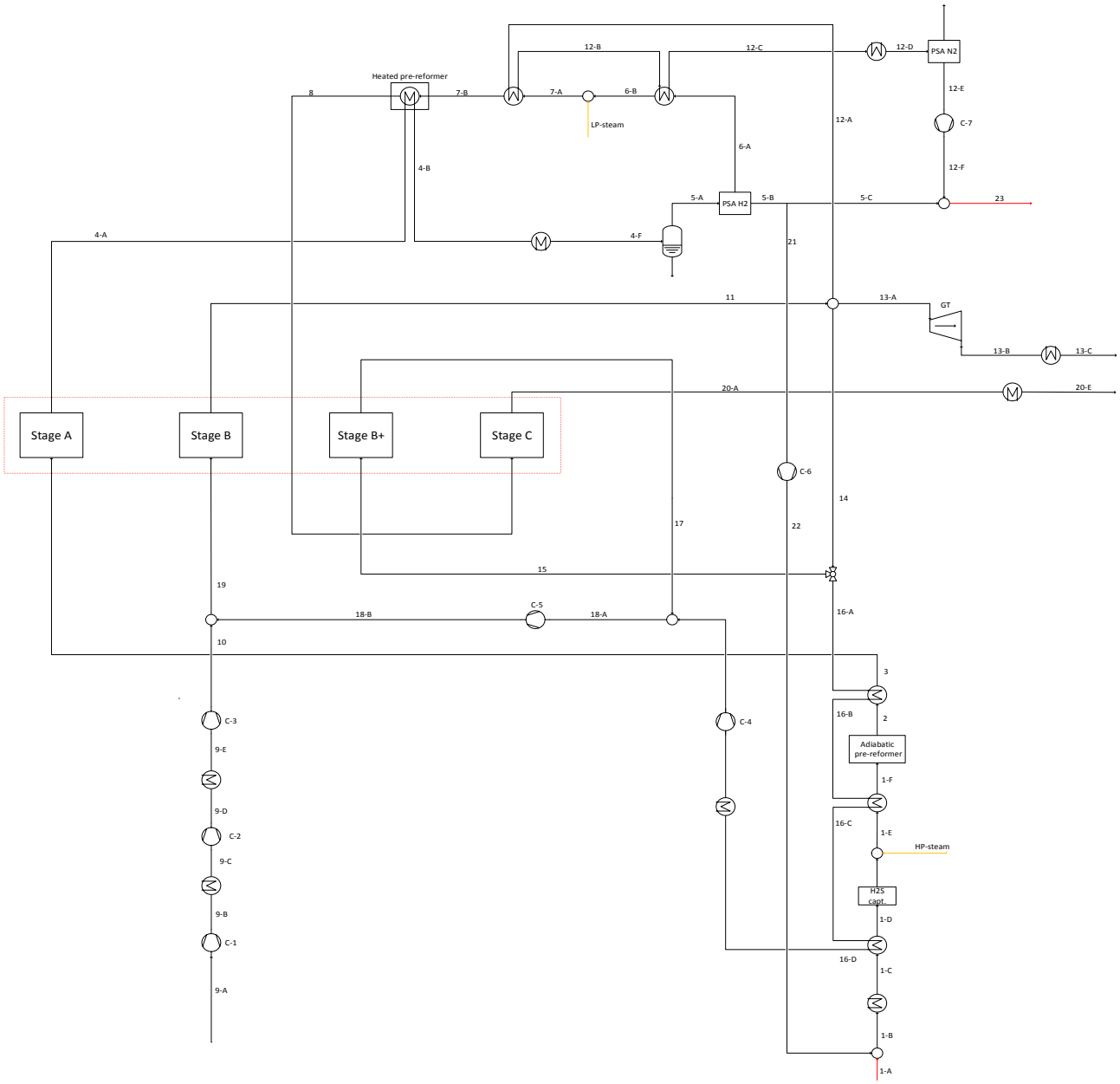

Figure 3: CaCu looping process for ammonia production plants, simplified scheme.

Figures 4 and 5 show the complete schemes of the CaCu process and the ammonia loop, with heat integration systems. As for the schemes in chapter 3, the black lines represent process gas streams, the light blue ones liquid water, the orange ones steam.

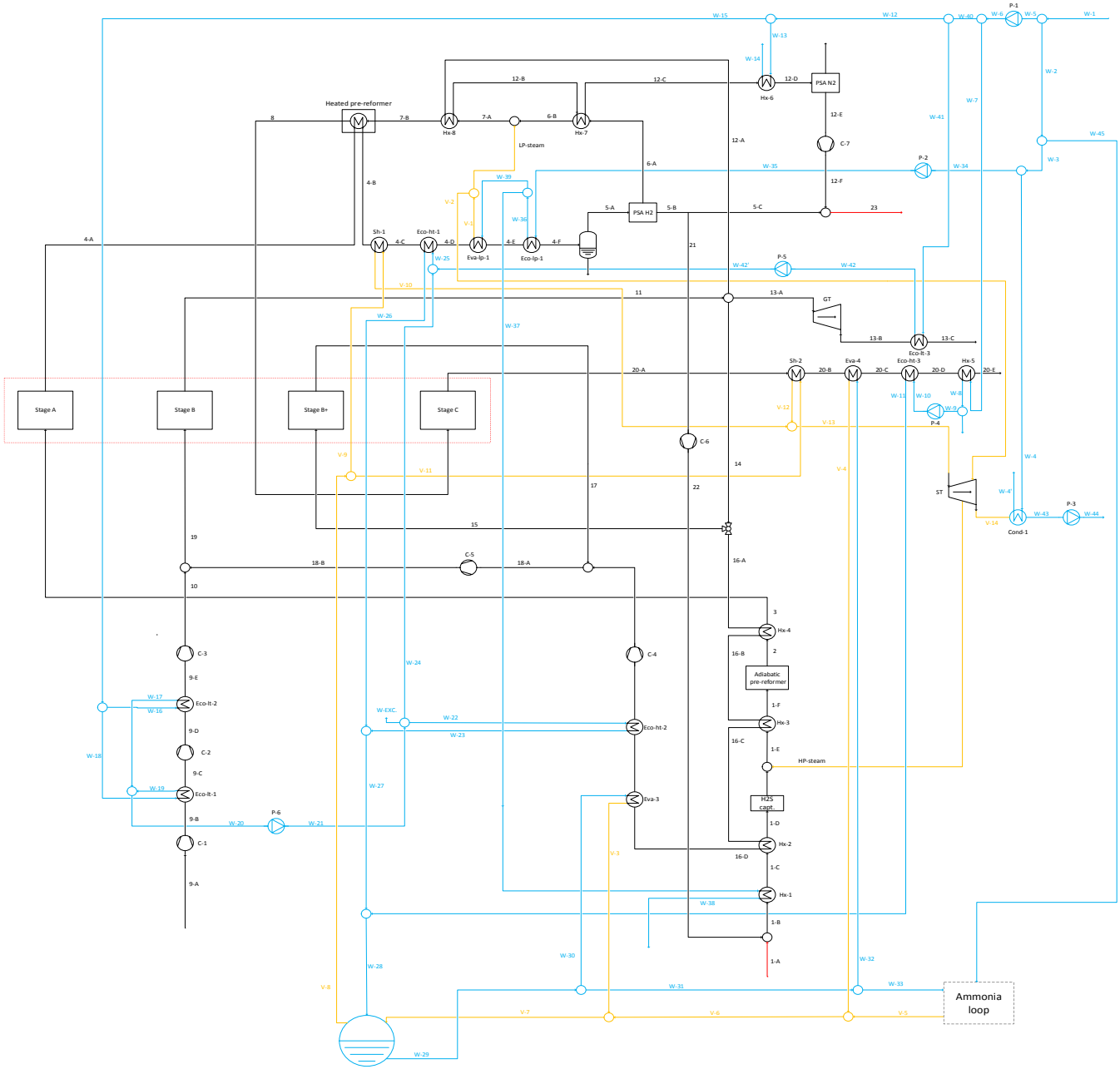

Figure 4: Complete Ca-Cu looping process scheme for ammonia production plants, case 1.

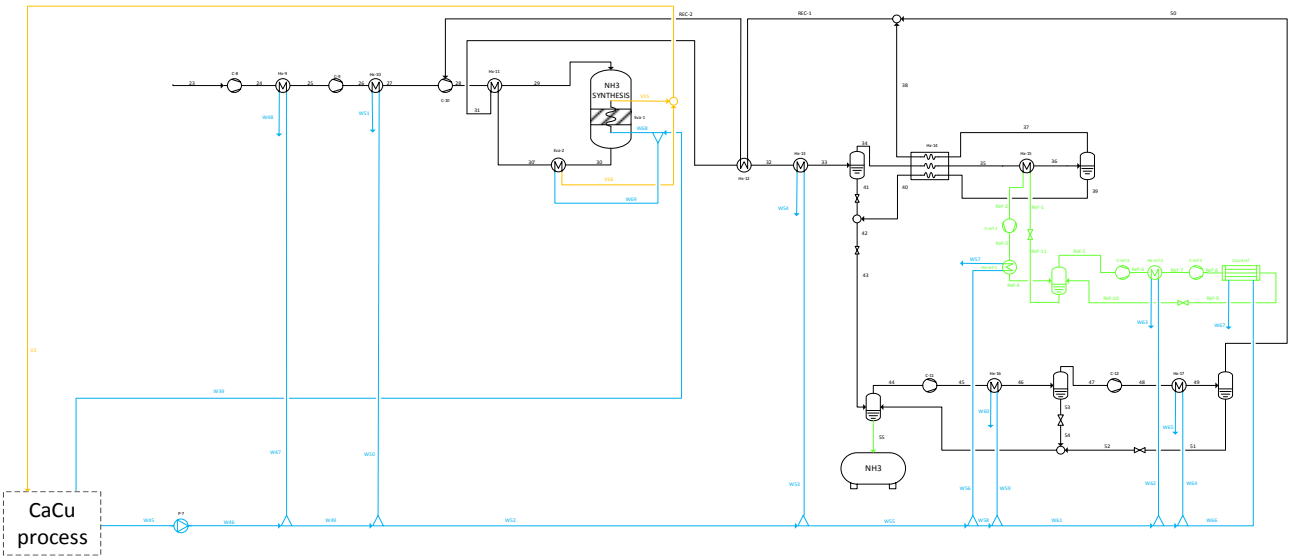

Figure 5: ammonia loop scheme, case 1.

As can be seen from the stream tables below, stage A inlet temperature has been slightly reduced below the 700 °C considered in chapter 4. In effect, if we use stage A outlet stream to sustain the pre-reforming of stage C inlet gas, the remaining hot streams are at stage B average outlet temperature, which is around 715-720 °C. Consequently, the approach temperature difference of the heat exchanger Hx-4 (see fig. 2) dictates the maximal $T_{,g,in,A}$: it is a very important parameter. We have imposed 26 °C as minimum value for such temperature difference, which determines a $T_{,g,in,A}$ of around 690°C.

The ammonia loop is very similar to that of a traditional ammonia plant, except for the already mentioned absence of inerts and so of the purge stream. The refrigeration cycle scheme is the same shown in chapter 3 (except for its heat duty), so we are not going to show its stream table. If not otherwise specified, the assumptions adopted for the traditional plant are retained.

Finally, the steam cycle. The plant performances are heavily influenced by the efficiency of the heat integration system (this can help explain its apparent complexity). In this case it is possible to produce steam at 110 bar and 510 °C, as for the traditional ammonia plant. Note that the hydrogen and the carbon dioxide streams (stream 4A and 20A respectively) contain a significant amount of steam, which, during their cooling condenses. When the condensation begins (in this case at 178 °C for the former flow and at 84 °C for the latter), the T-Q curve drastically reduces its slope (see fig. 7), meaning that a great amount of heat is available at low temperature. In the case of the hydrogen flow, some of the heat can be recovered to produce low-pressure steam (at 1,86 bar, corresponding to 118 °C of evaporation temperature), which is partly used as process steam (LP-steam) and partly fed into the steam turbine (stream V2).

The stream tables of the Ca-Cu looping process, of the ammonia loop and of the heat integration system are reported below. The temperature drops due to thermal dissipations through the reactors walls are taken into account (although they do not exceed 2 °C).

Ca-Cu LOOPING PROCESS STREAM TABLE													
					MOLAR COMPOSITION								
stream	T [°C]	P [bar]	m [kg/s]	n [kmol/s]	CH4	C2+	H2O	H2	N2	O2	CO	CO2	Ar
1-A	16,0	36,46	9,93	0,55	89,0%	8,1%	0,0%	0,0%	0,9%	0,0%	0,0%	2,0%	0,0%
1-B	16,4	36,46	9,95	0,56	87,3%	8,0%	0,0%	2,0%	0,9%	0,0%	0,0%	2,0%	0,0%
1-C	95,9	36,10	9,95	0,56	87,3%	8,0%	0,0%	2,0%	0,9%	0,0%	0,0%	2,0%	0,0%
1-D	365,0	35,74	9,95	0,56	87,3%	8,0%	0,0%	2,0%	0,9%	0,0%	0,0%	2,0%	0,0%
HP-steam	356,3	35,74	30,35	1,69	0,0%	0,0%	100,0%	0,0%	0,0%	0,0%	0,0%	0,0%	0,0%
1-E	358,9	35,74	40,30	2,25	21,8%	2,0%	75,0%	0,5%	0,2%	0,0%	0,0%	0,5%	0,0%
1-F	490,0	35,38	40,30	2,25	21,8%	2,0%	75,0%	0,5%	0,2%	0,0%	0,0%	0,5%	0,0%
2	439,6	34,85	40,30	2,34	23,1%	0,0%	68,0%	6,3%	0,2%	0,0%	0,0%	2,4%	0,0%
3	690,0	34,50	40,30	2,34	23,1%	0,0%	68,0%	6,3%	0,2%	0,0%	0,0%	2,4%	0,0%
4-A	834,8	34,48	24,58	2,81	4,6%	0,0%	30,2%	61,1%	0,2%	0,0%	2,8%	1,2%	0,0%
4-B	608,9	34,13	24,58	2,81	4,6%	0,0%	30,2%	61,1%	0,2%	0,0%	2,8%	1,2%	0,0%
4-C	393,3	33,79	24,58	2,81	4,6%	0,0%	30,2%	61,1%	0,2%	0,0%	2,8%	1,2%	0,0%
4-D	178,4	33,45	24,58	2,81	4,6%	0,0%	30,2%	61,1%	0,2%	0,0%	2,8%	1,2%	0,0%
4-E	135,7	33,12	24,58	2,81	4,6%	0,0%	30,2%	61,1%	0,2%	0,0%	2,8%	1,2%	0,0%
4-F	40,0	32,79	24,58	2,81	4,6%	0,0%	30,2%	61,1%	0,2%	0,0%	2,8%	1,2%	0,0%
5-A	40,0	33,79	10,28	2,02	6,4%	0,0%	2,6%	85,2%	0,2%	0,0%	3,9%	1,7%	0,0%
5-B	40,0	33,12	3,09	1,54	0,0%	0,0%	0,0%	100,0%	0,0%	0,0%	0,0%	0,0%	0,0%
5-C	40,0	33,12	3,07	1,53	0,0%	0,0%	0,0%	100,0%	0,0%	0,0%	0,0%	0,0%	0,0%
6-A	40,0	1,87	7,19	0,47	27,3%	0,0%	11,2%	36,4%	1,0%	0,0%	16,9%	7,1%	0,0%
6-B	122,9	1,86	7,19	0,47	27,3%	0,0%	11,2%	36,4%	1,0%	0,0%	16,9%	7,1%	0,0%
LP-steam	122,9	1,86	3,40	0,19	0,0%	0,0%	100,0%	0,0%	0,0%	0,0%	0,0%	0,0%	0,0%
7-A	122,9	1,86	10,58	0,66	19,5%	0,0%	36,6%	26,0%	0,7%	0,0%	12,0%	5,1%	0,0%
7-B	566,0	1,84	10,58	0,66	19,5%	0,0%	36,6%	26,0%	0,7%	0,0%	12,0%	5,1%	0,0%
8	700,0	1,80	10,58	0,84	4,8%	0,0%	15,2%	55,3%	0,6%	0,0%	16,9%	7,1%	0,0%
9-A	16,0	1,01	52,77	1,82	0,0%	0,0%	0,0%	0,0%	78,0%	21,0%	0,0%	0,0%	1,0%
9-B	172,6	3,34	52,77	1,82	0,0%	0,0%	0,0%	0,0%	78,0%	21,0%	0,0%	0,0%	1,0%
9-C	40,0	3,31	52,77	1,82	0,0%	0,0%	0,0%	0,0%	78,0%	21,0%	0,0%	0,0%	1,0%
9-D	206,2	10,74	52,77	1,82	0,0%	0,0%	0,0%	0,0%	78,0%	21,0%	0,0%	0,0%	1,0%
9-E	40,0	10,64	52,77	1,82	0,0%	0,0%	0,0%	0,0%	78,0%	21,0%	0,0%	0,0%	1,0%
10	206,2	34,50	52,77	1,82	0,0%	0,0%	0,0%	0,0%	78,0%	21,0%	0,0%	0,0%	1,0%
11	716,0	31,80	357,96	12,64	0,0%	0,0%	0,0%	0,0%	97,6%	0,0%	0,0%	1,1%	1,3%
12-A	716,0	31,80	18,53	0,65	0,0%	0,0%	0,0%	0,0%	97,6%	0,0%	0,0%	1,1%	1,3%
12-B	172,3	31,48	18,53	0,65	0,0%	0,0%	0,0%	0,0%	97,6%	0,0%	0,0%	1,1%	1,3%
12-C	105,2	31,16	18,53	0,65	0,0%	0,0%	0,0%	0,0%	97,6%	0,0%	0,0%	1,1%	1,3%
12-D	40	30,85	18,53	0,654	0,0%	0,0%	0,0%	0,0%	97,6%	0,0%	0,0%	1,1%	1,3%
12-E	40	30,24	14,31	0,511	0,0%	0,0%	0,0%	0,0%	100,0%	0,0%	0,0%	0,0%	0,0%
12-F	51	33,12	14,31	0,511	0,0%	0,0%	0,0%	0,0%	100,0%	0,0%	0,0%	0,0%	0,0%
13-A	716,0	31,80	22,69	0,80	0,0%	0,0%	0,0%	0,0%	97,6%	0,0%	0,0%	1,1%	1,3%
13-B	251,8	1,02	22,69	0,80	0,0%	0,0%	0,0%	0,0%	97,6%	0,0%	0,0%	1,1%	1,3%
13-C	40,0	1,01	22,69	0,80	0,0%	0,0%	0,0%	0,0%	97,6%	0,0%	0,0%	1,1%	1,3%
14	716,0	31,80	316,73	11,18	0,0%	0,0%	0,0%	0,0%	97,6%	0,0%	0,0%	1,1%	1,3%
15	716,0	31,80	173,59	6,13	0,0%	0,0%	0,0%	0,0%	97,6%	0,0%	0,0%	1,1%	1,3%
16-A	716,0	31,80	143,14	5,05	0,0%	0,0%	0,0%	0,0%	97,6%	0,0%	0,0%	1,1%	1,3%
16-B	555,0	31,48	143,14	5,05	0,0%	0,0%	0,0%	0,0%	97,6%	0,0%	0,0%	1,1%	1,3%
16-C	474,9	31,16	143,14	5,05	0,0%	0,0%	0,0%	0,0%	97,6%	0,0%	0,0%	1,1%	1,3%
16-D	427,3	30,85	143,14	5,05	0,0%	0,0%	0,0%	0,0%	97,6%	0,0%	0,0%	1,1%	1,3%
16-E	357,1	30,54	143,14	5,05	0,0%	0,0%	0,0%	0,0%	97,6%	0,0%	0,0%	1,1%	1,3%
16-F	284,5	30,24	143,14	5,05	0,0%	0,0%	0,0%	0,0%	97,6%	0,0%	0,0%	1,1%	1,3%
16-G	286,9	31,23	143,14	5,05	0,0%	0,0%	0,0%	0,0%	97,6%	0,0%	0,0%	1,1%	1,3%
17	299,6	31,23	173,59	6,13	0,0%	0,0%	0,0%	0,0%	97,6%	0,0%	0,0%	1,1%	1,3%
18	293,8	31,23	316,73	11,18	0,0%	0,0%	0,0%	0,0%	97,6%	0,0%	0,0%	1,1%	1,3%
18'	315,0	34,50	316,73	11,18	0,0%	0,0%	0,0%	0,0%	97,6%	0,0%	0,0%	1,1%	1,3%
19	300,0	34,50	369,50	13,00	0,0%	0,0%	0,0%	0,0%	94,9%	2,9%	0,0%	0,9%	1,2%
20-A	715,6	0,95	37,83	1,26	0,0%	0,0%	53,3%	0,0%	0,4%	0,0%	0,0%	46,3%	0,0%
20-B	497,3	0,94	37,83	1,26	0,0%	0,0%	53,3%	0,0%	0,4%	0,0%	0,0%	46,3%	0,0%
20-C	393,3	0,93	37,83	1,26	0,0%	0,0%	53,3%	0,0%	0,4%	0,0%	0,0%	46,3%	0,0%
20-D	84,0	0,92	37,83	1,26	0,0%	0,0%	53,3%	0,0%	0,4%	0,0%	0,0%	46,3%	0,0%
20-E	40	0,91	37,83	1,26	0,0%	0,0%	53,3%	0,0%	0,4%	0,0%	0,0%	46,3%	0,0%
21	40,0	33,12	0,02	0,01	0,0%	0,0%	0,0%	100,0%	0,0%	0,0%	0,0%	0,0%	0,0%
22	51,8	36,46	0,02	0,01	0,0%	0,0%	0,0%	100,0%	0,0%	0,0%	0,0%	0,0%	0,0%
23	42,7	33,12	17,38	2,04	0,0%	0,0%	0,0%	75,0%	25,0%	0,0%	0,0%	0,0%	0,0%

Table 1: CaCu looping process stream table, case 1

AMMONIA LOOP STREAM TABLE							
					molar composition		
stream	m [kg/s]	n [kmol/s]	T [°C]	P [bar]	H2	N2	NH3
23	17,41	2,05	42,7	33,1	75,0%	25,0%	0,0%
24	17,41	2,05	123,6	61,1	75,0%	25,0%	0,0%
25	17,41	2,05	40,2	60,6	75,0%	25,0%	0,0%
26	17,41	2,05	119,3	110,9	75,0%	25,0%	0,0%
27	17,41	2,05	40,2	109,9	75,0%	25,0%	0,0%
28	48,10	5,58	140,0	200,0	74,1%	24,7%	1,3%
29	48,10	5,58	320,2	199,0	74,1%	24,7%	1,3%
30	48,10	4,56	450,2	196,0	57,0%	19,0%	24,0%
30'	48,10	4,56	352,1	195,0	57,0%	19,0%	24,0%
31	48,10	4,56	217,5	194,0	57,0%	19,0%	24,0%
32	48,10	4,56	98,8	193,0	57,0%	19,0%	24,0%
33	48,10	4,56	30,2	192,0	57,0%	19,0%	24,0%
34	36,11	3,85	30,2	192,0	67,3%	22,4%	10,2%
35	36,11	3,85	9,3	191,0	67,3%	22,4%	10,2%
36	36,11	3,85	-19,9	190,0	67,3%	22,4%	10,2%
37	30,55	3,52	-19,9	190,0	73,5%	24,5%	1,9%
38	30,55	3,52	25,2	189,0	73,5%	24,5%	1,9%
39	5,56	0,33	-19,9	190,0	0,4%	0,1%	99,5%
40	5,56	0,33	25,2	189,0	0,4%	0,1%	99,5%
41	11,99	0,71	30,2	192,0	1,2%	0,4%	98,4%
42	17,55	1,04	28,6	189,0	0,9%	0,3%	98,8%
43	17,55	1,04	28,3	20,0	0,9%	0,3%	98,8%
44	0,40	0,03	28,4	20,0	30,8%	10,3%	58,9%
45	0,40	0,03	155,6	61,0	30,8%	10,3%	58,9%
46	0,40	0,03	40,2	60,7	30,8%	10,3%	58,9%
47	0,20	0,02	40,2	60,7	51,6%	17,2%	31,2%
48	0,20	0,02	185,1	190,0	51,6%	17,2%	31,2%
49	0,20	0,02	40,2	189,4	51,6%	17,2%	31,2%
50	0,13	0,01	40,2	189,4	64,9%	21,6%	13,6%
51	0,06	0,00	40,2	189,4	1,4%	0,5%	98,1%
52	0,06	0,00	34,7	20,0	1,4%	0,5%	98,1%
53	0,20	0,01	40,2	60,7	0,4%	0,1%	99,5%
54	0,20	0,01	37,8	20,0	0,4%	0,1%	99,5%
55	17,41	1,02	28,4	20,0	0,1%	0,0%	99,9%
REC-1	30,68	3,53	25,2	189,0	73,5%	24,5%	2,0%
REC-2	30,68	3,53	199,5	188,0	73,5%	24,5%	2,0%

Table 2: ammonia loop stream table, case 1

HEAT INTEGRATION SYSTEM (WATER)							
stream	m [kg/s]	T [°C]	p [bar]	stream	m [kg/s]	T [°C]	p [bar]
W-1	1030,5	20,0	1,01	W-45	254,5	20,0	1,01
W-2	815,4	20,0	1,01	W-46	254,5	20,0	4,55
W-3	561,0	20,0	1,01	W-47	14,4	20,0	4,55
W-4	504,5	20,0	1,01	W-48	14,4	104,0	4,55
W-4'	504,5	50,0	1,01	W-49	240,1	20,0	4,55
W-5	215,1	20,0	1,01	W-50	14,7	20,0	4,55
W-6	215,1	20,0	4,55	W-51	14,7	99,0	4,55
W-7	168,3	20,0	4,55	W-52	225,4	20,0	4,55
W-8	168,3	64,0	4,55	W-53	124,3	20,0	4,55
W-9	13,5	64,0	4,55	W-54	124,3	57,0	4,55
W-10	13,5	64,0	110,00	W-55	101,1	20,0	4,55
W-11	13,5	314,1	110,00	W-56	3,4	20,0	4,55
W-12	36,8	20,0	4,55	W-57	3,4	61,0	4,55
W-13	4,6	20,0	4,55	W-58	97,7	20,0	4,55
W-14	4,6	85,2	4,55	W-59	2,2	20,0	4,55
W-15	32,2	20,0	4,55	W-60	2,2	57,4	4,55
W-16	18,0	20,0	4,55	W-61	95,5	20,0	4,55
W-17	18,0	138,3	4,55	W-62	4,2	20,0	4,55
W-18	14,2	20,0	4,55	W-63	4,2	47,0	4,55
W-19	14,2	138,3	4,55	W-64	0,4	20,0	4,55
W-20	32,2	138,3	4,55	W-65	0,4	100,1	4,55
W-21	32,2	138,3	110,00	W-66	90,9	20,0	4,55
W-22	13,2	138,3	110,00	W-67	90,9	41,6	4,55
W-23	13,2	314,1	110,00	W-68	25,6	314,1	110,00
W-24	13,5	138,3	110,00	W-69	12,0	314,1	110,00
W-25	23,5	138,3	110,00				
W-26	23,5	314,1	110,00	V-1	12,8	122,9	1,86
W-27	36,7	314,1	110,00	V-2	9,4	122,9	1,86
W-EXC.	5,5	138,3	110,00	LP-steam	3,4	122,9	1,86
W-28	50,2	314,1	110,00	V-3	8,3	321,1	110,00
W-29	50,2	314,1	110,00	V-4	4,3	321,1	110,00
W-30	8,3	314,1	110,00	V-5	37,6	321,1	110,00
W-31	41,9	314,1	110,00	V-6	41,9	321,1	110,00
W-32	4,3	314,1	110,00	V-7	50,2	321,1	110,00
W-33	37,6	314,1	110,00	V-8	50,2	321,1	110,00
W-34	56,5	20,0	1,01	V-9	31,2	321,1	110,00
W-35	56,5	20,0	1,86	V-10	31,2	321,1	110,00
W-36	56,5	114,9	1,86	V-11	19,0	321,1	110,00
W-37	43,8	114,9	1,86	V-12	19,0	321,1	110,00
W-38	43,8	105,4	1,86	V-13	50,2	321,1	110,00
W-39	12,8	114,9	1,86	V-14	29,2	55,0	0,16
W-40	46,8	20,0	4,55	V-15	25,6	321,1	110,00
W-41	10,0	20,0	4,55	V-16	12,0	321,1	110,00
W-42	10,0	138,3	4,55	HP-steam	30,4	356,3	35,74
W-42'	10,0	138,3	110,00				
W-43	29,2	47,0	0,16				
W-44	29,2	47,0	1,50				

Table 3: heat integration system stream table, case 1

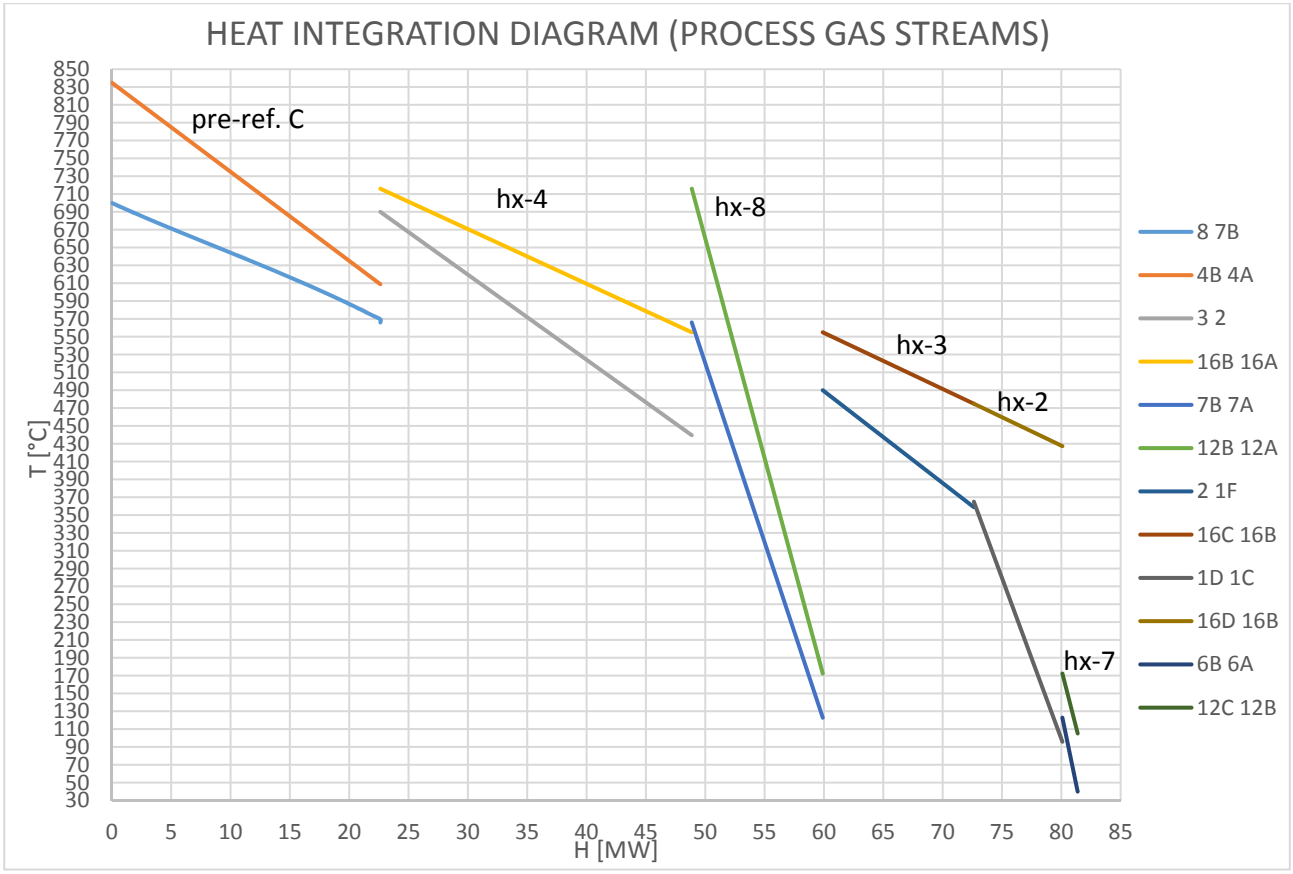

Figure 6: Heat integration system (process gas streams) T-Q diagram, case 1.

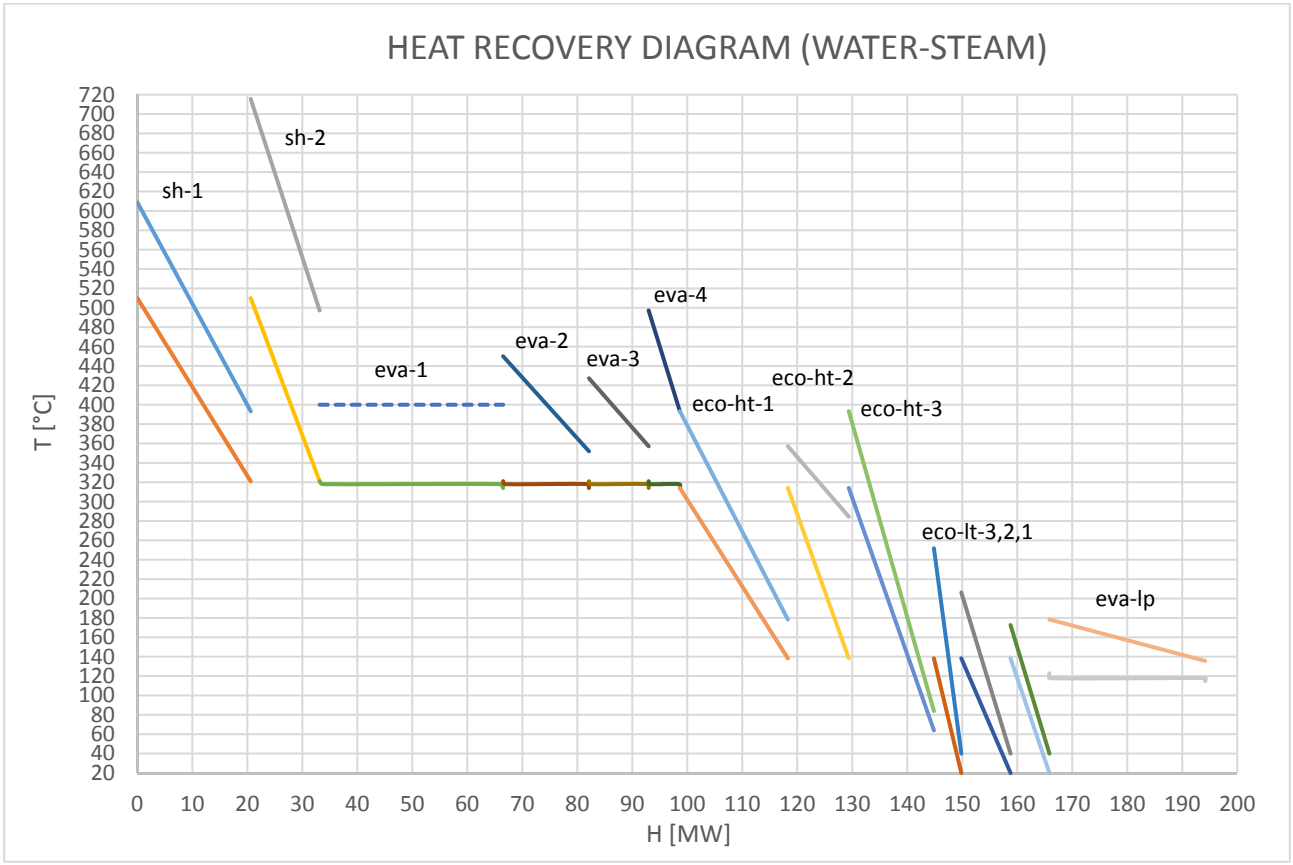

Figure 7: heat recovery (water-steam) T-Q diagram, case1.

The following table reports the (centrifugal) compressors and pumps mechanical power consumption and the mechanical power output of the steam turbine and the gas turbine. The power input of the refrigeration cycle compressors has been gathered in one only term (c,ref.); as pointed out in chapter 3 the refrigeration cycle has an energy efficiency ratio of 2,37. It can be seen that a significant electric power input is required to fulfil electric consumption in the compressors and pumps in the plant (12,7 MW in this case), although the steam turbine power output is higher than that of the reference plant and there is a gas turbine too. This feature is common to every CaCu looping configuration analysed and it is mainly due the high power consumption of the air compression. In this regard, note that the process air flow rate passes from 19,4 kg/s for the reference plant to 52,8 kg/s for this scheme, a great part of which is not expanded in the gas turbine, since the oxygen of the air is trapped by the solid bed and part of the nitrogen is sent into the PSA. Besides the turbine inlet temperature is quite low (716 °C in this case). The electric power input will be converted into a primary energy consumption (23 MW in this case) using a reference power production efficiency (55%), as already seen for the traditional ammonia plant, to determine the corrected primary energy consumption per ton of ammonia produced.

MECHANICAL POWER BALANCE	
compressors	
assumptions	
η,is.=	0,75
η,mech.=	0,98
results: power consumption [kW]	
c1 (air)	8319,0
c2 (air)	8869,0
c3 (air)	8901,0
c4 (bypass flow, stream 16D)	372,0
c5 (recycle flow, stream 18A)	7288,0
c6 (H2 for desulph., stream 21)	4,0
c7 (N2 flow, stream 12E)	146,0
c8 (H2/N2 flow, stream 23)	5015,7
c9 (H2/N2 flow, stream 25)	5059,4
c10 (H2/N2 flow, stream 27)	6188,0
c11 (incondensables, stream 44)	120,7
c12 (incondensables, stream 47)	81,8
c-ref (refrigeration cycle)	2748,4
P,comp.shaft tot.=	54197,0
pumps	
results: power consumption [kW]	
p1	76,2
p2	4,8
p3	4,0
p4	147,2
p5	109,4
p6	365,8
p7	90,2
P,pumps shaft tot.=	813,8
P,mech. required [kW]=	55010,8

gas turbine	
assumptions	
η,is.=	0,78
η,mech.=	0,98
P,in [bar]=	31,80
T,in [°C]=	716,0
m [kg/s]=	22,69
P,out [bar]=	1,02
results	
T,out [°C]=	251,8
P, shaft [kW]=	11511,1
steam turbine	
assumptions	
η,is.=	0,82
η,mech.=	0,98
P,in [bar]=	110
T,in [°C]=	510
P,out [bar]=	0,158
T,out [°C]=	55,0
results	
X,out=	0,90
P, shaft [kW]=	31322,6
P,mech. vailable tot [kW]=	42833,7
η,org.=	0,96
P,electric, in [kW]=	12684,5
η,el. ref.=	0,55
P, primary, plus [kW]=	23062,7

Table 4: mechanical power balance, case 1

Finally, table 5 shows a summary of the plant performance, pressure drops and beds size and cost for case 1. As already explained in chapter 3, the material cost shown below is representative only of the reactors (and valves) cost and not of the whole plant one. The results will be discussed in chapter 5.4.

PERFORMANCES					
carbon capture ratio=	97,3%		LHV,ng=	46,59	kg/s
carbon dioxide emissions=	0,0407	t,CO2/t,NH3	P, electric, input=	12,7	MW
cold gas efficiency=	80,2%		η, electric, ref.=	55%	
net primary energy consumption=	26,64	GJ/t,NH3	natural gas input=	46,59	MJ/kg
corrected prim. en. consumption=	27,97	GJ/t,NH3	ammonia yield=	1500	t/d
corrected CO2 emissions*=	0,116	t,CO2/t,NH3	S/C, stage A=	2,82	

BEDS SIZE, STAGES DURATION AND PRESSURE DROPS					
R, bed=	1,56	m	P,max,in=	34,5	bar
L, bed=	9,36	m	T, external wall=	70	°C
L, reactor=	10,8	m	T,steel, max =	300	°C
T,max,in=	863,3	°C			

	stage A	stage B	stage B+	stage C	
Number	4	3	3	1	
Δt [min] =	61,8	46,36	46,36	15,45	
V, max [m/s] =	0,5	2,93	1,27	11,27	
ΔP [bar] =	0,022	2,70	0,57	0,85	
ΔP/P,in [%] =	0,1%	7,8%	1,8%	47,3%	

MATERIAL COST			
valves per reactor=	8	cost per valve=	€ 50.000
N, valves, total=	88	total valves cost=	€ 4.400.000

reactor material	thickness [cm]	amount per reactor [m^3]	total amount [m^3]	cost [€/m^3]	total cost
fire bricks (internal refractory)	31,52	40,09	440,98	216	€ 95.251
steel (SA 516 grade 70)	9,62	13,69	150,56	5581,4	€ 840.338
mineral wool (external insulating)	15,37	23,47	258,17	750	€ 193.630

solid bed material (supported by alumina)	amount per reactor [t]	total amount [t]	support (Al2O3) mass fraction	cost [€/t]	total cost
CaO	72,82	801,02	15%	10000,00	€ 8.010.176
Cu	63,80	701,82	35%	15000,00	€ 10.527.278
Ni	18,57	204,26	82%	50000,00	€ 10.212.974
				total material cost=	€ 34.279.648

*Table 5: summary table, case 1.*considering a reference emission factor of 0,103 kg,CO2/MJe.*

5.2) Case 2: base case with P,A = P,B = 44 bar.

Since in chapter 4.7 we have seen that the operating pressure of stages A and B slightly affects the performance while it strongly affects the reactors' cost, here we analyse a high-pressure process. We will proceed as for case 1. Compared to that case, there are only minor changes in the plant scheme. The main is the air compression train, which in this case is split into four casings (instead of three), as the compression ratio required is higher (43,6). Secondly, the gas turbine flue-gas are used to produce low-pressure steam. Concerning the ammonia loop, there are no changes (except for the higher inlet pressure).

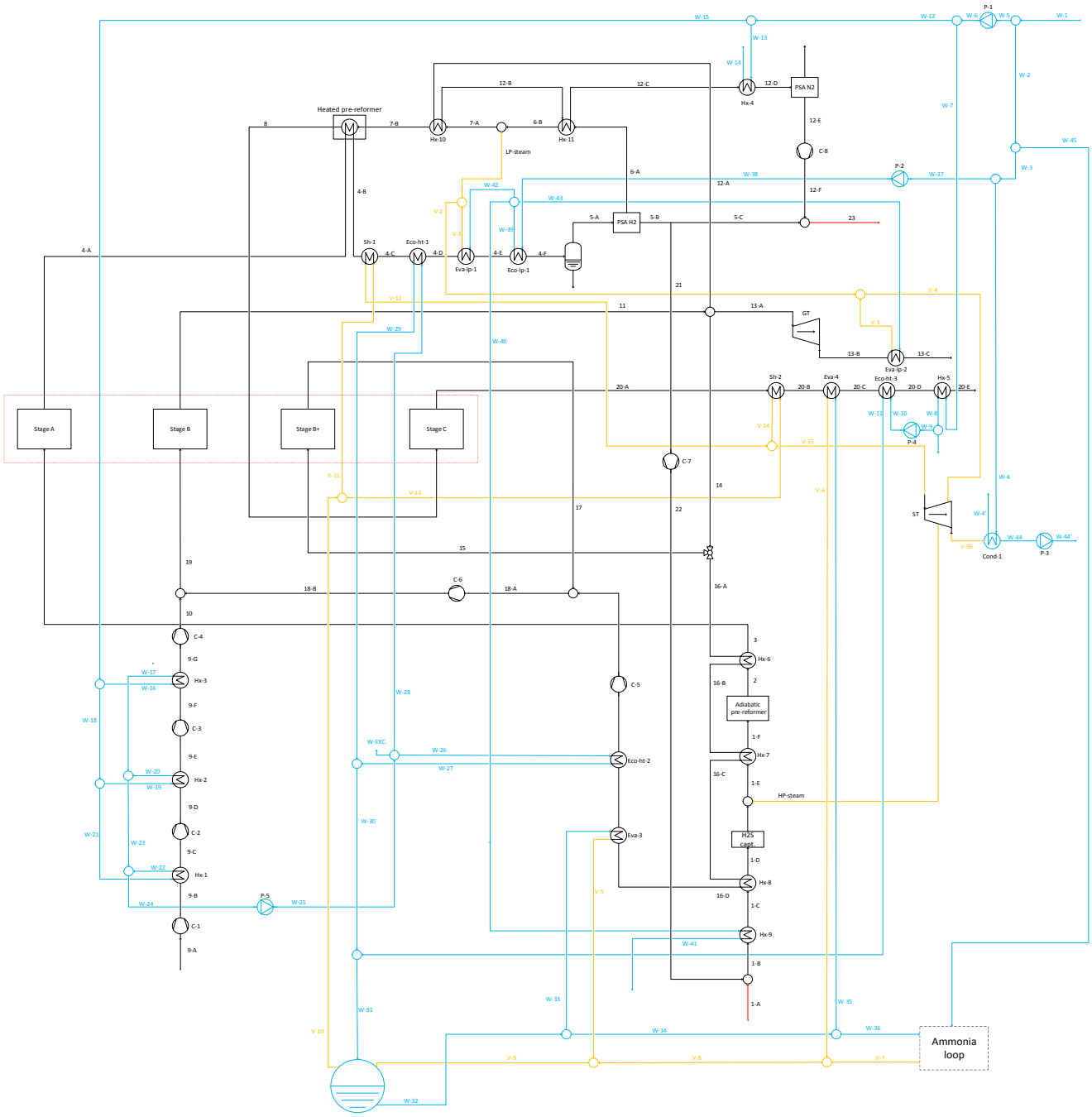

Figure 8: complete CaCu looping process scheme for ammonia production plants, case 2.

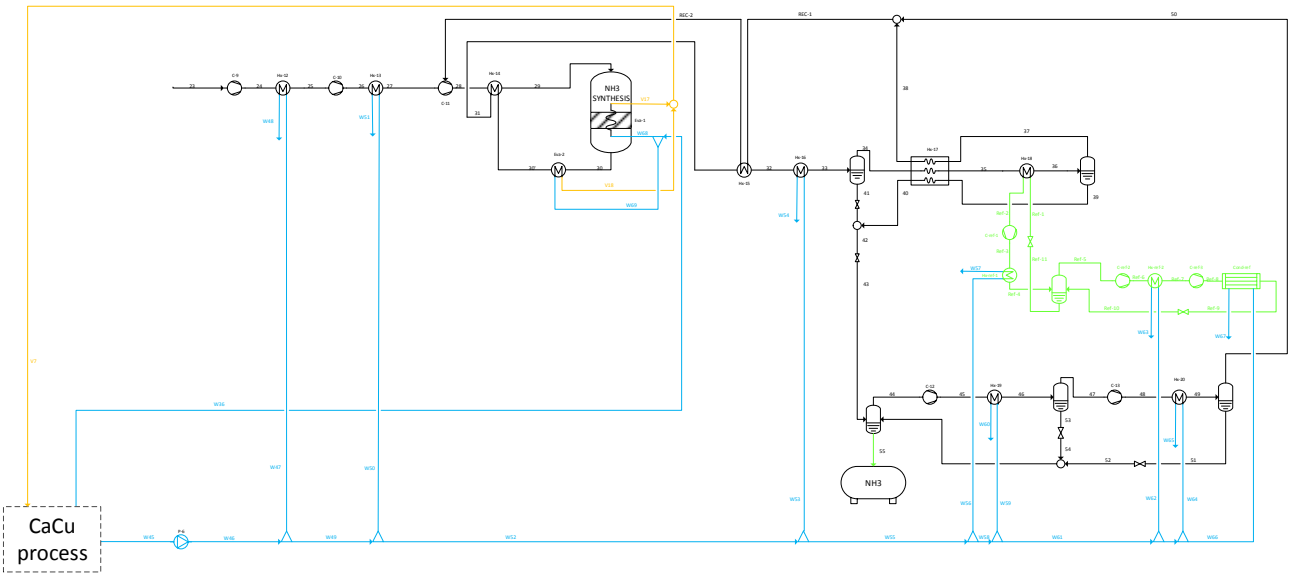

Figure 9: ammonia loop scheme, case 2.

Ca-Cu LOOPING PROCESS STREAM TABLE													
					MOLAR COMPOSITION								
stream	T [°C]	P [bar]	m [kg/s]	n [kmol/s]	CH4	C2+	H2O	H2	N2	O2	CO	CO2	Ar
1-A	16,0	46,50	10,00	0,56	89,0%	8,1%	0,0%	0,0%	0,9%	0,0%	0,0%	2,0%	0,0%
1-B	16,4	46,50	10,02	0,57	87,3%	8,0%	0,0%	2,0%	0,9%	0,0%	0,0%	2,0%	0,0%
1-C	97,2	46,04	10,02	0,57	87,3%	8,0%	0,0%	2,0%	0,9%	0,0%	0,0%	2,0%	0,0%
1-D	365,0	45,58	10,02	0,57	87,3%	8,0%	0,0%	2,0%	0,9%	0,0%	0,0%	2,0%	0,0%
HP-steam	386,4	45,58	32,11	1,78	0,0%	0,0%	100,0%	0,0%	0,0%	0,0%	0,0%	0,0%	0,0%
1-E	380,1	45,58	42,13	2,35	21,0%	1,9%	75,9%	0,5%	0,2%	0,0%	0,0%	0,5%	0,0%
1-F	490,0	45,12	42,13	2,35	21,0%	1,9%	75,9%	0,5%	0,2%	0,0%	0,0%	0,5%	0,0%
2	443,3	44,44	42,13	2,44	22,3%	0,0%	69,3%	5,9%	0,2%	0,0%	0,0%	2,3%	0,0%
3	694,0	44,00	42,13	2,44	22,3%	0,0%	69,3%	5,9%	0,2%	0,0%	0,0%	2,3%	0,0%
4-A	838,9	43,97	26,12	2,90	4,6%	0,0%	32,4%	59,1%	0,2%	0,0%	2,5%	1,1%	0,0%
4-B	613,8	43,53	26,12	2,90	4,6%	0,0%	32,4%	59,1%	0,2%	0,0%	2,5%	1,1%	0,0%
4-C	385,9	43,10	26,12	2,90	4,6%	0,0%	32,4%	59,1%	0,2%	0,0%	2,5%	1,1%	0,0%
4-D	191,5	42,67	26,12	2,90	4,6%	0,0%	32,4%	59,1%	0,2%	0,0%	2,5%	1,1%	0,0%
4-E	136,2	42,24	26,12	2,90	4,6%	0,0%	32,4%	59,1%	0,2%	0,0%	2,5%	1,1%	0,0%
4-F	40,0	41,82	26,12	2,90	4,6%	0,0%	32,4%	59,1%	0,2%	0,0%	2,5%	1,1%	0,0%
5-A	40,0	41,82	10,08	2,01	6,7%	0,0%	2,5%	85,4%	0,2%	0,0%	3,6%	1,6%	0,0%
5-B	40,0	40,98	3,09	1,54	0,0%	0,0%	0,0%	100,0%	0,0%	0,0%	0,0%	0,0%	0,0%
5-C	40,0	40,98	3,07	1,53	0,0%	0,0%	0,0%	100,0%	0,0%	0,0%	0,0%	0,0%	0,0%
6-A	40,0	1,89	6,99	0,47	28,9%	0,0%	10,8%	36,8%	1,1%	0,0%	15,5%	7,0%	0,0%
6-B	123,2	1,87	6,99	0,47	28,9%	0,0%	10,8%	36,8%	1,1%	0,0%	15,5%	7,0%	0,0%
LP-steam	123,2	1,87	3,40	0,19	0,0%	0,0%	100,0%	0,0%	0,0%	0,0%	0,0%	0,0%	0,0%
7-A	123,2	1,87	10,39	0,65	20,5%	0,0%	36,5%	26,2%	0,8%	0,0%	11,0%	5,0%	0,0%
7-B	123,2	1,86	10,39	0,65	20,5%	0,0%	36,5%	26,2%	0,8%	0,0%	11,0%	5,0%	0,0%
7-C	566,0	1,84	10,39	0,65	20,5%	0,0%	36,5%	26,2%	0,8%	0,0%	11,0%	5,0%	0,0%
8	700,0	1,80	10,39	0,84	5,1%	0,0%	14,8%	56,1%	0,6%	0,0%	16,7%	6,7%	0,0%

Continues

stream	T [°C]	P [bar]	m [kg/s]	n [kmol/s]	CH4	C2+	H2O	H2	N2	O2	CO	CO2	Ar
9-A	16,0	1,01	53,91	1,86	0,0%	0,0%	0,0%	0,0%	78,0%	21,0%	0,0%	0,0%	1,0%
9-B	151,6	2,91	53,91	1,86	0,0%	0,0%	0,0%	0,0%	78,0%	21,0%	0,0%	0,0%	1,0%
9-C	40,0	2,87	53,91	1,86	0,0%	0,0%	0,0%	0,0%	78,0%	21,0%	0,0%	0,0%	1,0%
9-D	167,8	7,33	53,91	1,86	0,0%	0,0%	0,0%	0,0%	78,0%	21,0%	0,0%	0,0%	1,0%
9-E	40,0	7,24	53,91	1,86	0,0%	0,0%	0,0%	0,0%	78,0%	21,0%	0,0%	0,0%	1,0%
9-F	167,8	18,46	53,91	1,86	0,0%	0,0%	0,0%	0,0%	78,0%	21,0%	0,0%	0,0%	1,0%
9-G	40,0	18,26	53,91	1,86	0,0%	0,0%	0,0%	0,0%	78,0%	21,0%	0,0%	0,0%	1,0%
10	159,1	44,00	53,91	1,86	0,0%	0,0%	0,0%	0,0%	78,0%	21,0%	0,0%	0,0%	1,0%
11	720,0	40,94	366,47	12,95	0,0%	0,0%	0,0%	0,0%	97,9%	0,0%	0,0%	0,9%	1,3%
12-A	720,0	40,94	18,47	0,65	0,0%	0,0%	0,0%	0,0%	97,9%	0,0%	0,0%	0,9%	1,3%
12-B	175,5	40,32	18,47	0,65	0,0%	0,0%	0,0%	0,0%	97,9%	0,0%	0,0%	0,9%	1,3%
12-C	108,3	39,92	18,47	0,65	0,0%	0,0%	0,0%	0,0%	97,9%	0,0%	0,0%	0,9%	1,3%
12-D	40,0	39,12	18,47	0,65	0,0%	0,0%	0,0%	0,0%	97,9%	0,0%	0,0%	0,9%	1,3%
12-E	40,0	38,34	14,31	0,51	0,0%	0,0%	0,0%	0,0%	100,0%	0,0%	0,0%	0,9%	1,3%
12-F	48,0	40,98	14,31	0,51	0,0%	0,0%	0,0%	0,0%	100,0%	0,0%	0,0%	0,9%	1,3%
13-A	720,0	40,94	23,50	0,83	0,0%	0,0%	0,0%	0,0%	97,9%	0,0%	0,0%	0,9%	1,3%
13-B	233,7	1,02	23,50	0,83	0,0%	0,0%	0,0%	0,0%	97,9%	0,0%	0,0%	0,9%	1,3%
13-C	136,2	1,01	23,50	0,83	0,0%	0,0%	0,0%	0,0%	97,9%	0,0%	0,0%	0,9%	1,3%
14	720,0	40,94	324,51	11,47	0,0%	0,0%	0,0%	0,0%	97,9%	0,0%	0,0%	0,9%	1,3%
15	720,0	40,94	177,30	6,27	0,0%	0,0%	0,0%	0,0%	97,9%	0,0%	0,0%	0,9%	1,3%
16-A	720,0	40,94	147,21	5,20	0,0%	0,0%	0,0%	0,0%	97,9%	0,0%	0,0%	0,9%	1,3%
16-B	557,0	40,53	147,21	5,20	0,0%	0,0%	0,0%	0,0%	97,9%	0,0%	0,0%	0,9%	1,3%
16-C	488,5	40,12	147,21	5,20	0,0%	0,0%	0,0%	0,0%	97,9%	0,0%	0,0%	0,9%	1,3%
16-D	442,3	39,72	147,21	5,20	0,0%	0,0%	0,0%	0,0%	97,9%	0,0%	0,0%	0,9%	1,3%
16-E	387,1	39,33	147,21	5,20	0,0%	0,0%	0,0%	0,0%	97,9%	0,0%	0,0%	0,9%	1,3%
16-F	300,7	38,93	147,21	5,20	0,0%	0,0%	0,0%	0,0%	97,9%	0,0%	0,0%	0,9%	1,3%
16-G	308,0	40,29	147,21	5,20	0,0%	0,0%	0,0%	0,0%	97,9%	0,0%	0,0%	0,9%	1,3%
17	299,6	40,29	177,30	6,27	0,0%	0,0%	0,0%	0,0%	97,9%	0,0%	0,0%	0,9%	1,3%
18	303,4	40,29	324,51	11,47	0,0%	0,0%	0,0%	0,0%	97,9%	0,0%	0,0%	0,9%	1,3%
18'	322,4	44,00	324,51	11,47	0,0%	0,0%	0,0%	0,0%	97,9%	0,0%	0,0%	0,9%	1,3%
19	300,0	44,00	378,42	13,33	0,0%	0,0%	0,0%	0,0%	95,1%	2,9%	0,0%	0,7%	1,2%
20-A	719,7	0,65	38,34	1,27	0,0%	0,0%	53,3%	0,0%	0,4%	0,0%	0,0%	46,3%	0,0%
20-B	535,1	0,64	38,34	1,27	0,0%	0,0%	53,3%	0,0%	0,4%	0,0%	0,0%	46,3%	0,0%
20-C	385,9	0,63	38,34	1,27	0,0%	0,0%	53,3%	0,0%	0,4%	0,0%	0,0%	46,3%	0,0%
20-D	75,0	0,63	38,34	1,27	0,0%	0,0%	53,3%	0,0%	0,4%	0,0%	0,0%	46,3%	0,0%
20-E	40,0	0,62	38,34	1,27	0,0%	0,0%	53,3%	0,0%	0,4%	0,0%	0,0%	46,3%	0,0%
21	40,0	40,98	0,02	0,01	0,0%	0,0%	0,0%	100,0%	0,0%	0,0%	0,0%	0,0%	0,0%
22	55,6	46,50	0,02	0,01	0,0%	0,0%	0,0%	100,0%	0,0%	0,0%	0,0%	0,0%	0,0%
23	42,0	40,98	41,41	2,04	0,0%	0,0%	0,0%	75,0%	25,0%	0,0%	0,0%	0,0%	0,0%

Table 6: CaCu looping process stream table, case 2.

AMMONIA LOOP STREAM TABLE							
					molar composition		
stream	m [kg/s]	n [kmol/s]	T [°C]	P [bar]	H2	N2	NH3
23	17,41	2,05	42,0	41,0	75,0%	25,0%	0,0%
24	17,41	2,05	112,8	70,5	75,0%	25,0%	0,0%
25	17,41	2,05	40,2	70,0	75,0%	25,0%	0,0%
26	17,41	2,05	109,8	119,7	75,0%	25,0%	0,0%
27	17,41	2,05	40,2	118,7	75,0%	25,0%	0,0%
28	48,10	5,58	128,0	200,0	74,1%	24,7%	1,3%
29	48,10	5,58	320,2	199,0	74,1%	24,7%	1,3%
30	48,10	4,56	450,2	196,0	57,0%	19,0%	24,0%
30'	48,10	4,56	353,0	195,0	57,0%	19,0%	24,0%
31	48,10	4,56	217,5	194,0	57,0%	19,0%	24,0%
32	48,10	4,56	98,8	193,0	57,0%	19,0%	24,0%
33	48,10	4,56	30,2	192,0	57,0%	19,0%	24,0%
34	36,11	3,85	30,2	192,0	67,3%	22,4%	10,2%
35	36,11	3,85	9,3	191,0	67,3%	22,4%	10,2%
36	36,11	3,85	-19,9	190,0	67,3%	22,4%	10,2%
37	30,55	3,52	-19,9	190,0	73,5%	24,5%	1,9%
38	30,55	3,52	25,2	189,0	73,5%	24,5%	1,9%
39	5,56	0,33	-19,9	190,0	0,4%	0,1%	99,5%
40	5,56	0,33	25,2	189,0	0,4%	0,1%	99,5%
41	11,99	0,71	30,2	192,0	1,2%	0,4%	98,4%
42	17,55	1,04	28,6	189,0	0,9%	0,3%	98,8%
43	17,55	1,04	28,3	20,0	0,9%	0,3%	98,8%
44	0,40	0,03	28,4	20,0	30,8%	10,3%	58,9%
45	0,40	0,03	155,6	61,0	30,8%	10,3%	58,9%
46	0,40	0,03	40,2	60,7	30,8%	10,3%	58,9%
47	0,20	0,02	40,2	60,7	51,6%	17,2%	31,2%
48	0,20	0,02	185,1	190,0	51,6%	17,2%	31,2%
49	0,20	0,02	40,2	189,4	51,6%	17,2%	31,2%
50	0,13	0,01	40,2	189,4	64,9%	21,6%	13,6%
51	0,06	0,00	40,2	189,4	1,4%	0,5%	98,1%
52	0,06	0,00	34,7	20,0	1,4%	0,5%	98,1%
53	0,20	0,01	40,2	60,7	0,4%	0,1%	99,5%
54	0,20	0,01	37,8	20,0	0,4%	0,1%	99,5%
55	17,41	1,02	28,4	20,0	0,1%	0,0%	99,9%
REC-1	30,68	3,53	25,2	189,0	73,5%	24,5%	2,0%
REC-2	30,68	3,53	199,5	188,0	73,5%	24,5%	2,0%

Table 7: ammonia loop stream table, case 2.

HEAT INTEGRATION SYSTEM (WATER)							
stream	m [kg/s]	T [°C]	p [bar]	stream	m [kg/s]	T [°C]	p [bar]
W-1	1114,3	20,0	1,01	W-46	254,5	20,0	3,99
W-2	862,2	20,0	1,01	W-47	14,5	20,0	3,99
W-3	607,7	20,0	1,01	W-48	14,5	93,0	3,99
W-4	553,1	20,0	1,01	W-49	240,0	20,0	3,99
W-4'	553,1	50,0	1,01	W-50	14,7	20,0	3,99
W-5	252,1	20,0	1,01	W-51	14,7	90,0	3,99
W-6	252,1	20,0	3,99	W-52	225,4	20,0	3,99
W-7	205,6	20,0	3,99	W-53	124,3	20,0	3,99
W-8	205,6	55,0	3,99	W-54	124,3	57,0	3,99
W-9	13,2	55,0	3,99	W-55	101,1	20,0	3,99
W-10	13,2	55,0	110,00	W-56	3,4	20,0	3,99
W-11	13,2	314,1	110,00	W-57	3,4	61,0	3,99
W-12	46,5	20,0	3,99	W-58	97,7	20,0	3,99
W-13	4,5	20,0	3,99	W-59	2,2	20,0	3,99
W-14	4,5	88,3	3,99	W-60	2,2	57,4	3,99
W-15	41,9	20,0	3,99	W-61	95,5	20,0	3,99
W-16	14,6	20,0	3,99	W-62	4,2	20,0	3,99
W-17	14,6	133,6	3,99	W-63	4,2	47,0	3,99
W-18	27,3	20,0	3,99	W-64	0,4	20,0	3,99
W-19	14,6	20,0	3,99	W-65	0,4	100,1	3,99
W-20	14,6	133,6	3,99	W-66	90,9	20,0	3,99
W-21	12,7	20,0	3,99	W-67	90,9	41,6	3,99
W-22	12,7	133,6	3,99	W-68	25,6	314,1	110,00
W-23	29,2	133,6	3,99	W-69	12,0	314,1	110,00
W-24	41,9	133,6	3,99				
W-25	41,9	133,6	110,00	V-1	15,7	123,2	1,87
W-26	15,9	133,6	110,00	V-2	12,3	123,2	1,87
W-27	15,9	314,1	110,00	LP-steam	3,4	123,2	1,87
W-EXC.	4,5	133,6	110,00	V-3	1,1	123,2	1,87
W-28	21,5	133,6	110,00	V-4	13,4	123,2	1,87
W-29	21,5	314,1	110,00	V-5	6,8	321,1	110,00
W-30	37,4	314,1	110,00	V-6	6,4	321,1	110,00
W-31	50,7	314,1	110,00	V-7	37,6	321,1	110,00
W-32	50,7	314,1	110,00	V-8	43,9	321,1	110,00
W-33	6,8	314,1	110,00	V-9	50,7	321,1	110,00
W-34	43,9	314,1	110,00	V-10	50,7	321,1	110,00
W-35	6,4	314,1	110,00	V-11	34,3	321,1	110,00
W-36	37,6	314,1	110,00	V-12	34,3	510,0	110,00
W-37	54,6	20,0	1,01	V-13	16,4	321,1	110,00
W-38	54,6	20,0	1,87	V-14	16,4	510,0	110,00
W-39	54,6	115,2	1,87	V-15	50,7	510,0	110,00
W-40	37,8	115,2	1,87	V-16	32,0	55,0	0,16
W-41	37,8	103,9	1,87	V-17	25,6	321,1	110,00
W-42	15,7	115,2	1,87	V-18	12,0	321,1	110,00
W-43	1,1	115,2	1,87	HP-steam	32,1	386,4	45,58
W-44	32,0	47,0	0,16				
W-44'	32,0	47,0	1,50				
W-45	254,5	20,0	1,01				

Table 8: heat integration system stream table, case 2.

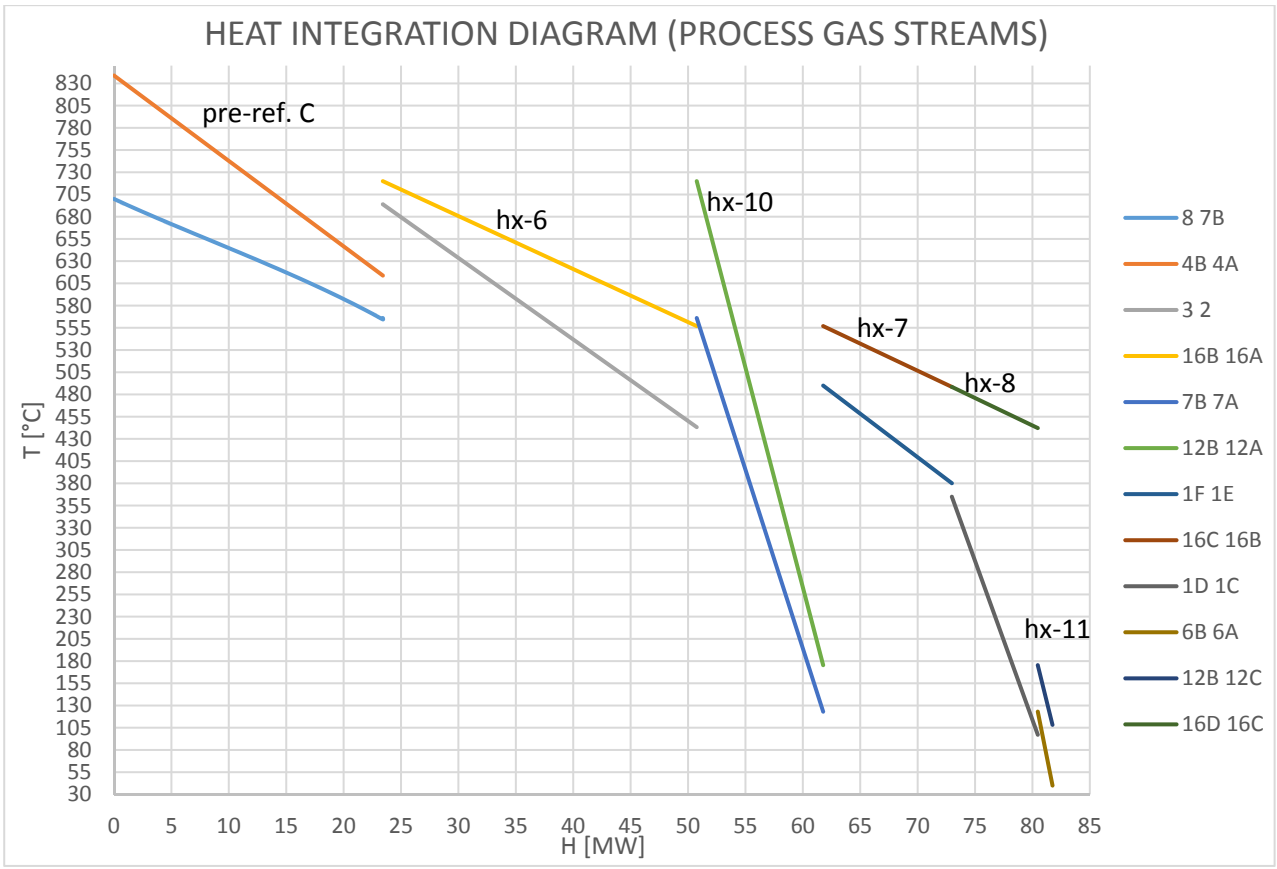

Figure 10: heat integration system (process gas streams) T-Q diagram, case 2.

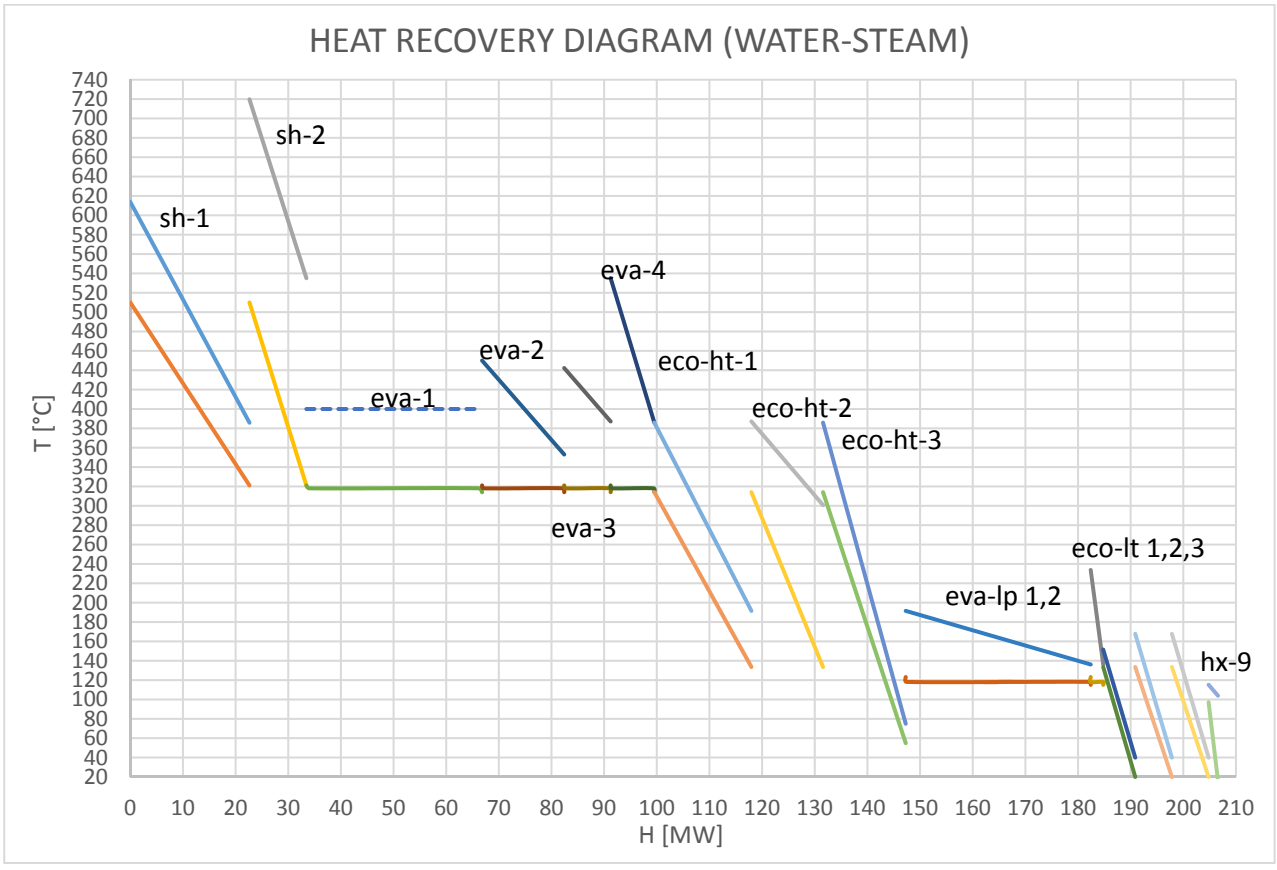

Figure 11: heat recovery (water-steam) T-Q diagram, case 2.

Table 9 shows that the overall compressors consumption has barely changed from case 1. Actually, this is due to the choice of splitting the air compression into four stages (instead of three, as in case 1). Generally speaking, an increase in pressure entails an increase in compression cost, for the reasons outlined above. Compared to case 1, the steam turbine power output slightly decreases, both because the steam to carbon required increases (as seen in fig. 35 of ch. 4.7, the S/C increases with pressure) and because the process steam is drawn at a higher pressure.

MECHANICAL POWER BALANCE					
compressors			**gas turbine**		
assumptions			assumptions		
η,is.=	0,75		η,is.=	0,78	
η,mech.=	0,98		η,mech.=	0,98	
results: power consumption [kW]			P,in [bar]=	40,94	
c1 (air)	7388,1		T,in [°C]=	720,0	
c2 (air)	6965,6		m [kg/s]=	23,50	
c3 (air)	6965,6		P,out [bar]=	1,02	
c4 (air)	6493,0		results		
c5 (bypass flow, stream 16D)	1153,0		T,out [°C]=	233,7	
c6 (recycle flow, stream 18A)	6602,0		P, shaft [kW]=	12442,3	
c7 (H2 for desulph., stream 21)	5,0				
c8 (N2 flow, stream 12E)	119,5		**steam turbine**		
c9 (H2/N2 flow, stream 23)	4327,0		assumptions		
c10 (H2/N2 flow, stream 25)	4347,0		η,is.=	0,82	
c11 (H2/N2 flow, stream 27)	5470,0		η,mech.=	0,98	
c12 (incondensables, stream 44)	120,7		P,in [bar]=	110	
c13 (incondensables, stream 47)	81,8		T,in [°C]=	510	
c-ref (refrigeration cycle)	2748,4		P,out [bar]=	0,158	
			T,out [°C]=	55,0	
P,comp.shaft tot.=	53864,0		results		
			X,out=	0,90	
pumps			P, shaft [kW]=	29158,6	
results: power consumption [kW]					
p1	89,3		P,mech. vailable tot [kW]=	41600,9	
p2	4,6				
p3	4,3				
p4	150,5				
p5	476,4				
p6	90,2				
			η,org.=	0,96	
P,pumps shaft tot.=	832,0		P,electric, in [kW]=	13640,8	
			η,el. ref.=	0,55	
P,mech. required [kW]=	54696,0		P, primary, plus [kW]=	24801,4	

Table 9: mechanical power balance, case 2

PERFORMANCES					
carbon capture ratio=	97,9%		LHV,ng=	46,59	MJ/kg
carbon dioxide emissions=	0,0325	t,CO2/t,NH3	P, electric, input=	13,6	MW
cold gas efficiency=	79,6%		η, electric, ref.=	55%	
net primary energy consumption=	26,83	GJ/t,NH3	natural gas input=	10,00	kg/s
corrected prim. en. consumption=	28,26	GJ/t,NH3	ammonia yield=	1500	t/d
corrected CO2 emissions =	0,114	t,CO2/t,NH3	S/C, stage A=	2,96	

BEDS SIZE, STAGES DURATION AND PRESSURE DROPS					
R, bed=	1,40	m	P,max,in=	44	bar
L, bed=	8,41	m	T, external wall=	70	°C
L, reactor=	9,7	m	T,steel, max =	300	°C
T,max,in=	878,7	°C			

	stage A	stage B	stage B+	stage C	
Number	4	3	3	1	
Δt [min] =	44,0	33,02	33,02	11,01	
V, max [m/s] =	0,5	2,91	1,27	14,05	
ΔP [bar] =	0,026	3,06	0,65	1,15	
ΔP/P,in [%] =	0,1%	7,0%	1,6%	64,1%	

MATERIAL COST					
valves per reactor=	8			cost per valve=	€ 50.000
N, valves, total=	88			total valves cost=	€ 4.400.000

reactor material	thickness [cm]	amount per reactor [m^3]	total amount [m^3]	cost [€/m^3]	total cost
fire bricks (internal refractory)	31,09	32,30	355,27	216	€ 76.738
steel (SA 516 grade 70)	8,65	10,11	111,22	5581,4	€ 620.753
mineral wool (external insulating)	15,33	19,32	212,50	750	€ 159.374

solid bed material (supported by alumina)	amount per reactor [t]	total amount [t]	support (Al2O3) mass fraction	cost [€/t]	total cost
CaO	52,83	581,09	15%	10000,00	€ 5.810.939
Cu	46,44	510,84	35%	15000,00	€ 7.662.595
Ni	13,47	148,18	82%	50000,00	€ 7.408.947
				total material cost=	€ 26.139.345

Table 10: summary table, case 2

5.3) Case 3: heated pre-reformer at stage A with P,A = P,B = 23,5 bar.

In this case the operating conditions have been chosen so that CaO hydration cannot occur. The main issue here is to provide the heat required to sustain both heated pre-reformers. As can be seen from the heat exchange diagram below (fig. 12), the heat duty of stage A pre-reformer is remarkable, and therefore the biggest hot flows available in the process (that exiting stage A and that bypassing stage B) must be used for this fulfilling this heat demand. The remaining two hot flows (that exiting stage C and that sent to the nitrogen PSA to feed the ammonia loop) must be used together to sustain stage C pre-reforming. With this heated pre-reformer configuration, stage A average outlet temperature increases compared to the previous cases, but, most importantly, there is no cold bed fraction (at $T_{,ad,A}$) at the end of stage A, therefore stage B and C outlet temperature significantly rise (roughly from 716 to 767 °C). Unfortunately, the high-temperature heat is not enough to reach chemical equilibrium at 700 °C at stage C pre-reformer, thus such temperature has been slightly decreased (to 670 °C).

The heat integration system has radically changed from the previous cases: except for the nitrogen flow (12B), which is quite small, the hottest flow available to produce high-pressure steam is the CO2-steam one (20C), which is at 483,7 °C after being cooled down in the heated pre-reformer of stage C and for heating the NG-steam fed to this pre-reformer. So, in this case, the steam temperature has been limited to 458,7 °C, at which 85 bar has been assumed as a reasonable pressure. Since a remarkable fraction of the high/medium-temperature heat available from the process streams has been successfully employed within the process for gas heating and pre-reformers, less amount of steam is produced and so the steam turbine power output is strongly reduced in comparison to the previous cases. As a result, a cold gas efficiency of 88,7% has been achieved in this case, which is noticeably higher than that reached for the previous cases (80,2% for case 2 and 79,6% for case 2, as seen before in Tables 5 and 10).

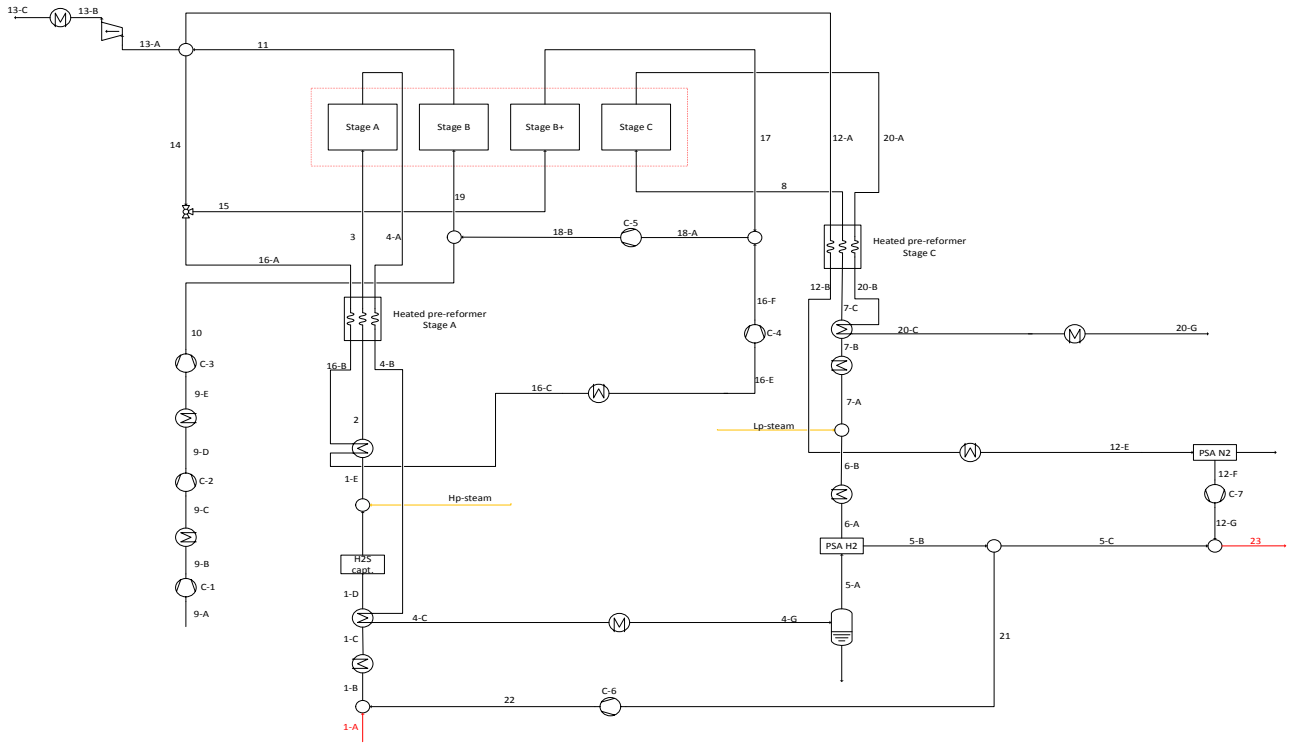

Figure 12: CaCu looping process for ammonia production plants, simplified scheme, case 3.

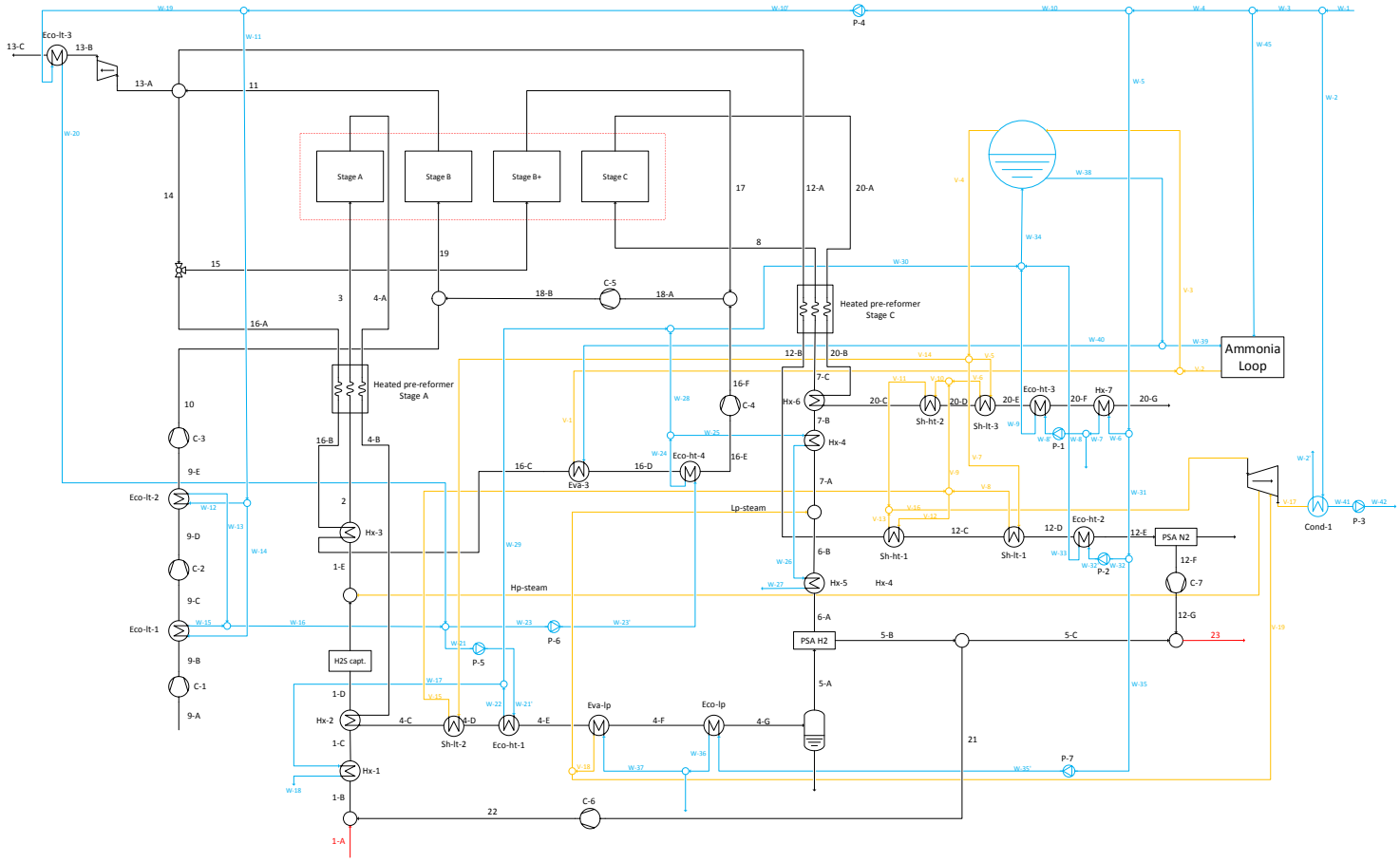

Figure 13: complete CaCu looping process scheme for ammonia production plants, case 3.

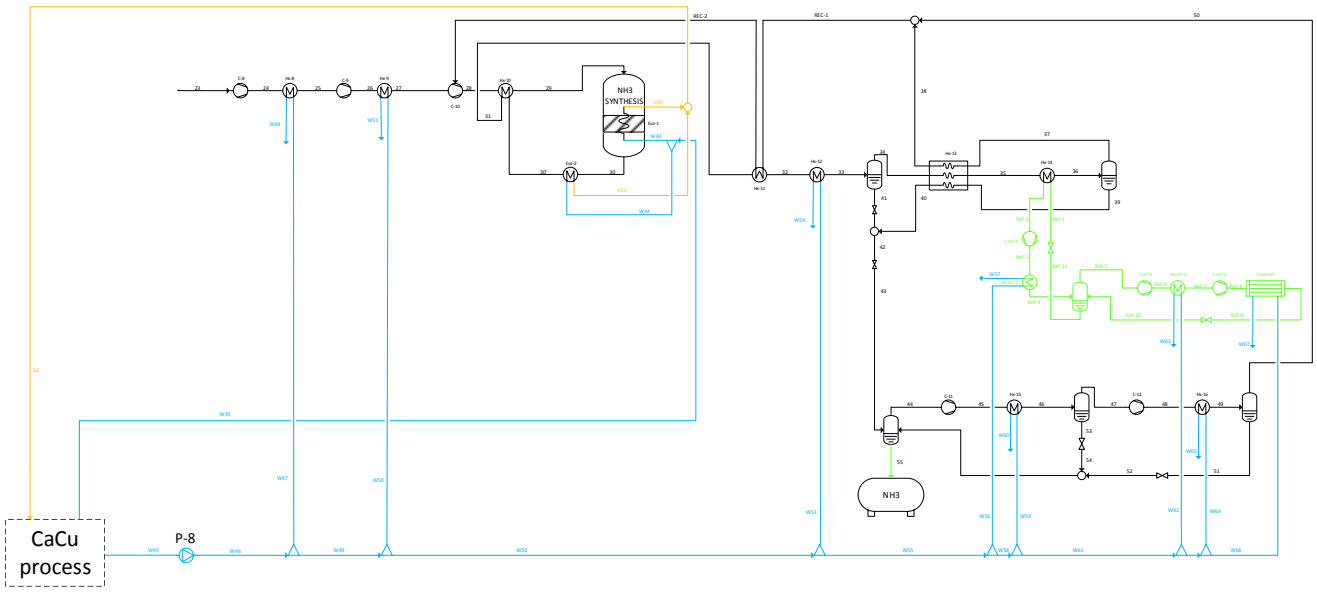

Figure 14: ammonia loop scheme, case 3.

The ammonia loop section has not changed compared to the previous cases.

Ca-Cu LOOPING PROCESS STREAM TABLE													
					MOLAR COMPOSITION								
stream	T [°C]	P [bar]	m [kg/s]	n [kmol/s]	CH4	C2+	H2O	H2	N2	O2	CO	CO2	Ar
1-A	16,0	24,96	8,98	0,50	89,0%	8,1%	0,0%	0,0%	0,9%	0,0%	0,0%	2,0%	0,0%
1-B	16,4	24,96	9,00	0,51	87,3%	8,0%	0,0%	2,0%	0,9%	0,0%	0,0%	2,0%	0,0%
1-C	277,3	24,71	9,00	0,51	87,3%	8,0%	0,0%	2,0%	0,9%	0,0%	0,0%	2,0%	0,0%
1-D	365,0	24,22	9,00	0,51	87,3%	8,0%	0,0%	2,0%	0,9%	0,0%	0,0%	2,0%	0,0%
hp-steam	300,6	24,46	31,26	1,74	0,0%	0,0%	100,0%	0,0%	0,0%	0,0%	0,0%	0,0%	0,0%
1-E	318,5	24,22	40,26	2,25	19,8%	1,8%	77,3%	0,4%	0,2%	0,0%	0,0%	0,4%	0,0%
2	425,0	23,98	40,26	2,25	19,8%	1,8%	77,3%	0,4%	0,2%	0,0%	0,0%	0,4%	0,0%
3	700,0	23,50	40,26	2,76	10,0%	0,0%	47,4%	32,9%	0,2%	0,0%	3,0%	6,6%	0,0%
4-A	856,1	23,48	27,37	2,89	2,1%	0,0%	32,0%	59,3%	0,2%	0,0%	4,4%	2,1%	0,0%
4-B	452,6	23,25	27,37	2,89	2,1%	0,0%	32,0%	59,3%	0,2%	0,0%	4,4%	2,1%	0,0%
4-C	427,5	23,01	27,37	2,89	2,1%	0,0%	32,0%	59,3%	0,2%	0,0%	4,4%	2,1%	0,0%
4-D	362,8	22,78	27,37	2,89	2,1%	0,0%	32,0%	59,3%	0,2%	0,0%	4,4%	2,1%	0,0%
4-E	166,0	22,56	27,37	2,89	2,1%	0,0%	32,0%	59,3%	0,2%	0,0%	4,4%	2,1%	0,0%
4-F	135,0	22,33	27,37	2,89	2,1%	0,0%	32,0%	59,3%	0,2%	0,0%	4,4%	2,1%	0,0%
4-G	40,0	22,11	27,37	2,89	2,1%	0,0%	32,0%	59,3%	0,2%	0,0%	4,4%	2,1%	0,0%
5-A	40,0	22,11	11,57	2,01	3,1%	0,0%	2,3%	85,1%	0,2%	0,0%	6,3%	3,0%	0,0%
5-B	40,0	21,67	3,09	1,54	0,0%	0,0%	0,0%	100%	0,0%	0,0%	0,0%	0,0%	0,0%
5-C	40,0	21,67	3,07	1,53	0,0%	0,0%	0,0%	100%	0,0%	0,0%	0,0%	0,0%	0,0%
6-A	40,0	1,88	8,48	0,47	13,1%	0,0%	9,8%	36,4%	0,9%	0,0%	26,9%	12,7%	0,0%
6-B	122,0	1,86	8,48	0,47	13,1%	0,0%	9,8%	36,4%	0,9%	0,0%	26,9%	12,7%	0,0%
lp-steam	122,0	1,86	3,64	0,20	0,0%	0,0%	100,0%	0,0%	0,0%	0,0%	0,0%	0,0%	0,0%
7-A	122,0	1,86	12,12	0,67	9,2%	0,0%	36,9%	25,5%	0,7%	0,0%	18,8%	8,9%	0,0%
7-B	277,3	1,84	12,12	0,67	9,2%	0,0%	36,9%	25,5%	0,7%	0,0%	18,8%	8,9%	0,0%
7-C	618,0	1,82	12,12	0,67	9,2%	0,0%	36,9%	25,5%	0,7%	0,0%	18,8%	8,9%	0,0%
8	670,0	1,80	12,12	0,74	3,6%	0,0%	22,5%	43,5%	0,6%	0,0%	15,7%	14,2%	0,0%
9-A	16,0	1,01	37,64	1,30	0,0%	0,0%	0,0%	0,0%	78,0%	21,0%	0,0%	0,0%	1,0%
9-B	158,2	3,04	37,64	1,30	0,0%	0,0%	0,0%	0,0%	78,0%	21,0%	0,0%	0,0%	1,0%
9-C	40,0	3,01	37,64	1,30	0,0%	0,0%	0,0%	0,0%	78,0%	21,0%	0,0%	0,0%	1,0%
9-D	183,1	8,45	37,64	1,30	0,0%	0,0%	0,0%	0,0%	78,0%	21,0%	0,0%	0,0%	1,0%
9-E	40,0	8,35	37,64	1,30	0,0%	0,0%	0,0%	0,0%	78,0%	21,0%	0,0%	0,0%	1,0%
10	183,4	23,50	37,64	1,30	0,0%	0,0%	0,0%	0,0%	78,0%	21,0%	0,0%	0,0%	1,0%

Continues

stream	T [°C]	P [bar]	m [kg/s]	n [kmol/s]	CH4	C2+	H2O	H2	N2	O2	CO	CO2	Ar
11	766,6	22,27	266,27	9,37	0,0%	0,0%	0,0%	0,0%	97,1%	0,0%	0,0%	1,6%	1,2%
12-A	766,6	22,27	18,69	0,66	0,0%	0,0%	0,0%	0,0%	97,1%	0,0%	0,0%	1,6%	1,2%
12-B	659,4	22,04	18,69	0,66	0,0%	0,0%	0,0%	0,0%	97,1%	0,0%	0,0%	1,6%	1,2%
12-C	427,5	21,82	18,69	0,66	0,0%	0,0%	0,0%	0,0%	97,1%	0,0%	0,0%	1,6%	1,2%
12-D	355,7	21,60	18,69	0,66	0,0%	0,0%	0,0%	0,0%	97,1%	0,0%	0,0%	1,6%	1,2%
12-E	40,0	21,17	18,69	0,66	0,0%	0,0%	0,0%	0,0%	97,1%	0,0%	0,0%	1,6%	1,2%
12-F	40,0	20,75	14,31	0,51	0,0%	0,0%	0,0%	0,0%	100%	0,0%	0,0%	0,0%	0,0%
12-G	45,5	21,67	14,31	0,51	0,0%	0,0%	0,0%	0,0%	100%	0,0%	0,0%	0,0%	0,0%
13-A	766,6	22,27	10,96	0,39	0,0%	0,0%	0,0%	0,0%	97,1%	0,0%	0,0%	1,6%	1,2%
13-B	314,5	1,02	10,96	0,39	0,0%	0,0%	0,0%	0,0%	97,1%	0,0%	0,0%	1,6%	1,2%
13-C	40,0	1,01	10,96	0,39	0,0%	0,0%	0,0%	0,0%	97,1%	0,0%	0,0%	1,6%	1,2%
14	766,6	22,27	236,62	8,33	0,0%	0,0%	0,0%	0,0%	97,1%	0,0%	0,0%	1,6%	1,2%
15	766,6	22,27	135,58	4,77	0,0%	0,0%	0,0%	0,0%	97,1%	0,0%	0,0%	1,6%	1,2%
16-A	766,6	22,27	101,04	3,56	0,0%	0,0%	0,0%	0,0%	97,1%	0,0%	0,0%	1,6%	1,2%
16-B	452,6	22,04	101,04	3,56	0,0%	0,0%	0,0%	0,0%	97,1%	0,0%	0,0%	1,6%	1,2%
16-C	362,0	21,82	101,04	3,56	0,0%	0,0%	0,0%	0,0%	97,1%	0,0%	0,0%	1,6%	1,2%
16-D	343,3	21,60	101,04	3,56	0,0%	0,0%	0,0%	0,0%	97,1%	0,0%	0,0%	1,6%	1,2%
16-E	302,7	21,39	101,04	3,56	0,0%	0,0%	0,0%	0,0%	97,1%	0,0%	0,0%	1,6%	1,2%
16-F	308,4	21,96	101,04	3,56	0,0%	0,0%	0,0%	0,0%	97,1%	0,0%	0,0%	1,6%	1,2%
17	299,5	21,96	135,58	4,77	0,0%	0,0%	0,0%	0,0%	97,1%	0,0%	0,0%	1,6%	1,2%
18-A	303,3	21,96	236,62	8,33	0,0%	0,0%	0,0%	0,0%	97,1%	0,0%	0,0%	1,6%	1,2%
18-B	317,9	23,50	236,62	8,33	0,0%	0,0%	0,0%	0,0%	97,1%	0,0%	0,0%	1,6%	1,2%
19	300,0	23,50	274,26	9,63	0,0%	0,0%	0,0%	0,0%	94,6%	2,8%	0,0%	1,4%	1,2%
20-A	766,3	1,32	33,00	1,07	0,0%	0,0%	50,7%	0,0%	0,4%	0,0%	0,0%	48,9%	0,0%
20-B	659,4	1,30	33,00	1,07	0,0%	0,0%	50,7%	0,0%	0,4%	0,0%	0,0%	48,9%	0,0%
20-C	483,7	1,29	33,00	1,07	0,0%	0,0%	50,7%	0,0%	0,4%	0,0%	0,0%	48,9%	0,0%
20-D	427,5	1,28	33,00	1,07	0,0%	0,0%	50,7%	0,0%	0,4%	0,0%	0,0%	48,9%	0,0%
20-E	355,7	1,27	33,00	1,07	0,0%	0,0%	50,7%	0,0%	0,4%	0,0%	0,0%	48,9%	0,0%
20-F	90,5	1,25	33,00	1,07	0,0%	0,0%	50,7%	0,0%	0,4%	0,0%	0,0%	48,9%	0,0%
20-G	40,0	1,24	33,00	1,07	0,0%	0,0%	50,7%	0,0%	0,4%	0,0%	0,0%	48,9%	0,0%
21	40,0	21,67	0,02	0,01	0,0%	0,0%	0,0%	100%	0,0%	0,0%	0,0%	0,0%	0,0%
22	57,5	24,96	0,02	0,01	0,0%	0,0%	0,0%	100%	0,0%	0,0%	0,0%	0,0%	0,0%
23	41,4	21,67	17,38	2,04	0,0%	0,0%	0,0%	75,0%	25,0%	0,0%	0,0%	0,0%	0,0%

Table 11: CaCu looping process stream table, case 3.

The CaO hydration becomes a serious problem where the water partial pressure is high and the temperature is low, that is at the beginning of stage A, when the inlet gas (at $T_{,g,in,A}$) meets the unconverted CaO (at $T_{,g,in,C}$). In this case, the water partial pressure in the inlet gas is 11,1 bar and the water partial pressure limit value at $T_{,g,in,C}$ (=670 °C) is 11,8 bar. At every other time and space the difference between the two is far larger (in particular, in zone "c", beyond the reaction front, where the gas is at $T_{,g,in,C}$, the water partial pressure is 8,1 bar).

As shown in fig. 15, since the feed gas entering stage A pre-reformer (stream 2) is not at chemical equilibrium at 425 °C, when it finds the catalyst, it reaches chemical equilibrium at the adiabatic temperature of 391 °C. In other words, there is an adiabatic section, at the pre-reformer inlet, in which the gas reaches its adiabatic equilibrium temperature (391 °C). Therefore, the cold gas inlet temperature difference at the pre-reformer of stage A is 62 °C and not 28 °C. Instead, we have set the gas inlet temperature of the stage C pre-reformer at its equilibrium value (618 °C), so that the approach temperature difference can be read from the table above (41,4 °C).

The ammonia loop remains the same, except for the lower inlet pressure, leading to a higher compression duty.

AMMONIA LOOP STREAM TABLE							
					molar composition		
stream	m [kg/s]	n [kmol/s]	T [°C]	P [bar]	H2	N2	NH3
23	17,41	2,05	41,4	21,7	75,0%	25,0%	0,0%
24	17,41	2,05	144,2	46,6	75,0%	25,0%	0,0%
25	17,41	2,05	40,2	46,1	75,0%	25,0%	0,0%
26	17,41	2,05	140,6	97,7	75,0%	25,0%	0,0%
27	17,41	2,05	40,2	96,7	75,0%	25,0%	0,0%
28	48,10	5,58	158,9	200,0	74,1%	24,7%	1,3%
29	48,10	5,58	320,2	199,0	74,1%	24,7%	1,3%
30	48,10	4,56	450,2	196,0	57,0%	19,0%	24,0%
30'	48,10	4,56	353,0	195,0	57,0%	19,0%	24,0%
31	48,10	4,56	217,5	194,0	57,0%	19,0%	24,0%
32	48,10	4,56	98,8	193,0	57,0%	19,0%	24,0%
33	48,10	4,56	30,2	192,0	57,0%	19,0%	24,0%
34	36,11	3,85	30,2	192,0	67,3%	22,4%	10,2%
35	36,11	3,85	9,3	191,0	67,3%	22,4%	10,2%
36	36,11	3,85	-19,9	190,0	67,3%	22,4%	10,2%
37	30,55	3,52	-19,9	190,0	73,5%	24,5%	1,9%
38	30,55	3,52	25,2	189,0	73,5%	24,5%	1,9%
39	5,56	0,33	-19,9	190,0	0,4%	0,1%	99,5%
40	5,56	0,33	25,2	189,0	0,4%	0,1%	99,5%
41	11,99	0,71	30,2	192,0	1,2%	0,4%	98,4%
42	17,55	1,04	28,6	189,0	0,9%	0,3%	98,8%
43	17,55	1,04	28,3	20,0	0,9%	0,3%	98,8%
44	0,40	0,03	28,4	20,0	30,8%	10,3%	58,9%
45	0,40	0,03	155,6	61,0	30,8%	10,3%	58,9%
46	0,40	0,03	40,2	60,7	30,8%	10,3%	58,9%
47	0,20	0,02	40,2	60,7	51,6%	17,2%	31,2%
48	0,20	0,02	185,1	190,0	51,6%	17,2%	31,2%
49	0,20	0,02	40,2	189,4	51,6%	17,2%	31,2%
50	0,13	0,01	40,2	189,4	64,9%	21,6%	13,6%
51	0,06	0,00	40,2	189,4	1,4%	0,5%	98,1%
52	0,06	0,00	34,7	20,0	1,4%	0,5%	98,1%
53	0,20	0,01	40,2	60,7	0,4%	0,1%	99,5%
54	0,20	0,01	37,8	20,0	0,4%	0,1%	99,5%
55	17,41	1,02	28,4	20,0	0,1%	0,0%	99,9%
REC-1	30,68	3,53	25,2	189,0	73,5%	24,5%	2,0%
REC-2	30,68	3,53	199,5	188,0	73,5%	24,5%	2,0%

Table 12: ammonia loop stream table, case 3.

HEAT INTEGRATION SYSTEM (WATER)							
stream	m [kg/s]	T [°C]	p [bar]	stream	m [kg/s]	T [°C]	p [bar]
W-1	693,0	20,0	1,01	W-44	10,8	297,3	85,00
W-2	214,4	20,0	1,01	W-45	254,7	20,0	1,01
W-2'	214,4	50,0	1,01	W-46	254,7	20,0	3,38
W-3	478,6	20,0	1,01	W-47	14,4	20,0	3,38
W-4	223,9	20,0	1,01	W-48	14,4	124,0	3,38
W-5	195,1	20,0	1,01	W-49	240,3	20,0	3,38
W-6	122,5	20,0	1,01	W-50	14,5	20,0	3,38
W-7	122,5	70,5	1,01	W-51	14,5	121,0	3,38
W-8	11,0	70,5	1,01	W-52	225,8	20,0	3,38
W-8'	11,0	70,5	85,00	W-53	124,2	20,0	3,38
W-9	11,0	297,3	85,00	W-54	124,2	57,0	3,38
W-10	28,8	20,0	1,01	W-55	101,6	20,0	3,38
W-10'	28,8	20,0	3,38	W-56	3,4	20,0	3,38
W-11	21,9	20,0	3,38	W-57	3,4	61,0	3,38
W-12	12,0	20,0	3,38	W-58	98,2	20,0	3,38
W-13	12,0	127,7	3,38	W-59	2,2	20,0	3,38
W-14	9,8	20,0	3,38	W-60	2,2	57,2	3,38
W-15	9,8	127,7	3,38	W-61	96,0	20,0	3,38
W-16	21,9	127,7	3,38	W-62	4,2	20,0	3,38
W-17	5,0	297,3	85,00	W-63	4,2	47,0	3,38
W-18	5,0	36,4	85,00	W-64	0,4	20,0	3,38
W-19	7,0	20,0	3,38	W-65	0,4	100,1	3,38
W-20	7,0	127,7	3,38	W-66	91,4	20,0	3,38
W-21	23,3	127,7	3,38	W-67	91,4	41,5	3,38
W-21'	23,3	127,7	85,00				
W-22	23,3	297,3	85,00	V-1	1,4	302,3	85,00
W-23	5,5	127,7	3,38	V-2	34,0	302,3	85,00
W-23'	5,5	127,7	85,00	V-3	35,4	302,3	85,00
W-24	5,5	297,3	85,00	V-4	35,4	302,3	85,00
W-25	4,4	297,3	85,00	V-5	10,7	302,3	85,00
W-26	4,4	142,0	85,00	V-6	10,7	382,2	85,00
W-27	4,4	74,8	85,00	V-7	4,7	302,3	85,00
W-28	1,1	297,3	85,00	V-8	4,7	382,2	85,00
W-29	18,3	297,3	85,00	V-9	1,8	382,2	85,00
W-30	19,4	297,3	85,00	V-10	12,5	382,2	85,00
W-31	72,6	20,0	1,01	V-11	12,5	458,7	85,00
W-32	5,0	20,0	1,01	V-12	22,9	382,2	85,00
W-32'	5,0	20,0	85,00	V-13	22,9	458,7	85,00
W-33	5,0	297,3	85,00	V-14	20,0	302,3	85,00
W-34	35,4	297,3	85,00	V-15	20,0	382,2	85,00
W-35	67,6	20,0	1,01	V-16	35,4	458,7	85,00
W-35'	67,6	20,0	1,86	V-17	12,4	55,0	0,16
W-36	115,0	20,0	1,86	V-18	11,8	122,0	1,86
W-37	11,8	20,0	1,86	V-19	8,2	122,0	1,86
W-38	35,4	297,3	85,00	V-20	23,2	302,3	85,00
W-39	34,0	297,3	85,00	V-21	10,8	302,3	85,00
W-40	1,4	297,3	85,00	HP-steam	31,3	300,6	24,46
W-41	12,4	47,0	0,16	LP-steam	3,6	122,0	1,86
W-42	12,4	47,0	1,50				
W-43	23,2	297,3	85,00				

Table 13: heat integration system stream table, case 3

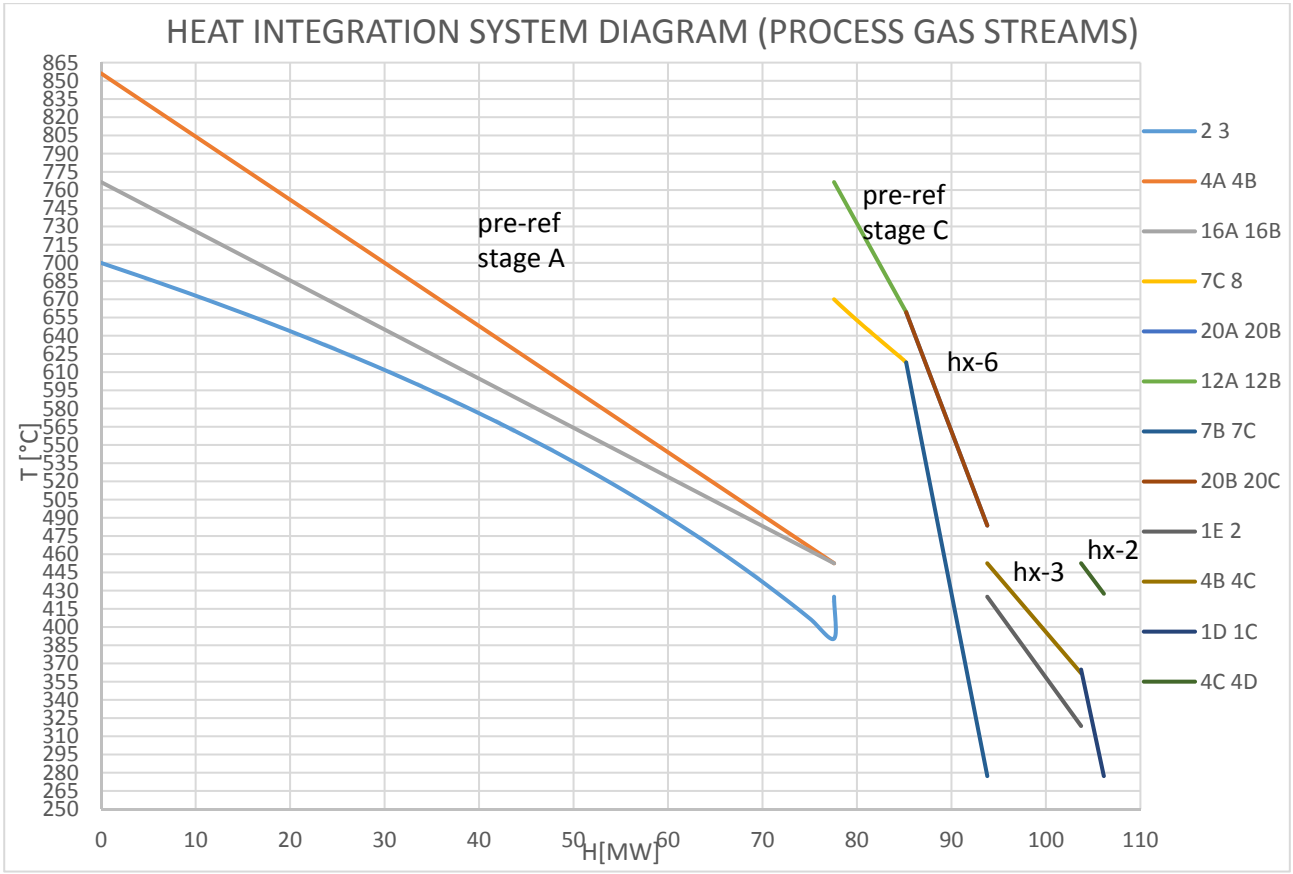

Figure 15: heat integration system (process gas streams) T-Q diagram, case 3.

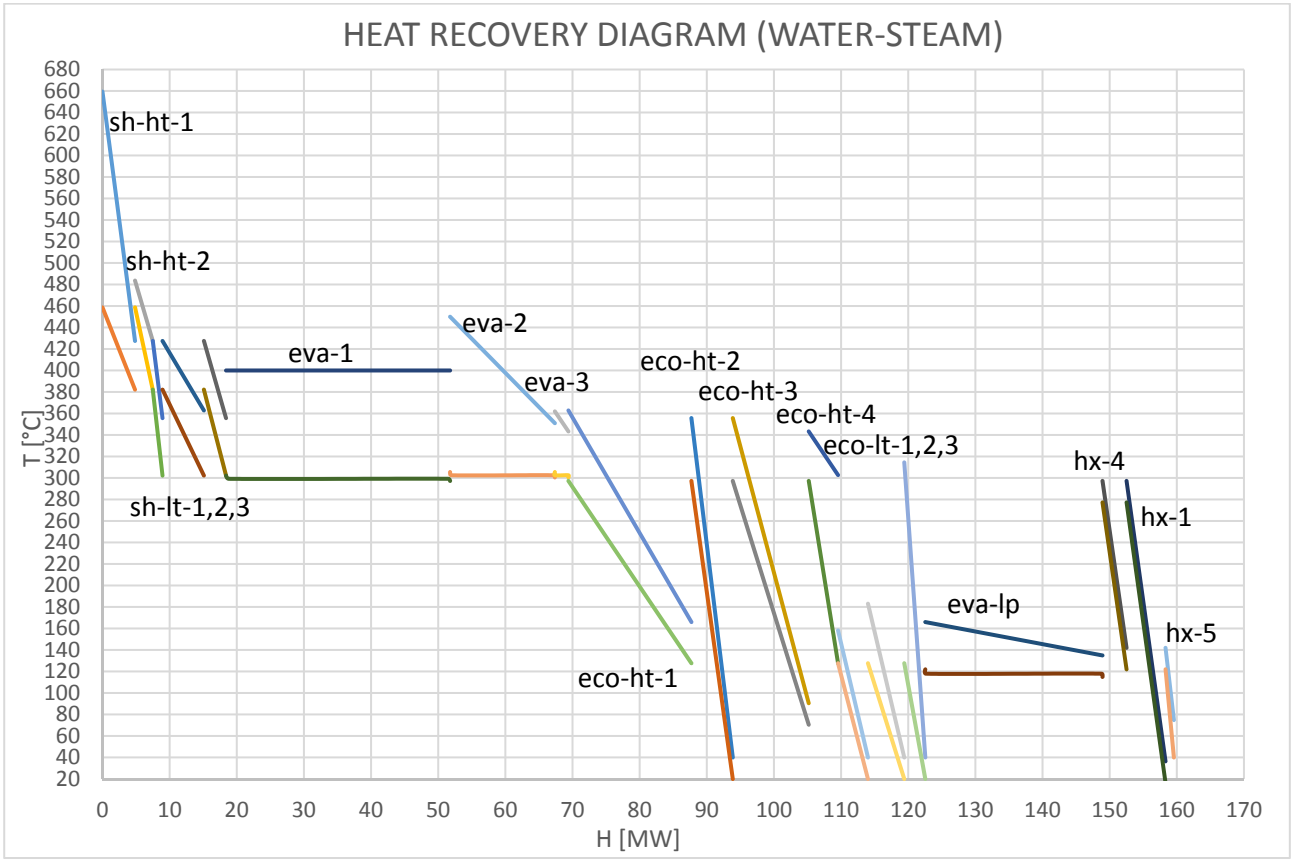

Figure 16: heat recovery (water-steam) T-Q diagram, case 3.

MECHANICAL POWER BALANCE			
compressors		**gas turbine**	
assumptions		assumptions	
η,is.=	0,75	η,is.=	0,78
η,mech.=	0,98	η,mech.=	0,98
results: power consumption [kW]		P,in [bar]=	22,27
c1 (air)	5383,6	T,in [°C]=	766,6
c2 (air)	5417,5	m [kg/s]=	10,96
c3 (air)	5429,2	P,out [bar]=	1,02
c4 (bypass flow, stream 16E)	608,1	results	
c5 (recycle flow, stream 18A)	3725,9	T,out [°C]=	314,5
c6 (H2 for desulph., stream 21)	5,1	P, shaft [kW]=	5474,2
c7 (N2 flow, stream 12F)	81,6		
c8 (H2/N2 flow, stream 23)	6219,0	**steam turbine**	
c9 (H2/N2 flow, stream 25)	6193,0	assumptions	
c10 (H2/N2 flow, stream 27)	7393,0	η,is.=	0,82
c11 (incondensables, stream 44)	120,7	η,mech.=	0,98
c12 (incondensables, stream 47)	81,8	P,in [bar]=	85
c-ref (refrigeration cycle)	2748,4	T,in [°C]=	458,7
		P,out [bar]=	0,158
P,comp.shaft tot.=	44292,8	T,out [°C]=	55,0
		results	
pumps		X,out=	0,90
results: power consumption [kW]		P, shaft [kW]=	14901,6
p1	92,6		
p2	41,9	P,mech. vailable tot [kW]=	20375,8
p3	1,7		
p4	6,9		
p5	202,5		
p6	48,3		
p7	5,7		
p8	61,0		
		η,org.=	0,96
P,pumps shaft tot.=	470,1	P,electric, in [kW]=	25403,2
		η,el. ref.=	0,55
P,mech. required [kW]=	44762,9	P, primary, plus [kW]=	46187,7

Table 14: mechanical power balance, case 3.

PERFORMANCES					
carbon capture ratio=	96,9%		LHV,ng=	46,59	MJ/kg
carbon dioxide emission=	0,0428	t,CO2/t,NH3	P, electric, input=	25,4	MW
cold gas efficiency=	88,7%		η, electric, ref.=	55%	
net primary energy consumption=	24,10	GJ/t,NH3	natural gas input=	8,98	kg/s
corrected prim. en. consumption=	26,76	GJ/t,NH3	ammonia yield=	1500	t/d
corrected CO2 emissions=	0,194	t,CO2/t,NH3	S/C, stage A=	3,21	

BEDS SIZE, STAGES DURATION AND PRESSURE DROPS					
R, bed=	1,89	m	P,max,in=	23,5	bar
L, bed=	11,34	m	T, external wall=	70	°C
L, reactor=	13,0	m	T,steel, max =	300	°C
T,max,in=	864,0	°C			

	stage A	stage B	stage B+	stage C	
Number	4	3	3	1	
Δt [min] =	139,8	104,82	104,82	34,94	
V, max [m/s] =	0,5	2,17	1,04	6,69	
ΔP [bar] =	0,02	1,23	0,30	0,48	
ΔP/P,in [%] =	0,1%	5,3%	1,4%	26,8%	

MATERIAL COST					
valves per reactor=	8			cost per valve=	€ 50.000
N, valves, total=	88			total valves cost=	€ 4.400.000

reactor material	thickness [cm]	amount per reactor [m^3]	total amount [m^3]	cost [€/m^3]	total cost
fire bricks (internal refractory)	32,23	59,12	650,37	216	€ 140.481
steel (SA 516 grade 70)	11,66	23,67	260,36	5581,40	€ 1.453.154
mineral wool (external insulating)	15,43	33,41	367,53	750	€ 275.649

solid bed material (supported by alumina)	amount per reactor [t]	total amount [t]	support (Al2O3) massic fraction	cost [€/t]	total cost
CaO	134,98	1484,79	15%	10000,00	€ 14.847.887
Cu	101,57	1117,26	35%	15000,00	€ 16.758.919
Ni	34,42	378,62	82%	50000,00	€ 18.931.056

total material cost=	€ 56.807.145

Table 15: summary table, case 3.

5.4) Performance comparison and discussion

PERFORMANCES COMPARISON				
	reference plant	CaCu case 3 (23,5 bar)	CaCu case 1 (34,5 bar)	CaCu case 2 (44 bar)
ammonia yield [t/d]	1500	1500	1500	1500
net natural gas input [t/d]	905,5	775,8	857,9	864
electric power output [MW]	3,9	-25,4	-12,7	-13,6
net primary energy consumption [GJ/t,NH3]	28,13	24,10	26,64	26,83
corrected primary energy consumption* [GJ/t,NH3]	27,72	26,76	27,97	28,26
net carbon dioxide emissions** [t,CO2/t,NH3]	0,363	0,043	0,041	0,032
corrected carbon dioxide emissions*** [t,CO2/t,NH3]	0,339	0,194	0,116	0,114
carbon dioxide recompression cost****[MWe]	9,8	10	12,7	14,4
cold water consumption [kg/s]	931,1	693,0	1030,5	1114,3
ammonia reactor inlet flow rate [kmol/s]	6,66	5,58	5,58	5,58
reactors and beds cost		€ 56.807.145	€ 34.279.648	€ 26.139.345

*Table 16: Plant performance comparison. Bear in mind that case 3 is different from the other two (since the pre-reformer of stage A is heated in this case). *the reference power production efficiency is 55%. **if the carbon dioxide captured is compressed and stored. ***considering an emission factor of 0,103 kg,CO2/MJe. ****recompression to 250 bar, using a compression train made of 5 centrifugal compressors (with the same performance of the other compressors), with inter-refrigeration to 40 °C.*

Two comparisons can be made, the first between the three Ca-Cu looping process configurations, the second between the Ca-Cu looping process and the traditional technology. Let us begin with the former.

The effect of the operating pressure (of stages A and B) can be inferred comparing case 1 and 2. On one hand, reducing the operating pressure entails a reduction in primary energy consumption and in CO2

recompression cost (the higher the pressure of stage A, the higher the pressure drops at stage C); on the other hand it leads to higher investment cost and CO2 slip from stage B (due to calcination). Therefore, the pressure optimal value has to be chosen based on a full economic analysis.

Comparing case 3 and 1, the positive effect of the heated pre-reformer of stage A on the energy performance is evident: the corrected primary energy consumption slips under 26,8 Gj/t,NH3, which is a remarkable result. Besides, the cold water consumption decreases. Unfortunately, the configuration of case 3 is the most expensive, mainly because of the reactors and beds cost but also because of the heated pre-reformers cost. Although a complete economic analysis would be required to prove it, this configuration seems to be quite promising (not least because it is the safest with respect to CaO hydration).

The second and most interesting comparison is between the Ca-Cu looping process proposed in this work and the conventional NH3 production technology. The results show that a primary energy saving, however small, is possible only in case 3. Anyway, the Ca-Cu process allows a reduction in the natural gas feed flow rate, balanced by the electric power input (which can be produced from renewable sources). This feature can be interesting in order to reduce the fossil fuels consumption, especially for importer countries (such as Europe). In this way, not only the ammonia production would become more sustainable, but it would be also less exposed to natural gas price instability and provision shortages. The argument gets stronger still if applied to the Italian energy market, characterized by a supply excess and a high renewable share.

In case of CO_2 compression and storage, another important point in favour of this new technology is the CO2 emissions, which are almost one order of magnitude lower than that of the reference plant in the case of a zero-emissions power production (net CO_2 emissions) and 43-67% lower if the power is produced by a combined cycle (corrected CO_2 emissions) . In fact, whereas in the reference plant there is a combustion flue-gas stream, in this case the only carbon dioxide emission is due to calcination in stage B. This feature is very important if we are aimed at limiting the global CO2 emissions in order to contain the temperature rise below 2 °C compared to the pre-industrial level (as pointed out at the United Nations Climate Change Conference of Paris, 2015). In this regard, we want to remind that the European Union, with the climate and energy framework adopted in October 2014, has set to 40% the target for greenhouse gas emissions reduction by 2030 (compared to 1990 levels).

Last but not least, the investment cost. Even though we have not performed an economic analysis, aimed at evaluating the plant cost for the cases analysed, some considerations can be made. Firstly, the fired tubular reformers are complex and expensive equipment (the FTR cost alone exceeds 28 M€) , and, to a much lesser extent, the same applies to auto-thermal reformers (remind that both are present in the reference plant). In the Ca-Cu process they are both replaced by fixed beds, which are much simpler and, reasonably, cheaper (their cost has been estimated above between 26 and 56 M€, depending on the case). But the main investment savings are believed to be downstream the syngas production. In traditional plants the raw syngas crosses several refining stages: water-gas shift, CO2 capture and methanation. Such stages are performed by big and expensive components. In the Ca-Cu process, two PSA, one for the hydrogen and one for the nitrogen stream, replace the aforementioned purification units in traditional NH3 production plants. This leads to another advantage: the purity of the hydrogen-nitrogen stream. This, as already outlined, allows to avoid the purge stream in the ammonia synthesis loop, and so the scrub and the PSA required for its treatment. Besides, as shown in table 16, the high purity of syngas leads a significant reduction in the molar flow rate crossing the ammonia reactor and in general the ammonia loop, which means a significant investment saving for the ammonia loop equipment.

6) Conclusions

In this work we have analysed a calcium-copper chemical looping process to produce the hydrogen and nitrogen stream required for the ammonia synthesis. As pointed out in chapter 5.4, it has several advantages over the traditional technology, in particular:

- A slightly lower primary energy consumption, which passes from 27,72 to 26,76 GJ/t,NH_3 in case 3
- A lower natural gas net input (up to 14,3% less)
- Lower carbon dioxide emissions, if we consider it compressed and stored, thanks to the absence of combustion. The figure drops from 0,339 t,CO_2/t,NH_3 for the reference plant to a maximum of 0,194 t,CO_2/t,NH_3 for case 3 (whereas, if we consider a zero-emissions reference power production, it is almost one order of magnitude lower than that of the reference technology)
- A lower investment cost (although we have not performed a full economic analysis, so we are not able to give a quantitative idea).

For these reasons, the technology seems very promising and further studies on the subject are worth to be carried out. A field research, with pilot and demonstration plants, is necessary to validate the calculation assumptions and confirm the process viability and profitability.

List of figures

Chapter 1

Chapter 2

List of tables

Bibliography

Chapter 1

1) Christian Egenhofer, Lorna Schrefler et al.; 2014; Final report for a study of composition and drivers of energy prices and costs in energy intensive industry: the case of the chemical industry – ammonia; Centre for European policy studies
2) Wikipedia: ammonia
3) Wikipedia: sodium nitrate
4) The Fertilizer Institute, http://www.firt.org/sites/default/files/2Vroomen.pdf
5) Wikipedia: urea production
6) http://www.essentialchemicalindustry.org/materials-and-applications/fertilizers.html
7) http://www.ehow.com/list_7421086_list-common-agricultural-fertilizers.html
8) Goldman Sachs Seventeenth Annual Agribusiness Conference
9) The Crop Site, http://www.thecropsite.com/articles/1720/fertilizer-controlling-costs-with-lower-crop-revenues/
10) Ullmann's encyclopedia of industrial chemistry, ammonia. Wiley-VCH Verlag GmbH & Co., 2002.

Chapter 2

1) The fertilizer Institute, http://www.firt.org/sites/default/files/2Vroomen.pdf
2) Wikipedia: sodium nitrate
3) Ullmann's encyclopedia of industrial chemistry, ammonia; Wiley-VCH Verlag GmbH & Co.; 2002.
4) Christian Egenhofer, Lorna Schrefler et al.; 2014; Final report for a study of composition and drivers of energy prices and costs in energy intensive industry: the case of the chemical industry – ammonia; Centre for European policy studies
5) Amonìaco y sus principale derivados, Tecnologìa Quimica Industrial, Diquima, Universidad Politecnica de Madrid
6) Idrogeno, slides del corso di Fondamenti di processi chimici, prof. Gianpiero Groppi, Politecnico di Milano
7) Ib Dybkjær, Torben Nørgaard, Jens Perregaard, Finn Joensen; Industria petrolchimica: prodotti di base e filiere petrolchimiche; Enciclopedia degli idrocarburi. Ammoniaca
8) Kent and Riegel's Handbook of industrial chemistry and biotechnology; James Kent editor; 11th edition
9) Howard F. Rase; Chemical reactor design for process plant; The University of Texas at Austin, Wiley and sons
10) Charles A. Hodge, Neculai N. Popovici; 1994; Pollution control in fertilizer production
11) DRP 235 421
12) Kohl, A., Nielsen, R.; 1997; Gas Purification, 5th ed. Gulf Publishing Company

Chapter 4

1) Wikipedia, Calcium oxide

2) J.R. Fernandez, J.C. Abanades, R. Murillo, G. Grasa; 2011; Conceptual design of a hydrogen production process from natural gas with CO2 capture using a Ca–Cu chemical loop

3) J.R. Fernandez, J.C. Abanades, R. Murillo; 2012; Modeling of sorption enhanced steam methane reforming in an adiabatic fixed bed reactor

4) Wen-Ching Yang; 2003; Handbook of fluidization and fluid-particles systems; Pittsburgh, USA

5) C. Qin, J. Yin, W. Liu, H. An and B. Feng; 2012; Behavior of CaO/CuO Based Composite in a Combined Calcium and Copper Chemical Looping Process

6) I. Martìnez, M.C Romano, J.R. Fernandez, P. Chiesa, R. Murillo, J.C. Abanades; 2013; Process design of a hydrogen production plant from natural gas with CO2 capture based on a novel Ca/Cu chemical loop

7) J.R. Fernandez, J.C. Abanades, G. Grasa; 2012; Modeling of sorption enhanced steam methane reforming—Part II: Simulation within a novel Ca/Cu chemical loop process for hydrogen production

8) R. Fernandez, J.C. Abanades, R. Murillo; 2012; Modeling of Cu oxidation in an adiabatic fixed-bed reactor with N2 recycling

9) S. Noorman, F. Gallucci, M. van Sint Annaland, J.A.M. Kuipers; 2010; A theoretical investigation of CLC in packed beds. Part 2: Reactor model

10) Abanades, J. C.; Murillo, R.; 2009; Method of capturing CO2 by means of CaO and the exothermic reduction of a solid; EP 2305366 B1

11) Lopez-Ortiz and Harrison; Ind. Eng. Chem. Res.;2001; Hydrogen Production Using Sorption-Enhanced Reaction

12) Harrison; Ind. Eng. Chem. Res.; 2008; Sorption-Enhanced Hydrogen Production: A Review

13) V. Spallina, F. Gallucci, M.C. Romano, P. Chiesa, G. Lozza, M. van Sint Annaland; 2013; Investigation of heat management for CLC of syngas in packed bad reactors

Ringraziamenti

Vorrei ringraziare il mio relatore, Matteo Romano, e la mia correlatrice, Isabel Martinez. Nel corso di questo lavoro, entrambi hanno dimostrato non solo grande professionalità e competenza, ma anche notevoli doti umane. Senza il loro ruolo di guida, supervisione e supporto questo lavoro non sarebbe stato possibile.